5-lipoxygenase (5-LO) regulation and activity in colorectal cancer cell lines

Dissertation

zur Erlangung des Doktorgrades der Naturwissenschaften

(Dr. rer. nat.)

vorgelegt beim Fachbereich Biochemie, Chemie und Pharmazie (14)

der Johann Wolfgang Goethe-Universität

in Frankfurt am Main

von

Tamara Jessika Göbel

aus Langen (Hessen)

Frankfurt am Main

2023

(D 30)

Vom Fachbereich Biochemie, Chemie und Pharmazie (14) der Johann Wolfgang Goethe-Universität als Dissertation angenommen.

Dekan: Prof. Dr. Clemens Glaubitz

Gutachter: Prof. Dr. Dieter Steinhilber

Prof. Dr. Andreas Weigert

Datum der Disputation:

Most fun I ever had
And I'd do it over and over and over again if I could

I Did Something Bad - Taylor Alison Swift, Karl Johan Schuster, Max Martin, 2017

Table of contents

List of abbreviations

1,25(OH)2-vitamin D3.....calcitriol
12-HHT.....12(S)-hydroxyheptadecatrienoic acid
12-LO.....platelet-type 12-lipoxygenase
15-LO-1.....15-lipoxygenase-1
15-LO-2.....15-lipoxygenase-2
2AG.....2-arachidonoylglycerol
2D.....two-dimensional
3D.....three-dimensional
5'UTR..... 5-prime untranslated region
5-H(p)ETE.... 5-hydroperoxyeicosatetraenoic acid
5-HETE.....5-hydroxyeicosatetraenoic acid
5-LO.....5-lipoxygenase
5-oxo-ETE..... 5-oxo-eicosatetraenoic acid
ADP.....adenosine diphosphate
AEA..... N-arachidonylethanolamine
AKBA...3-acetyl-11-keto-beta-boswellic acid
ALL..... acute lymphoblastic leukemia
ALOX5.....5-LO gene
AML..... acute myeloid leukemia
AMP.....adenosine monophosphate
AP-2..... activation protein 2
APS..... ammonium peroxydisulphate
ARA..... arachidonic acid
ASA.....acetylic salicylic acid
ATP..... adenosine triphosphate
BHT.....butylated hydroxytoluene
BSA.....bovine serum albumin
CAF.....cancer-associated fibroblast
CD14.....cluster of differentiation 14
cds..... coding sequence
CGM.....complete growth medium
CIMP..... CpG island methylator phenotype
CIN..... chromosomal instability
CLL.....chronic lymphocytic leukemia
CLP.....coactosine-like protein
CML.....chronic myeloid leukemia
CMS..... consensus molecular subtypes
CNS.....central nervous system
co.....control
Cobi.....Cobimetinib
COX-1/2.....cyclooxygenase 1/2
CRC..... colorectal cancer
CV..... control vector
CYP450..... cytochrome P450
CysLTs.....cysteinyl leukotrienes
DABCO..... 1,4-Diazabicyclo [2.2.2]octane
Dac.....Dactolisib
DAG.....diacylglycerol
DAPI..... 4',6-Diamidino-2-phenylindol
DC.....dendritic cells
DHA.....docosahexaenoic acid
DiHETE.....dihydroxyeicosatetraenoic acid
DMEM... Dulbecco's Modified Eagle Medium
DMSO..... dimethyl sulfoxide
DSMZ German Collection of Microorganisms and Cell Cultures
DNA.....deoxyribonucleic acid
DSS..... dextran sodium sulfate
DTT.....dithiothreitol
ECM.....extracellular matrix
EDTA.....ethylenediaminetetraacetic acid
Egr-1.....early growth response protein 1
eLO-3..... epidermis-type lipoxygenase-3
EMT..... epithelial-mesenchymal transition
EPA.....eicosapentaenoic acid
ERK-1/2.....extracellular signal-regulated kinase 1/2
Erlo..... Erlotinib
ETE..... eicosatetraenoic acid
EtOH..... ethanol
FA.....fatty acid
FCS..... fetal calf serum
FDA..... American Food and Drug Administration
FLAP.....5-lipoxygenase activating protein
Fluc.....firefly luciferase
fMLP.....N-formylmethionine-leucyl-phenylalanine
FTase..... farnesyltransferase
GDP..... guanosine diphosphate
GFP.....green fluorescent protein
GGTase.....geranyl-geranyl transferase
GM-CSF.....granulocyte-macrophage stimulating factor
GPCRs..... G-protein-coupled receptors
GPx..... glutathione peroxidase
GSH.....glutathione
GTP.....guanosine triphosphate
H(p)DHA hydroperoxydocosahexaenoic acid
H(p)EPE. hydroperoxyeicosapentaenoic acid
HEPES.....4-(2-hydroxyethyl)-1-piperazineethanesulfonic acid
H(p)ETE...hydroperoxyeicosatetraenoic acid
H(p)ODE hydroperoxyoctadecadienoic acid
HDAC..... histone deacetylase

HER2..... human epidermal growth factor receptor 2
HETE..... hydroxyeicosatetraenoic acid
HLM HLM006474
ICD-O3 .....International Classification of Diseases for Oncology
IL-4.....interleukin 4
INFγ .....interferon gamma
KLF .....Krüpple-like factor
KO.....knockout
LA .....linoleic acid
LB-medium.....Luria Broth Base Medium
LB LB42708
LC-MS/MS.....liquid chromatography-electrospray ionization tandem mass spectrometry
LDH .....lactate dehydrogenase
LLOQ ..... lower limit of quantification
LO .....lipoxygenases
LOX .....lipoxygenase gene
LSM .....Lymphocyte Separation Medium
LTA_4 .....leukotriene A4
$LTA4_H$ .....leukotriene A4 hydrolase
LTA_5 .....leukotriene A5
LTB_4 .....leukotriene B5
$LTC4_S$ .....cysteinyl leukotriene C4 synthase
LTs .....leukotrienes
LxA4 .....lipoxin A4
LxA5 .....lipoxin A5
LxB4 ..... 5(S),14(R),15(S)-triHETE
LxB5 .....lipoxin B5
MAPEG.... membrane-associated proteins in the eicosanoid and glutathione metabolism
MAPK ..... mitogen-activated protein kinase gene
MEK-1/2.... mitogen-activated protein kinase kinase
MaR1 ..... maresin-1
MaR2 ..... maresin-2
MAZ .....Myc-associated zinc finger protein
M-CSF macrophage colony-stimulating factor
MCTS ..... multicellular tumor spheroids
MDSCs.....myeloid-derived suppressor cells
MeOH ..... methanol
miRNA.....micro ribonucleic acid
MK2 ..... mitogen-activated protein kinase activated protein kinase 2
MLL1 .....N-methyltransferase 2A
MM6 .....Mono Mac 6
MMR ..... mismatch repair pathway
MMS ..... microsatellite stability
mRNA .....messenger ribonucleic acid
MSI ..... microsatellite instability
mTOR ..... mammalian target of rapamycin
mTORC-1 ..... mTOR complex 1
mTORC-2 ..... mTOR complex 2
MYBL2.....b-MYB gene
NAC .....N-acetylcysteine
NDGA .....nordihydroguaiaretic acid
NES .....nuclear export sequence
NFAT ..... nuclear factor of activated T-cells
NF-κB ..... nuclear factor kappa light-chain-enhancer of activated B cells
NIS .....nuclear import sequence
NK ..... natural killer
NPD1 ..... neuroprotectin 1
OAG 1-oleoyl-2-acetyl-sn-glycerol
OMS ....organotypic multicellular spheroids
p70S6K.....phosphorylation via ribosomal protein S6 kinase
Palbo .....Palbociclib
PBMCs ..... human peripheral blood mononuclear cells
PBS .....phosphate-buffered saline
PBSG ..... PBS glucose
PC ..... phosphatidylcholine
PCET .....proton-coupled electron transfer
PCRs ..... polymerase chain reactions
PD PD184352
PD1 ..... protectin D1
PE ..... phosphatidylethanolamine
PEI ..... polyethylenimine
PFA ..... paraformaldehyde
PG ..... phosphatidylglycerol
PGP .....Pro-Gly-Pro
pH_e ..... extracellular pH
pH_i ..... intracellular pH
PI .....propidium iodide
PPI ..... phosphatidylinositol
PI3K .....phosphoinositide 3-kinase
PKA ..... protein kinase A
PLA .....phospholipase
PMNL .....polymorphonuclear leukocytes
PPARα.....proliferator-activated receptor α
PS ..... phosphatidylserine
PUFA ..... polyunsaturated fatty acid
qPCR .....quantitative real-time polymerase chain reaction
RE .....response element
RGM ..... reduced growth medium
ROS .....reactive oxygen species
RPMI ..... Roswell Park Memorial Institute medium

RT ..... room temperature
RTK ..... receptor tyrosine kinase
RvD1 ..... resolvin D1
RvD2 ..... resolvin D2
RvD3 ..... resolvin D3
RvD5 ..... resolvin D5
RvE1 ..... resolvin E1
RvE2 ..... resolvin E2
RvE3 ..... resolvinE3
RvE4 ..... resolvin E4
SCH SCH772984
SDS ..... sodium dodecyl sulfate
sEH ..... soluble epoxide hydrolase
SH3 ..... c-Src homology 3
Sp1 ..... specificity protein 1
SPM ..... specialized pro-resolving lipid mediator
STORM ..... stochastic optical reconstruction microscopy
STRaND .... shuttling regulator of transcription
TAM ..... tumor-associated macrophage
TDTS ..... tissue-derived tumor spheres
TE ..... Trypsin-EDTA
TEMED ..... N,N,N',N'-tetramethylethylenediamine
TF ..... transcription factor
TGF-β ..... transforming growth factor beta
TIS ..... transcription initiation site
TME ..... tumor microenvironment
Tris ..... tris(hydroxymethyl)aminomethane
TSA ..... Trichostatin A
TSS ..... translation starting site
ULOQ ..... upper limit of quantification
UTP ..... uridine triphosphate
VDR ..... vitamin D receptor
VDRE ..... vitamin D response element
VEGF ..... vascular endothelial growth factor
WHO ..... World Health Organization
WM ..... wash medium
WST ..... water soluble tetrazolium
wt ..... wild-type

List of figures

List of tables

Abstract

This work aimed to investigate the regulation and activity of 5-lipoxygenase (5-LO), the central enzyme in leukotriene biosynthesis, in two colorectal cancer cell lines. The leukotriene pathway is positively correlated with the progression of several solid malignancies; however, factors regulating 5-LO expression and activity in tumors are poorly understood.

Cancer development, as well as cancer progression, are strongly dependent on the tumor microenvironment. In the conventional monolayer culture of cancer cell lines, cell-matrix and cell-cell interactions present in native tumors are absent. Furthermore, it is already known that various colon cancer cell lines dysregulate several important signaling pathways due to 3D growth. Therefore, the expression of the leukotriene cascade in HT-29 and HCT-116 colorectal cancer cells was investigated within a three-dimensional context using multicellular tumor spheroids to mimic a more physiological environment compared to conventional cell culture. Especially the expression of 5-LO, $cPLA_{2\alpha}$, and LTA_4 hydrolase was altered due to threedimensional (3D) cell growth, which was investigated by qPCR and Western blot analysis. High cellular density in monolayer cultures led to similar results. The observed 5-LO upregulation was found inversely correlated with cell proliferation, determined by cell cycle analysis, and activation of PI3K/mTORC-2- and MEK-1/ERK-dependent pathways, determined using pharmacological pathway inhibition, stable shRNA knockdown cell lines, and analysis via qPCR and Western blot analysis. Following, the transcription factor *E2F1* and its target gene *MYBL2* were identified to play a role in the repression of 5-LO during cell proliferation. For this purpose, several stable *MYBL2* over-expression and *ALOX5* reporter cell lines were prepared and analyzed. Since 5-LO was already identified as a direct p53 target gene, the influence of p53, which is variably expressed in the cell lines (HT-29, p53 R273H mut; HCT-116 p53 wt; HCT-116 p53 KO), was investigated as well. Furthermore, HCT-116 cells carrying a p53 knockout were investigated. The PI3K/mTORC-2- and MEK-1/ERK-dependent suppression of 5-LO was also found in tumor cells from other origins (Capan-2, Caco-2, MCF-7), which was determined using pharmacological pathway inhibition and following analysis via qPCR. This suggests that the identified mechanism might apply to other tumor entities as well.

5-LO activity was previously described as attenuated in HT-29 and HCT-116 cells compared to polymorphonuclear leukocytes, which express a highly active 5-LO. However, the present study showed that the enzyme activity is indeed low but inducible in HT-29 and HCT-116 cells. Of note, the general lipid mediator profile and the mediator concentrations were comparable to those of M2 macrophages. Finally, the analysis of substrate availability in HT-29 and HCT-116 cells revealed a vast difference between formed metabolite concentrations and supplemented fatty acid concentrations, indicating that the substrates are either transformed into lipoxygenase-independent metabolites or are esterified into the cellular membrane.

In summary, the data presented in this work demonstrate that 5-LO expression and activity are tightly regulated in HT-29 and HCT-116 cells and fine-tuned due to environmental conditions. The cells suppress 5-LO during proliferation but upregulate the expression and activity of the enzyme under cellular stress-triggering conditions. This implies a possible role of 5-LO in manipulating the tumor stroma to support a tumor-promoting microenvironment.

1 Introduction

1.1 Lipoxygenases

Lipoxygenases (LOs) are enzymes that introduce molecular oxygen into polyunsaturated fatty acids (PUFA) containing one (or more) (1Z,4Z)-pentadiene moieties to yield the respective (1S,2E,4Z)-hydroperoxide (Figure 1.1) (1–3). LOs have been identified in two of the three domains of life, namely bacteria and eukarya. In humans, six functional lipoxygenase isoforms are known, which are named according to the respective position of their oxygenation site within arachidonic acid [(5Z, 8Z, 11Z, 14Z)-eicosatetraenoic acid (ARA)]: 5-lipoxygenase (5-LO), platelet-type 12-lipoxygenase (12-LO), *R*-type 12-lipoxygenase (12R-LO), 15-lipoxygenase-1 (15-LO-1), 15-lipoxygenase-2 (15-LO-2), and epidermis-type lipoxygenase-3 (eLO-3). In contrast to the 5-LO gene (*ALOX5*) mapped on chromosome 10, the genes encoding the other lipoxygenases (*ALOX12*, *ALOX12B*, *ALOX15*, *ALOX15B*, and *ALOXE3*) are located in a joint gene cluster within chromosome 17. Nevertheless, *ALOX5* is not only unique due to its location: While all other *LOX* genes are similar in size (7-21 kb), *ALOX5* is much larger (71.9 kbp) (4).

All human LOs share a closely related two-domain protein structure: A small N-terminal β-barrel domain and a C-terminal mostly α-helical catalytic domain. The N-terminal domain has been implicated in Ca^{2+}-dependent membrane binding and activity regulation, while the C-terminal domain bears the catalytic center and the substrate-binding pocket. The size of the respective polypeptide chain ranges between 75-80 kDa (5). Within their catalytic centers LOs contain iron. Although the human LO enzymes share a highly conserved catalytic core, they strongly differ concerning the O_2 access and the U-shaped hydrophobic channel. This region hosts the PUFA substrate and determines by its invariant leucines, which (1Z,4Z)-pentadiene is aligned at the active site (6).

Depending on the type of human LO, the accepted substrates and the resulting products are divergent (7). Besides ARA, known substrates are linoleic acid (LA), docosahexaenoic acid (DHA), eicosapentaenoic acid (EPA), and endocannabinoids like *N*-arachidonoylethanolamine (AEA) and 2-arachidonoylglycerol (2AG) (see Figure 1.1 for structures of ARA, DHA, and EPA) (8). However, LO-metabolized products of those free fatty acids can also act as substrates. Free PUFAs are preferred over esterified PUFAs, but some enzymes also accept the esterified derivatives. Here, polyenoic fatty acids, as parts of phospholipids or cholesterol esters, serve as substrates (9, 10).

The proximity of the C-3 methylene group from the (1Z,4Z)-pentadiene and the central catalytic iron determines the oxygenation position. Depending on the substrate binding pocket and the orientation of the fatty acid substrate (carboxyl-end or ω-end first), different CH_2 groups are in position for hydrogen abstraction and the following oxygenation (7). Since LOs share closely related structures, their mechanism of introducing molecular oxygen to PUFAs is identical: Stereoselective hydrogen abstraction at C-3 of a (1Z,4Z)-pentadiene moiety, resulting in a radical, which migrates over the neighboring double bond and reacts with molecular oxygen at C-5 (in case of ARA and 5-LO), forming a peroxy radical (Figure 1.1) (11). Hydrogen abstraction and oxygen insertion proceed in an antarafacial relation, for example, on opposite sides of the

substrate. The hydrogen removal is proposed to be through a proton-coupled electron transfer mechanism (PCET), where the transfer of the electron and the proton proceed simultaneously (12). The radical is then converted into a peroxy anion and protonated to a hydroperoxide. The hydrogen abstraction is catalyzed by reducing the nonheme iron from Fe^{3+} (active, ferric form) to Fe^{2+} (inactive, ferrous form), while the peroxy anion formation is conversely catalyzed by oxidation of the nonheme iron from Fe^{2+} to Fe^{3+} (Figure 1.1). Therefore, the enzymes require oxidation to switch into their catalytically active form, which is accomplished by trace amounts of hydroperoxides. Nonenzymatic autoxidation can occur within a similar mechanism but without stereoselectivity (13).

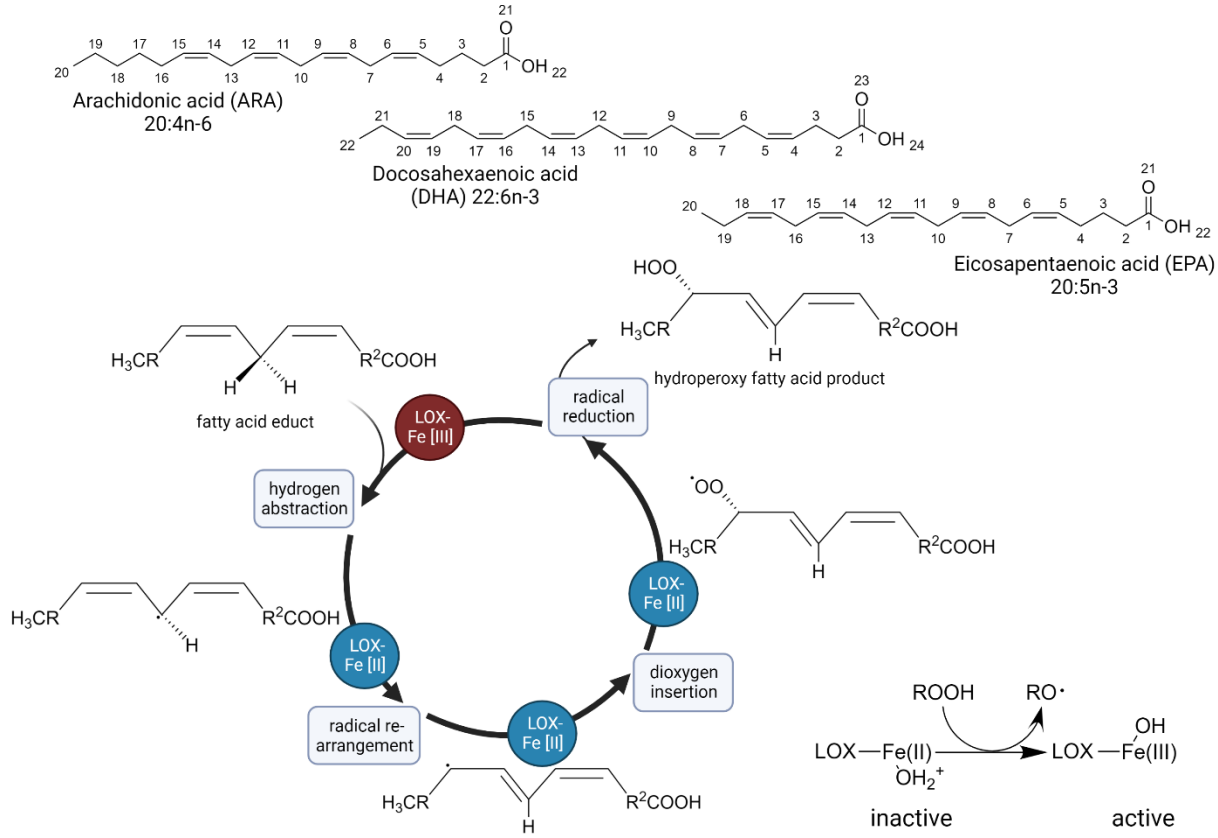

Figure 1.1: Examples for lipoxygenase substrates and scheme of the oxygenation mechanism. Adapted from (7) and (11).

Through their peroxidizing function, LOs contribute to the cellular redox status, but their activity simultaneously depends on the redox status. Due to this redox-regulating dependency, LOs have significant leverage on general physiological processes besides their canonical lipid-oxidizing and lipid mediator-producing function (5).

1.1.1 5-lipoxygenase

Like other LOs, 5-LO metabolizes ω-3 and ω-6 PUFAs into a broad range of eicosanoids. However, its preferred substrate is the ω-6 PUFA arachidonic acid. Leukotrienes (LTs), the main products of this reaction, are potent modulators of the immune system, and the enzyme itself is predominantly expressed in leukocytes. For this reason, 5-LO is considered part of the innate immune system. In the following sections the enzyme, its function, regulation, and its products will be described in more detail.

1.1.1.1 The *ALOX5* gene and its regulation

The human arachidonate *ALOX5* gene is located on chromosome 10q11.2 and consists of 14 exons separated by 13 introns. The regulatory five prime untranslated region (5'UTR) of the gene bears the *ALOX5* promoter with 10 GC-boxes, 8 of them within a GC-rich region. The promoter lacks TATA and CCA AAT boxes which generally, like multiple GC-boxes and a general GC-rich sequence, are a unique feature of housekeeping genes (14). Several transcription initiation sites (TIS) have been described, with the major TIS located at -65 relative to ATG (translation starting site (TSS)) (15). Investigations via reporter gene assay analysis of deletion mutants revealed three positive (-5900 to -3700 bp; -931 to -854 bp; -844 to -294 bp each relative to TSS) and two negative (-3400 to -1157 bp; -727 to -292 bp) regulatory regions within the *ALOX5* promoter (Figure 1.2) (15, 16).

The GC-rich region is mapped within the core promoter where several transcription factors were shown to bind. Five of the eight known GC-boxes are arranged in tandem (-176 to -147 bp, often referred to as GC0) and are recognized by the transcription factors Sp1 (specificity protein 1) and Egr-1 (early growth response protein 1) (17). The GC-rich region was also found to regulate the basal *ALOX5* promoter activity (18). Despite those GC-boxes, the core promoter harbors several other putative binding sites for additional transcription factors outside the GC-rich region: Binding sites for NF-κB (nuclear factor kappa light-chain-enhancer of activated B cells), AP-2 (activation protein 2), several PU.1 (SPI-1), NFAT (nuclear factor of activated T-cells), as well as a vitamin D response element (VDRE) and a SMAD binding element were identified (15, 16, 19). A Myb binding sequence was described downstream of the 10 GC-boxes (Figure 1.2) (15). Finally, quantitative proteomic analysis identified several other proteins that interact with the proximal *ALOX5* promoter in myeloid and B-lymphocytic cells. Among them the Krüpple-like factors (KLF) 13 and 16, several zinc finger proteins (e.g., the Myc-associated zinc finger protein MAZ), and the helicases BLM and DHX36 (20).

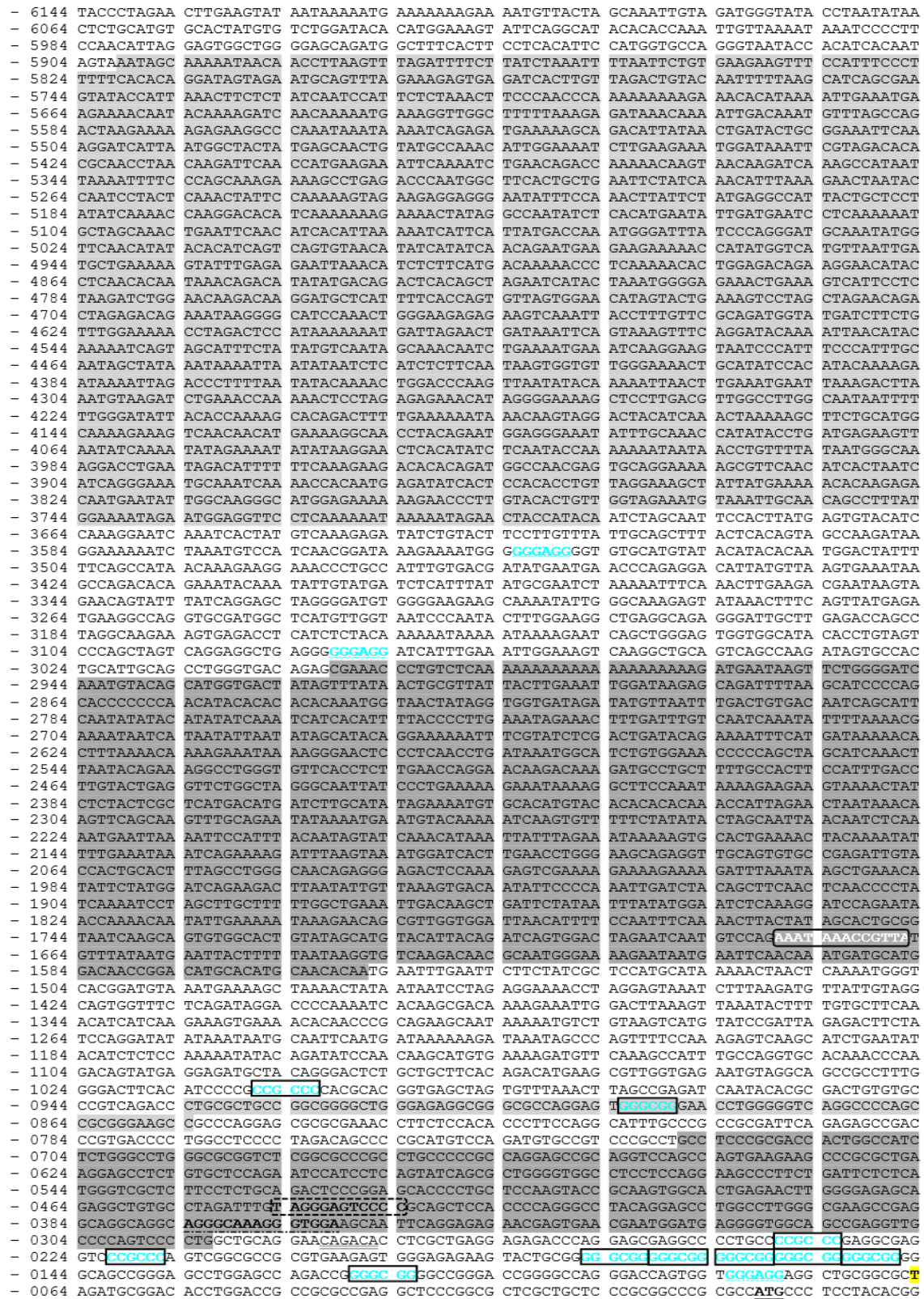

Figure 1.2: *ALOX5* promoter sequence overview.
Dark grey indicates negative regulatory regions, while light gray indicates positive regulatory regions. Yellow (T) marks the TIS. ATG marks the TSS. Angular boxes indicate classical GC-boxes (GGGCGG or CCGCCC). Turquoise indicates Sp1 binding sites (GGGCGG or GGGAGG). The rounded lined box indicates the MYB binding region (AAATAAACCGTTA). The DR3 type VDRE is marked with a dot-dash line (AGGGCAAAGGGTGGA). The NF-κB binding site is indicated by the rounded dash line box (TAGGGAGTCCCC).

Besides regulation via transcription factors, the 5-LO promoter was also found to be regulated by deoxyribonucleic acid (DNA) methylation and histone acetylation. Studies investigating 5-LO-positive and -negative cells of myeloid origin found that the 5-LO promoter was fully methylated in 5-LO-negative cell lines (U-937, HL-60TB). Cell lines that express 5-LO only after differentiation showed no 5-LO promoter methylation (21, 22). Furthermore, treatment of 5-LO-negative cells with the demethylating compound 5-Aza-2'-deoxycytidine led to 5-LO messenger ribonucleic acid (mRNA) expression in those cells (22). Therefore, DNA methylation was proposed to suppress *ALOX5* expression in cells of non-myeloid origin, e.g., adherent cancer cells (19). Further, it was shown that the pan-HDAC (histone deacetylase) inhibitor Trichostatin A (TSA) mediates 5-LO upregulation within the proximal *ALOX5* promoter in transfected HeLa and Mono Mac 6 (MM6) reporter cells (23). This effect was mediated through increased binding of Sp1 and Sp3 to GC-box 4 (GC-box upstream of the five tandem GC-boxes) (24). Furthermore, it was demonstrated in HeLa reporter cells that the histone-lysine *N*-methyltransferase 2A (MLL1) could induce *ALOX5* expression (25).

Naturally occurring mutations within the GC-rich region of the *ALOX5* promoter were shown to influence the gene expression by altering the number of Sp1 and Egr-1 binding sites. However, deletion and insertion of the identified mutations into reporter constructs and subsequent transfection of Hela cells led to a decreased reporter activity compared to the wild-type (wt) reporter construct. In contrast, it was shown that the mutated reporter constructs carrying the insertion increased the reporter activity compared to the wt reporter construct in Schneider cells (Drosophila SL2 cells) which do not express Sp1 or Egr-1. This discrepancy was explained by the possibility of unknown transcription factors interacting with this promoter region (26). Besides this, mutations were also found within the coding sequence (cds) in exons 1, 2, and 13 but led to no changes in the amino acid sequence (27).

In MM6 and HL-60 cells it was shown that myeloid cell differentiation by transforming growth factor beta (TGF-β) and calcitriol (1,25$(OH)_2$-vitamin D3) induces 5-LO expression (28, 29). The same treatment also activates SMAD3/4 in those cells, which are known to bind intron M of the *ALOX5* gene (30). Additionally, calcitriol activates the vitamin D receptor (VDR) that binds to the VDRE in the *ALOX5* gene, as described above. Besides the *ALOX5* promoter, VDREs are also found in exons 10, 12, and introns D and M. Regulation was especially shown for intron D (31). Therefore, *ALOX5* expression was also found to be regulated independently of the promoter by sequences within the gene's introns (Figure 3). The tumor suppressor p53 interacts with a p53RE in intron G of *ALOX5*. This interaction induced 5-LO expression in several p53 wt cell lines after genotoxic stress, while no change in expression was detected in p53 knockout and knockdown cells (32).

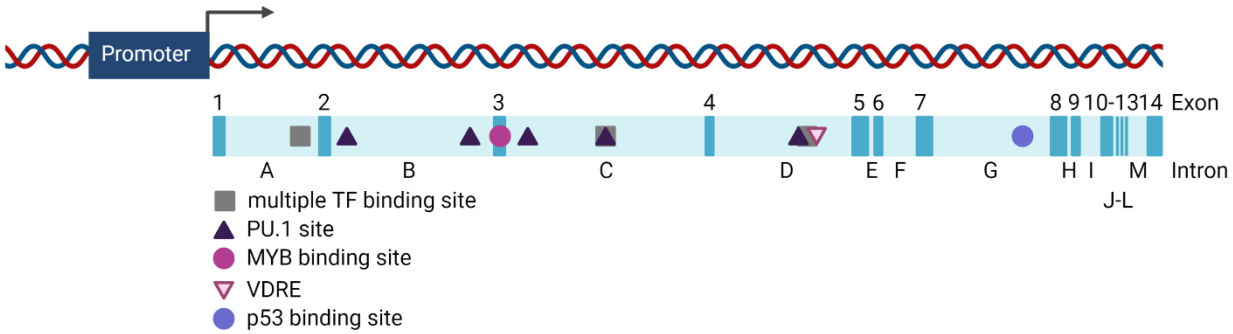

Figure 1.3: Schematic overview of the human *ALOX5* gene.
Figure adapted from (33).

Moreover, by analysis of ChIP-Seq data sets several master regulators (RUNX1, SMAD1, Wnt, C/EBPα, GATA2) of stem cell regeneration and differentiation were identified to bind to the *ALOX5* gene (introns C, D, and G) (33).

Besides the previously described actions, *ALOX5* expression can also be modified posttranscriptionally by alternative splicing. Several 5-LO mRNA isoforms have been identified that are not substrates to non-sense-mediated mRNA decay (34). Even though those isoforms show no canonical enzyme activity, it was shown that some (5-LOΔ13, 5-LOΔ4) could influence 5-LO wt activity (35, 36). While coexpression of wt 5-LO and 5-LOΔ13 in HEK293T cells reduced LT formation, coincubation of wt 5-LO with 5-LOΔ4 was found to have a stimulatory effect on LT formation. Interestingly, the cellular localization of expressed isoforms differs from the localization of wt 5-LO (37, 38).

1.1.1.2 5-LO enzyme expression

As already mentioned, 5-LO is mainly expressed in leukocytes which play a pivotal role in host defense. Specifically, 5-LO was found to be expressed in isolated human neutrophils, eosinophils, basophils, mast cells, B-lymphocytes, T-lymphocytes, dendritic cells, monocytes, and macrophages (33). The expression of 5-LO in B-lymphocytes was shown to depend on their differentiation and level of activation. 5-LO was shown to be highly expressed in the mantle zone area of lymph nodes, while 5-LO expression was not detectable in antibody-secreting plasma cells (39). Furthermore, activation of isolated human tonsillar B-lymphocytes induced 5-LO expression (40). While T-lymphocytes from human peripheral blood mononuclear cells (PBMCs) express 5-LO only when isolated freshly, 5-LO expression in macrophages depends on differentiation and polarization (41). 5-LO is strongly expressed in M1 macrophages, whereas 5-LO expression in M2 macrophages is relatively low (42). Freshly isolated $CD14^+$ (cluster of differentiation 14) monocytes express high levels of 5-LO, while immortalized human monocytic cell lines (THP-1, MM6) show a rather low 5-LO expression when not differentiated (20). However, cell differentiation using TGF-β and calcitriol as well as other differentiating agents strongly induce 5-LO expression over 100-fold (28). In contrast to freshly isolated T-lymphocytes, which loose 5-LO expression during cell cultivation, the MOLT-4 and Jurkat T-cell lines were shown to express high 5-LO amounts (43). In apoptotic Jurkat cells, 5-LO could be detected in lipid rafts (44). However, the findings for MOLT-4 and Jurkat cells are inconclusive since other studies showed

no *ALOX5* mRNA or protein expression in those cells (40, 45, 46). 5-LO is also expressed in several human immortalized B-cell lines like Rec-1, BL-41, JEKO-1, and Daudi cells (20, 45, 47).

Additionally to the status of cell differentiation, 5-LO expression was shown to correlate with cellular density, and cell proliferation led to a quick down-regulation of 5-LO expression (48).

In addition to healthy leukocytes and cancer cells from the monocytic lineage of hematopoietic origin, 5-LO is also expressed in various human malignant tissues and epithelial cancer cell lines (49). Expression of the enzyme was found in tumors of the gastrointestinal tract, the reproductive, and the central nervous system (50–53). However, these tissues do not express 5-LO under physiological conditions. The expression of 5-LO and its role in cancer will be discussed in detail in chapter 1.2.5.

1.1.1.3 Structure, cellular localization, and posttranslational modifications

As described in 1.1, LOs consist of a single polypeptide chain which, in the case of 5-LO, is 673 amino acids in length and approximately 78 kDa in size. 5-LO was found to form homo-dimers in aqueous solution, but dimerization is not required for leukotriene biosynthesis (54). Besides the typical two-domain LO structure, 5-LO bears some regulatory sites such as several nuclear import sequences (NIS), a nuclear export sequence (NES), an adenosine triphosphate (ATP) binding site (Trp75, Trp201), a calcium-binding site (Asn43, Asp44, Glu46), and a c-Src homology 3 (SH3)-binding motif which is assumed to be the primary interaction site of 5-LO with other proteins (55–58). However, until today only two direct interaction partners have been identified that interact with the N-terminal C-2-like domain of 5-LO: The coactosin-like protein (CLP) and the multidomain RNA helicase/RNase III Dicer (59). Besides binding of said proteins, this domain also binds phosphatidylcholine vesicles and diacylglycerol (60–62).

A crystal structure for wild-type human 5-LO is not available to date, but a model which is based on the crystal structure of stable-5-LO (63). Stable 5-LO lacks membrane insertion loops and harbors several stabilizing mutations. Comparison with the available crystal structures for rabbit 15-LO and black sea rod 8R-LO revealed that the secondary structure elements in the enzymes are conserved with the exception of helix α2 which is a short 3-turn helix in stable-5-LO, while it is a 6-7 turn helix in 15-LO and 8R-LO (64, 65). This unique position in stable-5-LO limits access to the catalytic iron and provides an encapsulated catalytic center, where the entry into the active site is not clearly evident. Therefore, site-directed mutagenesis studies were used to identify a possible substrate entry and the resulting new model supports active site access, which requires repositioning of Phe177 and Tyr181. While Phe177 appears to play a significant role in product specificity, Tyr181 serves as a gatekeeper to the active site (66). Recently, stable-5-LO was also crystallized in combination with the allosteric inhibitor AKBA (3-acetyl-11-keto-beta-boswellic acid) and the redox-type inhibitor NDGA (nordihydroguaiaretic acid), which provides a better understanding of inhibitor binding to 5-LO (67).

The intracellular localization of the soluble enzyme is strongly dependent on the cell type and state. In resting cells, 5-LO is predominantly located within the cytosol and the nuclear envelope (68). For example, in resting human polymorphonuclear leukocytes (PMNL, often referred to as neutrophils) analyzed by Western blot, 5-LO was mainly found in cytosolic fractions (69, 70). In contrast, resting alveolar macrophages and mast cells of human and murine origin have nuclear

5-LO (68). In resting and activated B-cells from patients with chronic lymphocytic leukemia, 5-LO was found predominantly within the nuclear fraction analyzed via Western blot (71). Furthermore, 5-LO was also found in the cytosol in HT-29 and HCT-116 colorectal cancer cells but within the nuclear envelope in U2-OS osteosarcoma cells (72). Cytosolic localization was also found in HEK 293T cells, stably transfected with wt 5-LO (37). After stimulation, the enzyme can translocate to the inner and outer sides of the nuclear membrane in several cells where its activity is increased. Translocation from the cytosol to the nuclear envelope is mediated via NIS of the enzyme (73, 74). In activated human PMNL, 5-LO and the 5-lipoxygenase activating protein (FLAP) were found in the nuclear envelope (75). Furthermore, two- and three-color STORM (stochastic optical reconstruction microscopy) analysis of activated murine neutrophils revealed co-localization of 5-LO and FLAP and co-localization of FLAP and $cPLA_{2\alpha}$ around the nuclear envelope (76).

The enzyme's localization was also shown to be dependent on posttranslational modifications, specifically on certain phosphorylation sites. Phosphorylation of 5-LO at Ser523 (mediated through protein kinase A (PKA)) in NIH-3T3 mouse fibroblast led to a permanent cytosolic location of the enzyme (77). This was caused by masking one of the NIS by phosphorylation at Ser523 (73, 78). This phosphorylation could be demonstrated in primary B-cells and B-cell lines but not in human PMNL (47). Furthermore, the phosphorylation site at Ser523 was validated via MALDI-MS analysis after *in vitro* phosphorylation (79). In contrast, phosphorylation of 5-LO at Ser271 (mediated through mitogen-activated protein kinase (MAPK), p38, and mitogen-activated protein kinase activated protein kinase 2 (MK2)) was described to be associated with nuclear localization of the enzyme (80). In addition, phosphorylation at Ser271 was reported to interfere with a nuclear export sequence of the enzyme. However, phosphorylation of 5-LO at Ser271 was described to inhibit nuclear export of the enzyme and, on the other hand, to induce nuclear export (80). This phosphorylation site at Ser271 could also be validated via MALDI-MS analysis and mutational studies (79, 81). Finally, a third phosphorylation site of 5-LO at Ser663 (mediated through extracellular signal-regulated kinase 2 (ERK-2)) was described *in vitro* (82). The influence on 5-LO localization by this phosphorylation is unknown. Furthermore, this phosphorylation could not be validated via MALDI-MS analysis and is therefore, the subject of controversial discussion (79).

1.1.1.4 Non-canonical functions

Besides 5-LO's canonical lipid transforming function, multiple studies implicated additional non-canonical functions of the enzyme. 5-LO was shown to be involved in the modulation of transcription, the translocation of β-Catenin and Runx2, p53 trafficking and transcriptional activity, and the modulation of micro ribonucleic acid (miRNA) processing.

Because 5-LO was found within the nuclear envelope and was shown to be associated with euchromatin in resting cells, the implication of 5-LO in transcription stands to reason (68). Knockout of 5-LO in mice was previously shown to have pleiotropic metabolic effects on adiposity and pancreatic function (83). Loss of 5-LO expression in leukemic cells reduced the activity of leukemic fusion proteins, which strongly activate canonical Wnt signaling. This was indicated to increase the self-renewal capacity of cancer stem cells (84). Furthermore, direct 5-LO and β-catenin interaction was shown, and 5-LO/β-Catenin interaction prevented β-Catenin from entering the nucleus (85). Additionally, a similar interaction could be demonstrated between 5-LO and

Runx2. There, the interaction promoted the nuclear localization of Runx2, which led to an increase of EGFR transcription in cardiomyocytes (86).

Finally, knockout of *ALOX5* in HT-29, HCT-116, U-2 OS, and MM6 cells significantly altered gene expression independent of the canonical 5-LO activity (72, 87). Since 5-LO is a highly mobile enzyme and bears NIS, 5-LO was suggested to act as a shuttling regulator of transcription (STRaND) and is not assumed to bind DNA directly (Figure 1.5). However, 5-LO was indicated to interact with histones and might stabilize histone acetylation and the nucleosome-free region. Therefore, it might promote the transcriptional activation or repression of transcription factors (TFs) (33, 87).

As discussed in 1.1.1.1, 5-LO expression is regulated by the tumor suppressor p53. 5-LO expression was induced by treatment with genotoxic compounds in various cancer cell lines, and p53 knockout completely abolished this effect (32, 88). Then again, 5-LO products were shown to influence the expression of pro-apoptotic p53 target genes (88). 5-LO and p53 were also shown to co-localize upon genotoxic stress, indicating a possible interaction. This interaction was shown by confocal microscopy and immunoprecipitation; therefore, 5-LO was suggested to be part of an autoregulatory negative feedback loop. This negative feedback loop might limit p53-dependent pro-apoptotic gene expression (32).

Dicer processes miRNAs, which posttranscriptionally regulate gene expression through translational repression or target transcript degradation. Therefore, their influence on cellular processes (e.g., cell proliferation, signal transduction, immune regulation) is of high impact. 5-LO was shown to interact with Dicer (see 1.1.1.3) and to modulate its activity *in vitro*. More specifically, the interaction of 5-LO with Dicer was shown to alter the miRNA processing activity of Dicer in a pre-miRNA-specific manner (89, 90). This provides a link between miRNA-mediated regulation of gene expression and inflammation.

1.1.2 12-, 15-lipoxygenase 1 & 2

Like the *ALOX5* promoter, *ALOX12*, *ALOX15*, and *ALOX15B* promoters lack TATA and CAAT boxes and show several regulatory TF binding sites (e.g., Sp1 and Sp3) (10, 91, 92). As discussed in 1.1.1, two different 12-LO enzymes are expressed in humans: Platelet type 12-LO (or 12-(*S*)-LO) and *R*-type 12-LO (12-(*R*)-LO). As the name indicates, the platelet type is primarily expressed in platelets and thus, in megakaryocytes, human islet cells, and keratinocytes (93). The enzyme comprises 663 amino acids with a molecular weight of 75 kDa (94). Furthermore, platelet type 12-LO was shown to form dimers like 5-LO (95). In contrast, the human *R*-type 12-LO is expressed in skin and hair follicles and comprises 694 amino acids with a molecular weight of approximately 80 kDa (96). The primary substrate of 12-LO is ARA yielding 12-HETE; however, 12-(*R*)-LO only shows a weak enzymatic activity toward ARA. A third 12-LO type is often discussed as “white blood cell type 12-LO” (93). This actually refers to 15-LO-1, a lipoxygenase with a 12/15-lipoxygenase activity encoded by *ALOX15*. 15-LO-1 is primarily expressed in M2 macrophages and eosinophils but is also found in various other cells (e.g., epithelial cells, smooth muscle, kidney) (97). The enzyme comprises 662 amino acids with a molecular weight of 75 kDa. Even though 15-LO-1 exhibits a 12/15-LO activity, its dual reaction specificity with ARA as substrate lies on the side of the 15-LO product (93%:7%). Utilizing the ω-3 PUFAs EPA and DHA, this ratio changes. With EPA and DHA as a substrate, the reaction specificity is still on the side

of the 15-LO product, however, to a lower percentage (EPA: 84%:16%, DHA: 60%:40%) (10). In contrast, 15-LO-2 exhibits a singular reaction specificity yielding the 15-LO products almost exclusively for all previously named PUFAs. Furthermore, 15-LO-2 is expressed in various human tissues and, in contrast to 15-LO-1, is constitutively expressed in human macrophages (98).

Furthermore, 12-LO, 15-LO-1, and 15-LO-2 are expressed in several cancer tissues and cell lines. However, compared to 5-LO, their role in cancer pathophysiology is even more elusive and researched to a lesser extent (98–100).

1.1.3 Formation of lipoxygenase-dependent oxylipins

Bioactive oxylipins are a vast class of important signaling molecules that modulate many molecular and cellular processes in tissue homeostasis and pathology. One important group of oxylipins are eicosanoids which function as mediators of inflammation, immune responses, pain, and many more physiological and pathophysiological processes. The term “eicosanoids” describes products of ARA or other C_{20} fatty acids, therefore not including eicosanoid-like products of longer fatty acids, e.g., DHA. The most prominent subgroups of eicosanoids are leukotrienes, prostaglandins, thromboxanes, epoxyeicosatrienoic acids, lipoxins, and resolvins. However, certain resolvins can also be formed from DHA. The lipid mediator class of specialized pro-resolving mediators (SPMs) includes lipoxins and resolvins formed from ARA, DHA, and EPA. The following sub-sections will discuss the process and regulation of predominantly 5-LO-dependent oxylipin formation.

1.1.3.1 The leukotriene cascade

5-LO is the central enzyme in leukotriene biosynthesis. As already described in 1.1.1.1 and 1.1.1.2, 5-LO expression is tightly regulated. However, 5-LO product formation is also strongly regulated, and proper 5-LO-dependent lipid mediator formation requires the interplay of several proteins and enzymes. In sequential reactions, ARA is released from the nuclear membrane by type A phospholipases and passed by FLAP to 5-LO. In a two-step dioxygenation, 5-LO initially forms the intermediate 5-hydroperoxyeicosatetraenoic acid (5-H(p)ETE) which is then subsequently metabolized into the unstable epoxide leukotriene A_4 (LTA_4). The intermediate 5-5-H(p)ETE can also be reduced to 5-HETE via glutathione peroxidases (GPx). Depending on the cellular components, LTA_4 can be converted to leukotriene B_4 (LTB_4) via leukotriene A_4 hydrolase (LTA_4H) or to cysteinyl LTs via cysteinyl leukotriene C_4 synthase (LTC_4S) (Figure 1.4) (13). However, those processes are not bound to occur inside one cell but can be shared between two cells due to transcellular metabolism (101–103). In fact, the transcellular metabolism of LTA_4 plays an important role in LT formation despite its unstable nature (104). Additionally, LTA_4 can be transformed to 6-*trans* LTB_4, 6-*trans*-12-*epi* LTB_4, 5(*S*),6(*S*)-DiHETE (dihydroxyeicosatetraenoic acid), or 5(*S*),6(*R*)-DiHETE via non enzymatic hydrolysis (69).

cPLA₂

The production of eicosanoids, in general, is highly dependent on substrate availability. In a physiological context, PUFAs are released by phospholipases which hydrolyze phospholipids from membranes (Figure 1.4). There, ARA, DHA, and EPA can be bound at the sn-2 position of phospholipids (105). These PUFAs can be released via hydrolysis of the ester bond at the sn-2

position by group A2 phospholipases (PLAs) (106). The three most important human PLA_2s include $cPLA_{2\alpha}$ (group IVA), a high molecular weight PLA_2 that is Ca^{2+}-dependent; $sPLA_2$ (group IIA), a secreted low molecular weight PLA_2 which is Ca^{2+} dependent as well; and $iPLA_2$ (group VIA), a Ca^{2+}-independent PLA_2 (107). They show unique substrate specificity on the sn-2 acyl chain towards ARA, EPA, and DHA. $cPLA_{2\alpha}$ was shown to be the most important enzyme for ARA release and, therefore, is a key component within the leukotriene cascade. The action of $cPLA_2$ depends on the enzyme's translocation, which is mediated by an increased intracellular Ca^{2+} concentration (108). Furthermore, $cPLA_2$ activity is known to be phosphorylation-dependent (109). Recently, it has been shown that $cPLA_2$ is not suited to process phosphatidylcholine (PC), phosphatidylglycerol (PG), or phosphatidylethanolamine (PE) 16:0-22:6 phospholipids but is capable of processing PE 16:0-20:5 phospholipids. Therefore, the release of DHA must be dependent on another PLA_2. However, $iPLA_2$ showed a preference for PE 16:0-20:5 compared to PE 16:0-22:4 and PE 16:0-20:5, indicating a preference of $iPLA_2$ for EPA compared to ARA and DHA. Finally, $sPLA_2$ prefers PC and PG 16:0-22:6 compared to PC and PG 16:0-20:4. Same results were found for PE 16:0-22:6, indicating a preference of $sPLA_2$ for DHA compared to ARA and EPA (110).

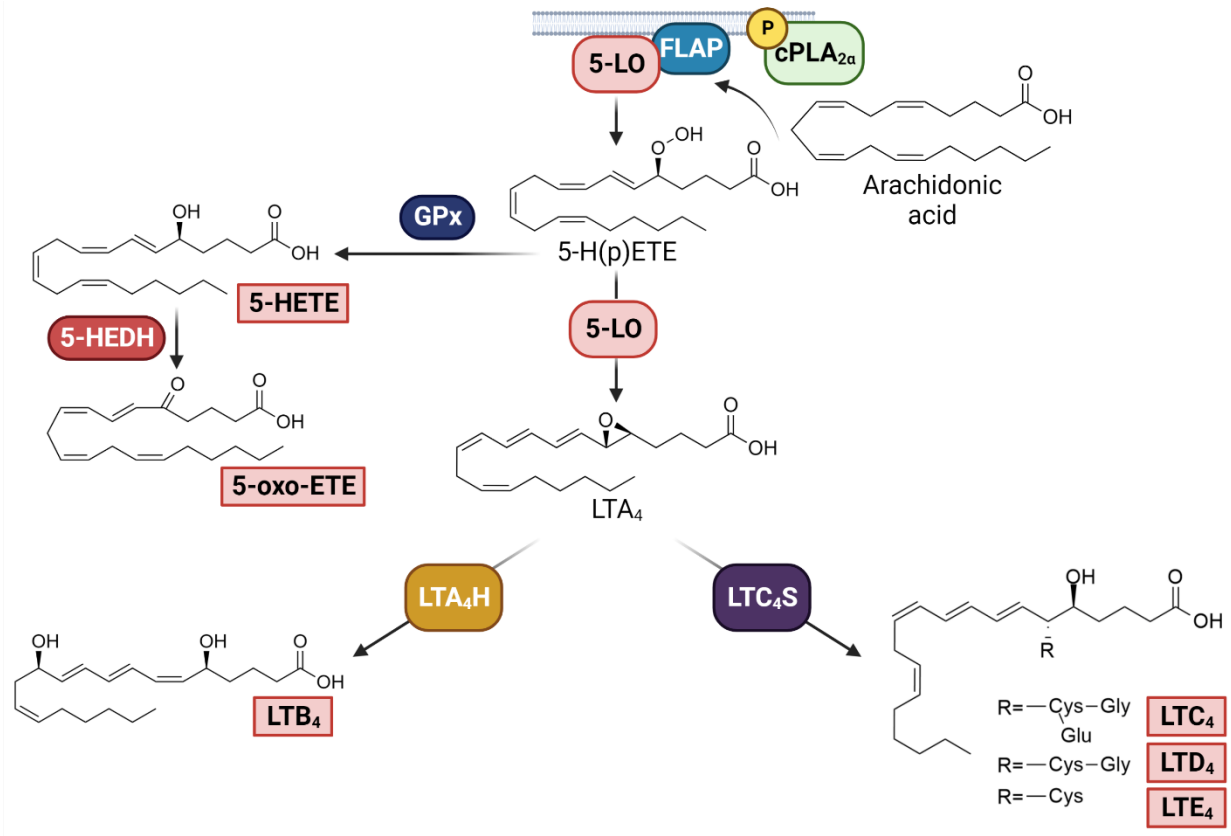

Figure 1.4: Schematic overview of the suggested biosynthetic pathway of arachidonic acid-derived leukotrienes. Scheme adapted from (69) and (13).

FLAP

The 5-lipoxygenase activating protein (FLAP) is another important member of the LT cascade. FLAP, which has no enzymatic activity, is an 18 kDa integral membrane protein, predominantly localized at the nuclear envelope and the endoplasmic reticulum (75, 111). It belongs to the membrane-associated proteins in the eicosanoid and glutathione metabolism (MAPEG) family. FLAP can form homotrimers within the nuclear membrane, but it was also found to be associated

with LTC_4S, another member of the MAPEG family (Figure 1.5) (112, 113). FLAP was shown to bind ARA, and in a FLAP/5-LO complex, it presents ARA to 5-LO (Figure 1.4) (114). In this context, Cys159, Cys300, Cys416, and Cys418 of 5-LO were identified to be essential for this interaction (115). 5-LO activity is rigorously depended on FLAP in intact cells. In cell-free assays and cellular homogenate preparations with the addition of an exogenous substrate, 5-LO is also active in absence of FLAP (116, 117). However, FLAP enhanced the reaction efficiency of 5-LO toward LTA_4 formation (118). Interestingly, it was indicated that the cellular localization of the FLAP/5-LO complex dictates 5-LO product formation. If the complex is located at the outer nuclear membrane, the formation of LTC_4 via LTC_4S is preferred. This is supported by a study that showed the localization of endogenous and overexpressed LTC_4S on the outer nuclear membrane (119). In contrast, if the complex is located at the inner nuclear membrane, the formation of LTB_4 via LTA_4H is favored (113). This is supported by a study showing the co-localization of LTA_4H and 5-LO in the nuclei of alveolar macrophages (120). Finally, it was shown that besides LT formation, FLAP is also crucial for the formation of lipoxins and resolvins (69, 121).

LTA_4H and LTC_4S

As already indicated, LTA_4H and LTC_4S are the main enzymes metabolizing LTA_4 to either LTB_4 or LTC_4. LTA_4H is a 69 kDa soluble metalloenzyme containing zinc within the catalytic domain. Besides its epoxide hydrolase function, which hydrolyzes LTA_4 to LTB_4, it also possesses an amino tripeptidase activity (122–124). This function was shown to cleave the chemoattractant matrikine Pro-Gly-Pro (PGP) (125). Therefore, LTA_4H can fulfill two opposing functions during an inflammatory response. Unlike 5-LO, LTA_4H is ubiquitously expressed at various levels (126). However, the enzyme is highly selective towards LTA_4 and undergoes suicide inactivation during catalysis (127, 128). In contrast, LTC_4S is a highly unstable 18 kDa glutathione S-transferase, which catalyzes the conjugation of LTA_4 with glutathione (GSH), yielding in LTC_4 (126). Like FLAP, LTC_4S forms homotrimers (129). Unlike LTA_4H, LTC_4S is not ubiquitously expressed but predominantly found in hematopoietic cells, which express 5-LO (130, 131). Like LTA_4H, LTC_4S was shown to be highly substrate-specific towards LTA_4. However, 5-oxo-ETE (5-oxo-eicosatetraenoic acid) (Figure 1.4) can be metabolized via LTC_4S to form the GHS adduct 5-oxo-7-glutathionyl-8,11,14-eicosatrienoic acid (132). Recently, it was shown that LTC_4S activity is regulated by phosphorylation via ribosomal protein S6 kinase (p70S6K) (133, 134).

1.1.3.2 Regulation of 5-LO activity

As described in 1.1.1.3, 5-LO bears various binding and interaction sites and is a highly mobile enzyme. Therefore, its enzymatic activity is regulated and influenced by members of the LT cascade and various other allosteric regulators or enzyme scaffolds. The following subchapter will, therefore, focus on the regulation of 5-LO activity. Figure 1.5 summarizes the translocation, activation, and regulation of 5-LO and the leukotriene biosynthetic complex.

Calcium

In contrast to other LOs, Ca^{2+} is one of the essential factors for 5-LO. Within the cellular context, 5-LO is activated by Ca^{2+} resulting in a rise of the enzymes V_{max}, shortening of the enzyme's lag phase, and increased 5-LO product formation (135). As indicated in 1.1.1.3, Ca^{2+} binds within the C2-like domain of 5-LO (2 mol Ca^{2+} per mol 5-LO) and increases its hydrophobicity (136). The reversible binding of Ca^{2+} enhances the 5-LO membrane interaction, leading to an increase in product formation (Figure 1.5). However, this could only be observed in the presence of scaffold proteins or factors like membrane components, e.g., PC (62). It was further shown that Ca^{2+} could be substituted with Mg^{2+} but higher ion concentrations were necessary to mediate the same effect (137). Despite the described dependency of 5-LO on Ca^{2+}, the enzyme shows basal activity in absence of Ca^{2+} (138). High concentrations of ARA (>20 µM) with or without PC also activate 5-LO and increase product formation. Ca^{2+} was also shown to induce 5-LO translocation towards the nuclear membrane (139). Furthermore, agents mobilizing intracellular Ca^{2+} such as calcium ionophore (A23187), N-formylmethionine-leucyl-phenylalanine (fMLP), LTB_4, or cytokines can induce this translocation and stimulate 5-LO product formation (140–143).

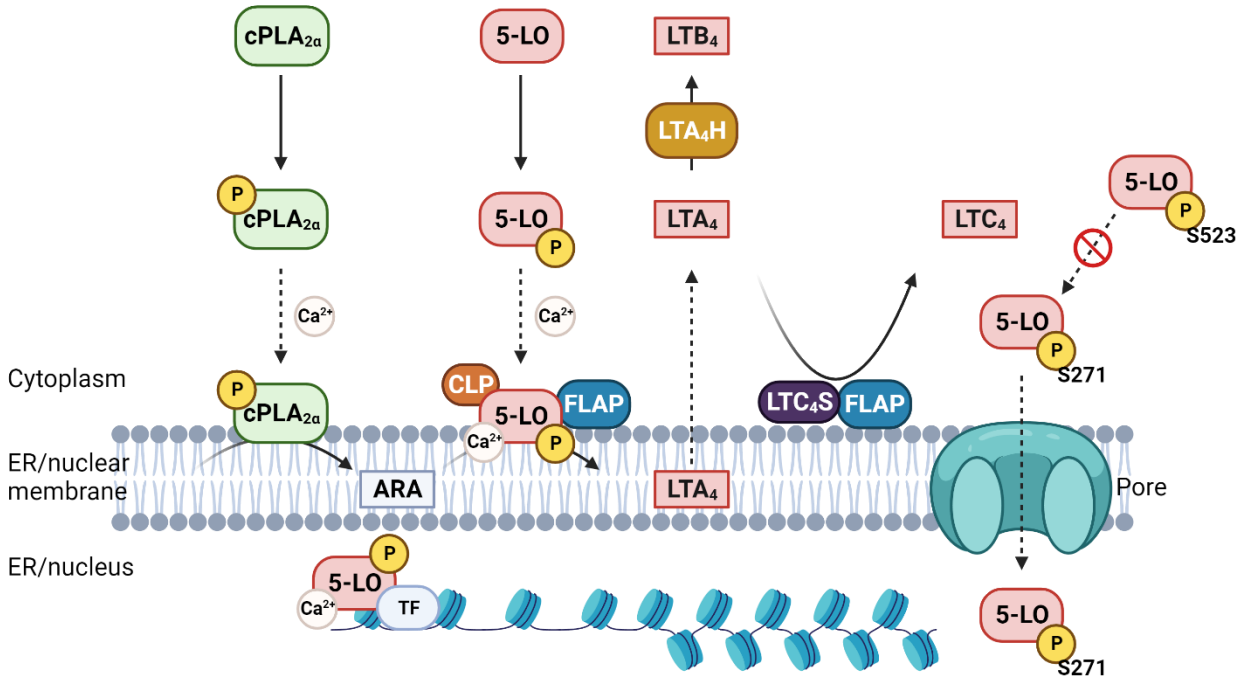

Figure 1.5: Schematic overview of 5-LO regulation, translocation, and assembly of the leukotriene biosynthetic complex.
Scheme adapted from (19) and (126).

ATP

Another regulating factor of 5-LO activity is ATP. It enhances 5-LO activity in the presence and absence of Ca^{2+} (144, 145). However, ATP is not involved in the enzymatic reaction and is not hydrolyzed during 5-LO's catalytic cycle (146). Nevertheless, it was shown that ATP is directly bound to 5-LO (1 mol ATP per mol 5-LO) and, therefore, allosterically activates 5-LO (147). Besides ATP, adenosine diphosphate (ADP), adenosine monophosphate (AMP), and uridine triphosphate (UTP) were shown to stimulate 5-LO activity as well; however, to a lesser extent than ATP (58).

Phosphorylation and localization

Both phosphorylation and localization affect the 5-LO's activity and product formation. As described in 1.1.1.3, 5-LO can change its localization depending on the phosphorylation status. Summarized, the association of 5-LO with a membrane after activation generally increases 5-LO product formation. Therefore, PKA-mediated phosphorylation at Ser523, which mediates a permanent cytosolic localization of 5-LO, and MAPK/MK2-mediated phosphorylation at Ser271, which mediates nuclear localization of 5-LO inhibit the enzyme's activity (77). However, phosphorylation at Ser271 only impairs 5-LO activity if the enzyme is not challenged with calcium ionophore (81). Even though the phosphorylation of Ser663 could not be confirmed by MALDI-MS analysis (1.1.1.3), mutation of stable-LOX at Ser663 to Asp, which mimics phosphorylation at amino acid 663, was shown to shift 5-LOs activity towards a 15-LO activity. Incubation of stable-LOX and stable-Asp663-LOX yielded in LxA_4 formation. Therefore, phosphorylation was indicated to play a role in regulating inflammation (148). However, those results were questioned within a study using wt 5-LO orthologs of different vertebrates (human, mouse, zebrafish). The study showed that the Ser- to Asp exchange at position 663 hardly impacts the 5-LO reaction specificity, wherefore 15-H(p)ETE was only detectable in trace amounts (149). Therefore, the previously indicated role of the phosphorylation at Ser663 in regulating inflammation within the physiological context is questionable.

Protein-protein interaction partners

Besides FLAP, 5-LO was shown to interact with the human filamentous actin-binding coactosin-like protein and the multidomain RNA helicase/RNase III Dicer (150).

The binding of 5-LO and CLP (1 mol CLP per mol 5-LO) was found to influence 5-LO activity. CLP was shown to bind F-actin and colocalize with actin stress fibers (151). Both 5-LO and CLP translocate toward the nuclear envelope after stimulation (152, 153). Therefore, it was hypothesized that 5-LO translocation might be realized through binding with CLP and transportation along F-actin. However, binding sites of CLP with F-actin and 5-LO were found close, indicating possible overlapping binding sites (154). Until now, a F-actin-CLP-5-LO complex has not been verified. Nevertheless, inhibition of 5-LO using hyperforin was shown to interrupt CLP-5-LO binding *in vitro,* which compromised 5-LO translocation in human PMNL (155). CLP-5-LO interaction increased 5-LO activity in the absence and presence of PC but only in the presence of Ca^{2+}. In particular, CLP binding to 5-LO promotes the formation of LTA_4 (152, 153). Albeit, the binding of CLP and 5-LO was shown to be independent of Ca^{2+} but might stabilize 5-LO by preventing turn-over inactivation (156).

The interaction of Dicer with 5-LO was found to support Ca^{2+}-mediated 5-LO activity, but not to the same extent as PC and CLP (90).

Intracellular redox tone

The most crucial factor for 5-LO activity is the redox state of its central catalytic iron. For enzymatic activity the active ferric state is required which is regulated by the intracellular redox tone of the cell (Figure 1.1 and Figure 1.5). The redox tone depends on lipid hydroperoxide levels and glutathione peroxidase activity. Lipid hydroperoxides (e.g., 5-, 12- and 15-H(p)ETE or 13-H(p)ODE (hydroperoxyoctadecadienoic acid)) promote 5-LO activity by shortening the enzyme's lag phase (157–159). However, high hydroperoxide levels inhibit the enzyme by irreversible turnover-dependent inactivation (160). Inorganic hydroperoxides were not capable of activating 5-LO in homogenates of PMNL but activated 5-LO in B-cells (158, 161).

Reducing conditions (e.g., dithiothreitol (DTT), high thiol concentrations) and glutathione peroxidases (GPx) suppress 5-LO activity (159, 162). GPxs reduce lipid hydroperoxides and, therefore, 5-LO activity. However, Ca^{2+} was shown to counteract GPx-mediated inactivation of 5-LO (117). Due to the binding of Ca^{2+} with the C2-like domain of 5-LO, lower hydroperoxide concentrations are sufficient to activate 5-LO activity (163). A similar effect was shown for 1-oleoyl-2-acetyl-sn-glycerol (OAG) (61).

Cellular membranes, phospholipids, and diacylglycerides

As already indicated by discussing the influence of Ca^{2+} on 5-LO, 5-LO associates with membranes via its C2-like domain. Interaction of purified 5-LO with membrane fractions was shown, which could be substituted with synthetic PC vesicles but not with PE, phosphatidylinositol (PPI), phosphatidylserine (PS), or DAG vesicles (164). Here, amino acids Trp13, Trp75, and Trp102 of 5-LO interact with PC. However, priming of PMNL with OAG and stimulation with fMLP induced 5-LO-dependent product formation. In contrast, EAG did not influence 5-LO product formation under the same conditions, with or without exogenous ARA (165). Furthermore, inhibition of DAG formation potently inhibited 5-LO product formation in PMNL, even after stimulation with calcium ionophore. This indicated a DAG formation-dependent 5-LO activation (166).

1.1.3.3 Formation of other oxylipins derived from 5-, 12-, and 15-lipoxygenases

Despite the classical 5-LO leukotriene formation route, 5-LO is also involved in the biosynthesis of other oxylipins. There, 5-LO metabolizes lipoxygenase products from 12- and 15-LO or vice versa. Like 5-LO, 12- and 15-LO insert molecular oxygen into ARA, DHA, and EPA according to the respective position of their oxygenation site within arachidonic acid (see 1.1).

Therefore, ARA turnover by 12- and 15-LO leads to 12- and 15-HETE or, more specifically, their hydroperoxide intermediates. 15-HETE can be metabolized by 5-LO, and 5-HETE can be metabolized by 15-LO, both yielding in 5(*S*),15(*S*)-DiHETE. This dihydroxylated fatty acid derivative can then be further metabolized to trihydroxylated fatty acids like lipoxin A_4 (LxA_4), 15(*R*)-LxA_4, and 6(*S*)-LxA_4. The same metabolites can be formed by metabolization of LTA_4 via 12-LO (167). Nevertheless, not all described routes are equally efficient (168). Furthermore, 15-HETE can be metabolized to 5(*S*),14(*R*),15(*S*)-triHETE (LxB_4); however, this requires several steps, including a second oxygenation step by 5-LO followed by hydrolysis of the formed 15(*S*)-hydroxy-5(6)-epoxy-ETE, presumably through epoxide hydrolases (169).

Besides the indicated routes displayed in Figure 1.6, ARA can be metabolized by cytochrome P450 (CYP450) and acetylated cyclooxygenase 2 (COX-2), yielding 15(*R*)-HETE, which was

further described to be metabolized via 5-LO yielding in the trihydroxilated fatty acids 15-epi-LxA$_4$ and 15-epi-LxB$_4$ (170). COX-2 can be acetylated at Ser530 by acetylsalicylic acid and, due to the acetylation, can only produce 15-(*R*) prostaglandins (171). Nitrosylation of COX-2 by statins was described to show the same effect (172).

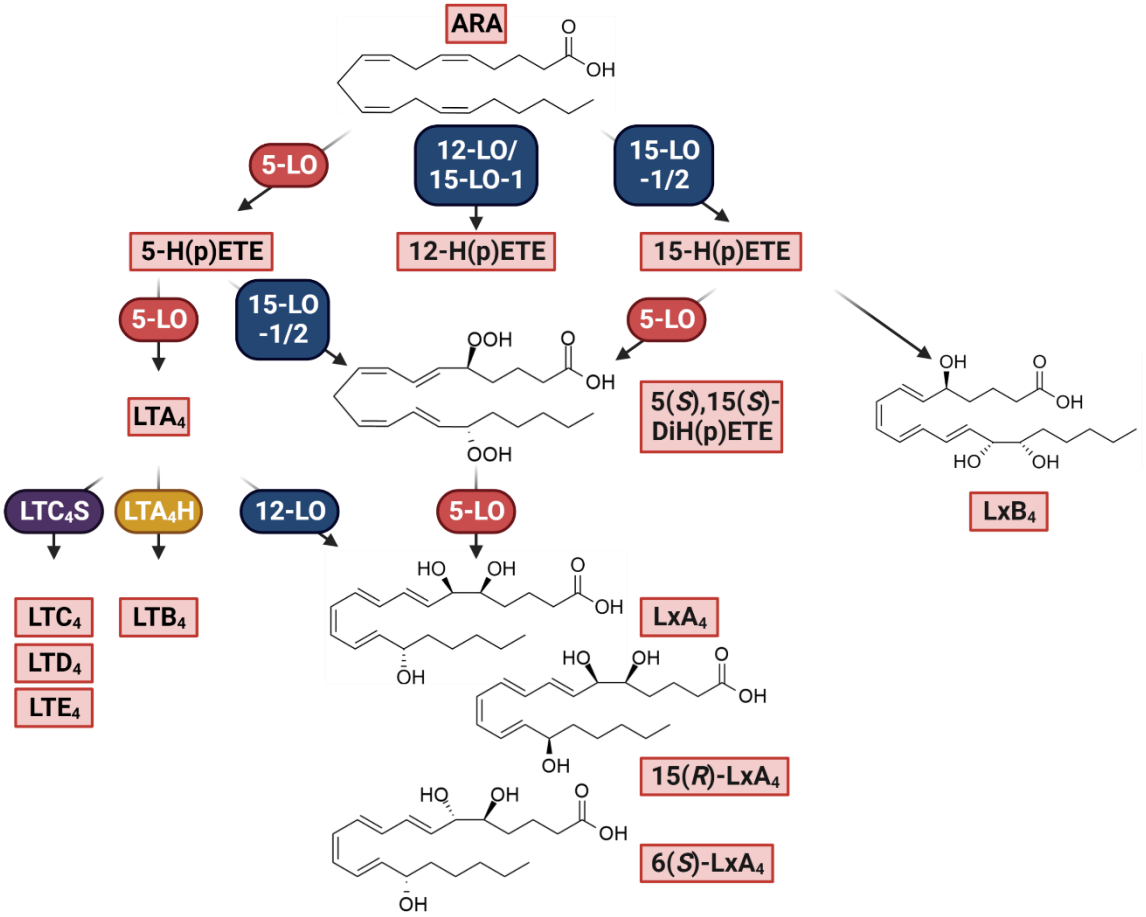

Figure 1.6: Schematic formation paths for ARA-derived LTs and SPMs.
Annotated enzymes are indicative. Some oxylipins can also be formed by other paths and via autoxidation. Note: Not all depicted paths are efficient. Figure adapted from (69) and (168).

As indicated, all described LOs were shown to turn over the ω-3 fatty acid DHA as well, yielding in the respective D-series resolvins. 5-LO metabolizes DHA to the hydroperoxide intermediates of 4-HDHA and 7-HDHA, while 15-LO-1 forms the hydroperoxide intermediates of 17-HDHA and 14-HDHA. These monohydroxylated derivatives are further metabolized to the dihydroxylated derivatives 4(*S*),17(*S*)H(p)DHA (by 15-LO via 4-H(p)DHA)) or 7(*S*),17(*S*)H(p)DHA (by 15-LO or 5-LO via 7-H(p)DHA or 17-H(p)DHA)). 14-H(p)DHA can be converted to 13,14-epoxy-maresin which can be further metabolized to the dihydroxylated maresin-1 (MaR1) (173). Resolvin D5 is formed by the conversion of 7(*S*),17(*S*)-H(p)DHA. However, 7(*S*),17(*S*)-H(p)DHA can also be converted to the trihydroxylated derivatives resolvin D1 (RvD1) or resolvin D2 (RvD2). Resolvin D3 (RvD3) is formed from 4(*S*),17(*S*)-H(p)HDHA (174, 175).

Besides the indicated formation routes in Figure 1.7, DHA can also be metabolized via acetylated COX-2 (176). The resulting *R*-stereoisomers are often referred to as aspirin-triggered resolvins. Maresin-2 (MaR2) can be formed via the soluble epoxide hydrolase (sEH), and protectin D1 (PD1, or neuroprotectin 1 (NPD1)) is formed by dual oxygenation of DHA via 15-LO (177, 178).

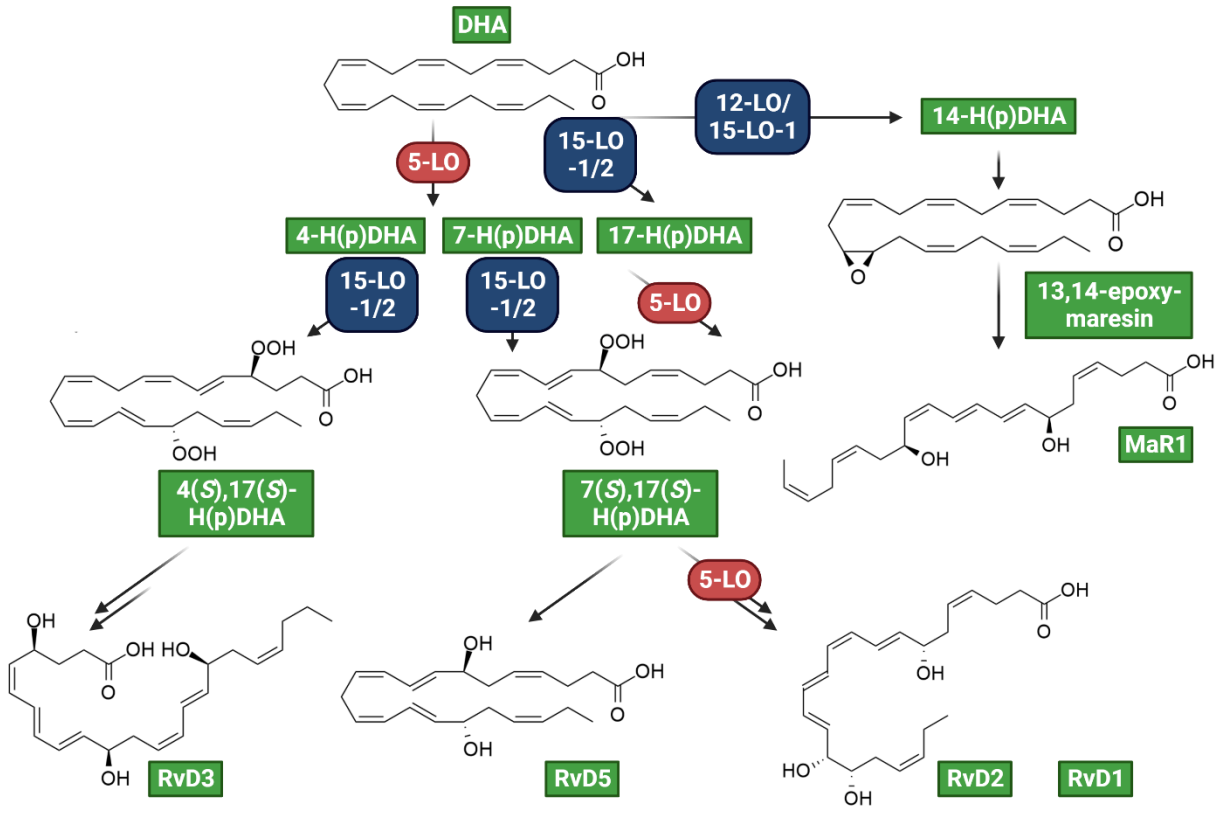

Figure 1.7: Schematic formation paths for DHA-derived oxylipins.
Annotated enzymes are indicative. Some oxylipins can also be formed by other paths and via autoxidation. Note: Not all depicted paths are efficient. Figure adapted from (69) and (168).

The turnover of the ω-3 fatty acid EPA by LOs yields 5-series leukotrienes, lipoxins, and E-series resolvins. Analog to 5-H(p)ETE, EPA can be transformed to 5-H(p)EPE via 5-LO, which can be metabolized to LTA_5 and LTB_5 in the following. Analogously to ARA-derived lipoxins, the intermediate LTA_5 can be transformed via 12/15-LO to lipoxins LxB_5, LxA_5, and 6(S)-LxA_5 (179). Besides 5-LO, 5-H(p)EPE can be metabolized via 15-LO-2, yielding the dihydroxylated derivative 5(*S*),15(*S*)DiH(p)EPE, which can be further transformed to resolvin E4 (RvE4) (180). Turnover of 5-H(p)EPE via acetylated COX-2 or CYP450 leads to 5(*S*),18(*R*)-DiH(p)EPE, which can be further transformed to resolvin E1 and E2 (RvE1, RvE2) (181). Those derivatives can also be formed by oxygenation of 18-(*R*)H(p)EPE yielding in 5(*S*),18(*R*)-DiH(p)EPE as well. Turnover of 18-(*R*)H(p)EPE by 15-LO yields in resolvin E3 (RvE3) (182). However, the origin of 18(*R*)-HEPE in biological systems is not finally determined (183).

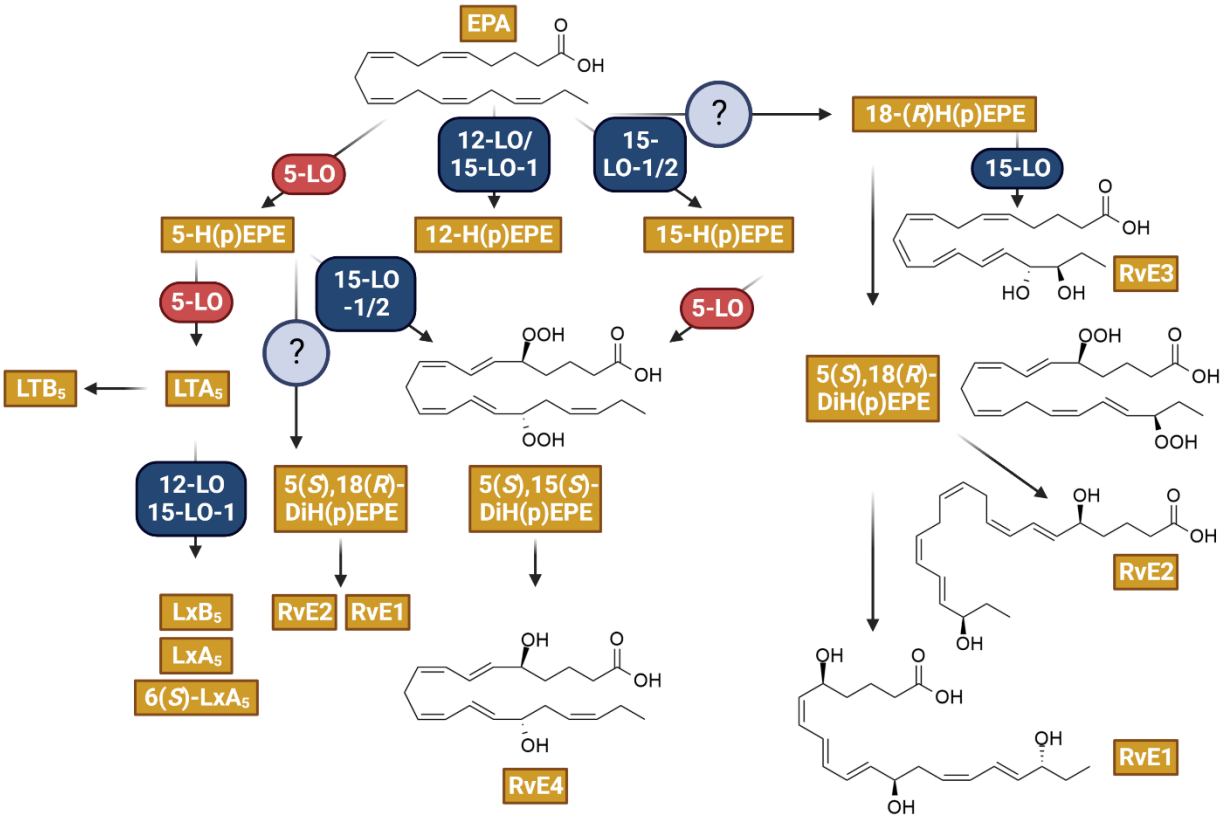

Figure 1.8: Schematic formation paths for EPA-derived LTs and SPMs.
Annotated enzymes are indicative. Some oxylipins can also be formed by other paths and via autoxidation. Note: Not all depicted paths are efficient. Figure adapted from (69) and (168).

All previously described derivatives are (if at all) predominantly detected in leukocytes, where the necessary enzymes are expressed in sufficient amounts. Besides 5-, 12-, 15-LO-1, and 15-LO-2, FLAP was shown to be crucial for the formation of SPMs (69, 121). Furthermore, transcellular metabolism, including different cell types, was shown to produce SPMs in cellular models (184). Although various cells express the necessary enzymes, the formation of dihydroxylated and especially trihydroxilated derivates is generally very low compared to the simultaneously formed monohydroxylated pro-inflammatory lipid mediators, even under non-physiological conditions (42, 69, 185).

Of note, many mono- and dihydroxylated precursors can be formed via autoxidation, and several formation routes were found to be inefficient, especially the ones where 5-LO employs precursors formed by other LOs (168, 186). In addition, the analysis of SPMs conducted via LC-MS/MS analysis is very complex due to their low endogenous concentrations, structural analogy, and sensitivity to oxidation (172).

1.1.4 Physiological and pathophysiological role of 5-LO-dependent oxylipins

A vast number of reports indicate the role of 5-LO-dependent fatty acid derivatives in a plethora of diseases and pathophysiological processes. However, LTs play a first and foremost role in the regulation of immune responses and tissue homeostasis. Therefore, they are often referred to as pro-inflammatory lipid mediators. SPMs were established as anti-inflammatory but were later termed pro-resolving since they were shown to stimulate and activate endogenous pathways that terminated inflammation (187). They mediate their actions through G-protein-coupled receptors (BLT1/2, CysLT1/2, ERV1, ALX, DRV1, DRV2, GPR37, and LGR6) placed within the cellular membrane of target cells. Leukotriene receptors (BLT1/2, CysLT1/2) and their ligand binding are generally better researched; therefore, their functions are less questioned (168, 188, 189). The following part will describe individual 5-LO-dependent mediators and receptors and their physiological and pathophysiological roles.

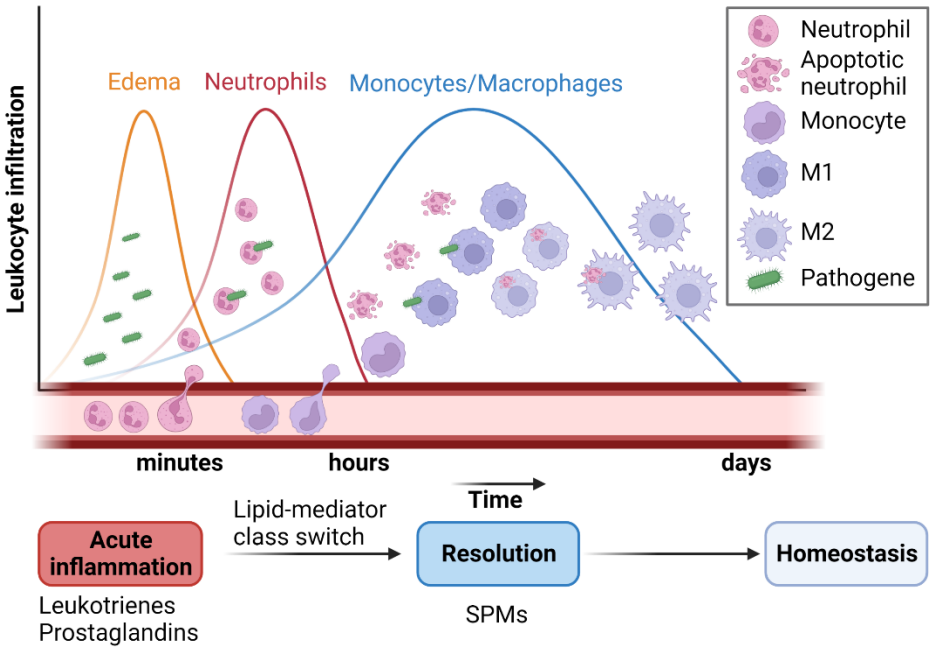

Figure 1.9: Schematic time course of the inflammatory response and resolution.
Figure adapted from (190) and (191).

1.1.4.1 Leukotrienes

As described, LTs are pro-inflammatory lipid mediators. They mediate pro-inflammatory actions, including the chemoattraction of leukocytes, inducing smooth muscle contractions, and increasing vascular permeability. Thereby, attracted PMNL can extravasate from the surrounding blood vessels invading the infected tissue (192) and oppose pathogens in the early inflammation phase through superoxide liberation and lysosomal enzyme release (193, 194). However, LTB_4 is also produced and released by PMNL, increasing their phagocytotic activity and the formation of reactive oxygen species (ROS) (195). LTB_4 also attracts monocytes, differentiating into macrophages within the invaded tissue (196). There, they are polarized to pro-inflammatory M1 macrophages, which switch to resolution phase M2 macrophages in response to local mediators and efferocytosis (see Figure 1.9 for time course) (191). Furthermore, LTB_4 also contributes to

the adaptive immune response by mediating the liberation of the immunoglobulins M, G, and E from B-lymphocytes (197, 198).

LTB_4 target cells, which express the respective receptor, are (besides leukocytes and lymphocytes) bronchial and vascular smooth muscle cells, endothelial cells, and peripheral sensory neurons (199). The effects of LTB_4 are predominantly mediated through BLT1, which bears a 20-fold higher affinity towards LTB_4 compared with the BLT2 receptor (200). BLT2 is ubiquitously expressed in various tissues and shows a high affinity for 12(*S*)-hydroxyheptadecatrienoic acid (12-HHT), a byproduct of thromboxane synthesis, but it also interacts with 12- and 15-HETE (201–203). The exact physiological role of BLT2 is still elusive. However, BLT2 was implicated in playing a role in wound healing and protecting or providing anti-inflammatory actions in dextran sodium sulfate (DSS)-induced colitis and allergic reactions (204–206). Furthermore, BLT1 and BLT2 were found to form an antagonistic sensitizing system in peripheral sensory neurons. There, activation of BLT2 caused desensitization of TRPV1-mediated calcium influx, indicating a possible role of BLT2 in the regulation of nociception (207). Besides the BLT receptors, LTB_4 also interacts with the peroxisome proliferator-activated receptor α (PPARα), which regulates the biosynthesis of enzymes involved in the metabolism of PUFAs (208, 209). Therefore, the interaction of PPARα with LTB_4 controls the duration of the inflammatory response by reducing the formation of LTB_4 (208).

In contrast, the LTB_4-BLT1 axis is also linked with many chronic diseases, predominantly inflammatory disorders with dysregulated immune responses, including autoimmune diseases, allergic conditions, and local as well as systemic inflammatory diseases (199). Therefore, the list of diseases with a possible association to the LTB_4-BLT1 axis is long: Asthma, allergic rhinitis, fibrotic diseases, pulmonary syndromes, arthritis, psoriasis, inflammatory bowel disease, rheumatoid arthritis, and cardiovascular diseases like atherosclerosis (to name a few). Only for some of the indicated diseases and conditions an association with the LTB_4-BLT1 axis has been established in small-scale or nonrandomized, placebo-controlled trials (210). Of note, the approval of Zileuton (5-LO inhibitor) by the American Food and Drug Administration (FDA) (for the treatment of asthma) highlights the critical role of LTs in asthma and allergic rhinitis; however, the role of LTs in other diseases still needs further investigation employing larger, randomized, double-blind, placebo-controlled clinical trials (199). Unfortunately, the use of Zileuton is limited due to hepatotoxic effects (211). In addition to the diseases mentioned above, LTs were also connected to hallmark events of cancer, which will be discussed in 1.2.5.

In contrast to LTB_4, cysteinyl leukotrienes mediate their actions predominantly in the respiratory system. There, they mediate strong bronchoconstriction, increase vascular permeability, and prompt mucus secretion (212). Like LTB_4, CysLTs attract leukocytes and exert their effects through GPCRs on the cell surface. CysLT1 is predominantly expressed in airway smooth muscle cells, vascular endothelial cells, and leukocytes (213). Therefore, CysLT1 mainly mediates the physiological functions of LTC_4. CysLT2, on the other hand, is similar to BLT2 more evenly distributed across tissues. CysLT2 expression can be found beside leukocytes in cardiovascular, cerebral, and nervous tissues (212). CysLTs are predominantly known for their effects on the progression of asthma; however, they were also implicated in cardiovascular diseases (atherosclerosis, vascular inflammation) and CNS diseases (multiple sclerosis, Alzheimer's disease, Parkinson's disease, Huntington's disease). There are three approved CysLT1 receptor antagonists for the treatment of asthma: Zafirlukast, Montelukast, and Pranlukast (214). However,

the FDA recently (2020) required a boxed warning and a revision for the indication of Montelukast (the most prescribed CysLT1 antagonist for asthmatic patients) for allergic rhinitis due to the risk of neuropsychiatric events (215, 216).

1.1.4.2 Specialized pro-resolving lipid mediators

The resolution phase of inflammation is already initiated with the peak of PMNL infiltration (Figure 1.9). Inflammation is considered a self-limiting, protective process to prevent unnecessary tissue damage and a chronic course of inflammation (217). Resolution of inflammation was considered a passive process for a long time, where pro-inflammatory cytokines and lipid mediators simply diffuse or dilute over time (218). With the identification and analysis of a new class of lipid mediators, SPMs, this passive-thought process was shown to be actively controlled and very complex. SPMs are, as described in 1.1.3, formed through the sequential oxygenation of different LOs. As only a few cells express several LOs, this process includes transcellular metabolism between different cell types.

The release of SPMs positively modulates the resolution and termination of inflammation by, e.g., reducing the number of infiltrated PMNL on the active inflammation site (219). They are known to promote resolution by counteracting the formation of prostaglandins and leukotrienes through the regulation of COX-2 expression and interaction with the BLT1 receptor (220–222). However, RvD1 was shown to upregulate COX-2 expression (223). Furthermore, lipoxins were shown to induce the secretion of anti-inflammatory cytokines like IL-10, which promotes efferocytosis by macrophages (224). Moreover, SPMs were recently proposed as anticancer molecules suitable for controlling cancer-associated inflammation (225). However, evidence gained through animal and human studies is rare or lacking (226).

Like LTs and CysLTs, SPMs mediate their resolution-promoting properties through GPCRs (188). However, some of the respective identified ligands for the receptors ERV1, ALX, DRV1, DRV2, GPR37, and LGR6 are discussed with dissent (168, 227, 228). Some of those receptors for pro-resolving lipid mediators were even shown to promote pro-inflammatory effects as well, depending on the respective ligand (168). SPMs are promoted as promising new non-immunosuppressive and non-opioid analgesic therapeutic options for many diseases (e.g., rheumatoid arthritis, chronic headaches, diabetic neuropathy) (229). SPMs were inversely associated with the pain score in arthritis patients, and several clinical studies link the supplementation with ω-3 PUFAs to reduced pain levels and higher SPM levels in various diseases (230–233). Unfortunately, many clinical studies investigating the effects of supplementation with ω-3 PUFAs do not analyze concentrations of pro-inflammatory LTs (234–236).

The utility of SPMs as mediators of active resolution of inflammation was questioned recently by a group of renowned scientists in the field (237). The reproducibility of SPM studies is difficult as there is no convention within the scientific community over measurement and detection criteria (238). Besides, lipid mediator profiles are sometimes presented as heatmaps, which only provide relative changes. Therefore, the often very low absolute concentrations are disregarded, and the presented result might be misleading (185). Furthermore, formation routes as well as receptor signaling are controversially discussed (168). Therefore, evidence proofing that pro-resolving lipid

mediators are formed in required concentrations to activate the proposed receptors during the resolution phase is missing (237).

1.2 Cancer

“Cancer” is the general term summarizing a large group of diseases centering on abnormal cell growth that has the potential to invade or spread from one distinct part to another in mammals. This includes all abnormal malignant neoplasms from different types of tissues. Cancer can be classified by the primary site (common by the general public) where the malignancy first developed and the type of tissue the cancer originates from (histological classification). The most common sites at which solid neoplastic malignancies develop are the skin, lungs, female breast, prostate, colon, rectum, cervix, and uterus. Those can be further subclassified by the type of cell they originate from, e.g., skin cancer can be classified into basal cell, squamous cell, and melanoma skin cancer (239). From the point of histology, hundreds of cancer types exist, which can be grouped into six major categories: Carcinoma, sarcoma, myeloma, leukemia, lymphoma, and mixed types. Carcinomas are the most common type, accounting for 80-90% of all cancer cases worldwide, and refer to malignant neoplasms of epithelial origin (240). Carcinomas can be further divided into adenocarcinomas (developed in organs or glands) and squamous cell carcinoma (originating in the squamous epithelium). Sarcomas originate from supportive and connective tissues like bones, muscles, fat, and tendons. The most common type of sarcoma is osteosarcoma (malignant neoplasm in the bone). Myeloma originates from plasma cells of the bone marrow.

Leukemia or “blood cancers” are neoplasms of the bone marrow, resulting in high numbers of abnormal, not fully developed leukocytes. It includes four main types: Acute lymphoblastic leukemia (ALL), acute myeloid leukemia (AML), chronic lymphocytic leukemia (CLL), and chronic myeloid leukemia (CML) (241). Lymphomas originate from glands and nodes of the lymphatic system, including the spleen, tonsils, and thymus. Lymphomas can be subclassified into Hodgkin and non-Hodgkin lymphomas, distinguished by the presence or absence of giant cells derived from B lymphocytes (Reed-Sternberg cells) (242). As the name indicates, mixed-type cancers are neoplasm malignancies from different categories or subcategories. Examples are adenosquamous carcinoma or carcinosarcoma. A detailed standardized medical classification by type, localization, and histology is given in the ICD-O3 (International Classification of Diseases for Oncology) provided by the world health organization (WHO) (243).

Cancer follows cardiovascular diseases as the leading cause of premature death in developed industrial countries. However, survival is worse in developing countries due to diminished treatment accessibility. In 2020, the number of estimated cancer cases exceeded the number of 19 million people of both sexes worldwide. Sadly, more than 9 million cases of death caused by cancer were assumed. This already high cancer burden is expected to be about 28 million cases in 2040 (a 47% rise compared to 2020). Today, the leading cancer type is female breast cancer (11.7% of all new cases). However, the mortality rate for female breast cancer is lower (6.9% of all cancer-related deaths) compared to lung cancer (18%) and colorectal cancer (9.4%), as shown in Figure 1.10 (244). Those numbers show the urgent need for broad, applicable, and affordable cancer treatments, which challenges science due to the vast complexity of cancer phenotypes.

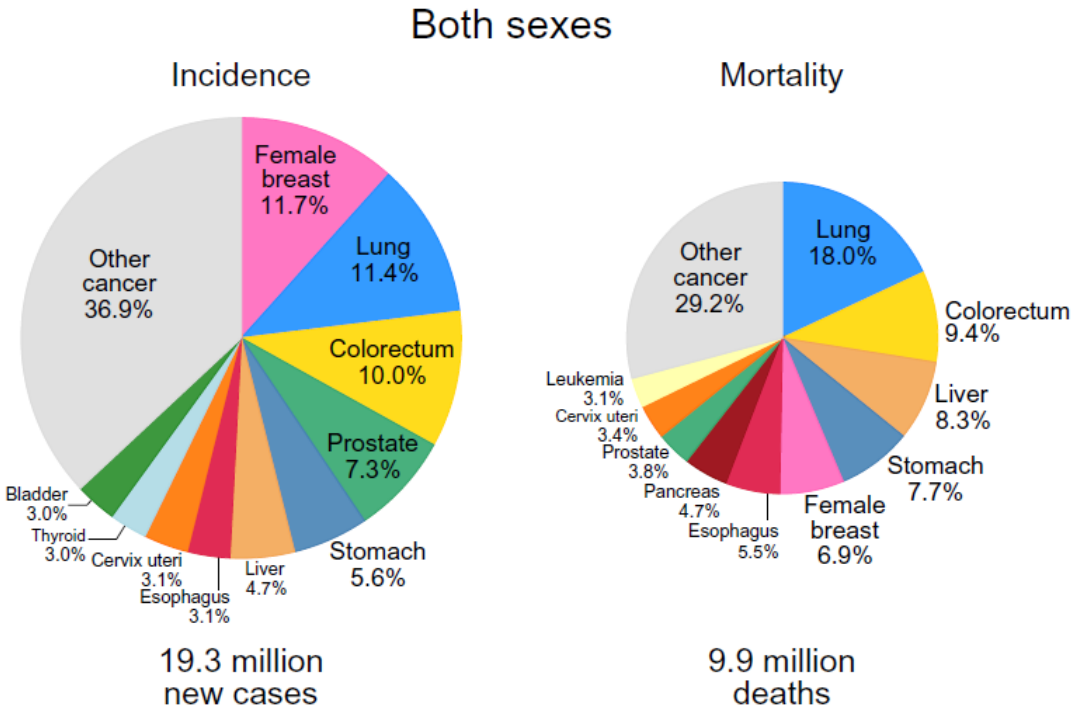

Figure 1.10: Global cancer statistics - incidence and mortality distribution by primary cancer sites in 2020. The figure is taken and modified from (244).

1.2.1 Hallmarks of cancer

Due to this vast complexity, Hanahan and Weinberg proposed in 2000 the simplification that cells must fulfill the so-called “hallmarks of cancer” to become a malignant neoplasm (245). Those hallmarks of cancer are, by today, eight biological capabilities that drain the vast complexity of cancer phenotypes into a set of underlying mechanisms and principles based on the fact that mammalian cells regulate their proliferation, differentiation, and cell death in similar ways. The six initially proposed hallmarks are: Self-sufficiency in growth signals, insensitivity to anti-growth signals, evading apoptosis, limitless replicative potential, sustained angiogenesis, tissue invasion, and metastasis (245). These were extended in 2011 by adding “avoiding immune destruction” and “deregulating cellular energetics” (summarized in Figure 1.11) (246). Even though the order and how those capabilities are obtained can differ vastly, achievement of all hallmarks is highly beneficial during tumorigenesis.

The afore-named hallmarks alone fail to explain the complexities of malignant neoplasms and how they obtain the previously described functional traits and aberrant phenotypic capabilities during development. Therefore, Hanahan and Weinberg added the concept of enabling characteristics, which explains how malignant neoplasms can accomplish those functional traits. Today, two enabling characteristics are assumed, namely “tumor-promoting inflammation”, as well as “genome instability and mutation” (Figure 1.11).

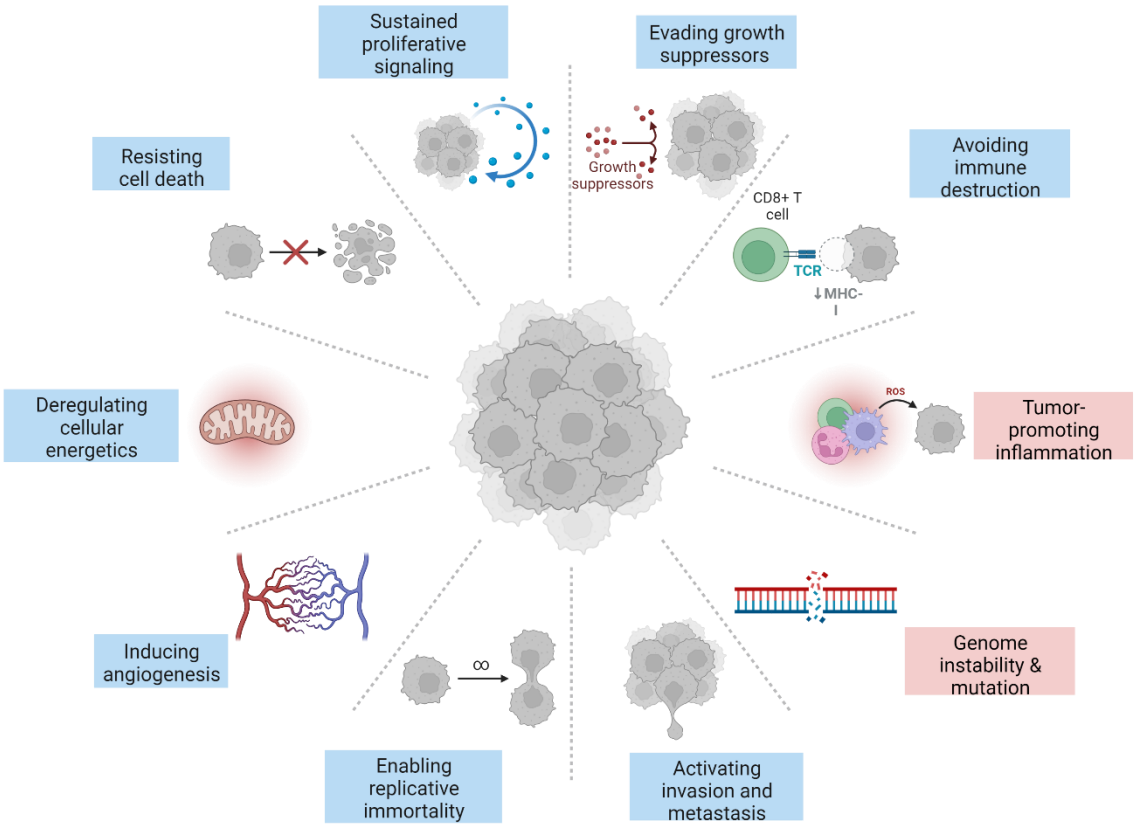

Figure 1.11: Schematic overview of the hallmarks of cancer (blue) and enabling characteristics (red).
Figure adapted from (246).

Due to the high amount of cancer research worldwide, new aspects emerge; cancer hallmarks and enabling characteristics are regularly updated with new proposals to boost scientific discussion and further research in this field. Therefore, Hanahan proposed 2022 “unlocking phenotypic plasticity” and “senescent cells” as new hallmarks and added “non-mutational epigenetic reprogramming” and “polymorphic microbiomes” as new enabling characteristics (Figure 1.12). The hallmarks of cancer concept also considers that even though all capabilities are conceptually distinguishable, parts of their regulation overlap and interconnect by canonical oncogenes, e.g., *KRAS*, *MYC*, *NOTCH*, and *TP53*. This highlights the importance of oncogenic signaling pathways within tumorigenesis.

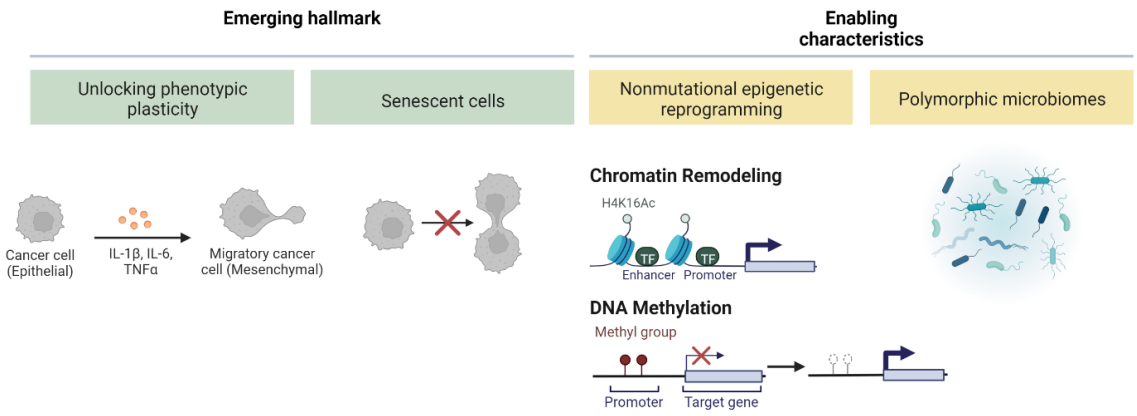

Figure 1.12: Schematic overview of the emerging hallmarks and proposed enabling characteristics (2022).
Figure adapted from (247).

1.2.2 Colorectal cancer

Colorectal cancer (CRC) ranks as the third most common neoplasm malignancy (10% estimate), with the second highest mortality rate (9.6% estimate) worldwide (Figure 1.10). Incidences of CRC are high in industrially developed countries (244). However, numbers are increasing in developing countries due to westernization. CRC is usually asymptomatic; if symptoms like abdominal pain, anemia, or rectal bleeding occur, advanced stages have already been reached (248). CRC is most often malignant, very aggressive, and metastatic. Late diagnosis is assumed to be chiefly responsible for the high mortality rate. Most CRC cases are sporadic (70-80%), while a lower proportion has a hereditary component. A midget proportion of CRC cases is attributable to inflammatory bowel diseases. CRC is a heterogeneous disease that can be classified into consensus molecular subtypes (CMS1-4), predominantly originating from genetic instability (249).

Therefore, most CRC subtypes are assumed to develop through the chromosomal (CIN) and microsatellite instability (MSI) pathway or the hypermethylation (CIMP, CpG island methylator phenotype) and mismatch repair pathway (MMR) (250).

The CIN pathway proposes an accumulation of changes that facilitate tumor growth and eventually lead to invasive malignancies. The starting point is often the truncation of the *APC* gene, followed by mutations of *KRAS*, *TP53*, and *PIK3CA*. Due to mutations of the *APC* gene, the Wnt pathway is hyperactivated. CRC without *APC* mutations often shows mutations or epigenetic changes of other Wnt signaling components. In contrast, CRC resulting through the MSI pathway is caused by mutations in short tandem repeats. Compared to CIN, CRC emanation from MSI predicts a better outcome. The CIMP pathway proposes epigenetic silencing of MMR components mediated through CpG island hypermethylation in promoter regions of MMR genes. Activating BRAF mutations like BRAF V600 are unique features of CRC emanation from CIMP (249–251).

1.2.3 Oncogenic signaling pathways

Cellular signaling is the major communication process of cells — one of the main properties of life in pro- and eukaryotes (252). This signaling includes the detection and production of signaling molecules and the regulation of transcription in response. Signaling molecules (ligands) include monoamines, amino acids, proteins, glycoproteins, lipids, phospholipids, and gases (253–258). They can bind to surface receptors that detect the signaling molecules and start signal transduction, transmitted by a multi-step sequence. This sequence often includes signal amplification and is most commonly transmitted through protein phosphorylation mediated by protein kinases (259). Due to their cellular function, most canonical signaling pathways necessary for proper cellular function include proto-oncogenes (260). These proto-oncogenes usually regulate processes like cell growth and differentiation, but when mutated, they become overactive and are named oncogenes (261). However, activation can also be triggered through general dysregulation, chromosome abnormality, and chromosomal translocation (262, 263). Oncogenic mutations can also occur in tumor suppressor genes. Tumor suppressor genes usually inhibit the cell cycle and growth, but when mutated or lost, they concede unrestricted cell division and growth (264). Mutations can also affect DNA repair genes or DNA mismatch, which then leads to the accumulation of mutations in other genes (265).

Several critical signaling pathways and molecular networks that regulate essential processes like proliferation, survival, translation, differentiation, and apoptosis contain oncogenes and are therefore stated as oncogenic signaling pathways (266). They have been identified as frequently altered in cancer (267–269). However, not all genes are activated or mutated within those pathways with equal frequencies. Furthermore, specific pathways like the RTK-RAS, cell cycle, and PI3K (Phosphoinositide 3-kinase) pathway are altered at high frequencies among many neoplastic malignancies. However, other pathways are only altered in particular subsets of tumor types (270).

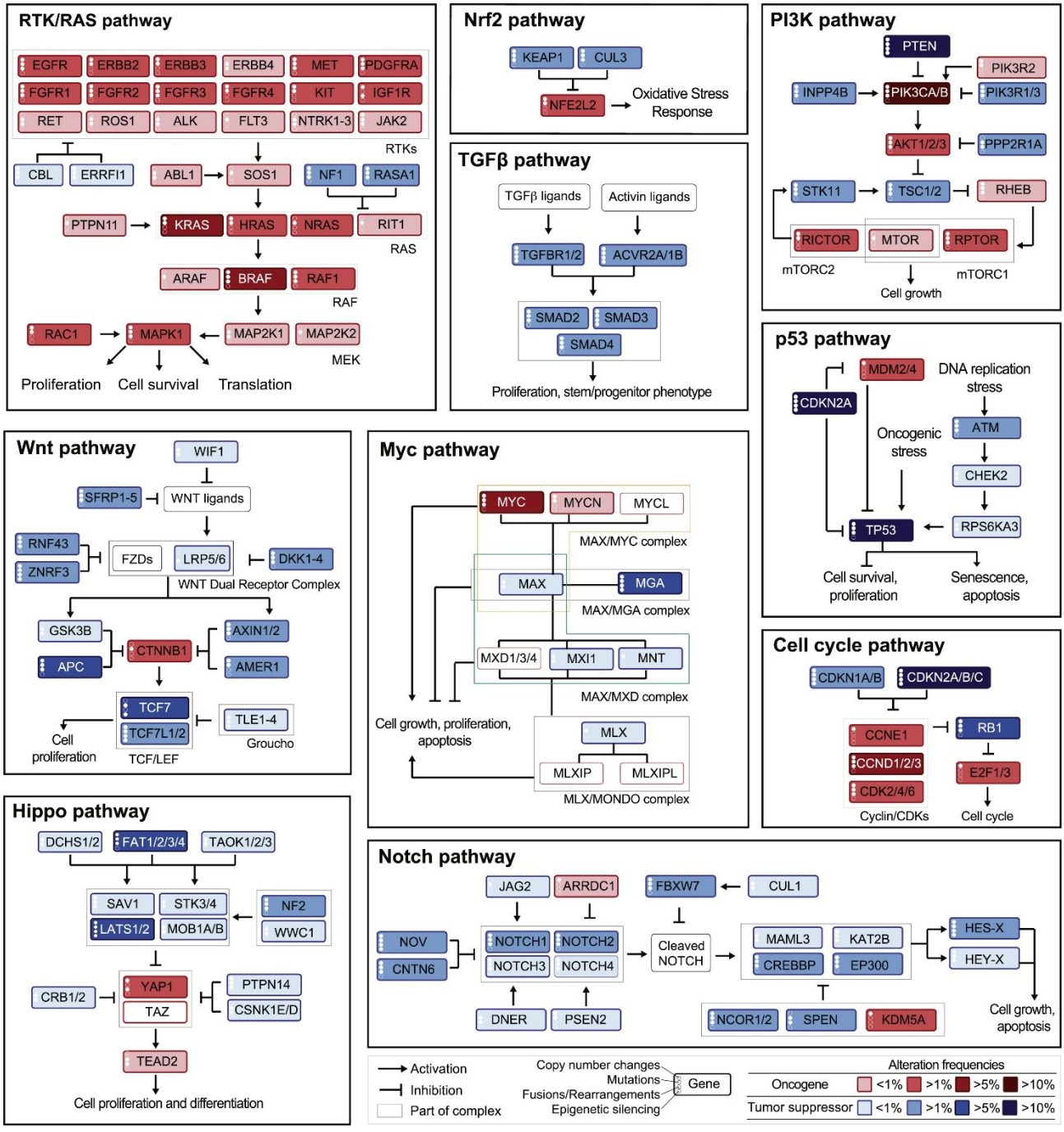

Figure 1.13: Overview of oncogenic signaling pathways with frequent genetic alterations from the cancer genome atlas. Interactions of pathway members in ten selected pathways. Gene alteration frequencies of oncogenic activation (red) and tumor suppressor inactivation (blue) are indicated by color intensity. Somatic alterations (copy number changes, mutations, fusions/rearrangements, epigenetic silencing) are indicated using white dots on the left side of each gene symbol. Note: Interpathway interactions are not displayed. Figure is taken from (270).

The ten most altered signaling pathways in cancer include the RTK/RAS, Nrf2, PI3K, TGF-β, Wnt, Myc, p53, cell cycle, Hippo, and Notch pathways. They are summarized in Figure 13. Displayed are the simplified interactions of pathway members and their gene alteration frequencies. Oncogenic activation is displayed in red, and tumor suppressor inactivation is displayed in blue. Furthermore, somatic alterations (copy number changes, mutations, fusions/rearrangements, epigenetic silencing) are marked as white dots. The displayed curated pathways result from the analysis of 9,125 tumor samples from 33 cancer types (270).

The RTK/RAS pathway bears the highest median alteration frequency across all cancer types (46% of samples). Tumor subtypes with the highest alterations in this pathway include Her2-enriched breast cancer (82% altered), genomically stable (CIMP) colorectal cancer (88% altered), and melanoma (94% altered). Among the most altered genes are BRAF (7%) and KRAS (9%). In addition to the linear signaling of the RTK/RAS pathway, it is highly interconnected with the PI3K pathway. This connection comprises several positive and negative feedback loops (271).

Regarding treatment, this complicates matters: E.g., inhibition of mTORC-1 (mammalian target of rapamycin complex 1) within the PI3K pathway via analogs of rapamycin (rapalogs) can lead to MAPK reactivation, leading to resistance against mTORC-1 inhibition (272). Besides this complex interference, several tumors often show multiple alterations that affect several pathways, and distinct pathways often occur co-altered. However, other tumors show mutual exclusive alterations (270). Especially the RAS, PI3K, p53, and cell cycle pathways exhibit multiple dynamic interactions, as explained in the example of mTORC-1 and MAPK, which can lead to a functional interference in multiple pathways, even though only one is altered (273). Alterations on RTK genes often promote the RAS or PI3K signaling, while the p53 and cell cycle pathways are often co-altered across multiple tumor types. Within the PI3K and cell cycle pathway, alterations are distributed over many genes, while alterations in the Wnt, Myc, and Nrf2 pathways are limited to only a few genes. Within the PI3K pathway, highly altered genes are PI3K and PTEN, most commonly found in breast cancer gastrointestinal and gynecological tumors (270).

1.2.4 Tumor microenvironment

Cancer cells are not solely regulated by their cellular signaling. Additionally, they highly interact with their surrounding microenvironment through cell-cell and cell-matrix interactions. Cancer cells can influence this microenvironment within their tumor mass by extracellular signals and vice versa (274). The tumor microenvironment (TME) varies between tumor types. However, most solid malignancies show hallmark compartments like stromal cells, blood vessels, immune cells, and extracellular matrix (ECM) (275).

The ECM consists of a variety of non-cellular component groups like proteoglycans, polysaccharides, proteins, and scaffold tissue which constitute the microenvironment of cells in nearly all tissues and organs. Those groups include collagen, elastin, fibronectin, laminin, heparan and keratan sulfate, and hyaluronic acid (276). The ECM can be categorized into two primary forms, which differ by location, composition, and function (277). While the interstitial form is a matrix that forms a three-dimensional (3D) network interconnecting cells in the stroma, the other form is described by the pericellular basement membrane — related to neoplastic malignancies; this membrane forms a stiff physical barrier around the tumor stroma (276). In principle, various cells can form and deposit ECM components. However, fibroblasts are the major

ECM producers. Therefore, cancer cells recruit and activate stromal cells through pro-fibrotic growth factors and inflammatory factors like TGF-α, TGF-β, EGF, and PDGF. When recruited, stroma cells (fibroblasts, pericytes, mesenchymal stem cells) can differentiate into cancer-associated fibroblasts (CAFs) by tumor-derived activation factors (278).

The ECM can possess both tumor-promoting and -suppressing properties. Therefore, the ECM is constantly changed and remodeled during cancer progression to promote cancer growth and migration (279).

A dedicated blood supply is essential for tumors, as access to oxygen and nutrients is crucial for growth, progression, and metastasis. Especially carcinomas depend on vascularization as their epithelial non-vascularized tissue origin prevents them from growing bigger than 1,000-2,000 µm (241). Therefore, cancer cells themselves induce angiogenesis by secreting various growth factors like vascular endothelial growth factor (VEGF) (242). Even after vascularization, solid neoplasm malignancies develop gradients of nutrients, oxygen, catabolites, pH value, soluble factors, and proliferative activity (Figure 13). The 3D structure of tumors often restricts anti-cancer therapy success due to a lack of drug penetration. Hypoxic areas emerge 100-200 µm away from functional blood vessels and cells from this area show only a low proliferation rate (243). In structures larger than 500 µm, nutrient deprivation, waste accumulation, and restriction in oxygen supply lead to a necrotic core region surrounded by a quiescent viable mantle encased by a proliferating outer rim (Figure 13).

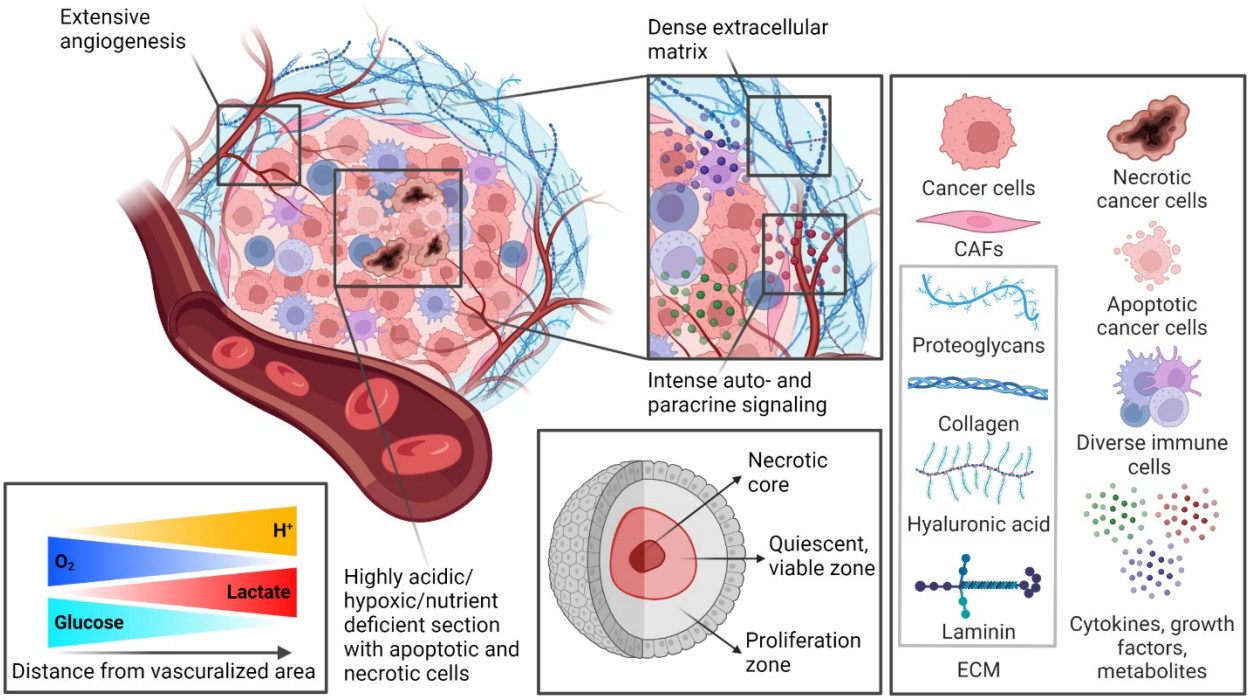

Figure 1.14: Schematic representation of the tumor microenvironment.
Figure adapted from (280) and (281).

Tumors get infiltrated with various immune cells performing pro- and antitumorigenic functions. Generally, immune cells can be categorized as innate and adaptive. Innate immune cells include macrophages, neutrophils, and dendritic cells, which carry out the innate immune response (282). Especially macrophages carry significant functions against pathogens and tissue damage. These functions include phagocytosis, antigen-presentation, and secretion of inflammatory chemo- and cytokines (283). The spectrum of macrophage activation is highly complex and fluent; however, in a more straightforward approach, they can be categorized as M1 and M2 macrophages, having a share in either inflammation and immune defense or regeneration and tissue homeostasis (284). Macrophages are thought to be recruited by local tumor conditions after the secretion of chemo- and cytokines (e.g., CSF-1, IL-34, IL-6) from cancer cells as a response to hypoxia and necrosis. Chronic inflammation due to persistent infection is a common starting point in tumorigenesis of several types of cancer (e.g., colorectal cancer) (285). However, macrophages are predominantly found in the M2 state as tumor-associated macrophages (TAMs) secreting IL-6, IL-8, IL-10, TGF-β, and VEGF within the TME (286).

Neutrophils provide the first line of defense against a wide variety of pathogens. In the early onset of tumorigenesis, neutrophils are recruited to the TME. Concerning the TME, neutrophils provide pro- and antitumorigenic functions dependent on the tumor type and stage of tumor progression. However, many more macrophages are recruited to the tumor than neutrophils, and the neutrophilic infiltration of tumors is generally associated with a worsened prognosis (287). Early on, IL-8 secreted by cancer cells, as well as apoptosis and necrosis, attract neutrophils. In turn, these neutrophils promote apoptosis by releasing ROS. In later stages of tumor development, neutrophils stimulate angiogenesis, tumor progression, local invasion and promote tumor growth by modifying the ECM.

Other immune cell subsets present in the TME are dendritic cells (DC), T-cells, B-cells, natural killer cells (NK), and other subsets of pathologically activated immature neutrophils and monocytes referred to as myeloid-derived suppressor cells (MDSCs) (288). MDSCs interact with T-cells, DCs, TAMs, B-cells, and NK cells. They participate in immune evasion, angiogenesis, and epithelial-mesenchymal transition (EMT). However, the suppression of immune cells is the most defining feature of MDSCs (289).

Due to the vast complexity and the high number of different cancer types, the cancer-specific TMEs and their cellular and molecular signaling networks remain only partly understood.

1.2.4.1 Short excursion: three-dimensional *in vitro* cell culture

As described in 1.2.4, solid malignancies are complex three-dimensional structures that develop heterogeneous gradients of nutrients, oxygen, pH value, soluble factors, catabolites, and proliferative activity. The 3D structure often restricts therapy success due to a lack of drug penetration. Therefore, culturing cells in a 3D context can provide several advantages compared to conventional two-dimensional cell culture (290–292). Spherical cancer cell models can be classified into four simplified groups, as proposed by Weiswald et al.: Multicellular tumor spheroids (MCTS), tumorspheres (abridged as CSC, since the model is predominantly used to study cancer stem cells), tissue-derived tumor spheres (TDTS), and organotypic multicellular spheroids (OMS) (293). MCTS are formed due to aggregation and compaction of cancer cell lines cultured under non-adherent or low-adherent conditions. CSC are cultured under similar conditions but are formed by clonal proliferation, usually in stem cell medium. Unlike this, TDTS are generated by the dissociation of tumor tissue followed by compaction during culture. OMS are cuttings from tumors cultured under non-adherent conditions, leading to rounding of the tissue (293).

Although all models share a round 3D structure, they display different intrinsic features. Therefore, the respective model should be chosen depending on the cancer type of interest and the aim of the study. For example, MCTS can be formed from various cancer cell lines (89, 294). They offer high reproducibility and are easiest to use for high throughput applications. MCTS show a very dynamic growth rate, similar to solid malignancies *in vivo*. This is characterized by an early exponential phase, followed by a period of limited growth associated with an increase in necrotic and non-proliferating cells (295). In contrast, monolayer cultures only show exponential cell proliferation under standard culture conditions (290). Cells in MCTS are more differentiated and were shown to develop ECM-like structures on their surface composed of fibronectin, laminin, collagen, and glycosaminoglycans (296). Even though MCTS are an established and valuable tool for *in vitro* investigations in drug discovery, drug repositioning, tumor physiology, cell response to cancer therapy, and general biomedical research, the model is limited to mimicking solid avascular malignancies or microvascularized malignancies if co-cultured with endothelial cells (292, 294, 297).

Nevertheless, the described physicochemical and growth properties are the primary advantage of MCTS. Thus, the complexity of the 3D cancer environment can be brought into the culture dish without the cost and accession limitations of animal models and human specimens.

1.2.5 The role of 5-LO and 5-LO dependent products in cancer

Apart from its role in the pathophysiology of various diseases (described in 1.1.4), 5-LO and its metabolites are also implicated in the pathophysiology of several types of cancer. 5-LO and its metabolites play an important role in leukemic malignancies. Since the enzyme is predominantly expressed in leukocytes, this is not astonishing (85). However, expression of the enzyme and LT formation were also found in solid cancers. Malignant tissues from the prostate, pancreas, lung, bladder, colon, and brain – tissue origins that do not express 5-LO under physiological conditions (Human Protein Atlas proteinatlas.org) readily express the enzyme (298–300).

5-LO-expressing tumors and cell lines show increased tumor growth, microvessel density, and metastasis (301–303). Therefore, 5-LO is implicated in several hallmark aspects of carcinogenesis, such as tumor cell proliferation, differentiation, apoptosis, migration, invasion, and angiogenesis. 5-LO expression was even outlined as a progressive biomarker for some cancer types (304, 305). However, high 5-LO expression in cancer tissues was also linked to poor prognosis concerning tumor progression, patient survival, and treatability (53, 306, 307).

Adding 5-LO products like 5-HETE and LTB_4 to cultured cancer cells induces mitogenic effects like cell proliferation and activation of anti-apoptotic signaling pathways. This was mediated through MAPK/AKT signaling in pancreas carcinoma cells (308, 309). Similar results were demonstrated for other cell lines (e.g., colon carcinoma, mammary carcinoma, gastric carcinoma) (310–312). The addition of 5-HETE, LTA_4, and ARA regulates VEGF expression in malignant mesothelioma, highlighting the involvement of 5-LO products in angiogenesis (313). Furthermore, CysLTs were shown to promote tumor cell proliferation and survival (314). Especially for LTD_4 enhanced cell proliferation via PKCε dependent ERK activation in intestinal epithelial cells could be detected (315).

As already mentioned above, 5-LO expression is, among other factors, associated with tumor-promoting functions. Treatment of cultured cancer cells using 5-LO inhibitors was shown to mediate anti-proliferative and cytotoxic effects. The fatty acid competitive inhibitor AA-861 attenuates the growth of human prostate, pancreas, breast, colon, esophageal, bladder, and myeloid cancer cell lines (316–321). However, those studies did not perform add-back experiments, demonstrating the reversibility of this effect by 5-LO products. Indirect inhibition of 5-LO using the FLAP inhibitor MK-886 triggered cell death in prostate and gastric cancer cells (322–324). The FDA-approved 5-LO inhibitor Zileuton was shown to trigger apoptosis in pancreatic and cervical cancer cells (325, 326). Furthermore, this inhibitor exerted anti-angiogenic effects by inducing apoptosis in HUVEC cells (327). Moreover, Zileuton loaded polymer micelles reduced circulating breast cancer cells and intratumoral cancer stem cells in orthotopic breast cancer models and mice (328).

Indeed, 5-LO inhibitors AA-861, MK-886, CJ-13,610, Rev-5901, and BWA4C can promote anti-proliferative and cytotoxic effects in several cancer cell lines. However, this effect was independent of 5-LO expression since 5-LO negative cell lines like HeLa, Panc-1, and U937 showed a concentration-dependent decrease in viability as well (329). Of note, the used concentrations capable of inducing anti-proliferative and cytotoxic effects were high (> 1 µM) in most studies (301).

However, 5-LO inhibitors have already been tested as potential cancer treatments in clinical trials. For example, NDGA completed a clinical phase II trial to treat prostate cancer. Nevertheless, it is essential to mention that the intended target of inhibition was not 5-LO but insulin-like growth factor receptor 1 (IGF-1R), and analysis showed no significant decline for the primary outcome measure (330). Likewise, in a clinical phase II trial, Zileuton was used to treat patients with head and neck or lung cancer suffering from bronchial dysplasia (331). The trial was completed in 2009; however, results have not been published by now (ClinicalTrials.gov Identifier: NCT00056004). Another clinical phase I trial aimed to treat advanced and/or metastatic solid tumors using the LTB_4 antagonist LY293111, but again, results were never published (ClinicalTrials.gov Identifier: NCT00006375). However, the same inhibitor was used for two other clinical phase II studies in combination with gemcitabine or gemcitabine-cisplatin to treat advanced adenocarcinoma of the pancreas and first-line non-small-cell lung cancer. Results for both studies did not demonstrate any benefit of adding LY293111 to the gemcitabine or gemcitabine-cisplatin therapy (332, 333).

Besides mediating anti-proliferative and cytotoxic effects in cancer cells, 5-LO inhibition was also shown to suppress vascular endothelial growth factor-induced angiogenesis in endothelial cells (334).

Independent of potential inhibitor-dependent off-target effects, several studies were still able to demonstrate the pro-proliferative and viability-promoting role of 5-LO using knockdown and knockout approaches. For example, 5-LO knockdown in human malignant pleural mesothelial cells significantly decreased cell viability time-dependent compared to scrambled and untreated controls (313). In the pancreatic cancer cell line SW1990 and the cervical cancer cell lines CaLo and Caski, 5-LO knockdown led to growth suppression and apoptosis (335). Furthermore, knockdown in SW1990 cells inhibits the growth of transplanted pancreatic tumors in a xenograft mouse model (336). A complete 5-LO knockout in the colon cancer cell lines HT-29, HCT-116, and the osteosarcoma cell line U-2 OS failed to demonstrate a substantial influence on overall cell viability (72).

Genetic deletion of 5-LO increased the numbers of tumor-infiltrating macrophages in Apc(Δ468) mice (polyposis model) and decreased neutrophil infiltration. Increased tumor-infiltrating macrophage density is linked to an improved prognosis in patients with colon cancer. This highlights the role of 5-LO in tumorigenesis and implicates 5-LO inhibitors as potential therapeutic agents for colorectal polyposis (337). In contrast, a global knockout mouse model where Lewis lung carcinoma cells were directly implanted into the lungs found increased primary tumor volume and liver metastases in 5-LO knockout mice. This implicated an antitumorigenic role for 5-LO products in the microenvironment during lung cancer progression (338).

Besides 5-LO, the other enzymes, receptors, and proteins of the LT cascade are overexpressed in various cancer cell lines and tissues alongside elevated LT formation. For example, FLAP is overexpressed in some epithelial cancer cell lines (72, 339). Its expression in breast cancer and the ovarian cancer microenvironment is, like the expression of 5-LO, an indicator of a poor prognosis regarding patients' survival (340, 341). Some cancer cell lines and primary tissue samples were even shown to express the complete LT cascade (72, 342). Finally, the BLT2 and CysLT2 receptors were found to be expressed in colorectal, breast, gastric, bladder, and pancreatic cancers (343–347).

2 Previous work and aim of the study

Previous findings leading to the presented study are, to a great extent, already published by Weisser et al. (72). In an initial screening of several tumor cell lines (pancreas: Capan-2, Panc-1; colon: HT-29, CaCo-2, HCT-116, SW1222; liver: HepG2; cervix: HeLa; prostate: LNCaP, DU-145; lung: A549; bone: U-2 OS; kidney: A498) four 5-LO expressing cell lines were identified (Figure 2.1A). Those cells were further analyzed to compare the expression of enzymes of the LT cascade (*LTC4S* expression was only analyzed on mRNA level due to a lack of a validated antibody) (Figure 2.1B, C). The identified 5-LO expressing cell lines HT-29, HCT-116, U-2 OS, and Capan-2 also expressed all enzymes important for LT formation. Thus, these cell lines should be capable of forming LTs after stimulation. However, 5-LO activity was relatively low in intact tumor cells compared to PMNL, which are known to express high amounts of active 5-LO (Figure 2.1E). Disruption of cellular integrity increased 5-LO product formation in U-2 OS and Capan-2 cells but did not affect product formation in HT-29 and HCT-116 cells.

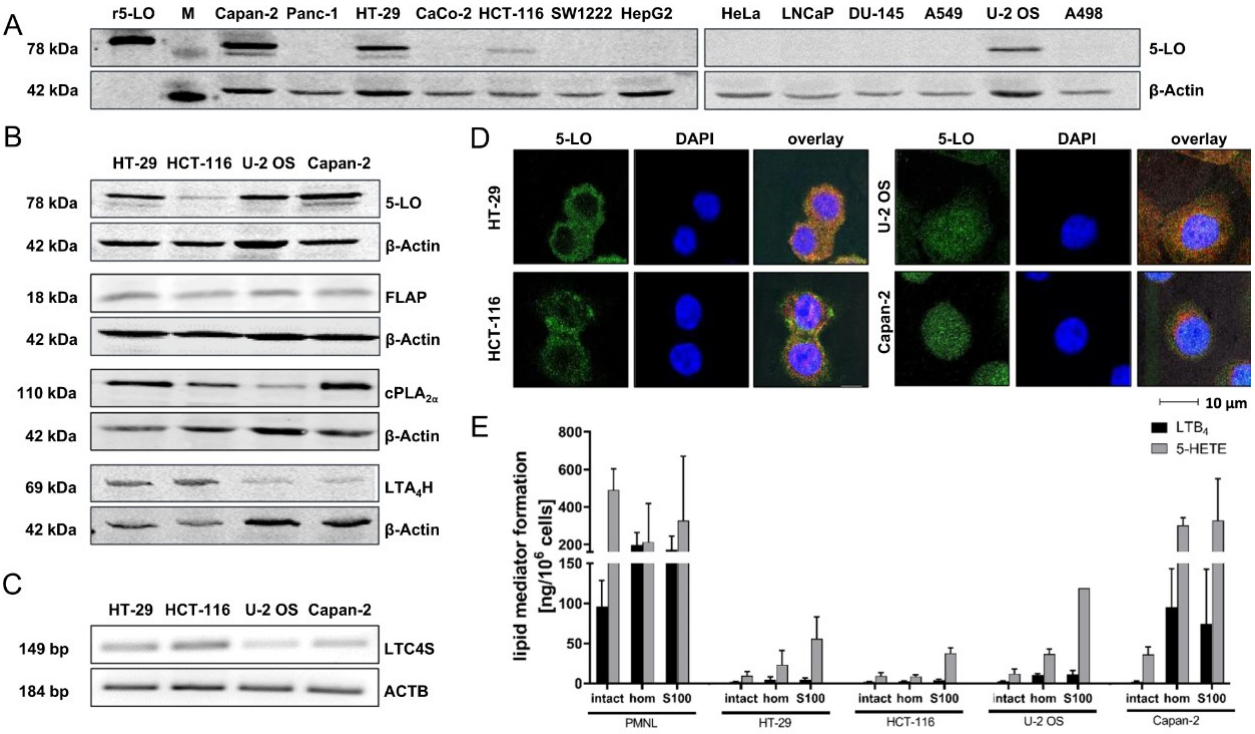

Figure 2.1: Previous findings on 5-LO expression and activity in tumor cell lines.
(A) 5-LO expression screening via Western blot analysis of various cancer cell lines. One representative blot from three individual experiments is shown. (B) Comparison of LT cascade enzyme and protein expression in 5-LO expressing cell lines via Western blot. One representative blot from three individual experiments is shown. (C) Comparison of *LTC4S* mRNA expression in 5-LO expressing cell lines. One representative gel from three individual experiments is shown. (D) Cellular 5-LO localization in 5-LO expressing cell lines analyzed via immunostaining and confocal microscopy analysis. Images were obtained using a Leica TCS-SP5 confocal microscope and analyzed using the LAS X software (both Leica, Wetzlar, Germany). (E) Comparison of 5-HETE and LTB_4 formation in intact cells, cell homogenates, and S100 supernatants of human PMNL and 5-LO expressing tumor cell lines. For the formation of 5-LO products, intact cells were stimulated with Ca^{2+} ionophore (A23187, 2.5 µM) in PBS/glucose 1 mg/mL (PBSG) buffer supplemented with 20 µM ARA and 1 mM Ca^{2+}. Homogenates and S100 supernatants received 1 mM ATP instead of Ca^{2+} ionophore. Samples were incubated for 10 min at 37°C, and lipid mediator formation was analyzed via LC/MS-MS. Presented are the mean + SD of 3–11 independent experiments.
Intact: Intact cells; hom: Cell homogenates; M: Size marker; r5-LO: Recombinant human 5-LO; S100: 100,000 rcf supernatants. Figure is taken from (72).

Finally, the segregation of membrane fractions via ultracentrifugation further elevated 5-LO product formation in the 100,000 rcf supernatants of all tumor cell lines tested but not in PMNL. Nevertheless, only disruption of cellular integrity in Capan-2 cells led to 5-LO product formation comparable to human PMNL (Figure 2.1E). Since the cellular localization of 5-LO is essential for LT formation, this was analyzed in cells stained by immunofluorescence using confocal microscopy. While 5-LO was predominantly localized within the cytosol in HT-29 and HCT-116 cells, the enzyme was evenly distributed between the cytosol and the nucleus in U-2 OS and Capan-2 cells (Figure 2.1D). This might explain the higher 5-LO product formation in U-2 OS and Capan-2 cells, combined with the higher 5-LO expression detected in those cells. However, this does not explain the elevated product formation in all tested tumor cell lines after the segregation of membrane fractions via ultracentrifugation.

Cancer development and progression are strongly dependent on the TME. In the monolayer culture of cancer cell lines, cell-matrix and cell-cell interactions present in native tumors are absent. There, cells develop artificial polarity due to cytoskeletal rearrangements as a cause of layer growth. Furthermore, it is already known that several colon cancer cell lines dysregulate essential signaling pathways due to 3D growth (348).

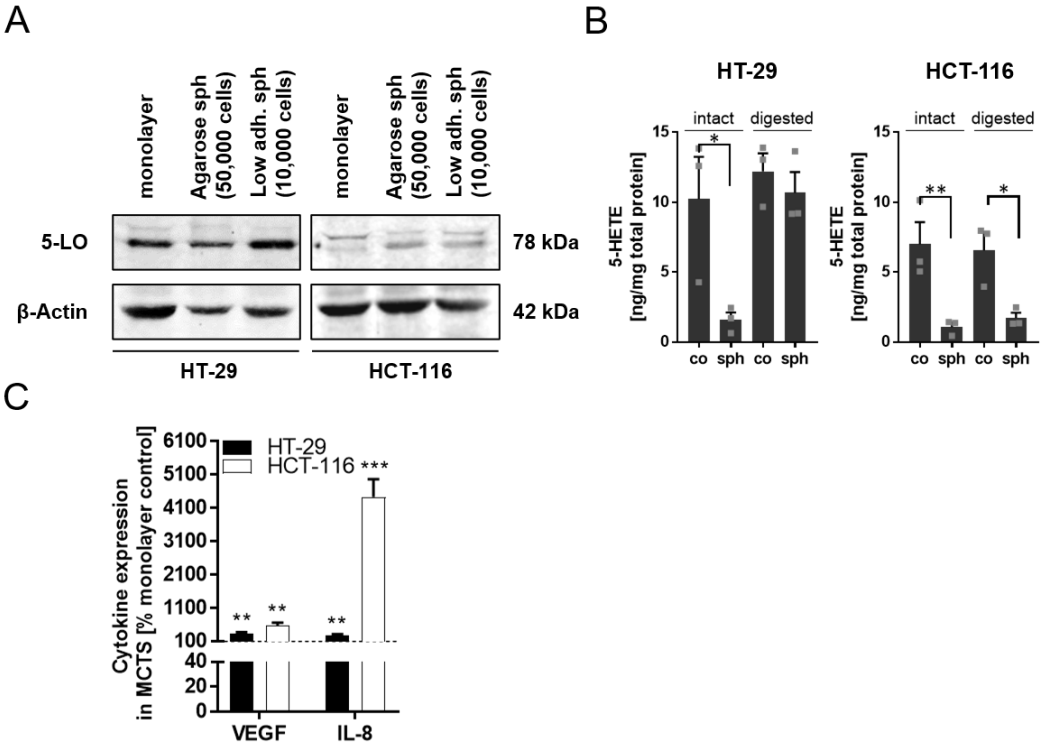

Figure 2.2: Previous findings on 5-LO expression, activity, and cytokine expression after MCTS formation.
(A) Analysis of 5-LO expression in monolayer and MCTS-grown HT-29 and HCT-116 cells via Western blot. Monolayer cells were taken from the respective maintenance culture while splitting the cells. For MCTS formation, indicated cell amounts were seeded in agarose-coated 24-well plates or special low adherence 96-well plates. Then, cells were incubated for 7 days at 37°C, 5% CO_2. (B) 5-HETE release from intact and (accutase) digested HT-29 and HCT-116 MCTS (10,000 cells seeded in 96-well low adh. plates grown for 7 days) and respective monolayer controls. For the formation of 5-LO products, intact cells were stimulated with Ca^{2+} ionophore (A23187, 2.5 µM) in PBSG buffer supplemented with exogenous ARA (20 µM) and Ca^{2+} (1 mM). 5-HETE formation was determined by LC-MS/MS analysis and normalized to the total protein content for each sample. (C) VEGF and IL-8 release from MCTS compared to the respective monolayer control (in %) grown for 7 days. Cytokines were determined via cytometric bead array (CBA; VEGF, IL-8). Mean release in cell monolayers: HT-29 (VEGF, 5388 pg/10^6 cells; IL-8, 272 pg/10^6 cells; HCT-116 (VEGF, 3830 pg/10^6 cells; IL-8, 50 pg/10^6 cells). Sph: Spheroids, low adh.: Low adherence, co: Control.

Therefore, 5-LO expression and activity were investigated after 3D growth of HT-29 and HCT-116 cells as MCTS during a master's thesis (Göbel 2017). U-2 OS and Capan-2 cells were excluded from MCTS formation experiments. U-2 OS cells only formed very loose and fragile spheroids in pre-testing, and Capan-2 cells did not form spheroid at all, probably due to their low proliferation rate and strong mucus secretion.

Compared to the respective monolayer-grown cells, culture of HT-29 and HCT-116 cells as MCTS for 7 days potently induced 5-LO expression (Figure 2.2A). However, the elevated 5-LO expression did not yield higher 5-HETE formation. Analysis of intact MCTS showed even diminished 5-HETE formation due to a lack of substrate availability attributable to the 3D structure (Figure 2.2B). MCTS of HT-29 and HCT-116 cells were further analyzed towards their VEGF and IL-8 expression, verifying that the initial seeding densities used resulted in MCTS sizes capable of forming oxygen and nutrient gradients (Figure 2.2C).

Summarizing the previous work, it was found that several tumor cell lines express 5-LO even though healthy tissue samples of the same origin do not express this enzyme. However, 5-LO product formation seems impaired in the cancer cells, even though they express the complete LT formation machinery. It was shown that 5-LO influences gene regulation in tumor cells with only low LT formation; however, for some genes, this regulation seemed to be 5-LO activity-dependent (72). Furthermore, 5-LO expression was elevated due to MCTS formation, highlighting the importance of more physiological culture conditions.

The described results led to the necessity of further investigations in order to understand the role of 5-LO in tumor cells. Therefore, the present study aimed to:

- Investigate the shown 5-LO upregulation after MCTS formation under more reproducible conditions, including improved controls
- Elucidate the underlying physicochemical parameters leading to 5-LO upregulation after MCTS formation
- Explore the mechanisms leading to the MCTS formation-dependent 5-LO upregulation
- Examine the cause of impaired 5-LO product formation in 5-LO-expressing tumor cells

3 Material and methods

3.1 Materials

3.1.1 Cell Culture

Following reagents and sterile ready-to-use buffers were especially used for cell culture applications and therefore obtained in cell culture appropriate quality.

All items in Table 1 were supplied from Thermo Fisher Scientific™ (Waltham, MA, USA), or their associated company Life Technologies™ (Carlsbad, CA, USA).

Table 1: Reagents and ready-to-use buffers for cell culture applications.

Reagents and ready-to-use buffers	Specifications
Dulbecco's Modified Eagle Medium (DMEM), powder, high glucose, pyruvate	L-glutamine, phenol red
DMEM, high glucose	L-glutamine, phenol red
DMEM, high glucose	no phenol red
Dulbecco's Phosphate-Buffered Saline (PBS)	without $CaCl_2$, without $MgCl_2$
L-Glutamine	200 mM
Lipofectamine™ LTX Reagent with PLUS™ Reagent	
McCoy's 5A (Modified) Medium, high glucose	L-glutamine, bacto-peptone, phenol red
Opti-MEM™ I Reduced Serum Medium	L-glutamine, no phenol red
Pen Strep	10,000 U/mL Penicillin, 10,000 µg/mL Streptomycin
Puromycin dihydrochloride	10 mg/mL
Roswell Park Memorial Institute medium (RPMI1640 Medium)	L-glutamine, phenol red
Sodium Pyruvate	100 mM
StemPro™ Accutase™ Cell Dissociation Reagent	
Trypan Blue Solution	0.4%
Trypsin-EDTA (TE)	0.5%, 10x diluted in 1x PBS (1:10) before use
UltraPure™ Agarose	Standard melting point

Reagents and ready-to-use buffers	Specifications
UltraPure™ Distilled Water	DNase/RNase-Free

Table 2: Fetal calf serum suppliers and used batches.

Fetal calf serum (FCS) suppliers	LOT
Capricorn Scientific GmbH, Ebsdorfergrund, Germany	CP16-1537 and CP19-2834
Gibco, Life Technologies™, (Thermo Fisher Scientific) Carlsbad, CA, USA	42Q4467K

Table 3: Cell culture materials and special consumables.

Cell culture materials and special consumables	Specifications	Distributor
CELLSTAR® Cell culture dishes	100/20 mm	Greiner Bio-One International, Kremsmünster, Austria
CELLSTAR® Cell culture flasks	650 mL, 175 cm^2	Greiner Bio-One International, Kremsmünster, Austria
CELLSTAR® Cell culture flasks	250 mL, 75 cm^2	Greiner Bio-One International, Kremsmünster, Austria
CELLSTAR® Cell culture flasks	50 mL, 25 cm^2	Greiner Bio-One International, Kremsmünster, Austria
CELLSTAR® Conical Bottom Tubes	15 mL, 50 mL	Greiner Bio-One International, Kremsmünster, Austria
CELLSTAR® Microplates	Cell-Repellent Surface, 96-well, F-Bottom	Greiner Bio-One International, Kremsmünster, Austria
CELLSTAR® Multiwell plates	6-well, 12-well, 24-well, 96-well	Greiner Bio-One International, Kremsmünster, Austria
Corning 96-well Spheroid Microplates		Corning Incorporated, New York, NY, USA

Cell culture materials and special consumables	Specifications	Distributor
Corning® Cell Lifter	19 mm	Corning Incorporated, New York, NY, USA
Corning® Microplates	96-well, TC-treated flat clear bottom, black	Corning Incorporated, New York, NY, USA
Corning® Ultra-Low Attachment Spheroid Microplate	96-well, clear, round bottom	Corning Incorporated, New York, NY, USA
Coverslips	Menzel (24x55 mm)	Thermo Fisher Scientific, Waltham, MA, USA
Cryo.s™ vials	2 mL, 12.5x48 mm, sterile	Greiner Bio-One International, Kremsmünster, Austria
EASYstrainer™	small, 20 µm	Greiner Bio-One International, Kremsmünster, Austria
FACS Tubes	12x75 mm, PS	Ratiolab, Dreieich, Germany
MicroAmp fast 96-well reaction plates		Applied Biosystems (Thermo Fisher Scientific), Waltham, MA, USA
Rotilabo®-syringe filters	PVDF, sterile, 0.45 µm pore size	Carl Roth
Superfrost™Plus Adhesion Microscope slides		Epredia Netherlands B.V., Breda, Netherlands
TC Dish 100 Cell+	100x20 mm, for challenging adherent cells	SARSTEDT AG & Co., Nümbrecht, Germany
Tissue-Tek® Cryomold®	Disposable Vinyl Specimen Molds, 15x15x5 mm	VWR International, Radnor, PA, USA
Trans-Blot Turbo RTA Mini 0.2 µm Nitrocellulose Transfer Kit		Bio-Rad Laboratories, Hercules, CA, USA

3.1.2 Chemicals and reagents

Table 4: General chemicals and reagents.

General chemicals and reagents	Distributor
1,4-Diazabicyclo [2.2.2]octane (DABCO)	Carl Roth GmbH + Co. KG, Karlsruhe, Germany
2-Propanol	VWR International, Radnor, PA, USA
4',6-Diamidino-2-phenylindol (DAPI)	Sigma-Aldrich, St. Louis, MO, USA
Acetic acid	PanReac AppliChem ITW Reagents, Darmstadt, Germany
Acrylamide 4K solution 30% (37.5:1)	PanReac AppliChem ITW Reagents, Darmstadt, Germany
APS (Ammonium peroxydisulphate)	Carl Roth GmbH + Co. KG, Karlsruhe, Germany
BD FACSFlow™	BD Biosciences, Franklin Lakes, New Jersey, USA
BHT (Butylated hydroxytoluene)	Cayman Chemical Company, Ann Arbor, MI, USA
BioWhittaker® Lymphocyte Separation Medium (LSM)	LONZA, Walkersville, MD, USA
Bromophenol blue	Merck KGaA, Darmstadt, Germany
Ca^{2+} Ionophore (A23187)	Sigma-Aldrich, St. Louis, MO, USA
Calcium chloride ($CaCl_2$) dihydrate	Carl Roth GmbH + Co. KG, Karlsruhe, Germany
Chloroform	PanReac AppliChem ITW Reagents, Darmstadt, Germany
Chloroquine diphosphate salt	Sigma-Aldrich, St. Louis, MO, USA
cOmplete™ Mini, EDTA-free Protease Inhibitor Cocktail	Roche Diagnostics GmbH, Mannheim, Germany
D-(+)-Glucose anhydrous	Carl Roth GmbH + Co. KG, Karlsruhe, Germany
Dextran from *Leuconostoc spp.*	Sigma-Aldrich, St. Louis, MO, USA
Dimethyl sulfoxide (DMSO)	PanReac AppliChem ITW Reagents, Darmstadt, Germany
Entellan™ mounting medium	Sigma-Aldrich, St. Louis, MO, USA
Eosin Y solution, alcoholic	Sigma-Aldrich, St. Louis, MO, USA

General chemicals and reagents	Distributor
Ethanol (EtOH) ROTIPURAN®	Carl Roth GmbH + Co. KG, Karlsruhe, Germany
Ethidium bromide solution (1%)	Carl Roth GmbH + Co. KG, Karlsruhe, Germany
Ethylenediaminetetraacetic acid (EDTA)	Merck KGaA, Darmstadt, Germany
Glycerol	PanReac AppliChem ITW Reagents, Darmstadt, Germany
Glycine	PanReac AppliChem ITW Reagents, Darmstadt, German
Hematoxylin solution, Mayer's	Sigma-Aldrich, St. Louis, MO, USA
HEPES (4-(2-hydroxyethyl)-1-piperazineethanesulfonic acid) for buffer solutions	PanReac AppliChem ITW Reagents, Darmstadt, Germany
Hydrochloric acid (HCl) 37%	VWR International, Radnor Pennsylvania, USA
Luria Broth Base (Miller's LB Broth Base)™	Thermo Fisher Scientific™, Waltham, MA, USA
Methanol (MeOH)	VWR International, Radnor Pennsylvania, USA
N,N,N',N'-Tetramethylethylenediamine (TEMED)	PanReac AppliChem ITW Reagents, Darmstadt, Germany
NP-40 (IGEPAL CA-630)	Sigma-Aldrich, St. Louis, MO, USA
Paraformaldehyde (PFA)	Sigma-Aldrich, St. Louis, MO, USA
PEG-8000	Sigma-Aldrich, St. Louis, MO, USA
PhosSTOP, Phosphatase Inhibitor Cocktail	Roche Diagnostics GmbH, Mannheim, Germany
Polybrene infection/transfection reagent	Sigma-Aldrich, St. Louis, MO, USA
Polyethylenimine (PEI) branched	Sigma-Aldrich, St. Louis, MO, USA
Propidium Iodide (PI)	Thermo Fisher Scientific, Waltham, MA, USA
Sodium acetate (NaAc)	Carl Roth GmbH + Co. KG, Karlsruhe, Germany
Sodium chloride (NaCl)	Carl Roth GmbH + Co. KG, Karlsruhe, Germany
Sodium dodecyl sulfate (SDS)	PanReac AppliChem ITW Reagents, Darmstadt, Germany

General chemicals and reagents	Distributor
Sodium hydroxide (NaOH) pellets	VWR International, Radnor, PA, USA
TISSUE FREEZING MEDIUM® for cryosectioning	Leica Biosystems Nussloch GmbH, Nussloch, Germany
Tris(hydroxymethyl)aminomethane (Tris)	PanReac AppliChem ITW Reagents, Darmstadt, Germany
Triton-X-100	PanReac AppliChem ITW Reagents, Darmstadt, Germany
Tween® 20	PanReac AppliChem ITW Reagents, Darmstadt, Germany
β-Mercaptoethanol	Sigma-Aldrich, St. Louis, MO, USA

Table 5: Used target inhibitors.

Inhibitors	Distributor
Cobimetinib	Cayman Chemical Company, Ann Arbor, MI, USA
Dactolisib (NVP-BEZ235)	Cayman Chemical Company, Ann Arbor, MI, USA
HLM006474	Cayman Chemical Company, Ann Arbor, MI, USA
LB42708	Cayman Chemical Company, Ann Arbor, MI, USA
NSC 66811	Cayman Chemical Company, Ann Arbor, MI, USA
Palbociclib	MedChemExpress LLC, South Brunswick, NJ, USA
PD184352	Cayman Chemical Company, Ann Arbor, MI, USA
Pifithrin-α	Cayman Chemical Company, Ann Arbor, MI, USA
Ro-3306	MedChemExpress LLC, South Brunswick, NJ, USA
SCH772984	Cayman Chemical Company, Ann Arbor, MI, USA
Temsirolimus	Cayman Chemical Company, Ann Arbor, MI, USA

Inhibitors	Distributor
Wortmannin	Cayman Chemical Company, Ann Arbor, MI, USA

Table 6: Kits, proteins, enzymes, and special consumables.

Kits, proteins, and enzymes	Distributor
BSA (Bovine Serum Albumin)	Sigma-Aldrich, St. Louis, MO, USA
Cell proliferation reagent WST-1	Sigma-Aldrich, St. Louis, MO, USA
DNA Gel Loading Dye (6x)	Thermo Fisher Scientific, Waltham, MA, USA
DNase I, RNase-free	Thermo Fisher Scientific, Waltham, MA, USA
EveryBlot blocking buffer	Bio-Rad Laboratories, Hercules, CA, USA
Gel Loading Dye, Purple (6X)	New England BioLabs, Ipswich, MA, USA
GeneRuler 1 kb DNA ladder	Thermo Fisher Scientific, Waltham, MA, USA
GeneRuler 100 bp DNA Ladder	Thermo Fisher Scientific, Waltham, MA, USA
GlycoBlue™ Coprecipitant	Thermo Fisher Scientific, Waltham, MA, USA
High-capacity RNA-to-cDNA™ Kit	Thermo Fisher Scientific, Waltham, MA, USA
NEBuilder® HiFi DNA Assembly	New England BioLabs, Ipswich, MA, USA
NucleoBond Xtra Maxi EF, Maxi kit for endotoxin-free plasmid DNA	Macherey-Nagel, Düren, Germany
NucleoSpin Plasmid, Mini kit for plasmid DNA	Macherey-Nagel, Düren, Germany
PageRuler™ Plus Prestained Protein Ladder	Thermo Fisher Scientific, Waltham, MA, USA
Pierce™ BCA Protein Assay Kit	Thermo Fisher Scientific, Waltham, MA, USA
Power SYBR™ Green Master Mix	Applied Biosystems, Thermo Fisher Scientific, Waltham, MA, USA
Q5® High-Fidelity DNA Polymerase	New England BioLabs, Ipswich, MA, USA
Recombinant Human GM-CSF	PeproTech, London, United Kingdom
Recombinant Human IL-4	PeproTech, London, United Kingdom
Recombinant Human INF-γ	PeproTech, London, United Kingdom
Recombinant Human M-CSF	PeproTech, London, United Kingdom
RiboRuler High Range RNA Ladder	Thermo Fisher Scientific, Waltham, MA, USA
RiboRuler High Range RNA Ladder	Thermo Fisher Scientific, Waltham, MA, USA
RNase A, DNase, and protease-free (10 mg/mL)	Thermo Fisher Scientific, Waltham, MA, USA

Kits, proteins, and enzymes	Distributor
Roche Cytotoxicity Detection Kit (LDH)	Sigma-Aldrich, St. Louis, MO, USA
Spectra™ Multicolor High Range Protein Ladder	Thermo Fisher Scientific, Waltham, MA, USA
TRIzol™ Reagent	Thermo Fisher Scientific, Waltham, MA, USA

Table 7: Used fatty acids.

Lipids	Specification
Arachidonic acid (ARA)	Peroxide free
Docosahexaenoic acid (DHA)	
Eicosapentaenoic acid (EPA)	Peroxide free

3.1.3 Antibodies

Table 8: Primary antibodies.

Primary antibodies	Cat. No.	Distributor
5-LO	66326-1-Ig,	Proteintech, Rosemont, IL, USA
5-LO	ab169755	Abcam, Cambridge, United Kingdom
5-LO (6A12)		in house produced
b-Myb	711708	Thermo Fisher Scientific, Waltham, MA, USA
Cleaved Caspase 3	9664S	Cell Signaling Technology, Danvers, MA, USA
$cPLA_{2\alpha}$	sc-438	Santa Cruz Biotechnology, Dallas, TX, USA
ERK (p44/42)	#9102	Cell Signaling Technology, Danvers, MA, USA
FLAP	ab53536	Abcam, Cambridge, United Kingdom
Ki67	ab15580	Abcam, Cambridge, United Kingdom
LTA_4H	sc-390567	Santa Cruz Biotechnology, Dallas, TX, USA
MEK1	#2352	Cell Signaling Technology, Danvers, MA, USA
mTOR	PA5-34663	Thermo Fisher Scientific, Waltham, MA, USA

Primary antibodies	Cat. No.	Distributor
mTOR	ab134903	Abcam, Cambridge, United Kingdom
p53	sc-126	Santa Cruz Biotechnology, Dallas, TX, USA
p70S6K	sc-8418	Santa Cruz Biotechnology, Dallas, TX, USA
phospho-ERK	sc-7383	Santa Cruz Biotechnology, Dallas, TX, USA
phospho-p70S6K	#9205	Cell Signaling Technology, Danvers, MA, USA
PIK3CA	MA5-14870	Thermo Fisher Scientific, Waltham, MA, USA
PRKCζ	sc-17781	Santa Cruz Biotechnology, Dallas, TX, USA
Raptor	sc-81537	Santa Cruz Biotechnology, Dallas, TX, USA
Rictor	sc-271081	Santa Cruz Biotechnology, Dallas, TX, USA
α-Tubulin	sc-5286	Santa Cruz Biotechnology, Dallas, TX, USA
α-Tubulin	ab176560	Abcam, Cambridge, United Kingdom

Table 6: Secondary antibodies.

Secondary antibodies	Conjugate	Distributor
Donkey anti-Mouse IgG (H+L) Highly Cross-Adsorbed Secondary Antibody	Alexa Fluor™ Plus 488	Thermo Fisher Scientific, Waltham, MA, USA
Donkey anti-Rabbit IgG (H+L) Highly Cross-Adsorbed Secondary Antibody	Alexa Fluor™ Plus 647	Thermo Fisher Scientific, Waltham, MA, USA
IRDye® 680RD Donkey anti-Mouse IgG (H + L)	IRDye 680RD	LI-COR Biosciences GmbH, Bad Homburg, Germany
IRDye® 680RD Donkey anti-Rabbit IgG (H + L)	IRDye 680RD	LI-COR Biosciences GmbH, Bad Homburg, Germany

IRDye® 800CW Donkey anti-Mouse IgG (H + L)	IRDye 800CW	LI-COR Biosciences GmbH, Bad Homburg, Germany
IRDye® 800CW Donkey anti-Rabbit IgG (H + L)	IRDye 800CW	LI-COR Biosciences GmbH, Bad Homburg, Germany

3.1.4 Buffers

Table 9: Used buffer stocks, compositions, and dilutions.

Buffers	Buffer composition and dilution
10x Running buffer for SDS-PAGE	0.25 M Tris, 1.92 M Glycerine, 35 mM SDS for use, 100 mL 10x buffer were diluted with 900 mL ultrapure water
10x Tris-buffered saline (TBS)	0.5 M Tris, 1 M NaCl pH was adjusted with HCl to 7.4. For use, 100 mL 10x buffer was diluted with 900 mL ultrapure water
12.5x Towbin transfer buffer for protein immunoblotting	0.31 M Tris, 2.4 M Glycine for use, 80 mL buffer was diluted with 720 mL ultrapure water and mixed with 200 mL 100% MeOH
4x Lenti-X-Concentrator	40% (W/V) PEG-8000, 1.2 M NaCl pH 7.2 sterile filtered (0.2 µM)
50x TAE buffer for agarose gels	2 M Tris, 1 M acetic acid, 50 mM EDTA
$CaCl_2$	0.4 M
Mowiol mounting medium	6 g Glycerin, 2.4 g Mowiol 4-88, 6 mL ultrapure water, 12 mL Tris-HCl (pH 8.5), 25 mg DABCO/mL
PBS glucose (PBSG) buffer	20 mg/mL α-D-Glucose stock diluted to 1 mg/mL for further use
Trans-Blot Turbo transfer buffer	200 mL 5x buffer was diluted with 600 mL ultrapure water and 200 mL 100% EtOH
RIPA lysis buffer	20 mM TRIS-HCl (pH 7.4), 150 mM NaCl, 2 mM EDTA, 1% Triton-X-100, 0.5% NP-40
5x loading buffer	250 mM TRIS-HCl (pH 6.8), 5 mM EDTA, 50% Glycerol (v/v), 10% SDS (w/v), 0.05% (w/v) Bromophenol blue

3.1.5 Plasmids

The following plasmids can be found at Addgene (Watertown, MA, USA).

Table 10: Used plasmids and respective Addgene numbers.
The following plasmids were obtained from Addgene or gifted from elsewhere but can be found at Addgene, including the respective maps.

Plasmid	Addgene number
psPAX2	#12260
p-CMV-VSV-G	#8454
pSBtet-GP	#60495
pSBbi-GP	#60511

The plasmid pcGlobin2-SB100X was kindly gifted by Prof. Dr. Zoltan Ivics (Paul-Ehrlich-Institut, Langen, Germany).

3.1.6 Instruments and software

3.1.6.1 Centrifuges

- Sigma 3K30, Sigma Laborzentrifugen, Osterode, Germany; rotor type 12154-H
- Heraeus Multifuge X3 FR, Thermo Fisher Scientific, Waltham, MA, USA; rotor type 75003180
- Centrifuge 5424 R, Eppendorf, Hamburg, Germany; rotor type FA-45-24-11
- Beckmann Ultrazentrifuge Optima LE-80K; rotor type 70.1 Ti
- Varifuge 3.0RS, Heraeus Sepatech, Hanau, Germany; rotor type #8080E
- Heraeus 400R, Heraeus, Hanau, Germany; rotor type #8177
- Sorval LYNX 4000, Thermo Fisher Scientific, Waltham, MA, USA; rotor type F14-14x50cv, F14-6x250y

3.1.6.2 Gel electrophoresis and transfer

Agarose gel electrophoresis

- MIDI 1 Electrophoresis Unit, Carl Roth GmbH + Co. KG, Karlsruhe, Germany
- Power PAC 300, Bio-Rad, Hercules, CA, USA

Protein electrophoresis and transfer

- Mini-PROTEAN Tetra Cell, Bio-Rad, Hercules, CA, USA
- PowerPAC Basic Power Supply, Bio-Rad, Hercules, CA, USA
- Mini Trans-Blot® Electrophoretic Transfer Cell, Bio-Rad, Hercules, CA, USA
- Thermo cycler
- peqSTAR 96 Universal Gradient, Peqlab Biotechnologie, Erlangen, Germany
- Applied Biosystems™ Veriti™ 96-Well Thermal Cycler, Applied Biosystems™, Forster City, CA, USA
- StepOnePlus™ Real-Time PCR System, Applied Biosystems™, Forster City, Ca, USA

3.1.6.3 Microscopes

All used microscopes and software for image analysis were obtained from Carl Zeiss, Oberkochen, Germany.

- Axio Vert.A1
- Zeiss LSM 780 AxioObserver.Z1
- Zen black software
- Zen blue software (version 2.6)
- Zen core software (version 2.6)

3.1.6.4 Flow cytometer

- BD FACSuite™ software, Becton Dickinson BD Biosciences, Franklin Lakes; NJ, USA
- BD FACSVerse™ flow cytometer, Becton Dickinson BD Biosciences, Franklin Lakes, NJ, USA
- FlowJo V10.6 software, Becton Dickinson BD Biosciences, Ashland, OR, USA

3.1.6.5 Plate reader

All plate readers and software for data acquisition and analysis were obtained from the Tecan Group, Männedorf, Switzerland

- i-control™ software for Tecan microplate readers
- infinite® M200 plate reader
- Spark® multimode plate reader

3.1.6.6 Others

- Bandelin Sonopuls HD 200, BANDELIN electronic, Berlin, Germany
- Biovision 1000/26mx, Vilber Lourmat, Marne-la-Vallée, France
- NanoDrop™ 2000 spectrophotometer, Thermo Fisher Scientific, Waltham, MA, USA
- Odyssey® 9120 infrared imaging system, LI-COR Biosciences, Lincoln, NE, USA
- Cryostat, CryoStar™ NX50, Thermo Fisher Scientific, Waltham, MA, USA

3.2 Human cell culture

3.2.1 Cell lines and general culture conditions

All cell handling and experiments were performed under a laminar flow bench to ensure sterile conditions. Therefore, sterile materials and solutions were used. All cell lines were cultured in a humidified atmosphere of 5% CO_2 at 37°C. Cultivation of cells was carried out in 75 cm^2 or 175 cm^2 flasks, and cultures were split twice a week using 1x TE. Table 11 states all specifications and sources of the cell lines used. The listed general growth conditions also apply to all genetically altered cell lines generated for this thesis.

3.2.2 Thawing of frozen cells

Frozen cells (3-5x10^6) were thawed fast and directly diluted in 13 mL complete growth medium (CGM). After centrifugation (340 rcf, 5 min at RT), the supernatant was discarded, and the cell pellet was resuspended in 5 mL of fresh CGM. The cell suspension was transferred into a 25 cm^2 culture flask. CGM for HT-29, MCF-7, Capan-2, and Caco-2 cells was supplemented with an additional 10% of FCS. The medium was replaced after 20-24 h to discard nonadherent cells.

3.2.3 Cryopreservation

All parental or genetically altered cell lines were cryopreserved in their respective cryopreservation medium (CGM and 5% DMSO) using 3-5x10^6 cells/mL in 2 mL cryovials. The vials were placed in an isopropanol-containing cryo-freezing container (Mr. Frosty, Nalgene®, max. 18 vials) or within tissue paper coiled like a ball (max. 20 vials per ball, approximately 13 cm in diameter) to enable a temperature reduction of about 1°C per minute.

3.2.4 Cellular morphology

To determine morphological changes due to different treatments and to verify GFP expression after transfection experiments, cells were monitored using a Zeiss Axio Vert.A1 microscope with an Axiocam 305 color. For fluorescence excitation, LED modules with 385 nm, 470 nm, and 590 nm were used. The Zeiss filter sets 49 (excitation: G365, beamsplitter: FT395, emission: BP445/50), 38 (excitation: BP470/40, beamsplitter: FT495, emission: BP525/50), and 64 (excitation: BP587/25 (HE), beamsplitter: FT605 (HE), emission: BP647/70 (HE)) were used to avoid excitation of untargeted fluorophores. Pictures were analyzed and processed using the Zeiss Zen core software.

Table 11: Used cell lines and their respective specifications.

Cell line	HT-29	HCT-116	HCT-116 p53 -/- (349)	MCF-7	U-2 OS	Capan-2	Caco-2	Lenti-X-293T
Origin	Human colorectal adenocarcinoma cells, established in 1964 from the primary tumor of a 44-year-old woman with colon adenocarcinoma	Human colorectal carcinoma cells, established from the primary colon carcinoma of an adult man	Cells were generated from the HCT-116 cell line using two promoterless targeting vectors to sequentially disrupt the two p53 alleles (349)	Human breast adenocarcinoma cells, established in 1970 from a 69-year-old woman with metastatic mammary carcinoma (after radio- and hormone therapy)	Human osteosarcoma cells, established in 1964 from a moderately differentiated osteogenic sarcoma of a 15-year-old girl	Human pancreas adenocarcinoma cells, established in 1975 from the tumor of a 56-year-old man	Human colon adenocarcinoma cells, established in 1974 from the primary colon tumor of a 72-year-old man	293T clone selected for high-titer lentivirus production
General growth conditions, including respective CGM	McCoy' s 5A medium supplemented with 10% FCS, 100 U/mL Penicillin, 100 µg/mL Streptomycin (PS), and 1 mM sodium pyruvate	DMEM high glucose medium supplemented with 10% FCS, 100 U/mL Penicillin, 100 µg/mL Streptomycin, and 1 mM sodium pyruvate	DMEM high glucose medium supplemented with 10% FCS, 100 U/mL Penicillin, 100 µg/mL Streptomycin, and 1 mM sodium pyruvate	DMEM high glucose medium supplemented with 10% FCS, 100 U/mL Penicillin, 100 µg/mL Streptomycin, and 1 mM sodium pyruvate	DMEM high glucose medium supplemented with 10% FCS, 100 U/mL Penicillin, 100 µg/mL Streptomycin, and 1 mM sodium pyruvate	McCoy' s 5A medium supplemented with 10% FCS, 100 U/mL Penicillin, 100 µg/mL Streptomycin, and 1 mM sodium pyruvate	DMEM high glucose medium supplemented with 10% FCS, 100 U/mL Penicillin, 100 µg/mL Streptomycin, 1 mM sodium pyruvate, and 1% NEAA	DMEM high glucose medium supplemented with 10% FCS, 100 U/mL Penicillin, 100 µg/mL Streptomycin, and 1 mM sodium pyruvate
Split ratio and doubling time	1:5 – 1:7 40-60 h	1:10 – 1:20 25-40 h	1:10 - 1:20	1:5-1:10 50 h	1:10-1:20 25-30 h	1:4 50-70 h	1:5-1:10 80 h	1:10 – 1:20
Source	**DSMZ ACC 299**	**DSMZ ACC 581**	**Bert Vogelstein, Johns-Hopkins University, Baltimore**	**DSMZ ACC 115,**	**ATCC HTB-96™**	**DSMZ ACC 245**	**DSMZ ACC 169**	**Takara Bio Inc. Cat. #632180**

3.2.5 Isolation of human leukocytes from leukocyte concentrates

Leukocyte concentrates and human plasma was obtained from the DRK blood donor service (Frankfurt am Main, Germany). Donors gave written consent for use in research. If living cells were required for further analysis after differentiation, testing certificates for HAV, HBV, HCV, HEV, HIV, and Lues were obtained.

3.2.5.1 Heat inactivation of human plasma

Human plasma (Industrieplasma C I0052) of identical blood groups was pooled and transferred into 50 mL tubes. After incubation at 56°C for 1 h in a water bath and centrifugation (872 rcf, 30 min at RT), the heat-inactivated human serum was transferred to fresh 50 mL tubes and stored at - 20°C until further use.

3.2.5.2 PBMC and PMNL separation by density gradient centrifugation

The leukocyte concentrates were transferred to beakers (separated by donor) and diluted with PBS to 80 mL. Diluted leukocyte concentrates were transferred to 50 mL tubes and mixed with 5 mL dextran solution (5% (w/v) dextran in PBS). After erythrocyte sedimentation for 30 min, the upper plasma phase was collected, and separated erythrocytes were discarded. The plasma fraction was slowly layered over 10 mL lymphocyte separation medium (LSM) and centrifuged (10 min, 1153 rcf, at RT) without deceleration. PBMCs formed a layer upon the LSM, and PMNL formed a pellet.

3.2.5.3 Isolation and differentiation of monocytes from isolated PBMCs

PBMC layers from each donor were transferred to 50 mL tubes, washed twice (10 min, 558 rcf, at RT), and the supernatants were discarded. For seeding, isolated and washed PBMCs were resuspended in 40 mL of warm wash medium (WM, RPMI 1680 supplemented with 5% PS). Cell suspensions of each donor were transferred into 100 mm Cell+ dishes (5 mL per dish, 8 dishes per donor) and diluted with 5 mL WM. After 1-2 h at 37°C, 5% CO_2, non-adherent cells were discarded, and each dish was washed harshly using 5 mL warm WM twice.

Table 12: Monocyte differentiation and polarization conditions.

	Differentiation	Polarization
Incubation times and wash conditions	Differentiation for seven days. The medium was replaced 48 and 120 h after seeding. Cells were washed harshly using 5 mL WM before each medium change.	Polarization within the last 48 h of differentiation.
M1	CM supplemented with 10 ng/mL GM-CSF.	CM supplemented additionally with 10 ng/mL INF-γ.
M2	CM supplemented with 10 ng/mL M-CSF. Treatment for seven days.	CM supplemented additionally with 10 ng/mL IL-4.

For differentiation of isolated monocytes to M1 or M2 macrophages, cells were incubated with culture medium (CM, RPMI 1680 supplemented with 5% PS and 5% heat-inactivated human serum) and treated with granulocyte-macrophage colony-stimulating factor (GM-CSF) or macrophage colony-stimulating factor (M-CSF). For polarization, interferon-gamma (INF-γ) or interleukin 4 (IL-4) was added to the culture for the final 48 h. Concentrations, conditions, and exact time points are further described in Table 12 and Figure 3.1.

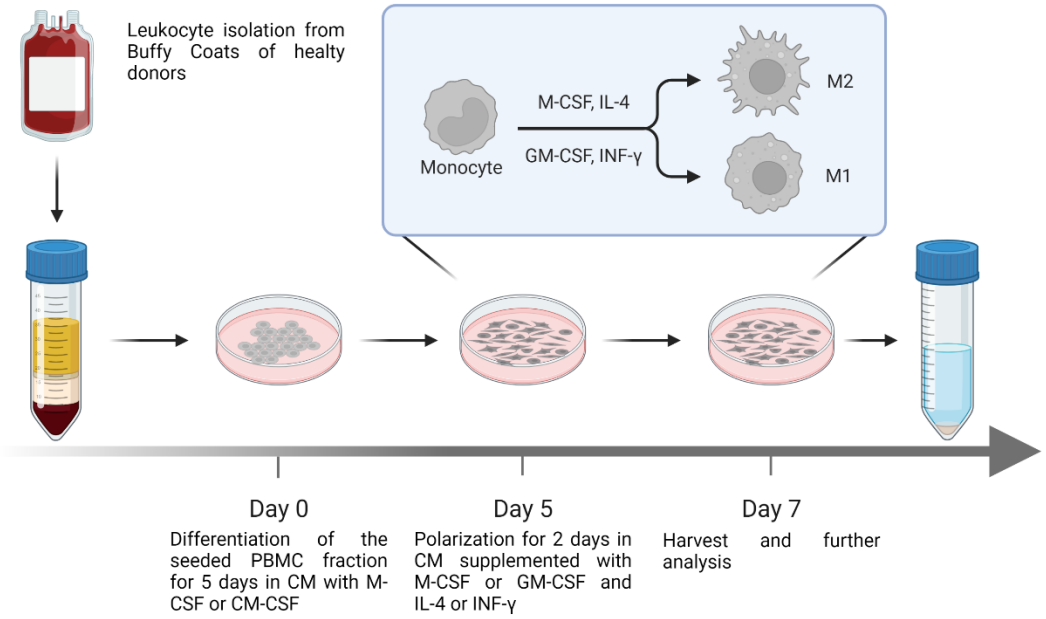

Figure 3.1: Workflow and time schedule for *in vitro* differentiation and polarization of human blood-derived monocytes to macrophages.

3.2.5.4 PMNL purification via hypotonic lysis

PMNL pellets were washed with 10 mL PBS and centrifuged (558 rcf, 10 min, at RT) twice. Pellets were mixed with 5 mL ice-cold ultrapure water for 45 secs to remove remaining erythrocyte contaminations. Hypotonic lysis was stopped by adding 40 mL of ice-cold PBS. Donor samples were analyzed individually or were pooled (3-6 donors) via centrifugation (558 rcf, 10 min, at RT) and resuspended in 2-10 mL ice-cold PBSG buffer, depending on the number of donors pooled. Prior to further experiments, cell numbers were determined using a Burker chamber.

3.2.6 Generation of stably transfected cell lines using the sleeping beauty system

The sleeping beauty system was used to generate stably transfected cell lines with various reporter constructs and target proteins. The parental plasmids pSBbi-GP and pSBtet-GP were kindly provided by Erik Kowarz (350), and cloning for all constructs is described under 3.8.

3.2.6.1 General procedure and antibiotic selection

For each construct, HT-29 (0.5-0.7x10^6) or HCT-116 (0.5-0.65x10^6) cells were seeded into 6-well plates using 3 mL CGM per well. Cells were left to adhere for 24 h in a humidified atmosphere (at 37°C, with 5% CO_2). For transfection, the medium was changed to 2 mL OptiMEM with no additional supplements. Transfection was performed using the Lipofectamine™ LTX Reagent according to the manufacturer's protocol. 24 h after transfection medium was changed to CGM. 48 h after transfection, the medium was changed to CGM supplemented with 3 µg/mL puromycin, and antibiotic selection was performed for nine days. The medium was changed every other day.

Transfection with pSBGP reporter constructs

DNA mixes were prepared in 325 µL OptiMEM containing different DNA concentrations depending on the cell line (see Table 13) and PLUS™ Reagent. LTX mixes were prepared in OptiMEM containing 0.125 µL LTX reagent per µL OptiMEM (DNA/LTX ratio 1:5) for HT-29 and 0.05 µL (DNA/LTX ratio 1:3) LTX reagent per µL OptiMEM for HCT-116 cells. 160 µL DNA mix was added dropwise to 160 µL LTX mix to prepare DNA-LTX mixes. DNA-LTX mixes were incubated for 30 min at RT before transfection. 300 µL transfection mixes (containing 3.75 µg total DNA for HT-29 and 2.5 µg total DNA for HCT-116 cells) were added dropwise to the cells.

Table 13: DNA mix composition for transfection of pSBGP reporter constructs

	HT-29	HCT-116
pSBGP vector	7.72 µg	5.15 µg
pcGlobin2-SB100x	0.41 µg	0.27 µg
Total DNA	8.13 µg	5.42 µg
PLUS™ Reagent	8.13 µL	5.42 µL

Transfection with pSBbi and pSBtet constructs

DNA mixes were prepared in 325 µL OptiMEM containing 5.42 µg total DNA (0.27 µg pcGlobin2-SB100x, 5.15 µg pSBGP vector) and 5.42 µL PLUS™ Reagent. LTX mixes were prepared in OptiMEM containing 0.125 µL LTX reagent per µL OptiMEM (DNA/LTX ratio 1:5) for HT-29 and 0.05 µL (DNA/LTX ratio 1:3) LTX reagent per µL OptiMEM for HCT-116 cells. 160 µL DNA mix was added dropwise to 160 µL LTX mix to prepare DNA-LTX mixes. DNA-LTX mixes were incubated for 30 min before transfection. 300 µL of transfection mixes (containing 2.5 µg total DNA) were added dropwise to the cells.

3.2.7 Generation of stable knockdown cell lines using lentiviral transduction

To generate stable knockdown cell lines for various targets, several MISSION shRNA bacterial clones and a non-mammalian pLKO.1-puro shRNA control vector (SHC002, 5'-CCG GCA ACA AGA TGA AGA GCA CCA ACT CGA GTT GGT GCT CTT CAT CTT GTT GTT TTT-3') were purchased from Sigma-Aldrich Inc., Missouri, USA. Bacterial culture, transformation, and vector preparations are described under 3.8. Table 14 lists the respective target genes, the clone IDs, and their respective specifications. The packaging vector psPAX2 was obtained via Addgene as a gift from Didier Trono, and the envelope vector pCMV-VSV-G was obtained via Addgene as a gift from Bob Weinberg.

Table 14: Used shRNA plasmids and specifications (insert sequence).

Target gene	Clone ID	TRCN	Insert sequence 5`-3`	Region	Internal name
MAP2K1	NM_002755.2-2032s1c1	0000199799	CCG GCC CAT ATC CAA GTA CCA ATG CCT CGA GGC ATT GGT ACT TGG ATA TGG GTT TTT TG	3´UTR	pLKO.1-puro_shMAP2K1
MTOR	NM_004958.2-4662s1c1	0000038678	CCG GGC ATG GAA GAA TAC ACC TGT ACT CGA GTA CAG GTG TAT TCT TCC ATG CTT TTT G	CDS	pLKO.1-puro_shMTOR
MYB	NM_005375.2-	0000288599	CCG GCC AGA TTG TAA ATG CTC ATT TCT	3´UTR	pLKO.1-puro_shMYB

	2596s21c1		CGA GAA ATG AGC ATT TAC AAT CTG GTT TTT G		
MYBL2	NM_002466.2-2515s1c1	0000020519	CCG GGC TAA CAA CAA AGT TCC ACT TCT CGA GAA GTG GAA CTT TGT TGT TAG CTT TTT	3´UTR	pLKO.1-puro_shMYBL2
PIK3CA	NM_006218.2-3471s1c1	0000196582	CCG GGC ATT AGA ATT TAC AGC AAG ACT CGA GTC TTG CTG TAA ATT CTA ATG CTT TTT TG	3´UTR	pLKO.1-puro_shPIK3CA
PRKCZ	NM_002744.x-1806s1c1	0000001218	CCG GCG CGT GAT TGA CCC TTT AAC TCT CGA GAG TTA AAG GGT CAA TCA CGC GTT TTT	3´UTR	pLKO.1-puro_shPRKCZ
RICTOR	NM_152756.2-2620s1c1	0000074291	CCG GCG TCG GAG TAA CCA AAG ATT ACT CGA GTA ATC TTT GGT TAC TCC GAC GTT TTT G	CDS	pLKO.1-puro_shRICTOR
RPTOR	NM_020761.1-4325s1c1	0000039770	CCG GCG ACT ACT ACA TCT CCG TGT ACT CGA GTA CAC GGA GAT GTA GTA GTC GTT TTT G	CDS	pLKO.1-puro_shRPTOR

Table 15: Used shRNA plasmids and specifications (target sequence*).

Target gene	**Clone ID**	**TRCN**	**Target sequence 5'-3'***	**Region**	**Internal name**
PIK3CB	NM_006219	0000010025	CGA CAA GAC TGC CGA GAG ATT	CDS	pLKO.1-puro_shPIK3CB
PIK3CD	NM_005026	0000033276	GAC CCA GAA GTG AAC GAC TTT	CDS	pLKO.1-puro_shPIK3CD
PIK3CG	NM_002649	0000199330	CTC CAG ATC TAC TGC GGT AAA	CDS	pLKO.1-puro_shPIK3CG

*Merck changed the provided information and only furnished the target sequence instead of the insert sequence.

3.2.7.1 Generation of virus particles

For each shRNA vector, $4x10^6$ Lenti-X™ 293T cells were seeded into 100 mm Petri dishes using 10 mL CGM per dish. Cells were left to adhere for 24 h in a humidified atmosphere at 37°C, with 5% CO_2. Cells were then transported to the S2 lab using a safety transport box. The medium of each dish was changed to 10 mL CGM supplemented with 25 µM chloroquine. Dishes were placed back in a humidified atmosphere at 37°C, 5% CO_2, while transfection mixes were prepared. Transfection mixes were prepared by dripping 500 µL PEI mix (500 µL OptiMEM containing 88 µg PEI) into 500 µL of the respective DNA mix (478 µL OptiMEM + respective vector; amounts are listed in Table 16). After inversion, transfection mixes were incubated for 15 min at RT. Afterward, transfection mixes were added dropwise to the chloroquine-treated cells.

Lenti-X™ 293T cells were incubated with their respective transfection mixes for 17 h in a humidified atmosphere at 37°C, with 5% CO_2.

Table 16: Used vectors for lentiviral particle generation and their respective specifications.

Vector	[bp]	[pmol]/[µg] DNA	[µg]	[pmol] ratio
pLKO.1-puro_shRNA	7086	0.214	10	2
psPAX2	10709	0.141	7.5	1
pCMV-VSV-G	6507	0.233	4.5	1

After this duration, the medium of all dishes was changed to 10 mL CGM without other supplements, and cells were incubated for another 48 h. Next, the supernatants of each dish were collected and individually filtered using a 0.45 µm PVDF filter. 3 volumes of clarified supernatant (9 mL) were mixed with 1 volume (3 mL) 4x Lenti-X-Concentrator within 15 mL tubes and gently inverted. After incubation for 30 min at 4°C, the virulent supernatants were centrifuged (1,500°rcf, for 45°min at 4°C). Supernatants were discarded, and the remaining pelleted virus particles were resuspended in 1 mL OptiMEM, further referred to as transduction mixes.

3.2.7.2 Lentiviral transduction and antibiotic selection

HT-29 and HCT-116 cells were seeded into 6-well plates 24 h before lentiviral transduction. Therefore, $0.307x10^6$ HT-29 and $0.3x10^6$ HCT-116 cells were seeded in 3 mL of the respective CGM. Before transduction, 6-well plates were transported to the S2 area, and the medium was changed to 1 mL RGM supplemented with 8 µg/mL polybrene per well. 500 µL of prepared transduction mixes were added dropwise for each cell line. Transduced cells were then incubated for 24 h in a humidified atmosphere at 37°C, with 5% CO_2.

After that, the medium was changed to the respective CGM for 48 h. Then, cells were washed, and the medium was changed every two days to CGM supplemented with 3 µg/mL puromycin for antibiotic selection. Cells were cultured for 11 days after transduction within the S2 area to ensure the complete depletion of lentiviral particles. Depending on their growth, cells were transferred

into 75 cm^2 flasks within this duration, but medium change and puromycin treatment were carried out nevertheless.

Cells were transferred into the S1 area after the indicated time for further experiments and cryopreservation.

3.3 Cell culture experiments

3.3.1 Monolayer culture experiments

For monolayer culture experiments (used for protein and RNA analysis), different culture dish sizes and, therefore, seeding cell numbers were used. Table 17 states the used dish sizes, medium volumes, and the respective cell seeding density. If the seeding/synchronization procedure is not mentioned for an experiment within the results section, cells were directly collected from the maintenance culture during cell splitting.

Table 17: Culture dishes and cell seeding densities.

Cultures dish	Cell number [x10^6]	Medium [mL]
6-well (RNA)	0.4	2
100 mm dish (Protein)	3	10

3.3.1.1 Reversible cell cycle synchronization via serum deprivation

For serum-induced cell cycle synchronization, cells were seeded in a reduced growth medium (RGM) containing only 0.5% FCS. After 22-24 h medium was changed to CGM for 2 h to release cells from cell cycle arrest prior to treatment. Figure 3.2 summarizes the general cell culture workflow, including cell cycle synchronization and further treatment.

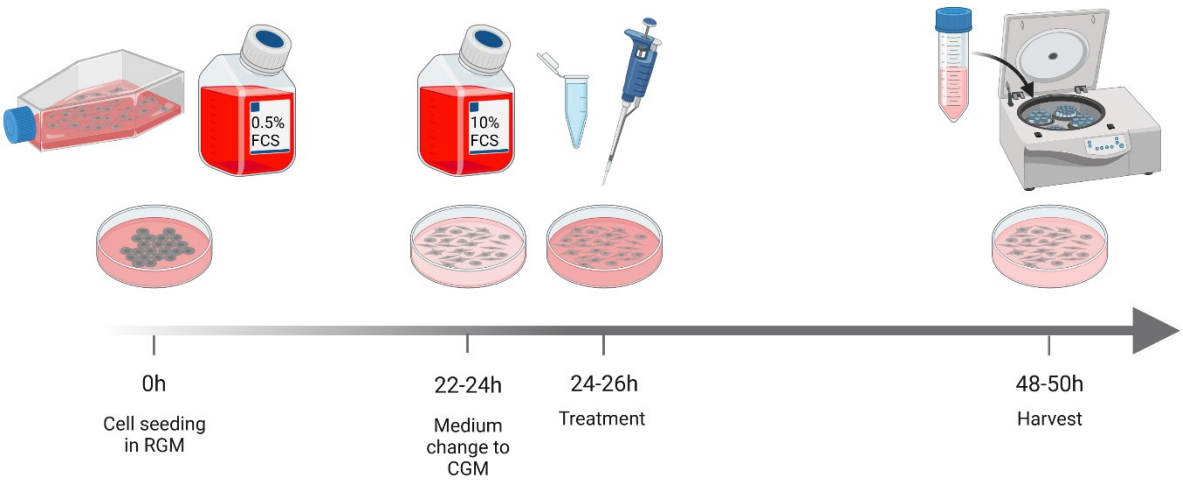

Figure 3.2: General cell culture workflow for cell cycle synchronization and following treatment.

3.3.1.2 Inhibitor treatment

For inhibitor treatment experiments, cells were seeded according to 3.3.1. After cell cycle synchronization, as described in 3.3.1.1 medium was changed to the respective CGM, according to Figure 3.2. 2 h after this, cells were treated with DMSO as the vehicle control or the indicated inhibitors for 24 h.

3.3.1.3 High cellular density

For high cellular density experiments, different amounts of cells were seeded into 6-well (mRNA) or 100 mm dishes (protein, cell cycle). Table 18 provides the respective cell numbers and volumes. For better reproducibility, cells were seeded in RGM for reversible cell cycle synchronization, as described in 3.3.1.1. After 24 h, the medium was changed to CGM according to Figure 3.2, and cells were incubated for 24 h at 37°C, 5% CO_2.

Table 18: Cell seeding densities for high cellular density experiments.

Seeding density (6-well) x10^6	[mL] (6-well)	Seeding density (100 mm) x10^6	[mL] (100 mm)
0.4	2	2.4	12
0.8	2	4.7	12
1	2	5.9	12
2	2	11.8	12
3	2	17.7	12

3.3.1.4 Low extracellular pH

For pH treatment experiments, cells were seeded according to 3.3.1. After 24 h, the medium was changed to pH-adjusted CGM prepared according to Table 19, and cells were incubated for 24 or 48 h. Cells treated with standard CGM (DMEM for both cell lines, since no McCoys 5A powder medium is available) or prepared CGM with an adjusted pH of 7.4 served as controls.

Table 19: Composition of pH-adjusted DMEM medium

pH	Composition	Supplements
pH 7.4 pH 6.8 pH 6.5	6.69 g powdered DMEM, 2.98 g HEPES, and 3.78 g PIPES dissolved in a final volume of 500 mL ultra-pure water. pH was first adjusted to 8.5 to dissolve PIPES using NaOH, then adjusted to the indicated pH using HCl	10% FCS,1% PS, 1% sodium pyruvate

3.3.2 Multi-cellular tumor spheroid culture

For MCTS formation, $0.05x10^6$ cells were seeded into low adherence 96-well plates (CellCarrier Spheroid ULA microplate, Perkin Elmer, Waltham, MA, USA) using 200 µL CGM or into agarose coated 24-well plates (1% ultra-pure agarose in PBS, 300 µL) using 700 µL CGM. Spheroids were allowed to grow for 4 or 7 days. The respective monolayer controls were prepared as described in 3.3.1, with a medium change after 24 h, and were harvested after 48 h. 4-day and 7-day monolayer cells were seeded in 12-well plates at a density of $0.05x10^6$ per well in 2 mL CGM, with no medium change during their culture.

For cell cycle analysis experiments, 4-day and 7-day monolayer cells were seeded in 100 mm dishes, using $0.81x10^6$ cells in 10 mL CGM, with no medium change during their culture.

3.3.3 General cell harvest procedure

3.3.3.1 RNA samples

If cells were cultured for RNA extraction and further analysis, the culture medium was discarded after the indicated incubation time. Then, the wells were washed once using 2 mL ice-cold PBS. Afterward, cells were lyzed as described in 3.4.1.

3.3.3.2 Protein samples

If cells were cultured for protein analysis, the culture medium was discarded after the indicated incubation time, and the dishes (100 mm) were washed once using 10 mL ice-cold PBS. Afterward, cells were scraped off the plate using a cell lifter while overlayed with 10 mL of ice-cold PBS. The cell suspension was transferred to 50 mL tubes previously placed on ice. Dishes were washed with another 10 mL of ice-cold PBS. After centrifugation (340 rcf, 5 min, 4°C), the supernatant was discarded, and the remaining pellet was resuspended in 1 mL ice-cold PBS. The cell suspension was transferred into a 1.5 mL tube. After centrifugation (357 rcf, 5 min, 4°C), the supernatant was again discarded, and the remaining cell pellet was lyzed, as described in 3.5.1.

The same procedure was performed for MCTS. However, spheroids were collected with their CGM from the wells; therefore, an extra centrifugation step (340 rcf, 5 min, 4°C) was performed before washing the spheroids.

If cells were cultured in well-formats smaller than 100 mm, cells were detached using TE. Therefore, wells were washed with appropriate amounts of warm PBS and detached using 0.5 mL warm TE per well (12-well plate, 1 mL per well for 6-well plates). After 5-10 min, the reaction was stopped using 1.5-2 mL CGM. Cell suspensions were pooled, and supernatants were discarded after centrifugation (340 rcf, 5 min, RT). The remaining Pellet was washed once using 10 mL of ice-cold PBS. After centrifugation (340 rcf, 5 min, 4°C), the supernatant was discarded, and the remaining pellet was resuspended in 1 mL ice-cold PBS. The cell suspension was transferred into a 1.5 mL tube. After centrifugation (357 rcf, 5 min, 4°C), the supernatant was again discarded, and the remaining cell pellet was lyzed, as described in 3.5.1.

3.3.3.3 Intact cells

If cells were cultured for lipid mediator analysis, cells were detached using TE. Therefore, cells were washed with 5 mL warm PBS and detached using 3 mL warm TE. After 5-10 min, the reaction was stopped using 7 mL CGM. After centrifugation (340 rcf, 5 min, RT), the supernatant was discarded. The remaining pellet was washed once using 10 mL of ice-cold PBS. After centrifugation (340 rcf, 5 min, 4°C), the supernatant was discarded again, and the remaining pellet was resuspended in ice-cold PBSG.

3.3.4 Cell viability and cytotoxicity

3.3.4.1 General cell culture procedure for viability and cytotoxicity assays

The influence of used inhibitors on cell proliferation and cytotoxicity was determined by WST-1 and LDH assay. Therefore, $0.03x10^6$ HT-29 and $0.03x10^6$ HCT-116 cells per well were seeded into 96-well plates using 100 µL RGM. For LDH assays, medium without phenol red and pyruvate was used. After 22 h medium was changed to CGM for 2 h. Then, the medium was changed to 100 µL CGM containing DMSO or inhibitors. Cells were treated with medium containing 1% Triton-X-100 to determine the maximal LDH activity for the respective cell line.

WST-1 cell proliferation assay

For determination of cell proliferation, cells treated with inhibitors for 24 h were incubated with 10 µL WST-1 reagent for 1 h at 37°C. Absorbance was measured at 450 nm/690 nm using the infinite M200 plate reader.

LDH cytotoxicity assay

For determination of cytotoxicity, 100 µL supernatant of cells treated with inhibitors for 24 h were transferred into a new 96-well plate. Supernatants were then mixed with 100 µL reaction mixture (according to the manufacturer's protocol) and incubated for 30 min, protected from light. Absorbance was measured at 490 nm/620 nm using the infinite M200 plate reader. In order to determine the percentage of cytotoxicity, the average absorbance values of the triplicates were calculated, and the average absorbance of the background control was subtracted from each sample. Then, samples were normalized to the Triton-X-100 control, and values were multiplied by 100.

3.3.5 Cell cycle analysis

3.3.5.1 General cell culture procedure and harvest for cell cycle analysis

For cell cycle analysis after serum starvation, cells were harvested after 22 h. Cells for cell cycle analysis after inhibitor treatment were subjected to a medium change using 10 mL CGM. Samples were treated after 2 h for a period of 24 h using 10 µL DMSO or the indicated inhibitors.

After serum starvation or inhibitor treatment, cells were washed using 10 mL PBS and harvested using 3 mL TE per 100 mm dish. The reaction was stopped using 7 mL of fresh CGM. The resuspended cells were separated using a 20 µm cell strainer and placed into a 15 mL tube. After counting, cells were centrifuged (340 rcf, 5 min at RT). The supernatant was discarded, and the

pellet was resuspended in 5 mL PBS. Following another centrifugation step, cells were resuspended according to $4x10^6$ cells/mL and placed on ice.

3.3.5.2 Fixation and staining

For fixation, 500 µL of the prepared cell suspensions were added dropwise to 4.5 mL ice-cold EtOH while vortexing to avoid clumping. Afterward, the tubes were placed at -20°C overnight. Before staining, fixed cells were centrifuged (873 rcf, 5 min at RT) and washed using 10 mL ice-cold PBS twice. The cell pellet was resuspended in 500 µL staining buffer (PBS + 0.1% Triton-X-100, 0.2 mg/mL RNAse A, 0.02 mg/mL PI) and placed into FACS tubes. Staining was performed for 30 min at RT, light protected. Afterward, samples were stored at 4°C.

3.3.5.3 Flow cytometer measurements and analysis

Samples were measured using a FACSVerse flow cytometer. Samples were vortexed properly before measurement. BD FACSFlow™ was used as sheath fluid. The percentages of G0/G1, S, and G2/M cells were calculated using FlowJo (V10.6) software. Before applying the cell cycle analysis tool, sample sets were gated, plotting PI-A vs. PI-W to determine single cells.

3.4 Investigations on RNA level

3.4.1 RNA extraction and purification

Total RNA was extracted from cells using TRIzol reagent. Therefore, 1-10x10^6 cells were lyzed in 1 mL TRIzol. After at least 24 h at -80°C, RNA was extracted with chloroform, according to the manufacturer's protocol. For precipitation, 1 µL GlycoBlue™ coprecipitant was used per sample. Extracted RNA pellets were resuspended in 20-30 µL warm RNase/DNase-free water. RNA concentrations and purity were determined using a NanoDrop™ 2000 spectrophotometer based on the absorbance ratios A260/280 and A260/230.

3.4.2 DNAse I digestion and RNA precipitation

Extracted RNA was digested with DNase I, according to the manufacturer's protocol. Digested preparations (11 µL per sample) were mixed with 55 µL 100% EtOH, 1.1 µL 3 M NaAc, and 0.5 µL GlycoBlue™ coprecipitant for precipitation. Mixes were scaled up if necessary, and samples were stored at -80°C overnight. Samples were incubated for 10 min on ice prior to centrifugation for 30 min, 12,000 rcf, 4°C. Pellets were washed with 500 µL ice-cold RNase-free 70% EtOH twice. Finally, purified RNA pellets were resuspended in 20 µL warm RNase/DNase-free water. RNA concentrations and purity were determined using a NanoDrop™ 2000 spectrophotometer based on the absorbance ratios A260/280 and A260/230.

3.4.3 RNA integrity

To make sure that the RNA purification led to intact RNA, the integrity was determined. Therefore, 1 µg RNA in a total volume of 2 µL was mixed with 2 µL of 2x RNA loading dye. Samples, as well as RiboRuler High Range RNA Ladder, were incubated for 10 min at 70°C. Samples were separated by gel electrophoresis (1% agarose gel, Ethidium bromide 0.001%, TAE buffer) for 45 min at 100 V. Bands were visualized on a Biovision 1000/26mx system, and 28s/18s rRNA ratios were checked.

3.4.4 cDNA synthesis

cDNA was prepared using DNAse I digested purified RNA (2 µg). Therefore, the High-Capacity RNA-to-cDNA™ Kit was used according to the manufacturer's protocol. Samples were diluted afterward according to 10 ng/µL RNA equivalents (1:10).

3.4.5 qPCR analysis

Relative quantification of mRNA content was performed by qPCR analysis using 20 ng (if not indicated otherwise) cDNA (RNA equivalent) with the Power SYBR™ Green PCR Master Mix on a StepOnePlus System. Reactions were performed in a final volume of 20 µL. Reaction mix compositions are described in Table 20. Sample measurements were performed in triplicates for every individual experiment. Table 21 states the exact PCR temperature and time parameters applied. A list with all specific primer target sequences is provided in Table 22.

Table 20: qPCR reaction mix composition.

Master mix components for one reaction	**[µL]**
Power SYBR™ Green	10
H_2O	7.88
Forward primer [100 pmol/µL stock]	0.06
Reverse primer [100 pmol/µL stock]	0.06

Table 21: qPCR program sequence and parameters.

Sequence	**Temperature [°C]**	**Time**
Initial denaturation	95	10 min
40 cycles	95	15 sec
	60	1 min
Melt curve	95	15 sec
	60	1 min
	0.3 steps up to 95	

Table 22: qPCR Primer and respective nucleotide accession numbers (NM).

Gene	**Forward primer 5´-3´**	**Reverse primer 5´-3**	**NM**	**Product size [bp]**
ACTB	AGA GCT ACG AGC TGC CTG AC	AGC ACT GTG TTG GCG TAC AG	NM_001101.5	184
ALOX5	CCC GGG AGA TGA GAA CCC TA	CCA GCA GCT TGA AAA TGG GG	NM_000698.5	200
BAX	CCC GAG AGG TCT TTT TCC GAG	CCA GCC CAT GAT GGT TCT GAT	NM_001291430.2	155
E2F1	GAG GAG ACC GTA GGT GGG AT	GGA CAA CAG CGG TTC TTG C	NM_005225.3	183
E2F2	GAG TCA GAG GAT GGG GTC CT	AAA CAT TCC CCT GCC TAC CC	NM_004091.4	156
E2F3	GGA GCT AGG AGA AAG CGG TC	TGA GGG AGA TTT TGG AGT TTT TGG	NM_001949.5	115
E2F4	TGC AGA TGC TTT GCT GGA GAT	CCA GCA GAA CCT CAA TGG GA	NM_001950.4	148

Gene	Forward primer 5´-3´	Reverse primer 5´-3	NM	Product size [bp]
E2F5	GTT CTG GAT CTC AAA GCG GC	CAG CAC CTA CAC CTT TCC ACT	NM_001951.4	141
FOXO1	TCG TCA TAA TCT GTC CCT ACA CA	CGG CTT CGG CTC TTA GCA AA	NM_002015.4	168
FOXO3	CGG ACA AAC GGC TCA CTC T	GGA CCC GCA TGA ATC GAC TAT	NM_001455.4	150
MYB	GCA GGT GCT ACC AAC ACA GA	CGA GGC GCT TTC TTC AGA TA	NM_001130173.2	175
MYBL2	CCA GCC ACT TCC CTA ACC G	CAG TGT CCA CTG CTT TGT GC	NM_002466.4	152
MYC	GTC AAG AGG CGA ACA CAC AAC	TTG GAC GGA CAG GAT GTA TGC	NM_002467.6	162
SP1	AGT TCC AGA CCG TTG ATG GG	GTT TGC ACC TGG TAT GAT CTG T	NM_138473.3	101
TP53	CTG GAT TGG CAG CCA GAC T	TCC GGG GAC AGC ATC AAA TC	NM_000546.6	180
LTC4S	GTC TAC CGA GCC CAG GTG AA	GCG TAG CCC TGG AAG TAG C	NM_145867.1	149
ALOX15	GGG GCA AGG AGA CAG AAC TC	GCG CTA ACA AGG GAA CCT GA	NM_001140.5	167
ALOX15B	CTA CAG GCT GGC TCT GCT TT	GGA TCA GGA CAG GGT TGA GA	NM_001039130.2	199
PIK3CB	TAT TTG GAC TTT GCG ACA AAG ACT	TCG AAC GTA CTG GTC TGG TAG	NM_006219.3	190
PIK3CD	AAG GAG GAG AAT CAG AGC GTT	GAA GAG CGG CTC ATA CTG GG	NM_005026.5	138
PIK3CG	GGC GAA ACG CCC ATC AAA AA	GAC TCC CGT GCA GTC ATC C	NM_002649.3	150
PTGS1	TCT TGC TGT TCC TGC TCC TG	CAC AGG CCA GGG ATG GTG	NM_000962.4	196
PTGS2	CTC CCT TGG GTG TCA AAG GTA AA	GGC CCT CGC TTA TGA TCT GT	NM_000963.4	172

3.5 Investigations on protein level

3.5.1 Cell lysis

All samples (except PMNL) for Western blot analysis were lyzed in 100-200 µL (dependent on the used cell number) of RIPA lysis buffer. Before use, the lysis buffer was supplemented with fresh protease (cOmplete™ Mini) and phosphatase (PhosSTOP™) inhibitors, as described in the manufacturer's protocols. Lysates were kept on ice for 10 min before storing the samples overnight or until further use at -80°C. After thawing on ice, lysates were sonicated (MS72, Bandelin Sonopuls HD 200) three times for 10 sec at the lowest pulse rate to remove DNA jelly. The remaining debris was removed through centrifugation (10,000 rcf, for 10 min at 4°C). Supernatants were transferred into new 1.5 mL tubes, and pellets were discarded. Lysates were stored at -20°C.

Freshly isolated PMNL were lyzed in 200 µL hot (95°C) SDS lysis buffer. Before use, the lysis buffer was supplemented with fresh protease (cOmplete™ Mini 2x) and phosphatase (PhosSTOP™) inhibitors, as described in the manufacturer's protocols. After lysis, samples were incubated for 10 min at 95°C. Then, lysates were sonicated (MS72, Bandelin Sonopuls HD 200) three times for 10 sec at the lowest pulse rate to remove DNA jelly. The remaining debris was removed through centrifugation (10,000 rcf, for 10 min at 4°C). Supernatants were transferred into new 1.5 mL tubes, and pellets were discarded. Lysates were stored at -80°C. Samples were further processed for SDS-PAGE and Western blot analysis on the same day.

3.5.2 Determination of protein concentration

Protein concentrations were quantified using the Pierce™ BCA Protein Assay Kit according to the manufacturer's protocol. Absorbance was measured with an infinite M200 multiplate reader at 562 nm. Concentrations were calculated by preparing a dilution series of BSA with each assay to fit a standard curve.

3.5.3 SDS-PAGE

For SDS-PAGE, protein samples were diluted and mixed with 5x loading dye and boiled at 96°C for 5 min. Identical total protein amounts per lane (30-60 µg in 10-30 µL) were separated using 10% self-cast (1 mm or 1.5 mm) or 4-15% (1 mm) pre-cast gels. PageRuler™ Plus Prestained Protein Ladder or Spectra™ Multicolor High Range Protein Ladder were used as molecular weight markers. Gels were run using ice-cold 1x running buffer, applying the parameters listed in Table 23.

Table 23: Used SDS-PAGE parameters.

Gel	Parameters
10%	10 min, 100 V ~45 min, 200 V
4-15%	45 min, 200 V

3.5.4 Protein immunoblotting

Western blot transfer to nitrocellulose membranes (0.2 µm) was performed employing the classic wet tank method or a semi-dry method using the Trans-Blot Turbo transfer system. Therefore, ice-cold 1x Towbin transfer buffer or 1x Trans-Blot Turbo buffer was used. Transfer stacks were packed according to the manufacturer's protocol. Used parameters for protein transfer to nitrocellulose membranes are provided in Table 24.

Table 24: Used protein immunoblot methods and parameters.

Method	Parameters
Wet tank blotting	100 V, 85 min, ice-cold buffer
Semi-dry (TransBlot Turbo)	Mixed MW, 2 gels, 1 mm: 2.5 A, up to 25 V, 7 min (12 min if 1.5 mm gels were used) High MW, 2 gels. 1 mm: 2.5 A, up to 25 V, 10 min

After blotting, membranes were blocked with EveryBlot Blocking Buffer for 1 h at RT. Then, membranes were incubated with primary antibodies directed against the respective target proteins, as stated in Table 25. Membranes were washed with TBST (3x) at RT. Afterward, membranes were incubated with the respective fluorescence-conjugated secondary antibodies (diluted 1:15,000) for 1 h at RT. After washing with TBST (3x) and TBS (1x), the protein antibody complexes were visualized using the Odyssey Infrared Imaging System, and immune reactive bands were quantified with the Image Studio 5.2 software.

Table 25: Used primary antibodies, dilutions, and incubation conditions.

Antibody	Species	Dilution	Incubation condition
5-LO (abcam)	rabbit	1:1,000	4°C, overnight
5-LO (ProteinTech)	mouse	1:2,000	4°C, overnight or 3 h, RT
b-Myb	rabbit	1:500	4°C, overnight
$cPLA_{2\alpha}$	rabbit	1:500	4°C, overnight
ERK 1/2	rabbit	1:1,000	4°C, overnight
FLAP	goat	1:500	4°C, overnight
LTA_4H	mouse	1:500	3 h, RT
MEK-1	mouse	1:2,000	3 h, RT
mTOR	rabbit	1:1,000	4°C, overnight
p110α	rabbit	1:1,000	3 h, RT
p53	mouse	1:1,000	4°C, overnight
p70S6K	mouse	1:500	4°C, overnight
Phospho-ERK1/2	mouse	1:200	4°C, overnight
Phospho-p70S6K	rabbit	1:1,000	4°C, overnight
PRKCζ	mouse	1:400	3 h, RT
Raptor	mouse	1:400	3 h, RT
Rictor	mouse	1:400	3 h, RT
α-Tubulin (SantaCruz)	mouse	1:1,000	1 h, RT
α-Tubulin (abcam)	rabbit	1:5,000	1 h, RT

3.5.5 Histological and immunofluorescent staining of MCTS cryosections

3.5.5.1 Spheroid embedding and cryosectioning

For embedding spheroids prior to cryosectioning, half of a 96-well plate (per cell line, per time point) was transferred into a 50 mL tube. After settling the spheroids, the supernatant was discarded, and the spheroids were transferred into 1.5 mL tubes. Spheroids were washed with 1 mL ice-cold PBS and fixated with 1 mL 4% paraformaldehyde (PFA) solution in PBS for 30 min (800 rpm, at RT, Eppendorf Thermomixer). Afterward, spheroids were washed with 1 mL ice-cold PBS and placed in a serial dilution of PBS buffered sucrose solution (10%, 20%, 30%, at 28°C, 800 rpm, Eppendorf Thermomixer). Solutions were replaced every 30 min.

Embedding was carried out in Tissue-Tek® Cryomold® embedding molds. Spheroids were placed at the center of an embedding mold, and the remaining sucrose solution was carefully removed. The embedding mold was slowly filled with tissue freezing medium and immediately placed onto a metal block precooled to -80°C. When fully frozen, samples were stored at -80°C.

Before sectioning, preparations were tempered at -20°C. For sectioning, a CryoStar cryostat microtome was used. Mold-embedded samples were attached to a cryostat specimen chuck using tissue-freezing medium. After 5-10 min, the probed specimen chuck was fastened to the cryostat, and sections of 14 µm were prepared. Specimens were mounted on Superfrost®Plus adhesive microscope slides. Afterward, samples were dried for 2 h at room temperature before storage at -80°C.

3.5.5.2 Histological sample preparation

For histological sample preparation of spheroid cryosections, stored slides were thawed at RT for 10 min. Adhesive tissue freezing medium was removed by rinsing the slides with PBS. Then, the slides were incubated for 30 sec in Mayer´s Hematoxylin. After washing with PBS, nuclei were blued in Scott's tap water solution for 20 sec. Samples were then dehydrated in 70% and 95% EtOH for 30 sec, successively. For counterstaining, slides were incubated in alcoholic eosin for 30 sec. Before mounting, samples were washed through 2 changes of 95% EtOH and 3 changes of 100% EtOH before clearing through three changes of xylene. Finally, slides were mounted with coverslips using ~200 µL of Entellan rapid mounting medium. After 30 min, samples were sealed using clear lacquer.

3.5.5.3 Immunofluorescent sample preparation

For immunofluorescent sample preparation of spheroid cryosections, stored slides were thawed at RT for 10 min. Adhesive tissue freezing medium was removed by rinsing the slides intensively with ice-cold PBS for 10 min. Samples were blocked using 1% BSA with 2.2% glycine in PBS for 1 h at RT. Then, a Super PAP Pen was used to circle the specimens on the slides to reduce the amount of primary and secondary antibody solution necessary for staining. Samples were stained with primary antibodies (see Table 26) diluted in PBSB (PBS containing 1% BSA) for 3 h at RT or overnight at 4°C. After intensive rinsing with PBS, samples were incubated with secondary antibodies diluted in PBSB (1:2,000) for 1 h at RT (light protected). Samples were rinsed

intensively with PBS, and counterstaining was performed using DAPI diluted in PBS (1:1,000) for 1 h at RT (light protected). Stained slides were mounted using 150-200 µL Mowiol mounting medium with Menzel coverslips. Mounted samples were left to dry overnight at RT and sealed using clear nail polish.

Prepared samples were imaged on a Zeiss 780 AxioObserver.Z1 laser-scanning confocal microscope, equipped with an Argon laser and a He/Ne 633 nm laser, using a Zeiss Plan-Neofluar 40x/1.3 NA oil lens. The same pinhole size was applied for all measurements. In separate tracks, samples were excited with 405, 488, and 633 nm lasers. 3 x 3 or 4 x 4 tile scans were acquired using GaAsP and PMT detectors. A line average of 8 was applied to all channels. Pictures were analyzed and processed using the Zeiss Zen blue software. Identical linear histogram adjustments were applied to each channel to adjust brightness and contrast. 5-LO knockout cells and secondary antibody control stainings were used to adjust optimal gain and digital offset parameters for each measurement.

Table 26: Primary antibodies used for indirect immunofluorescent confocal microscopy.

Antibody	**Species**	**Dilution**	**Incubation condition**
5-LO (ProteinTech)	mouse	1:50	4°C, overnight
Ki67	rabbit	1:1,000	4°C, overnight
Cleaved Caspase-3	rabbit	1:400	4°C, overnight

3.6 Lipid mediator analysis

3.6.1 5-LO activity assay

For lipid mediator formation in intact untreated or inhibitor-treated HT-29 and HCT-116 cells, cells were prepared according to Figure 3.2. After harvest, cells were washed and resuspended in ice-cold PBSG buffer (according to $10x10^6$ cells/mL).

For lipid mediator formation in intact human PMNL, cells were prepared as described in 3.2.5.4. Cells were resuspended in ice-cold PBSG buffer. The concentration was dependent on the respective experiment (typically $5x10^6$ or $10x10^6$ cells/mL).

For lipid mediator formation in intact human macrophages, cells were prepared as described in 3.2.5.3. Cells were resuspended in ice-cold PBSG buffer. Here, four 100 mm dishes of each donor were harvested, and cells were washed. After centrifugation (314 rcf, 5 min, 4°C), cells were resuspended in 1 mL ice-cold PBSG buffer. Since macrophage cell numbers were highly donor-dependent, total protein amounts for each sample were analyzed, and lipid mediator formation was normalized to total protein content. The same procedure was performed if tumor cells and human PMNL were compared with human macrophages.

Lipid mediator formation was initiated by stimulation with 2.5 µM Ca^{2+} ionophore (A23187) or 5 µM S1P and 20 µM ARA or a mixture of 6 µM ARA, DHA, and EPA. After 10 min, the reactions were stopped by the addition of 1 mL ice-cold methanol. Supernatants were separated by centrifugation (872 rcf, 10 min, 4°C) and stored at -80°C until further analysis.

A mixture of PBSG buffer and 100% MeOH (1:2) was prepared as a surrogate matrix for dilution purposes during lipid mediator extraction.

3.6.2 Liquid chromatography electrospray ionization MS/MS analysis

Lipid mediators were analyzed by liquid chromatography-electrospray ionization tandem mass spectrometry (LC-ESI-MS/MS). Therefore, 200 µL assay supernatant (or 10 µL sample diluted to 200 µL with surrogate matrix) was spiked with 20 µL MeOH, 20 µL methanolic IS working solution, and 100 µL 0.15 M EDTA solution. Mixtures were extracted twice using 600 µL ethyl acetate in amber tubes. Organic phases were combined after extraction, following centrifugation (3 min at 20,000 rcf), and were evaporated at 45°C under a gentle stream of nitrogen in amber glass vials. Extracted samples were reconstituted in 50 µL MeOH/water (70:30, v/v) containing 0.0001% BHT. Reconstituted samples were transferred into inserts and injected into the LC-MS system. Calibration standards and quality control samples were prepared by spiking 200 µL surrogate matrix with 20 µL of the methanolic standard working solution and processed as described for the samples.

The LC-MS system consisted of a triple quadrupole mass spectrometer QTRAP 6500+ (Sciex, Darmstadt, Germany) equipped with a Turbo V Ion Spray source operated in negative electrospray ionization mode and an Agilent 1290 Infinity LC-system with binary HPLC pump, column oven and autosampler (Agilent, Waldbronn, Germany). The chromatographic separation was performed using an Acquity UPLC BEH C18 2.1x100 mm column and VanGuard Pre-Column 2.1 × 5 mm (both with a particle size of 1.7 µm, from Waters, Eschborn, Germany) for reversed-

phase separation of 34 analytes. A Lux Amylose-1® column (250 × 4.6 mm, 3 µm, 1,000 Å, from Phenomenex, Aschaffenburg, Germany) was used for chiral separation of 15R/S-HETE and 17R/S-HDHA. Analytes were eluted with gradient elution using water (solvent A) and acetonitrile (solvent B) containing 0.0025% formic acid, respectively. More information about calibration ranges, gradient programs, and mass spectrometric parameters can be found in the appendix.

Data acquisition was performed using Analyst Software 1.7.1 (Sciex, Darmstadt, Germany), and quantification was executed using MultiQuant Software 3.0.3 (Sciex, Darmstadt, Germany), employing the internal standard method (isotope dilution mass spectrometry). Calibration curves were calculated by linear regression with 1/x weighting.

LM extraction and analysis were performed by the Gurke/Thomas laboratory at the Institute of Clinical Pharmacology (Pharmazentrum Frankfurt, ZAFES, Goethe-University).

3.7 Reporter gene experiments

For reporter gene assays, an in-house produced substrate buffer was developed, and results were normalized to cellular GFP expression.

Therefore, $0.03x10^6$ cells (stably transfected HT-29 or HCT-116 reporter cells) were seeded into black 96-well µCLEAR® plates using 100 µL RGM per well. For faster and stronger adherence, plates were centrifuged (300 rcf, 5 min, RT). After 22 h, 100 µL CGM with 17.5% FCS was added to each well to achieve the final FCS concentration of CGM. After 2 h of incubation (37°C, 5% CO_2), the medium was changed to CGM containing the respective inhibitors or the vehicle control (DMSO). After 24 h of inhibitor incubation (37°C, 5% CO_2), GFP expression and firefly luciferase (Fluc) activity were measured using the Spark multimode plate reader. Therefore, the medium was removed, and cells were washed with 100 µL warm PBS once. The GFP signal was measured in 75 µL warm PBS (Ex 485(20)/Em 520(10), optimal gain). To measure Fluc activity, 75 µL substrate buffer (Table 27) per well was added, and plates were agitated at low speed for 20 min at RT, light protected. Then, 140 µL of each well was transferred into white LUMITRAC 96-well plates, and the Fluc activity was measured (1,000 ms integration time). For analysis, the ratio of measured Fluc activity and the GFP expression signal was determined. Results were then normalized to the respective vehicle control.

Table 27: Substrate buffer composition for reporter gene assay.

Component	Concentration
HEPES pH 7.8	74.9 mM
DTT	49.9 mM
$MgSO_4$	4 mM
AMP	895 µM
EDTA	785 µM

Component	Concentration
ATP	488 µM
D-luciferin	469 µM
NaS_2O_4	287 µM
Coenzyme A	135 µM
Tween20	0.33%
Triton-X-100	1%

3.8 Cloning

Respective maps of all plasmids prepared, as well as a list of all primers used for cloning, can be found in the appendix. Table 28 states all prepared plasmids.

A human cDNA clone of ‘homo sapiens b-Myb’ was purchased from BioCat GmbH, Heidelberg, Germany.

Table 28: Prepared plasmids with used backbones and inserts.

Plasmid name	Backbone	Description
pSBbiGP_MYBL2	pSBbiGP	MYBL2 gene
pSBGP_LUC	pSBGP_LUC	pSBtet-GP, promoterless, carries the firefly luciferase gene
pSBGP_BaxLUC	pSBGP_LUC	Bax promoter construct
pSBGP_p53LUC	pSBGP_LUC	p53 promoter construct
pSBGP_pN0LUC	pSBGP_LUC	pN0 promoter construct
pSBGP_pN10LUC	pSBGP_LUC	pN10 promoter construct
pSBGP_pN10p53LUC	pSBGP_LUC	pN10p53 promoter construct
pSBGP_pN6LUC	pSBGP_LUC	pN6 promoter construct
pSBGP_pN6ΔMYBLUC	pSBGP_LUC	pN6 promoter construct, deleted MYB binding site
pSBGP_SV40_5LOcds 1600delLUC	pSBGP_LUC	SV40 promoter, shortened 5LO gene (1600 nts deleted from 3' end), fusion protein with firefly luciferase
pSBGP_SV40_5LOcds 1600delmutMYBLUC	pSBGP_LUC	SV40 promoter, shortened 5LO gene (1600 nts deleted from 3' end, mutated cds MYB

Plasmid name	Backbone	Description
		binding side) fusion protein with firefly luciferase
pSBGP_SV40_5LOcds 1699delLUC	pSBGP_LUC	SV40 promoter, shortened 5LO gene (1699 nts deleted from 3' end) fusion protein with firefly luciferase
pSBGP_SV40LUC	pSBGP_LUC	SV40 promoter construct, control
pSBtetGP_LV	pSBtetGP	non-coding sequence in MCS
pSBtetGP_MYBL2	pSBtetGP	MYBL2 gene

3.8.1 Methods for DNA preparation

3.8.1.1 Polymerase chain reaction

Polymerase chain reactions (PCRs) were carried out using the Q5® High-Fidelity DNA Polymerase. Reaction mixes were prepared according to the manufacturer's protocol. Table 29 states the exact PCR temperature and time parameters applied.

Table 29: Standard protocol for PCR reactions using Q5® High-Fidelity DNA Polymerase.

	Temperature [°C]	Time
Initial denaturation	98°C	30 sec
30 cycles	98°C	10 sec
	61°C	20 sec
	72°C	30-50 sec/kb
Final elongation	72°C	2 min
Storage	4°C	∞

Used primers were designed with an annealing temperature of approximately 56°C calculated using the 'Oligo Calc webtool'. PCR products were purified using the GeneJET PCR purification kit (if only the desired product emerged) or by agarose gel electrophoresis (see DNA isolation and purification) and the GeneJET Gel Extraction Kit. Both GeneJET PCR and GeneJET Gel Extraction and Purification Kits were used according to the manufacturer's protocol.

3.8.1.2 Restriction digest

Restriction digests were performed using restriction enzymes from NEB. In general, 1 µg DNA was digested in a 50 µL reaction, using one or two restriction enzymes with 1x Cutsmart buffer. Restriction digests were performed at 37°C for either 1 h or 15 min if 'time-safer qualified' enzymes were used. Depending on the respective enzyme, reaction mixtures were heat

inactivated at 65°C for 15 min or at 80°C for 20 min. If the digestion reaction was used for plasmid linearization, the product was purified using the GeneJET PCR Purification Kit according to the manufacturer's protocol. If a specific DNA fragment was needed, digested samples were separated by gel electrophoresis, and fragments were purified using the GeneJET Gel Extraction Kit.

3.8.1.3 DNA isolation and purification

Agarose concentration was adapted depending on the size of the expected product according to the manufacturer's protocol. For quantitative separation, the sample was taken and mixed with the respective amount of 6x DNA loading dye. Analytical gel electrophoresis was performed using only 5 µl of the respective sample mixed with 1 µl of 6x DNA loading dye. Agarose gel electrophoresis was performed in 1x TAE at 120 V for 25 min if only one fragment or fragments with large size differences (>1 kb) were analyzed. If separation of fragments with similar sizes was necessary, gels were run at 100 V for 45 min.

For the isolation of DNA fragments, bands were visualized at 312 nm using a UV-transilluminator. Samples were cut from the gel and transferred to 2 mL reaction tubes. Gel pieces were purified using the GeneJET Gel Extraction Kit according to the manufacturer's protocol.

3.8.1.4 Ligation and assembly of multiple DNA fragments

DNA fragments digested as described in 3.8.1.2 were ligated using T4 DNA Ligase (New England Biolabs). A molar ratio of 1:3 (vector to insert) was used for most reactions (calculated using the NEBioCalculator online tool). Ligation reactions (standard composition is shown in Table 30) were performed for 30 min at RT, followed by inactivation for 10 min at 65°C. Then, the reaction mix was placed on ice until transformation into *E. coli* was performed.

Table 30: Standard ligation composition.

Components	**Final amount**
T4 DNA ligase buffer (10x)	1x
Vector DNA	50-100 ng
Insert 1	3x molar amount of vector DNA
Insert 2 (optional)	3x molar amount of vector DNA
T4 DNA ligase	1 µL
H_2O	to 20 µL

For more complex cloning projects that could not be accomplished as described before, the NEBuilder® HiFi DNA Assembly Master Mix was used according to the manufacturer's protocol. This allowed the combination of up to five DNA fragments simultaneously. Vector DNA was linearized by PCR or by restriction digest, while inserts were prepared by PCR. Respective adjacent fragments were prepared to share a homologous region of about 20 bp. DNA fragments were combined by incubation for 15-60 min at 50°C following the manufacturer's manual.

3.8.2 Plasmid preparation

3.8.2.1 Transformation in *E. coli* and antibiotic selection

DNA was transformed into DH5a competent cells for vector amplification. Competent cells were thawed on ice for approximately 10 min. 50 µl of DH5α cells were incubated with 1 µl of DNA (50-100 ng) on ice for 30 min. After this, a heat shock was performed at 42°C for 45 s in a thermocycler, and cells were put on ice for 1 min afterward. Then, 500 µl SOC medium was added, and the transformed cells were incubated for 1 h at 37°C, 350 rpm. For antibiotic selection, cells were centrifuged (1,000 rcf, 2 min, RT), and the supernatant was discarded by inverting the tubes. The pellet was resuspended in the small amount of remaining supernatant, and 20 µl cell suspension was transferred on LB-agar plates containing the respective selection antibiotic. Plated agar plates were incubated at 37°C overnight until colony formation was visible. Colonized plates were stored at 4°C for up to one month.

Storage of transformed E. coli

E. coli cells were stored as glycerol stocks at -80°C. Glycerol stocks were prepared by diluting 800 µl of an overnight culture (in LB-medium containing the respective selection antibiotics) with 250 µl of 87% glycerol in cryovials. The tubes were directly stored at -80°C without any pre-cooling steps.

3.8.2.2 Vector DNA preparation

The amplification of vector DNA was either done in mini cultures (8 mL LB-medium) for newly assembled constructs or as maxi cultures (500 mL LB-medium) for already sequenced plasmids. MiniPrep amplifications were performed in LB-medium containing the respective selection antibiotic, inoculated with a clone from a selection LB-agar plate, and incubated at 37°C, 180 rpm overnight. MaxiPrep amplifications were performed in LB-medium containing the respective selection antibiotic and inoculated either with a clone from an LB-agar selection plate or with 500 µL transformation mix of an already sequenced plasmid. Incubation conditions were the same as described for small-scale amplifications.

Cells were harvested for either 10 min, 4°C, 4,000 rcf (MiniPrep) or 20 min, 4°C, 4,000 rcf (MaxiPrep). The amplified DNA was isolated from the cell pellets using either a MiniPrepKit (MiniPrep) or a MaxiPrepKit (MaxiPrep), according to the manufacturer's manual.

DNA concentrations were determined using a NanoDrop™ 2000 spectrophotometer.

3.8.2.3 DNA sequencing

Verification of new plasmids or sequence confirmation of bought plasmids was achieved using Sanger sequencing (Microsynth AG, Schweiz). Therefore, 1,000 ng DNA were used.

3.9 Statistical analysis

Statistical analysis was performed using GraphPad Prism7 (San Diego, CA, USA). Used statistic tests are described in each figure legend for the respective data set. Data are presented as mean + SEM.

4 Results

4.1 Expression of enzymes of the leukotriene cascade in MCTS of HT-29 and HCT-116 CRC cells

Tumor cells underlie various physicochemical parameters *in vivo,* which are not adequately mirrored during conventional monolayer culture. Thus, MCTS of the colorectal cancer cell lines HT-29 and HCT-116 were analyzed regarding their profile of enzymes of the leukotriene cascade. As described in chapter 2, this was already performed partly during a preliminary master's thesis in 2017. However, this time the aim was to examine if 5-LO expression is already upregulated within a shorter incubation period and to implement and investigate better-suited monolayer controls than cells taken from the respective maintenance culture. The cell lines U-2 OS and Capan-2 were excluded for MCTS formation from this study even though their 5-LO expression was the highest among the tested cell lines (Figure 2.1A). This decision was made due to the very loose spheroid formation seen for U-2 OS cells and insufficient formation of Capan-2 spheroids.

For MCTS formation, HT-29 and HCT-116 cells were seeded in special low adherence 96-well- or 24-well plates coated with ultra-pure agarose. Identical cell numbers were seeded for MCTS and monolayer controls. Due to their higher proliferation rate in monolayer culture, monolayer controls were seeded in 12-well plates instead. After growth for 4 or 7 days, spheroids and monolayers were harvested. During this incubation period, the medium was neither renewed nor changed. Hence, another monolayer control (co) was prepared to display optimal growth conditions. For this purpose, cells were seeded and harvested after 48 h with an approximate confluency of 70-80%. Medium was changed 24 h after seeding. All samples were analyzed via Western blotting towards the protein expression of 5-LO, $cPLA_{2\alpha}$, LTA_4H, and FLAP (Figure 4.1). MCTS formation already induced 5-LO expression significantly after 4 days. This induction was comparable to the results obtained after 7 days of culture independent of the method used for spheroid formation (densitometric data for 5-LO, $cPLA_{2\alpha}$, LTA_4H, and FLAP are displayed in App. Figure 7.1).

Interestingly, monolayer growth for 4 and 7 days also induced 5-LO expression in HT-29 (after 7 days) and HCT-116 cells (after 4 and 7 days). An inverse expression pattern was found for $cPLA_{2\alpha}$. Here, spheroid formation and monolayer growth for 7 days led to a downregulation of the protein expression. LTA_4H expression was strongly influenced by MCTS formation as well. No basal expression was found for HT-29 cells, but MCTS formation strongly induced LTA_4H expression. In HCT-116 cells, moderate LTA_4H expression was measurable; however, expression was again induced by MCTS formation and monolayer growth for 7 days. The expression of FLAP was not influenced under all tested conditions.

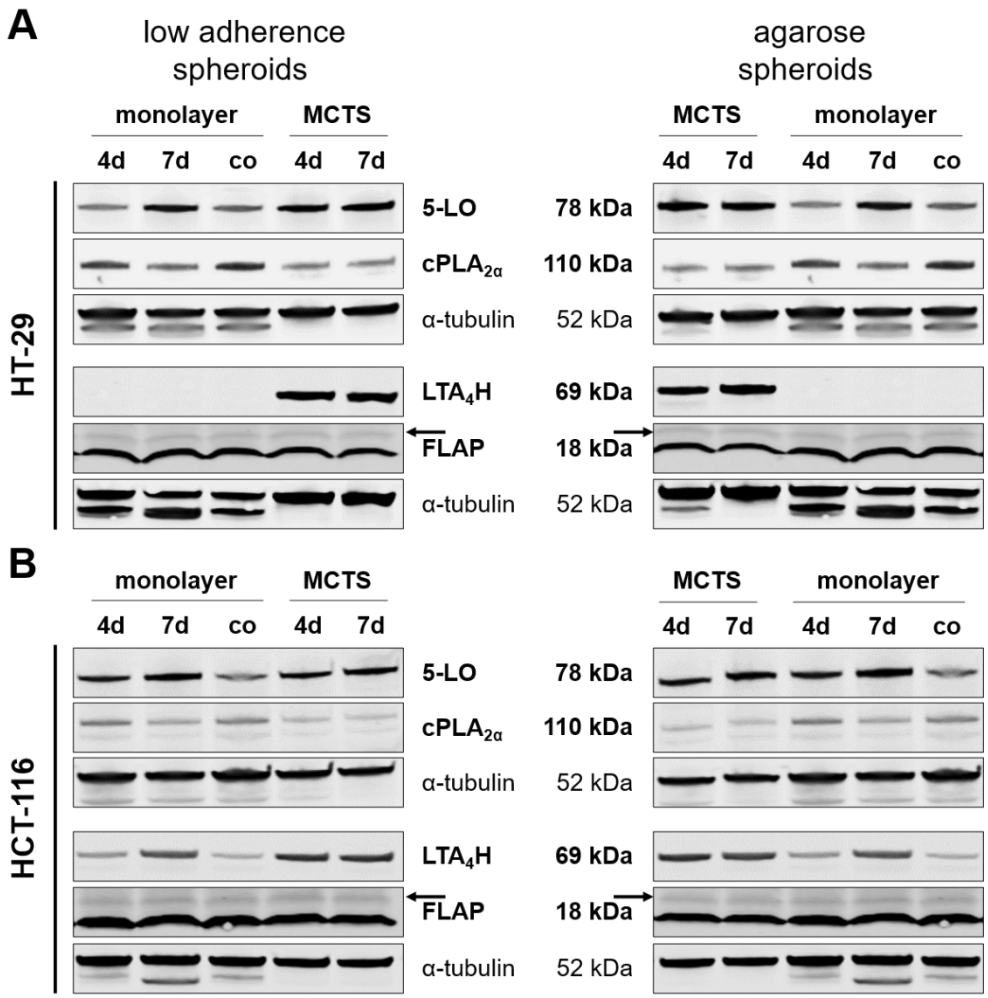

Figure 4.1: Protein expression of 5-LO and other members of the LT cascade in MCTS.
Protein expression of 5-LO, $cPLA_{2\alpha}$, LTA_4H, and FLAP in HT-29 (A) and HCT-116 (B) cells analyzed via Western blot. MCTS were either grown for 4 or 7 days in 96-well low adherence plates or 24-well plates coated with ultra-pure agarose (1%). Respective monolayer controls were seeded in 12-well plates. Identical cell amounts ($0.05x10^6$ cells/well) were used. The subconfluent monolayer controls (co) were seeded in 100 mm dishes ($3x10^6$ cells per dish), received a medium change after 24 h, and were harvested after 48 h. Same monolayer controls are displayed on the low-adherence and agarose spheroid blots. One representative blot out of 3 is shown.

Additionally, mRNA expression of *ALOX5*, *LTC4S,* and *ALOX15* was investigated via qPCR analysis. Results obtained for 5-LO protein expression could be confirmed on mRNA level; however, induction of *ALOX5* after MCTS formation and growth for 7 days was more pronounced in HCT-116 cells. Investigation of *LTC4S* expression revealed the same pattern as for *ALOX5*. *LTC4S* induction after MCTS formation and 7-day monolayer growth was more pronounced in HT-29 cells (up to 20-fold) than in HCT-116 cells (up to 3-fold). Unfortunately, the lack of a suitable antibody made it impossible to investigate LTC_4S protein expression. Notably, basal *LTC4S* expression was lower in HT-29 and HCT-116 monolayers than *ALOX5* expression (Figure 4.2B). To summarize, MCTS and monolayer growth for 4 or 7 days influenced the expression of members of the LT cascade potently, independent of the used MCTS formation method.

Interestingly, MCTS formation and 7-day monolayer growth induced *ALOX15* mRNA expression in both cell lines as well. However, basal *ALOX15* expression in monolayer-grown cells, as already seen for *LTC_4S,* was relatively low compared to *ALOX5* expression (Figure 4.2B). Nevertheless, basal *ALOX15* mRNA expression was more pronounced in HCT-116 cells

compared to HT-29 cells. Additionally, mRNA expression of *PTGS1* and *PTGS2* was analyzed (App. Figure 7.2). Like *ALOX5*, *PTGS1* expression was upregulated due to MCTS formation and monolayer growth for 7 days. *PTGS2* expression was predominantly upregulated after MCTS formation after 4 and 7 days. Basal *PTGS1* expression was higher compared to *PTGS2* expression in both investigated cell lines. However, the expression of *PTGS1* and *PTGS2* was more pronounced in HT-29 cells compared to HCT-116 cells.

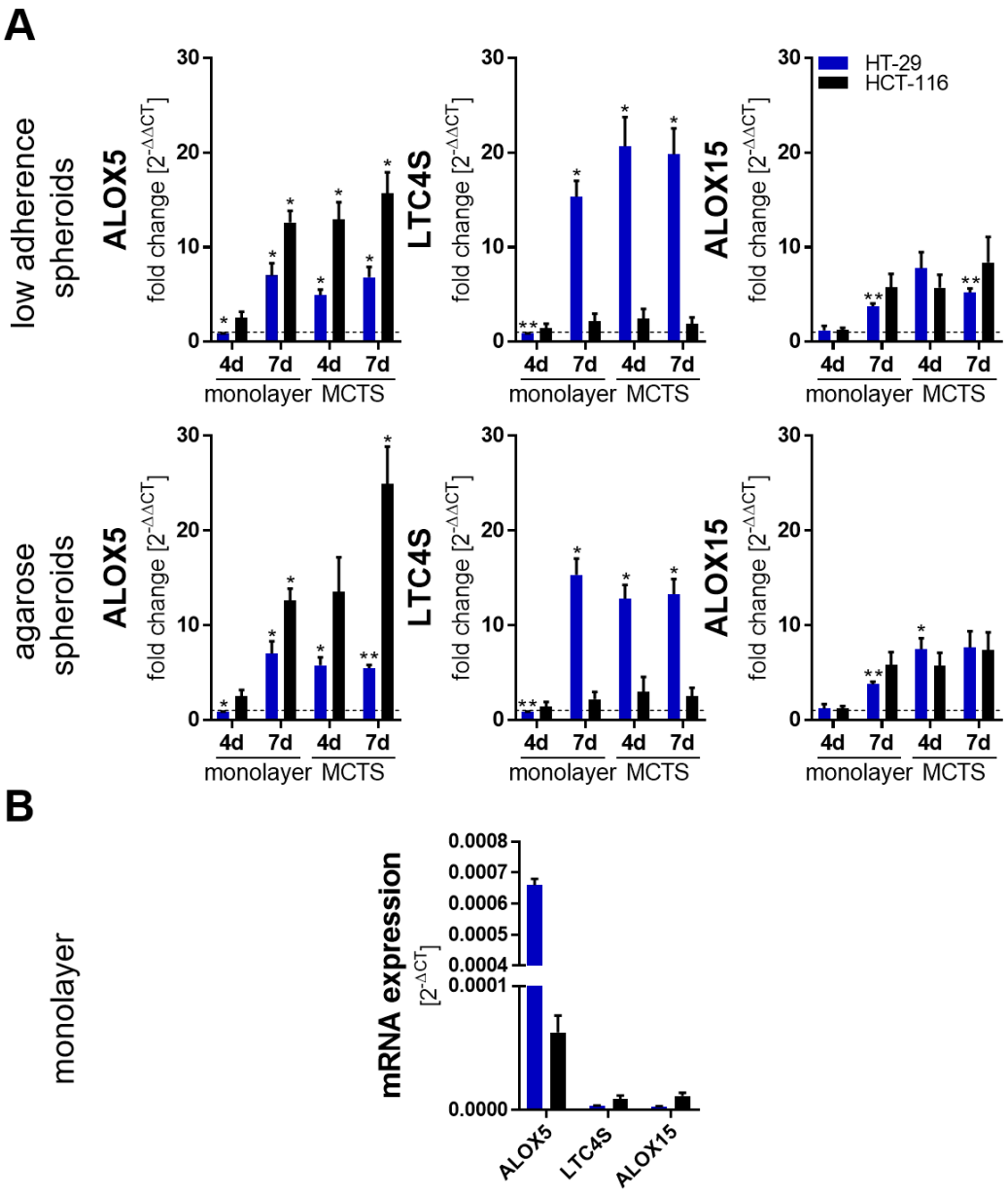

Figure 4.2: mRNA expression of *ALOX5*, *LTC4S,* and *ALOX15* in MCTS.
MCTS were either grown for 4 or 7 days in 96-well low adherence plates or 24-well plates coated with ultra-pure agarose (1%). Respective monolayer controls were seeded in 12-well plates. Same cell amounts ($0.05x10^6$ cells/well) were used. The subconfluent monolayer controls (co) were seeded in 6-well plates ($0.4x10^6$ cells per well), received a medium change after 24 h, and were harvested after 48 h. (A) Gene expression determined via qPCR analysis was normalized to the housekeeping gene *ACTB* and the respective monolayer control ($2^{-\Delta\Delta CT}$ method). (B) Comparison of monolayer gene expression normalized to *ACTB* ($2^{-\Delta CT}$). Results are depicted as mean + SEM from 3 independent experiments. Asterisks indicate significant changes vs. co determined by unpaired two-tailed student's t-test with Welch's correction. * (P<0.05), ** (P<0.01), *** (P<0.001).

4.1.1 Characterization of established MCTS and monolayer models

For further characterization, pictures of monolayers and MCTS were taken and analyzed. After 4 days of growth, both cell lines showed compact MCTS formation independent of the preparation method (Figure 4.3). However, growth for 7 days did not significantly increase the spheroid size any further. Comparing MCTS from both cell lines, HCT-116 cells formed generally bigger spheroids (Figure 4.4A).

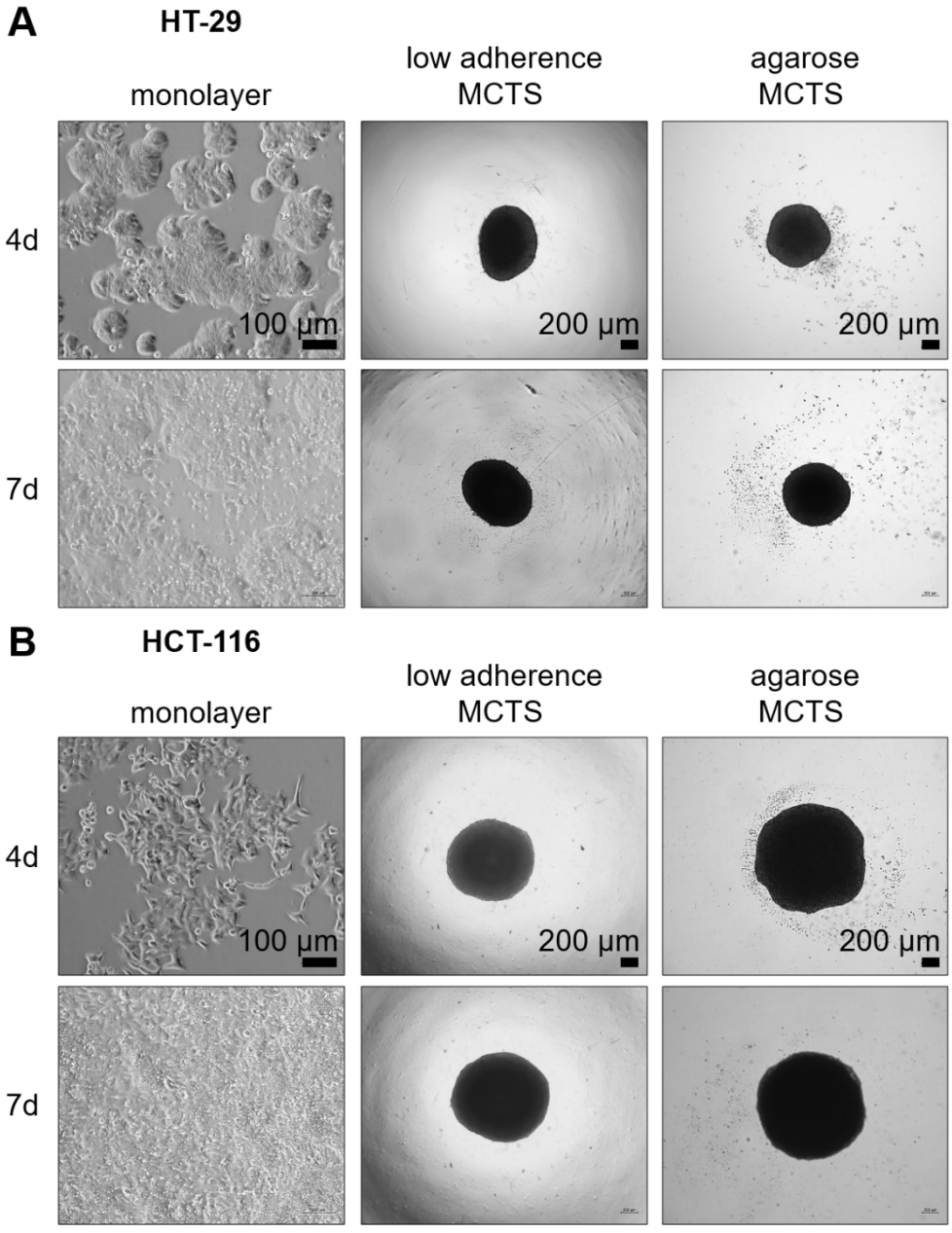

Figure 4.3: Monolayer and MCTS appearance after 4 and 7 days of growth.
Transmitted light microscope pictures of HT-29 (A) and HCT-116 (B) MCTS and monolayers. MCTS were either grown for 4 or 7 days in 96-well low adherence plates or 24-well plates coated with ultra-pure agarose (1%). Respective monolayer controls were seeded in 12-well plates. Identical cell numbers ($0.05x10^6$ cells/well) were seeded. Pictures were taken employing a light microscope (monolayers, scale bar: 100 µm; MCTS, scale bar: 200 µm). One representative picture out of 3 is shown.

Furthermore, no significant differences in MCTS size after 4 and 7 days could be observed comparing both formation methods. Nevertheless, spheroid formation and especially compaction progressed faster using the 96-well low adherence plates compared to 24-well agarose-coated plates (Figure 4.4B). Monolayers of both cell lines cultured for 7 days were visibly overgrown. Culture for 4 days led to a confluency of ~70-80% for both cell lines, but cells formed very densely grown islets, especially in the case of HT-29 cells (Figure 4.3).

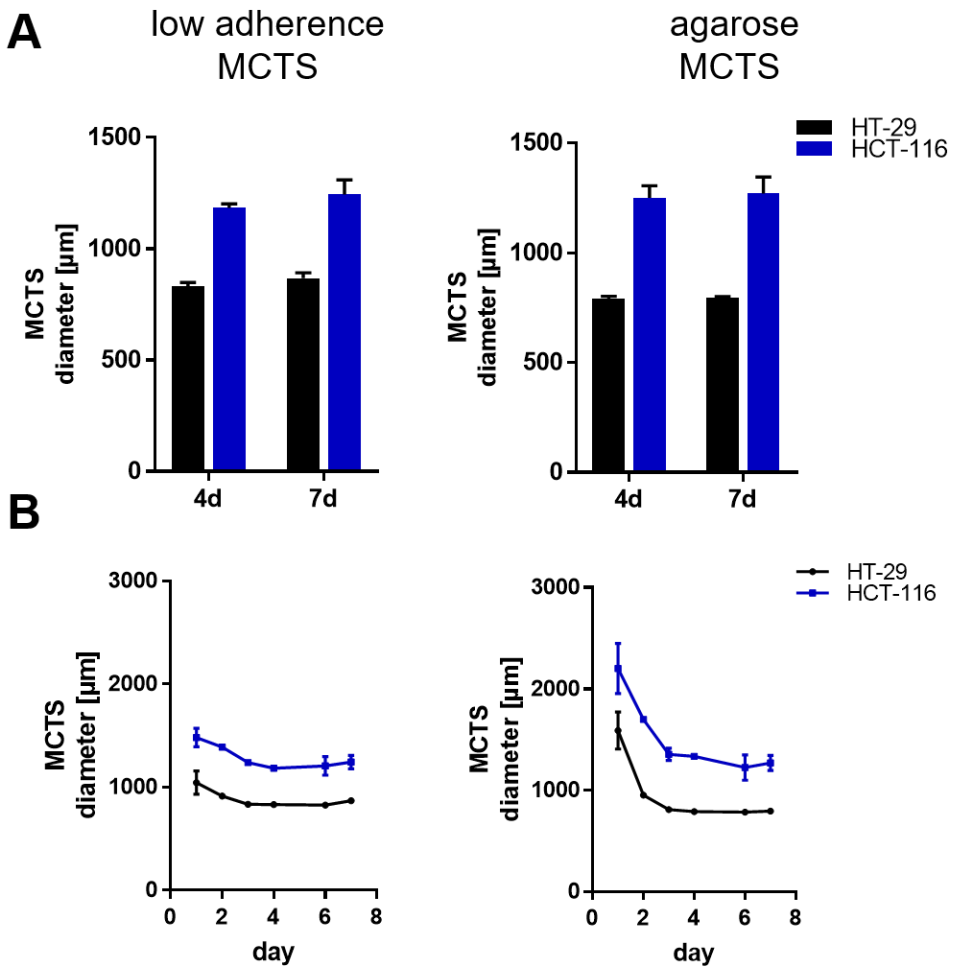

Figure 4.4: Size profile of MCTS.
Average diameters after 4 and 7 days (A) and during growth for 7 days (B). MCTS were either grown for 4 or 7 days in 96-well low adherence plates or 24-well plates coated with ultra-pure agarose (1%). Identical cell numbers ($0.05x10^6$ cells/well) were used. Pictures were taken employing a light microscope, and diameters were analyzed using the ZEN core 2.6 software. Results are depicted as mean + SEM from 6 (A) or 2-6 (B) independent experiments.

For further characterization, 14 µm cryosections of MCTS were prepared and stained using hematoxylin and eosin. Because no significant size differences were noticed between both spheroid formation methods, only samples from the 96-well low adherence plates were prepared due to practicability. MCTS of both cell lines showed a thick outer rim region (Figure 4.5). Beyond, HT-29 MCTS showed a looser core region already recognizable after 4 days; however, this rim was more pronounced and delimited in spheroids grown for 7 days. Interestingly, MCTS of HCT-116 cells showed a capsulated empty inner core region after growth for 4 days. This empty core region was even more prominent after 7 days. There, the core encapsulating rim seemed very unstable and was surrounded by a looser cell structure. The fissures visible in MCTS after 7 days in both cell lines are no characteristic features but artifacts originating from the cutting process.

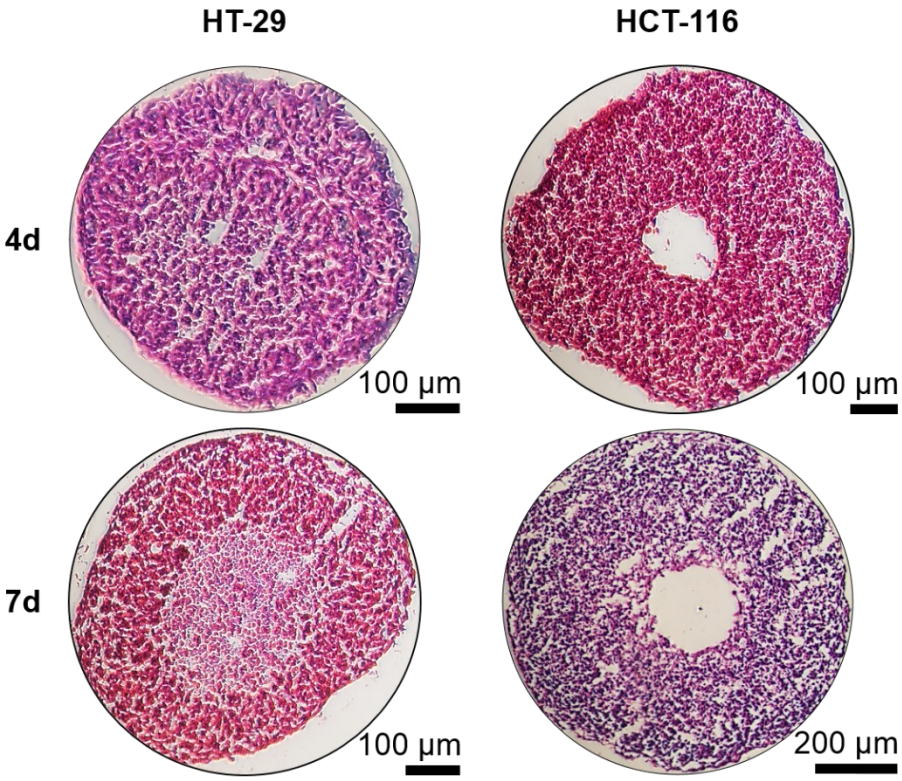

Figure 4.5: Hematoxylin and eosin staining of MCTS cryosections.
Cryosections (14 µm) of HT-29 and HCT-116 MCTS stained with hematoxylin (nuclei, purple/blue) and eosin (cytosol and ECM, pink). MCTS were grown for 4 or 7 days in 96-well low adherence plates. Identical cell numbers ($0.05x10^6$ cells/well) were used. Pictures were taken employing a light microscope. One of 3 independent experiments is shown, respectively.

To ensure better comparability of monolayer-grown cells and MCTS, no medium change was performed during the 4- and 7-days of culture. As a result, acidification of the medium was observed due to phenol red pH indication. Medium supernatants of cells cultured for 7 days were bright yellow, indicating a pH range of 6.0-6.5. Similar pH conditions were observed for medium supernatants of MCTS after 4 and 7 days for both cell lines. Medium supernatants of HCT-116 monolayers cultured for 4 days also showed those pH conditions. In contrast, supernatants of HT-29 monolayers cultured for 4 days were more orange, indicating a pH range of 6.5-7.0. The medium supernatant of the subconfluent monolayer controls showed an orange/red color, indicating a pH range of 7.0-7.5.

As both cell lines were visibly overgrown after 7 days of culture and showed strong induction of 5-LO expression, cell cycle analysis was performed. In line with the monolayer appearance, culture for 7 days triggered a G0/G1 cell cycle arrest in both cell lines (Figure 4.6). Interestingly the proportion of cells in G0/G1 was higher for HT-29 cells than for HCT-116 cells. However, the culture of HCT-116 cells for 4 days also triggered G0/G1 arrest, but the proportion of cells in the G0/G1 phase was lower compared to HCT-116 cells cultured for 7 days (Figure 4.6). The subconfluent monolayer control showed the lowest G0/G1 percentage for both cell lines. Interestingly, no difference was observable between the 4-day cultured monolayer and the subconfluent control for HT-29 cells despite the pronounced formation of tightly grown cell islets (Figure 4.6A). An example of the gating strategy applied to the obtained sample sets before cell cycle analysis can be found in App. Figure 7.3.

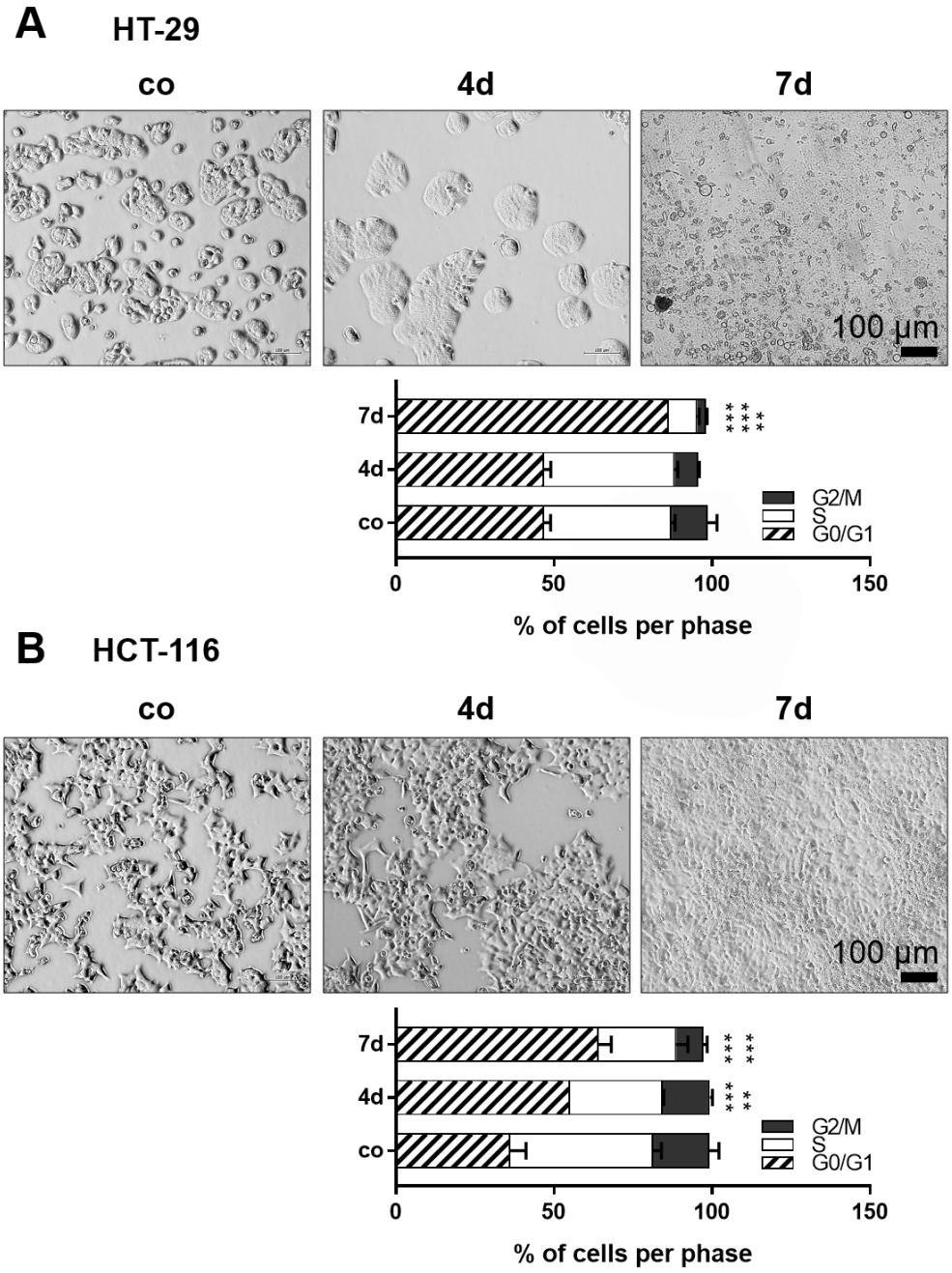

Figure 4.6: Cell cycle distribution of monolayers.
HT-29 cells (A) and HCT-116 cells (B) were grown for 4 or 7 days ($0.81x10^6$ cells/100 mm dish) and compared to monolayer controls (co, $3x10^6$ cells/100 mm dish), which were harvested after 48 h of culture and received a medium change after 24 h. Pictures were taken employing a light microscope. One representative picture out of 3 independent experiments is shown. Cells were analyzed via flow cytometry, and cell cycle analysis was performed using FlowJo software 10. Results are depicted as mean + SEM from 3 independent experiments. Asterisks indicate significant changes vs. co determined by two-way ANOVA coupled with Bonferroni post-test for multiple comparisons. * ($P<0.05$), ** ($P<0.01$), *** ($P<0.001$).

4.2 Influence of extracellular acidic pH and cellular density on 5-LO expression

Regarding the findings on 5-LO expression obtained for over-confluent and nearly-confluent monolayer cultured cells, the effects of extracellular acidic pH and high cellular density on 5-LO expression were investigated.

Beforehand, reversible cell cycle synchronization via serum deprivation was established for HT-29 and HCT-116 cells. As the obtained results implied a possible cell cycle dependency, this was necessary to ensure optimal conditions for subsequent experiments. Cell cycle synchronization can be reached by removing or depleting serum for ~ 24 h (exit into G_0 quiescence). Then, serum is added to stimulate cell cycle entry (early G_1 phase) (351). Therefore, cells were seeded either in their respective complete growth medium (CGM) or reduced growth medium (RGM) for cell cycle synchronization (see Figure 3.2 for workflow). After 22-24 h, cells were prepared for cell cycle analysis to review the synchronization. Furthermore, samples were collected to investigate the influence of reversible cell cycle synchronization on 5-LO expression. As expected, cell cycle synchronization inhibited cell proliferation and led to a shift toward G0/G1 in HT-29 and HCT-116 cells. Importantly, 5-LO expression was not affected through synchronization (see App. Figure 7.4). For further experiments, CGM was added for 2 h after synchronization before starting the experiment to stimulate cell cycle entry.

In order to investigate the influence of extracellular acidic pH, cells were seeded in RGM and left to adhere for 22 h. Cells were then incubated with CGM for 2 h before they were washed and treated with the pH-adjusted medium. Using the normal ready-to-use CGM for pH adjustment was impossible since cell culture media usually contain a sodium bicarbonate buffer system, allowing physiological pH maintenance when cultured in a 5-10% CO_2 environment. Therefore, DMEM powder in combination with a HEPES/PIPES buffer system was used. Unfortunately, no McCoys 5A powdered medium was available; therefore, HT-29 cells were also treated using DMEM. Medium adjusted to pH 7.4 served as the control medium and was compared with medium adjusted to pH 6.5 and 6.8. Cells were incubated with the ready-to-use, commercially obtained DMEM medium (CGM) as an additional control. All used media were supplemented with 10% FCS, 1% PS, 1% pyruvate and prepared under sterile conditions.

Treatment with acidified medium significantly induced *ALOX5* expression in both cell lines (Figure 4.7). In HT-29 cells, the induction was more pronounced after 24 h at pH 6.8 compared to pH 6.5. On the contrary, after 48 h, induction of *ALOX5* was more pronounced for HT-29 cells treated with pH 6.5; however, the observed induction of *ALOX5* at pH 6.8 was less pronounced compared to 24 h. Furthermore, the use of DMEM on HT-29 cells influenced *ALOX5* expression and led to a reduction of expression compared to the control (Figure 4.7A). For HCT-116 cells, treatment with pH 6.5 led to a less pronounced *ALOX5* induction than treatment with pH 6.8 after 24 h. However, both effects were nearly abolished after 48 h.

Next, the influence of cellular density on 5-LO expression was investigated. Therefore, cells were seeded in RGM using different cell densities (cells/cm^2). After 24 h medium was changed to CGM, and cells were incubated for 24 h.

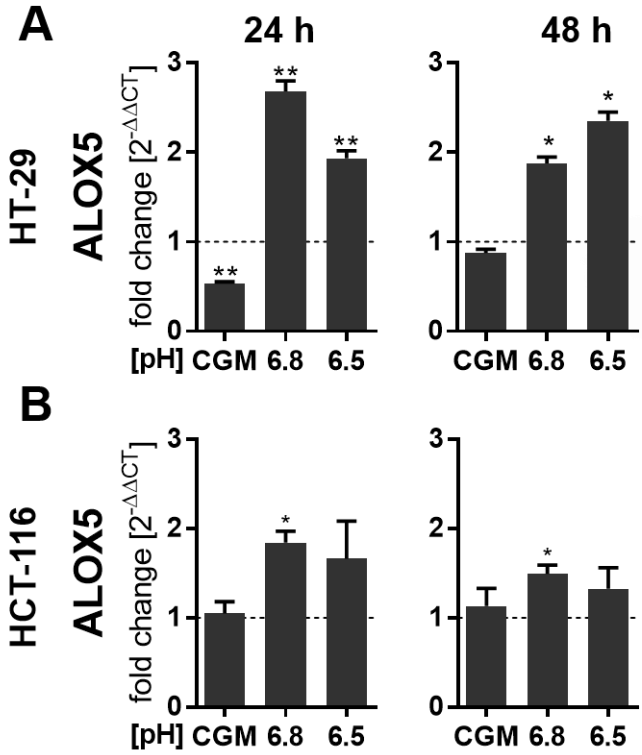

Figure 4.7: mRNA expression of *ALOX5* after treatment with acidified CGM medium.
HT-29 (A) and HCT-116 cells (B) were seeded in 6-well plates using RGM ($0.4x10^6$ cells/well). After 22 h, medium was changed to CGM for 2 h. Then, cells were washed and incubated for 24 h or 48 h using pH-adjusted medium. For comparison, cells were also incubated with commercially obtained ready-to-use medium (CGM) and self-prepared medium adjusted to pH 7.4 served as a control. *ALOX5* expression was determined via qPCR analysis. Expression was normalized to the housekeeping gene *ACTB* and the respective adjusted pH 7.4 control ($2^{-\Delta\Delta CT}$ method). Results are depicted as mean + SEM from 3 independent experiments. Asterisks indicate significant changes vs. pH 7.4 control determined by unpaired two-tailed student's t-test with Welch's correction. * (P<0.05), ** (P<0.01), *** (P<0.001).

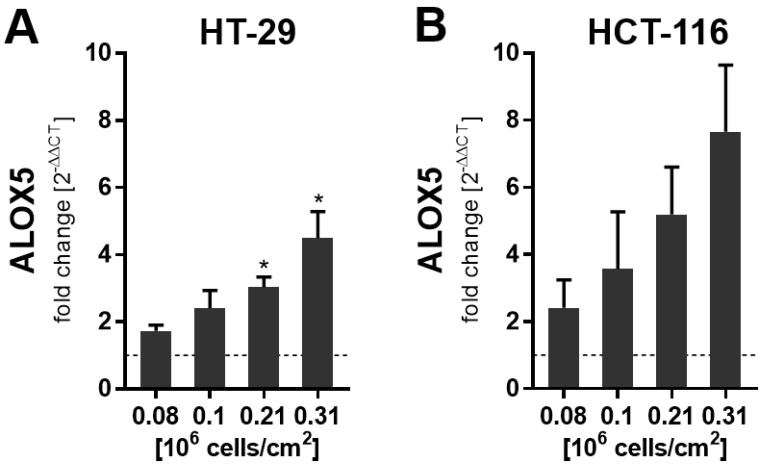

Figure 4.8: mRNA expression of *ALOX5* after growth in different cellular densities.
HT-29 (A) and HCT-116 (B) cells were seeded into 6-well plates using RGM. After 24 h, medium was changed to CGM. Cells were harvested after another 24 h. *ALOX5* expression was determined via qPCR analysis. Expression was normalized to the housekeeping gene *ACTB* and the respective 70-80% confluency control ($0.042x10^6$ cells/cm^2 seeding density, $2^{-\Delta\Delta CT}$ method). Results are depicted as mean + SEM from 3 independent experiments. Asterisks indicate significant changes vs. pH 7.4 controls determined by unpaired two-tailed student's t-test with Welch's correction. * (P<0.05), ** (P<0.01), *** (P<0.001).

ALOX5 mRNA expression was examined first. For this purpose, cells grown in a density of $0.042x10^6$ cells/cm^2 (equal to $0.4x10^6$ cells/well on a 6-well plate) served as a subconfluent monolayer control (70-80% confluency). For both cell lines, increasing cellular density led to an induction of *ALOX5* expression (Figure 4.8). However, results were only significant in HT-29 cells seeded at $0.21x10^6$ and $0.31x10^6$ cells/cm^2 (Figure 4.8A). It is essential to mention that despite the medium change after 24 h, acidification of the medium supernatant in the high-density samples was visible. Since the induction of *ALOX5* due to high cellular density was more pronounced for both cell lines compared to treatment with acidified CGM, the expression of 5-LO was also investigated on protein level. In both cell lines, an increase in 5-LO expression was observed via Western blot analysis due to increased cellular density (Figure 4.9A).

Since high cellular density mediated through cell-cell contact can trigger cell cycle arrest in the early G1 phase, cell cycle analysis was performed as well. Surprisingly, high cellular density did not trigger cell cycle arrest in HT-29 cells but led to a significant and density-dependent shift towards the G0/G1 phase in HCT-116 cells (Figure 4.9B).

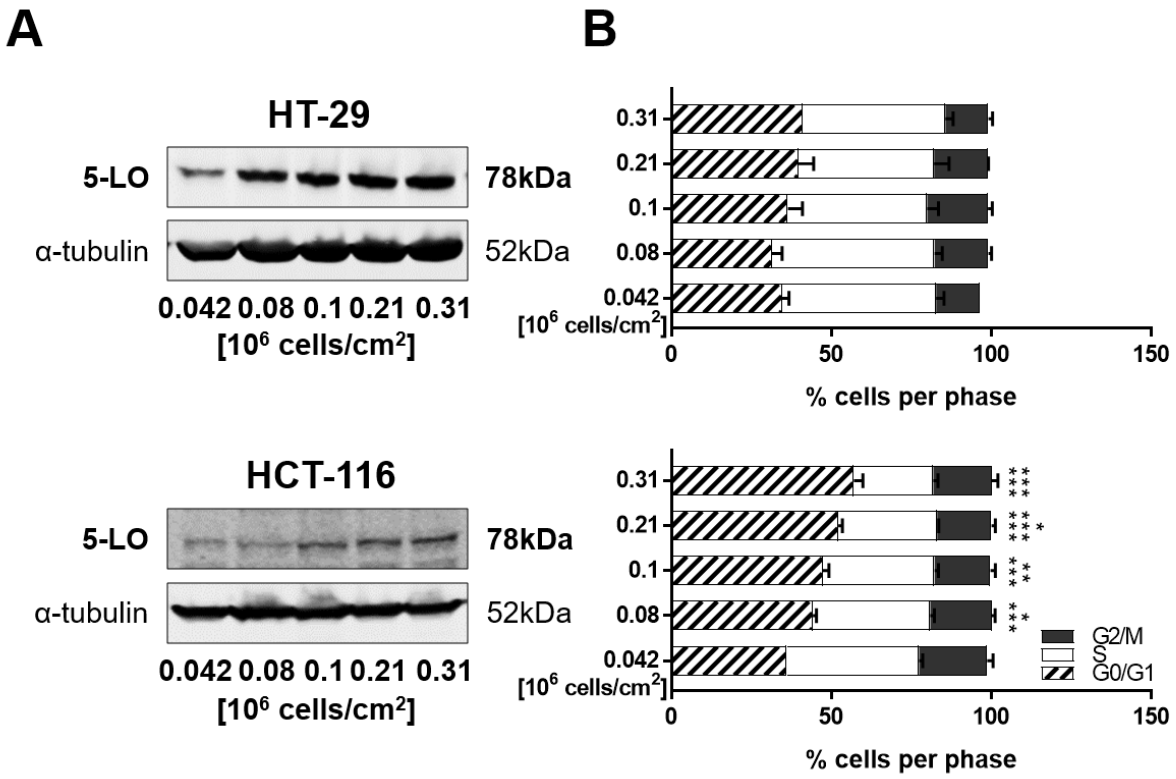

Figure 4.9: 5-LO protein expression and cell cycle distribution in monolayer grown cells seeded in different densities. HT-29 and HCT-116 cells were seeded into 100 mm plates in RGM. After 24 h, medium was changed to CGM. Cells were harvested after another 24 h. (A) Protein expression of 5-LO in HT-29 and HCT-116 cells. One representative Western blot out of 3 is shown. (B) Cell cycle distribution in HT-29 and HCT-116 cells grown in different densities. Results are depicted as mean + SEM from 3 independent experiments. Asterisks indicate significant changes vs. the 70-80% confluency control ($0.042x10^6$ cells/cm^2) determined by two-way ANOVA coupled with Dunnett's post-test for multiple comparisons. * ($P<0.05$), ** ($P<0.01$), *** ($P<0.001$).

4.3 Influence of pro-proliferative and survival pathways on 5-LO expression

Since 3D culture of HT-29 and HCT-116 induced 5-LO expression (4.1), another aim of this work was to elucidate pathways that might be involved in this regulation. Recently, Riedl et al. demonstrated that 3D growth of HT-29 and HCT-116 CRC cells attenuates AKT-mTOR-S6K and MEK-1/ERK signaling (348). Both pathways are commonly altered signaling routes regulating cell growth, proliferation, survival, and metabolism in CRC. Their dysregulation has also been implicated in CRC progression (352). Therefore, the effects of pharmacological inhibition and knockdown of these pathways on 5-LO expression were investigated. Furthermore, the possible involvement of p53 was investigated since 5-LO is a direct p53 target gene that is upregulated in HCT-116 cells after treatment with genotoxic compounds (32).

4.3.1 Compound-mediated pathway inhibition

To investigate the involvement of the PI3K/mTOR and MEK/ERK axis in the regulation of 5-LO expression, HT-29 and HCT-116 monolayer grown cells were treated with several inhibitors targeting multiple members of both signaling cascades. As established in Chapter 4.2, cell cycle synchronization via serum starvation was performed prior to the inhibitor treatment (see Figure 3.2 for workflow). Treatment with the pan-PI3K inhibitor Wortmannin (1 µM), the mTOR inhibitor Temsirolimus (3 µM), and the dual pan-PI3K and mTOR inhibitor Dactolisib (3 µM) led to a significant induction (1.2-1.9-fold) of 5-LO protein expression in HT-29 cells (see App. Figure 7.5 for structures of the respective inhibitors).

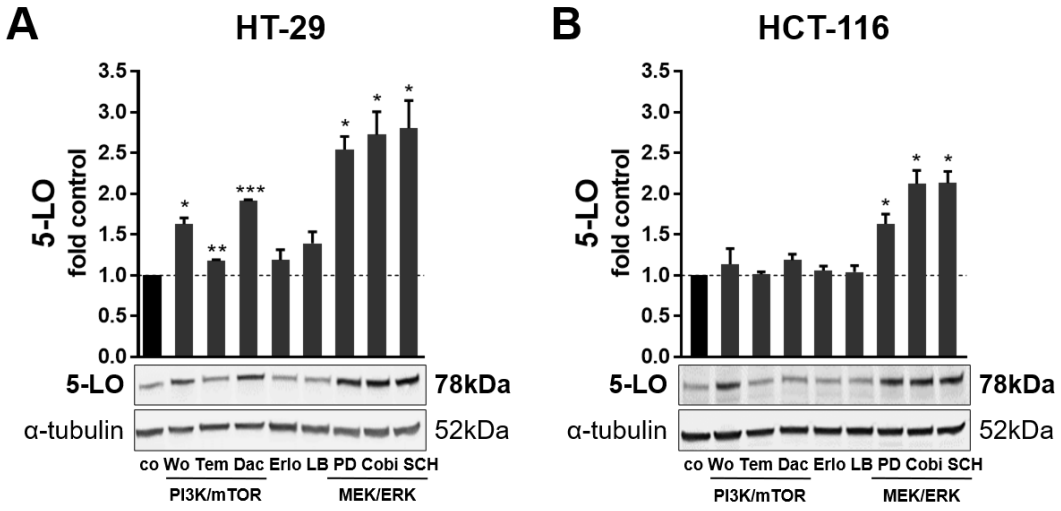

Figure 4.10: 5-LO protein expression after 24 h of treatment with inhibitors of the PI3K/mTOR and MEK/ERK pathway in monolayer grown cells.
HT-29 (A) and HCT-116 (B) cells were seeded ($3x10^6$ cells/100 mm dish) and cell cycle was synchronized by serum starvation using RGM 22 h before treatment. Then, medium was changed to CGM for 2 h and cells were treated for 24 h with the indicated inhibitors Wortmannin (Wo) 1 µM; Temsirolimus (Tem) 3 µM; Dactolisib (Dac) 3 µM, Erlotinib (Erlo) 5 µM; LB42708 (LB) 1 µM; PD184352 (PD) 1 µM; Cobimetinib (Cobi), 0.5 µM; SCH772984 (SCH) 1 µM. The vehicle control (co) received DMSO instead. Densitometric values were determined and values were normalized to the loading control α-tubulin followed by normalization to the DMSO vehicle control (co). Results are depicted as mean + SEM from 3 independent experiments. Asterisks indicate significant changes vs. DMSO vehicle control determined by unpaired two-tailed student's t-test with Welch's correction * (P<0.05), ** (P<0.01), *** (P<0.001).

Interestingly, pan-PI3K/mTOR inhibition failed to induce 5-LO protein expression in HCT-116 cells (Figure 4.10). Targeting of the EGF receptor using Erlotinib (5 µM) and inhibition of Ras farnesylation essential for Ras activation using LB42708 (1 µM) did not alter 5-LO protein expression significantly in any of the cell lines. In contrast, inhibition of MEK1/2 using PD184352 (1 µM), MEK-1 using Cobimetinib (0.5 µM), and ERK-1/2 using SCH772984 (1 µM) induced 5-LO protein expression in both cell lines significantly. However, the induction of 5-LO expression was more pronounced for HT-29 cells (2.5-2.8-fold) than for HCT-116 cells (1.6-2.1-fold).

Obtained data for *ALOX5* mRNA expression support the results for 5-LO protein expression. However, induction of *ALOX5* mRNA was even more pronounced than 5-LO protein expression. Of note, treatment of HCT-116 cells with Dactolisib led to an elevated but not significantly altered *ALOX5* mRNA expression (2.6-fold, Figure 4.11B).

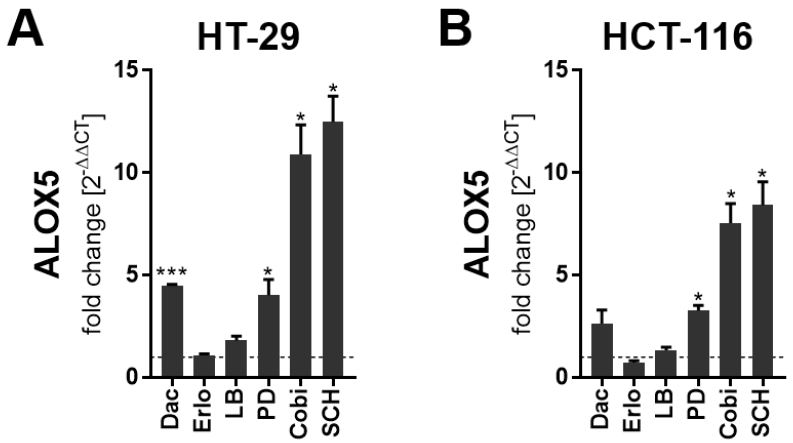

Figure 4.11: mRNA expression of *ALOX5* after 24 h of treatment with inhibitors of the PI3K/mTOR and MEK/ERK pathway in monolayer grown cells.
HT-29 (A) and HCT-116 (B) cells were seeded ($0.4x10^6$ cells/well, 6-well plate) and cell cycle was synchronized by serum starvation using RGM 22 h before treatment. Then, medium was changed to CGM for 2 h and cells were treated for 24 h with the indicated inhibitors Dactolisib (Dac) 3 µM, Erlotinib (Erlo) 5 µM; LB42708 (LB) 1 µM; PD184352 (PD) 1 µM; Cobimetinib (Cobi), 0.5 µM; SCH772984 (SCH) 1 µM. The vehicle control received DMSO instead. *ALOX5* expression was determined via qPCR analysis. Expression was normalized to the housekeeping gene *ACTB* and the respective vehicle control ($2^{-\Delta\Delta CT}$ method). Results are depicted as mean + SEM from 3 independent experiments. Asterisks indicate significant changes vs. DMSO controls determined by unpaired two-tailed student's t-test with Welch's correction. * ($P<0.05$), ** ($P<0.01$), *** ($P<0.001$).

To assure that the obtained results for induction of 5-LO expression after treatment with inhibitors of the PI3K/mTOR and MEK/ERK pathway are independent of compound cytotoxicity, WST-1 cell viability and LDH cytotoxicity assays were performed (Figure 4.12). Therefore, indicated compounds were tested in three different concentrations after cell cycle synchronization. Reduced viability or proliferation was detected after treatment with the PI3K/mTOR inhibitors Wortmannin in HCT-116 cells (75% viability compared to the DMSO-treated control) and Dactolisib in both cell lines (55% viability). Furthermore, the viability or proliferation of both cell lines was affected after treatment with the highest tested concentration of Erlotinib (10 µM, 80% viability). Further decreases in cell viability or proliferation were detected after MER/ERK inhibition using Cobimetinib and SCH772984 in both cell lines but were only significant in HCT-116 cells.

Importantly, concentrations used to investigate mRNA and protein expression influenced cell viability or proliferation only in the case of Dactolisib (3 µM, both cell lines ~ 55%) and Cobimetinib (0.5 µM, both cell lines ~ 75%). No elevated cytotoxicity (>10%) was detected in both cell lines with any tested inhibitor concentration compared to the respective DMSO treated (0%) and Triton-X-100 (100%) control.

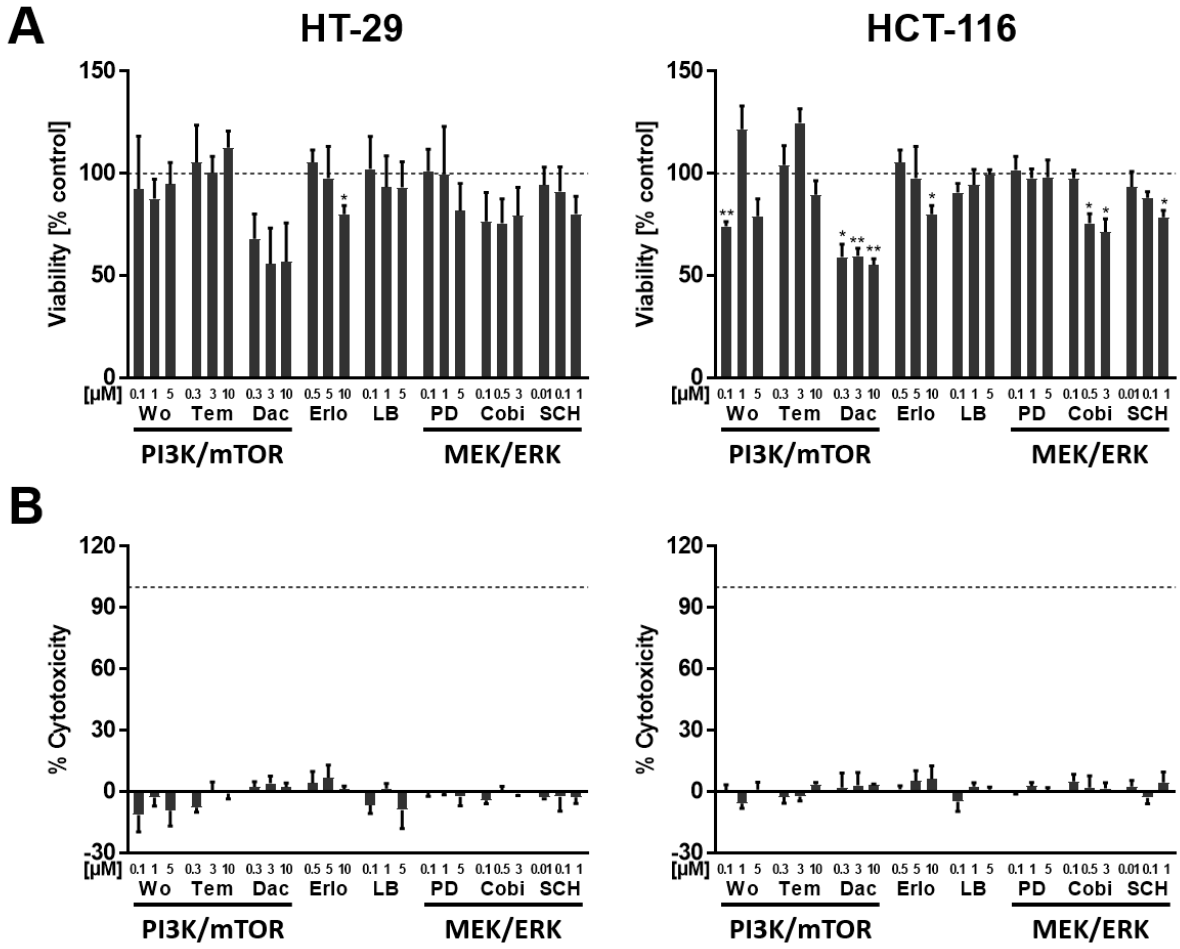

Figure 4.12: Cell viability and cytotoxicity after 24 h of treatment with inhibitors of the PI3K/mTOR and MEK/ERK pathway in monolayer grown cells.
HT-29 and HCT-116 cells were seeded in 96-well plates ($0.03x10^6$ cells/well) using RGM for cell cycle synchronization. After 22 h medium was changed to CGM for 2 h and cells were treated for 24 h with the indicated inhibitors Wortmannin (Wo), Temsirolimus (Tem), Dactolisib (Dac), Erlotinib (Erlo), LB42708 (LB), PD184352 (PD), Cobimetinib (Cobi), SCH772984 (SCH). The vehicle control received DMSO instead. Cell viability was determined using a WST-1 assay (A). Results were normalized to the respective DMSO control (100%). Compound cytotoxicity was determined using an LDH assay (B). To determine the percentage of cytotoxicity, average absorbance of the respective background control was subtracted from each sample. Then, samples were normalized to the Triton-X-100 control (100%) and the respective DMSO control (0%). Results shown are depicted as mean + SEM from 3 independent experiments. Asterisks indicate significant changes vs. controls determined by unpaired two-tailed student's t-test with Welch's correction. * (P<0.05), ** (P<0.01), *** (P<0.001).

Since some of the tested inhibitors were described to induce G0/G1 cell cycle arrest in a variety of cancer cell lines (353, 354), cell cycle analysis of treated HT-29 and HCT-116 cells was performed as well. After cell cycle synchronization and treatment for 24 h using the established workflow (Figure 3.2), inhibition of PI3K/mTOR using Dactolisib and inhibition of MEK/ERK using PD184352, Cobimetinib, and SCH772984 significantly shifted the cell population of both cell lines

towards the G0/G1 phase compared to the respective DMSO control (co). Interestingly, treatment of HT-29 cells using Wortmannin and Temsirolimus, which both slightly altered 5-LO protein expression in this cell line (Figure 4.10A), did not affect the cell population in G0/G1. However, treatment with Wortmannin increased the proportion of cells in the S phase and decreased the proportion of cells in the G2/M phase. Treatment of HT-29 cells with LB42708 even decreased the proportion of cells in G0/G1 phase and increased the cell population in S phase. In contrast, treatment of HCT-116 cells with Wortmannin and Temsirolimus reduced the proportion of cells in S phase and increased the cellular population in G2/M phase. Same results were obtained after treatment of HCT-116 cells with LB42708. In general, HCT-116 control cells showed a lower proportion of cells in the G0/G1 phase compared to the HT-29 control (35% HCT-116, 42% HT-29).

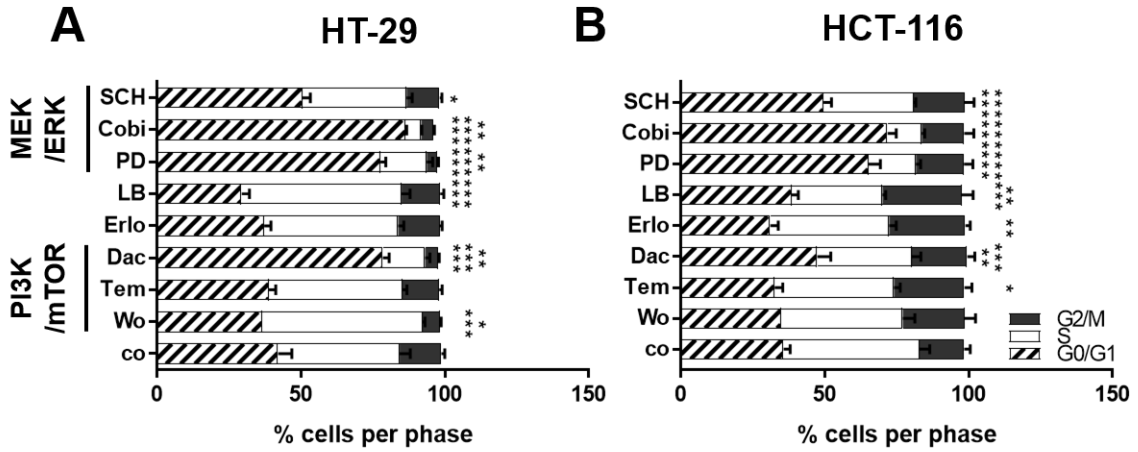

Figure 4.13: Cell cycle analysis after 24 h of treatment with inhibitors of the PI3K/mTOR and MEK/ERK pathway in monolayer grown cells.
HT-29 (A) and HCT-116 (B) cells were seeded ($3x10^6$ cells/100 mm plate) and cell cycle was synchronized by serum starvation using RGM 22 h before treatment. Then, medium was changed to CGM for 2 h and cells were treated for 24 h with the indicated inhibitors Wortmannin (Wo) 1 µM; Temsirolimus (Tem) 3 µM; Dactolisib (Dac) 3 µM, Erlotinib (Erlo) 5 µM; LB42708 (LB) 1 µM; PD184352 (PD) 1 µM; Cobimetinib (Cobi), 0.5 µM; SCH772984 (SCH) 1 µM. The vehicle control (co) received DMSO instead. Asterisks indicate significant changes vs. DMSO vehicle co determined by two-way ANOVA coupled with Dunnett's post-test for multiple comparisons. * ($P<0.05$), ** ($P<0.01$), *** ($P<0.001$).

4.3.2 Phosphorylation status of p70S6K and ERK after MCTS formation

Because Riedl et al. used HT-29 and HCT-116 cells but deployed different incubation parameters (low cell number per well $0.03x10^6$, short incubation time of 48 h), it was important to examine the phosphorylation state of ERK and p70S6K for the investigated MCTS in this study. Therefore, the sample set of MCTS and controls of both cell lines (introduced in 4.1.1) were investigated for ERK phosphorylation at Tyr202/204 mediated via MEK and p70S6K phosphorylation at Thr389 mediated via mTOR, as well as the individual target expression. Here, only samples from the low attachment plate formation method were investigated since no noticeable differences were observed between both methods for the previously shown experiments. As expected, MCTS formation for 4 and 7 days reduced the phosphorylation of ERK significantly in HT-29 cells compared to the control (co) (Figure 4.14A). Interestingly, monolayer culture for 4 days without any medium changes even elevated the phosphorylation of ERK in those cells. Surprisingly, the analyzed sample set for HCT-116 cells showed a reversed pattern for the ERK phosphorylation (Figure 4.14C). The control and 4-day monolayer showed a comparable low ERK phosphorylation, whereas the 7-day monolayer incubations and MCTS formation for 4 and 7 days strongly induced ERK phosphorylation. Similar results were obtained regarding the p70S6K phosphorylation for the HCT-116 sample set (Figure 4.14D).

For HT-29 cells in general, detecting pp70S6K was difficult since no phosphorylation was detectable on 2 of 3 Western blots. Therefore, this was not further analyzed. However, the expression of p70S6K itself was affected by growth of MCTS for 7 days and growth of monolayer controls for 7 days (Figure 4.14B).

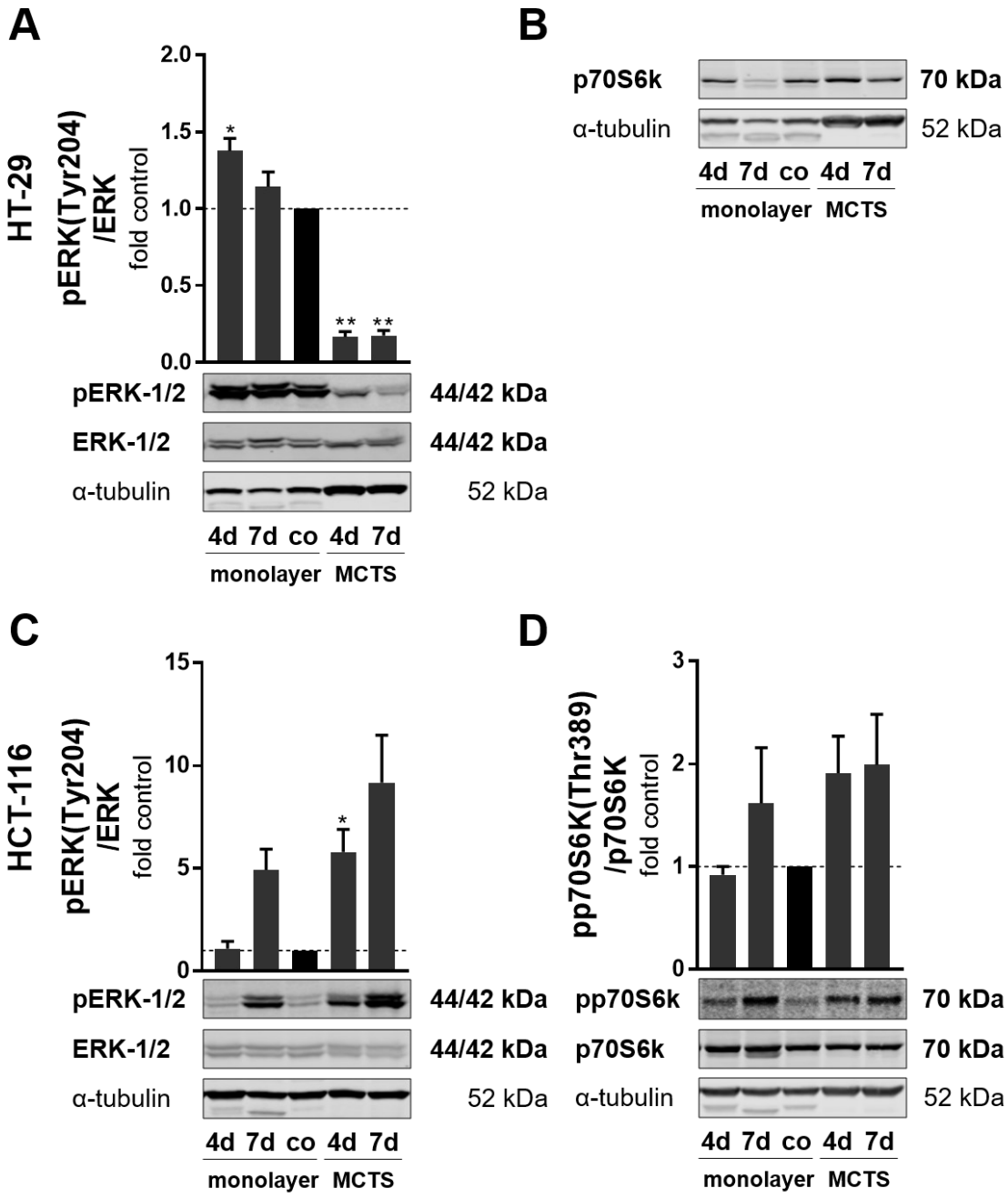

Figure 4.14: Phosphorylation state of ERK and p70S6K in MCTS.
Protein expression of pERK (Tyr202/204) and total ERK, as well as pp70S6K (Thr389) and total p70S6K analyzed via Western blot. MCTS were either grown for 4 or 7 days in 96-well low adherence plates. Respective monolayer controls were seeded in 12-well plates. Identical cell numbers ($0.05x10^6$ cells/well) were used. The subconfluent monolayer controls (co) were seeded in 100 mm dishes ($3x10^6$ cells per dish), received a medium change after 24 h, and were harvested after 48 h. One representative blot out of 3 is shown. Densitometric values were determined, coefficients calculated and normalized to the respective subconfluent monolayer control (co). α-Tubulin served as a loading control. Results are depicted as mean + SEM from 3 independent experiments. Asterisks indicate significant changes vs. co. determined by unpaired two-tailed student's t-test with Welch's correction * ($P<0.05$), ** ($P<0.01$), *** ($P<0.001$).

4.3.3 Influence of p53

Gilbert et al. were able to demonstrate that *ALOX5* is a direct p53 target gene. This was investigated in several cancer cell lines expressing wt p53, which were treated with genotoxic agents (32). Therefore, it was important to investigate if the observed 5-LO upregulation after treatment with PI3K/mTOR and MEK/ERK inhibitors might be p53 dependent.

Therefore, *TP53* and *BAX* expression was investigated via qPCR after 24 h of treatment with inhibitors of the PI3K/mTOR and MEK/ERK pathway in HCT-116 cells expressing the p53 wt. Treatment with the previously tested inhibitors, except for Erlotinib, led to a significant but low induction of *TP53* expression (Figure 4.15A). However, the treatment did not significantly affect the expression of BAX, a direct p53 target gene (353) (Figure 4.15B).

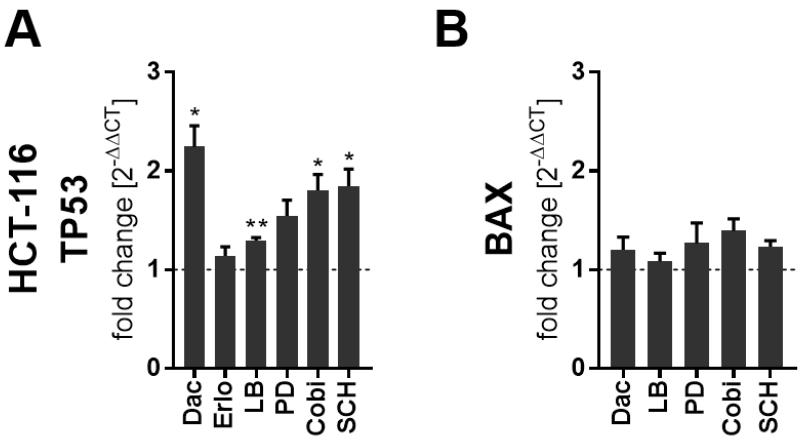

Figure 4.15: mRNA expression of *TP53* and *BAX* after 24 h of treatment with inhibitors of the PI3K/mTOR and MEK/ERK pathway in HCT-116 cells.
Cells were seeded ($0.4x10^6$ cells/well, 6-well plate) and cell cycle synchronized by serum starvation using RGM 22 h before treatment. Then, medium was changed to CGM for 2 h and cells were treated for 24 h with the indicated inhibitors Dactolisib (Dac) 3 µM, Erlotinib (Erlo) 5 µM; LB42708 (LB) 1 µM; PD184352 (PD) 1 µM; Cobimetinib (Cobi), 0.5 µM; SCH772984 (SCH) 1 µM. The vehicle control received DMSO instead. *TP53* (A) and *BAX* (B) expression were determined via qPCR analysis. Expression was normalized to the housekeeping gene *ACTB* and the respective vehicle control ($2^{-\Delta\Delta CT}$ method). Results are depicted as mean + SEM from 3 independent experiments. Asterisks indicate significant changes vs. DMSO co determined by unpaired two-tailed student's t-test with Welch's correction. * ($P<0.05$), ** ($P<0.01$), *** ($P<0.001$).

To assess if the observed induction of *TP53* expression is the reason behind the induced 5-LO expression due to PI3K/mTOR and MEK/ERK inhibition, HCT-116 cells were treated with the p53 inhibitor Pifithrin-α (30 µM) and the MDM2 antagonist NSC 66811 (5 µM). But, both compounds failed to affect 5-LO protein expression. However, combined treatment of Dactolisib or Cobimetinib with Pifithrin-α further increased 5-LO protein expression compared with the respective controls (Figure 4.16A). Notably, treatment with Pifithrin-α affected the viability (75%) of HCT-116 cells and showed cytotoxic effects (35%), whereas NSC 66811 did not affect the viability but also mediated cytotoxic effects (35%) (Figure 4.16B, C).

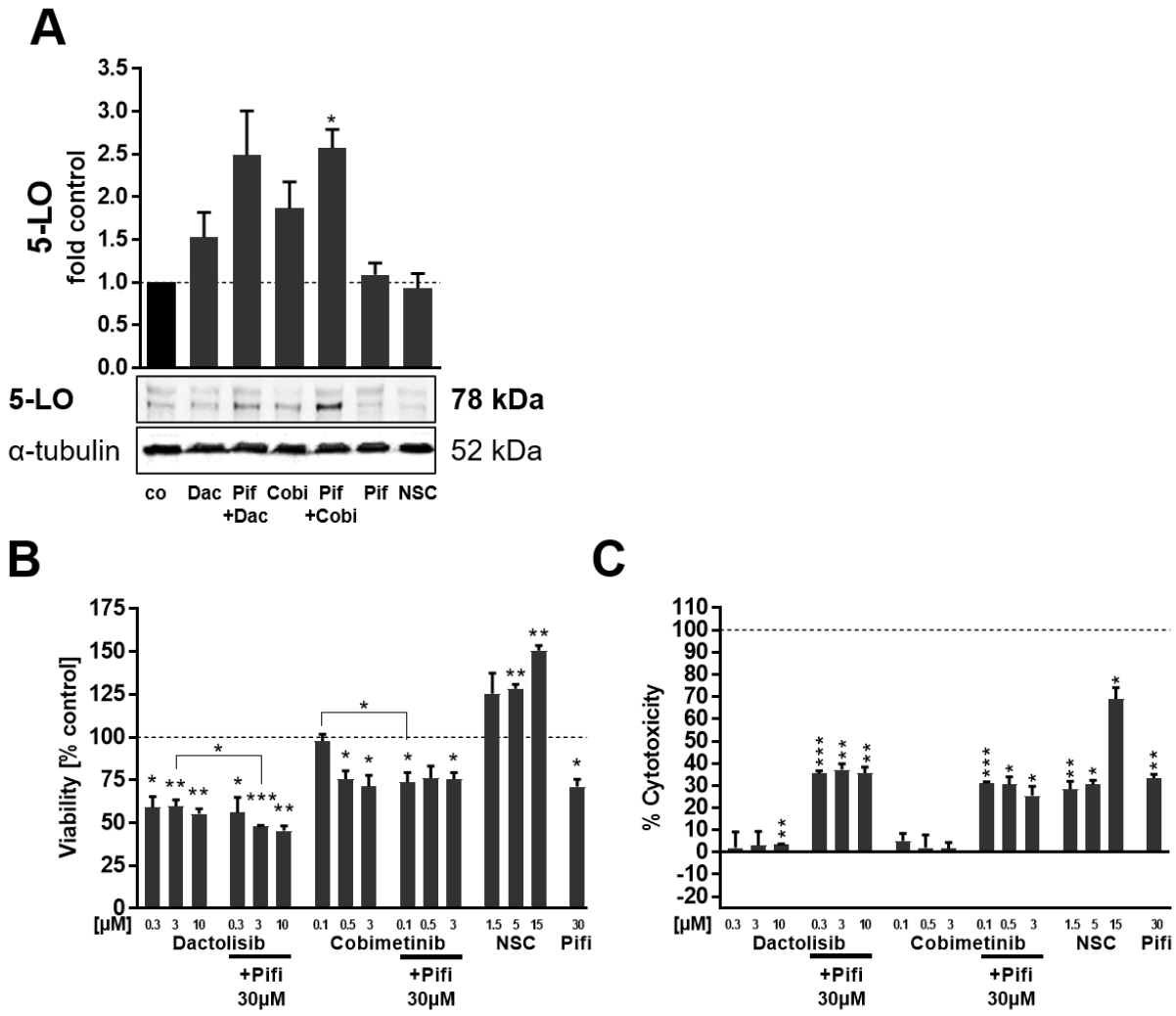

Figure 4.16: 5-LO protein expression, viability, and cytotoxicity after 24 h of treatment with inhibitors of the PI3K/mTOR, MEK/ERK, and p53 pathways in monolayer grown HCT-116 cells.
Cells were seeded ($3x10^6$ cells/100 mm plate (A); $0.03x10^6$ cells/well, 96-well plate) and cell cycle was synchronized by serum starvation using RGM 22 h before treatment. Then, medium was changed to CGM for 2 h and cells were treated for 24 h with the indicated inhibitors Dactolisib (Dac) 3 µM; Cobimetinib (Cobi), 0.5 µM; NSC 66811 (NSC) 5 µM, and Pifithrin-α (Pifi) 30 µM. The vehicle control received DMSO instead. (A) 5-LO protein expression in treated HCT-116 cells determined via Western blot analysis. Densitometric values were determined and values were normalized to the loading control α-tubulin followed by normalization to the DMSO vehicle control (co). Cell viability was determined using a WST-1 assay (B). Results were normalized to the respective DMSO control (100%). Compound cytotoxicity was determined using an LDH assay (C). To determine the percentage of cytotoxicity, average absorbance of the respective background control was subtracted from each sample. Then, samples were normalized to the Triton-X-100 control (100%) and the respective DMSO control (0%). Asterisks indicate significant changes vs. DMSO vehicle co determined by unpaired two-tailed student's t-test with Welch's correction (A) or two-way ANOVA coupled with Dunnett's post-test for multiple comparisons (B, C). * ($P<0.05$), ** ($P<0.01$), *** ($P<0.001$).

Next, HCT-116 cells carrying a p53 knockout (HCT-116 p53 -/-) (344) were treated with selected PI3K/mTOR and MEK/ERK inhibitors. As already shown for the parental cell line HCT-116, the MEK/ERK inhibitors induced *ALOX5* mRNA expression (Figure 4.11B). Although this induction is comparable between the parental and p53 knockout cell line, the basal *ALOX5* mRNA expression is lower in p53 -/- cells.

Therefore, it was no surprise that 5-LO protein expression was not detectable in HCT-116 p53 -/- cells even after treatment with PI3K/mTOR and MEK/ERK inhibitors (Figure 4.17A). Beyond

that, those inhibitors still induced a significant G0/G1 cell cycle shift after treatment for 24 h (Figure 4.17C). The proportion of cells in the G0/G1 phase was generally lower in HCT-116 p53 -/- cells compared to their parental wt cells (cf. Figure 4.13B).

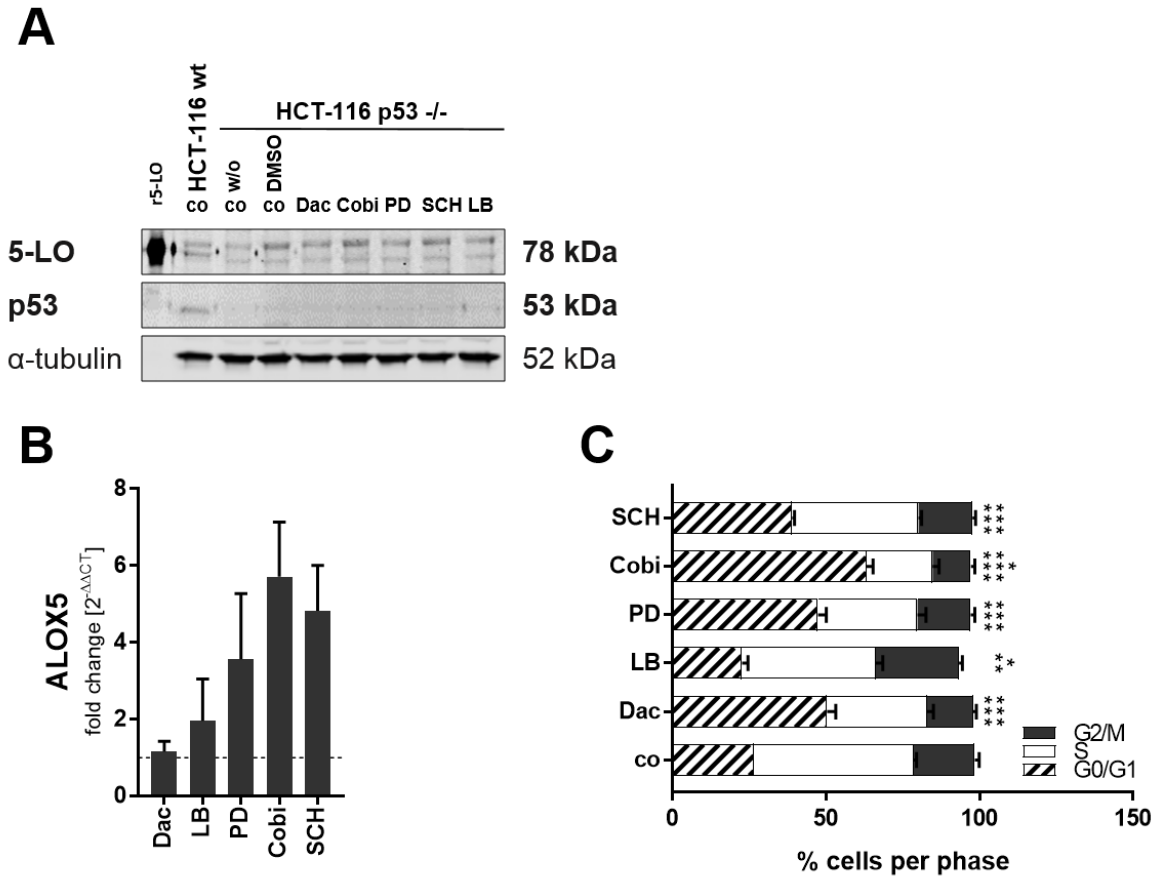

Figure 4.17: 5-LO protein and mRNA expression as well as cell cycle analysis after 24 h of treatment with inhibitors of the PI3K/mTOR and MEK/ERK pathways in monolayer grown HCT-116 p53 -/- cells.
Cells were seeded ($3x10^6$ cells/100 mm plate (A, C); $0.4x10^6$ cells/well, 6-well plate) and cell cycle was synchronized by serum starvation using RGM 22 h before treatment. Then, medium was changed to CGM for 2 h and cells were treated for 24 h with the indicated inhibitors Dactolisib (Dac) 3 µM; PD184352 (PD) 1 µM; Cobimetinib (Cobi), 0.5 µM; SCH772984 (SCH) 1 µM; LB42708 (LB) 1 µM. The vehicle control received DMSO instead. (A) 5-LO and p53 protein expression in treated HCT-116 p53 -/- cells determined via Western blot analysis. HCT-116 wt p53 expressing cells and recombinant purified 5-LO (r5-LO) served as a control. (B) *ALOX5* mRNA expression was determined via qPCR analysis. Expression was normalized to the housekeeping gene *ACTB* and the respective vehicle control ($2^{-\Delta\Delta CT}$ method). (C) Cell cycle analysis after inhibitor treatment of HCT-116 p53 -/- cells. Asterisks indicate significant changes vs. DMSO vehicle co determined by unpaired two-tailed student's t-test with Welch's correction (B) or two-way ANOVA coupled with Dunnett's post-test for multiple comparisons (C). * (P<0.05), ** (P<0.01), *** (P<0.001).

Cellular viability and compound cytotoxicity were also tested for HCT-116 p53 -/- cells, but only treatment with Dactolisib influenced the cellular viability/proliferation (40%). At the same time, this did not mediate cytotoxic effects (App. Figure 7.6A, B). Finally, it was tested if the 3D culture of HCT-116 p53 -/- cells would induce 5-LO protein expression, but as shown for the PI3K/mTOR and MEK/ERK inhibitors, no 5-LO protein expression was detectable (App. Figure 7.6C).

4.3.4 Knockdown of PI3K/mTOR and MEK/ERK pathway members

As inhibition of the PI3K/mTOR and MEK/ERK pathways led to pronounced 5-LO protein expression in both investigated cell lines, several stable knockdowns of members of both signaling pathways were established in HT-29 and HCT-116 cells. By this, the involved central members of both pathways should be identified and the previously presented result should be further validated. The used specific shRNA sequences were directed against the different isoforms of the catalytic subunit of PI3K, namely p110α (*PIK3CA*), p110β (*PIK3CB*), p110δ (*PIK3CD*), p110γ (*PIK3CG*), as well as Rictor (*RICTOR*), Raptor (*RPTOR*), mTOR (*MTOR*), MEK-1 (*MAP2K1*), and PKCζ (*PRKCZ*).

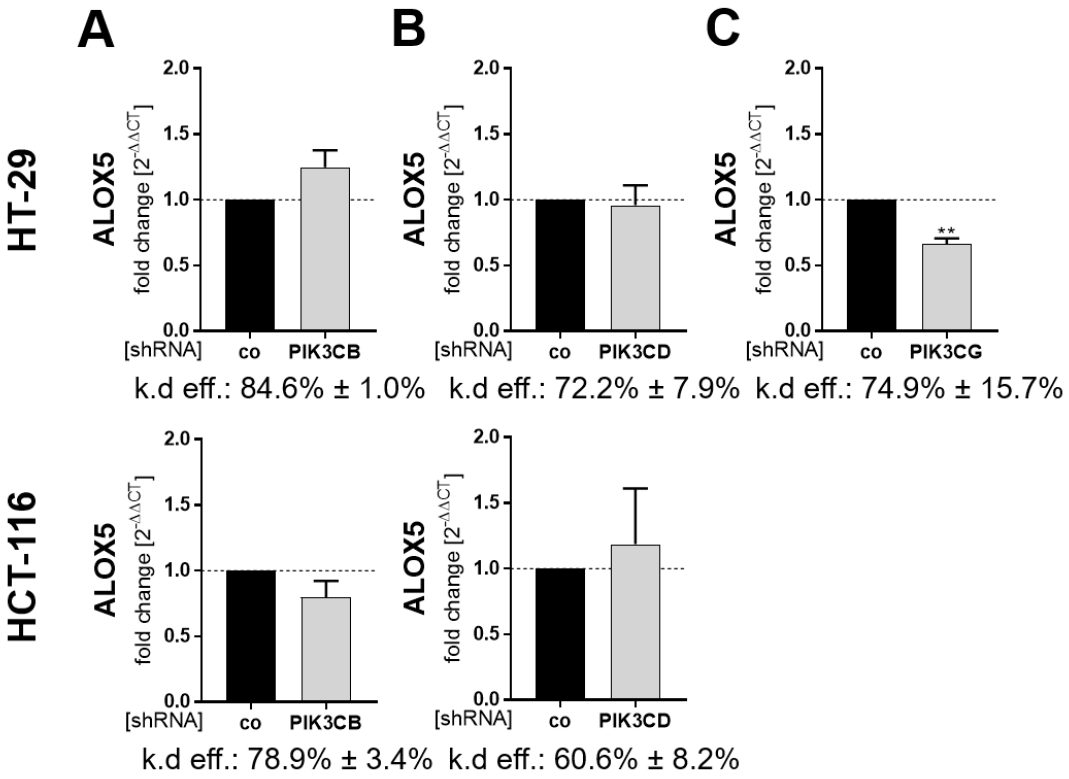

Figure 4.18: mRNA expression of *ALOX5* and knockdown efficiencies after stable knockdown of the PI3K catalytic subunits PI3KCB, PI3KCD, and PI3KCG in HT-29 and HCT-116 cells.
Cells were seeded (0.4×10^6 cells/well, 6-well plate) in CGM and cultured for 48 h with a medium change after 24 h. *ALOX5* mRNA expression and target knockdown efficiencies of PI3KCB (A), PI3KCD (B), and PI3KCG (C) were determined via qPCR analysis. Expression was normalized to the housekeeping gene *ACTB* and the respective control cell line (co) expressing a non-mammalian shRNA ($2^{-\Delta\Delta CT}$ method). Asterisks indicate significant changes vs. DMSO vehicle co determined by unpaired two-tailed student's t-test with Welch's correction. * ($P<0.05$), ** ($P<0.01$), *** ($P<0.001$).

A stable knockdown of the respective targets was introduced using a vector-based shRNA expression in combination with lentiviral transduction. Due to the number of targets, a stable lentiviral-based procedure was preferred over a transient procedure regarding cell yield and cost-benefit efficiency. A non-mammalian shRNA vector was used for the respective control cells (co).

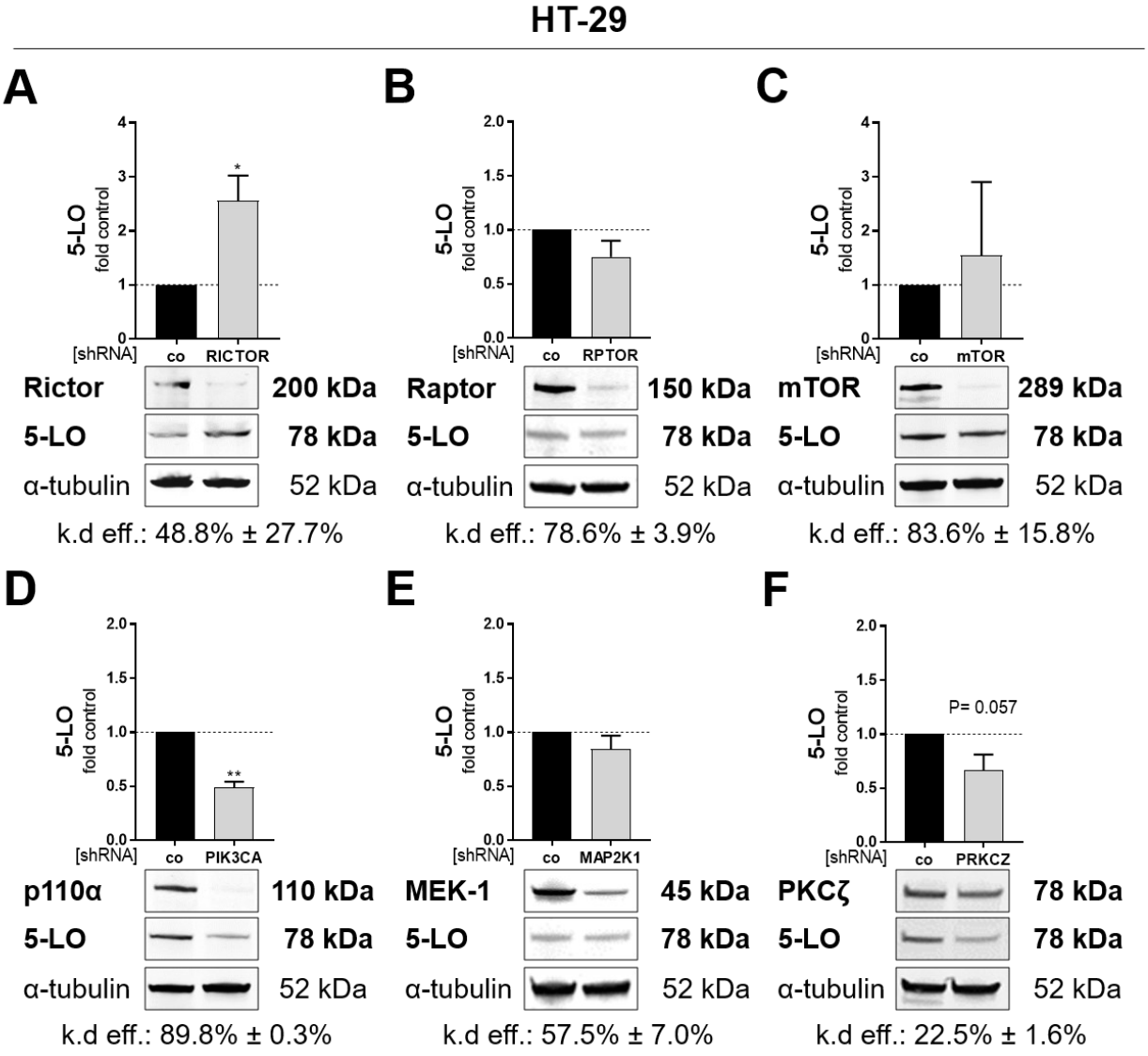

Figure 4.19: 5-LO and knockdown target protein expression after stable knockdown of members from the PI3K/mTOR and MEK/ERK cascades in HT-29 cells.
5-LO and (A) Rictor, (B) Raptor, (C) mTOR, (D) p110α, MEK-1 (E), and PKCζ (F) expression in stable knockdown cells determined via Western blot. Knockdown efficiencies are depicted as mean ± SD and were determined via densitometric analysis of the respective knockdown target in non-mammalian shRNA expressing control cells (co) and respective knockdown cells. Densitometric values were normalized to the loading control α-tubulin followed by normalization to the non-mammalian shRNA expressing control (co). Results are depicted as mean + SEM from 3 independent experiments. One representative blot is shown. Asterisks indicate significant changes vs. control determined by unpaired two-tailed student's t-test with Welch's correction. * (P<0.05), ** (P<0.01), *** (P<0.001).

Acquisition of knockdown efficiencies and analysis of 5-LO expression was performed via Western blot analysis (p110α, Rictor, Raptor, mTOR, MEK-1, PKCζ) or qPCR analysis if a specific antibody was not available (p110β, p110δ, p110γ) (Figure 4.18, Figure 4.19, Figure 4.20). After transduction, antibiotic selection and culture expansion, most of the established knockdown cell lines and the controls showed comparable morphology and growth properties. However,

knockdown of p110α and PKCζ in HT-29 cells and knockdown of PKCζ in HCT-116 cells impaired growth of the respective cell lines compared to the established control cell lines.

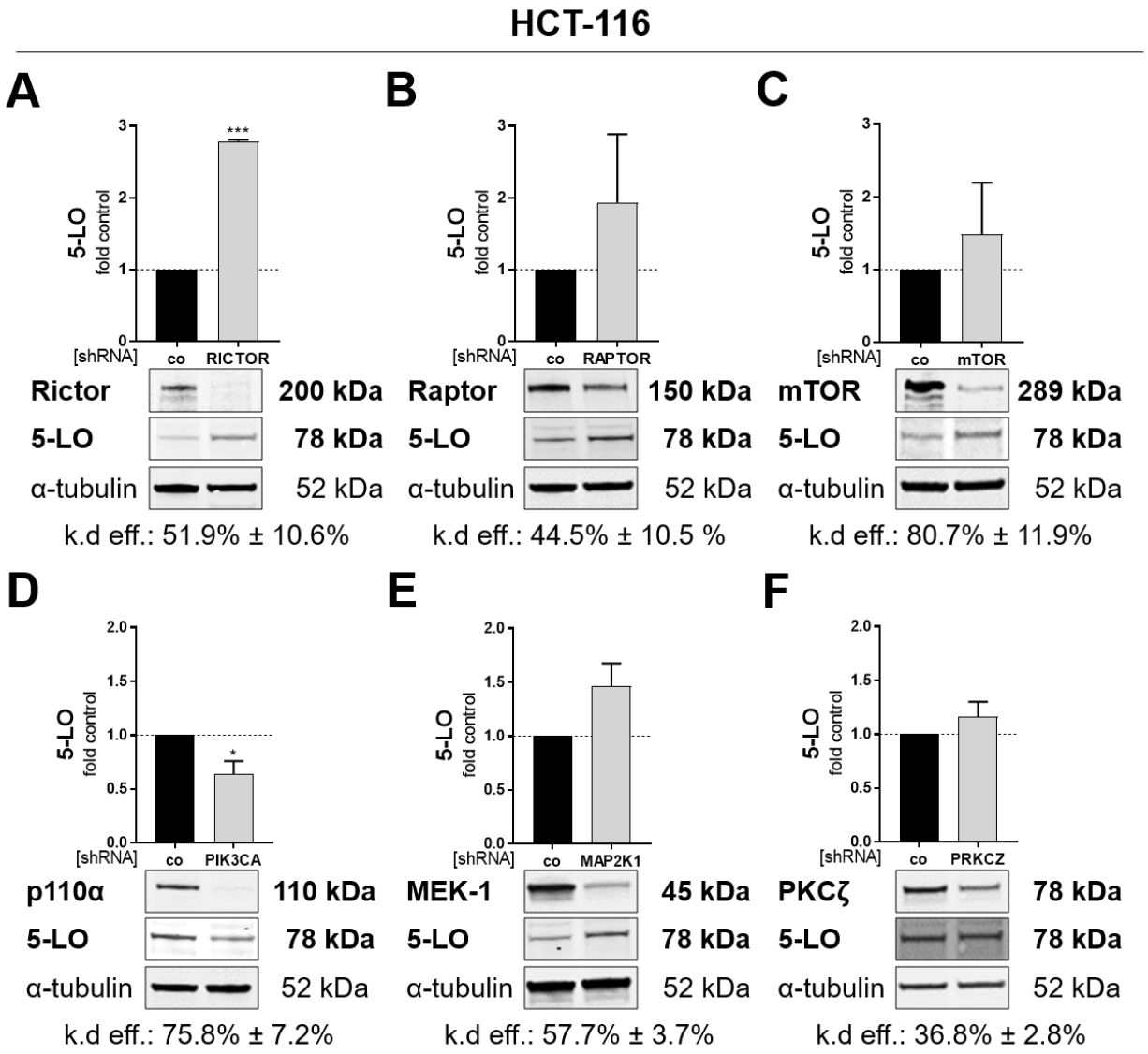

Figure 4.20: 5-LO and knockdown target protein expression after stable knockdown of members from the PI3K/mTOR and MEK/ERK cascades in HCT-116 cells.
5-LO and (A) Rictor, (B) Raptor, (C) mTOR, (D) p110α, MEK-1 (E), and PKCζ (F) expression in stable knockdown cells determined via Western blot. Knockdown efficiencies are depicted as mean ± SD and were determined via densitometric analysis of the respective knockdown target in non-mammalian shRNA expressing control cells (co) and respective knockdown cells. Densitometric values were normalized to the loading control α-tubulin followed by normalization to the non-mammalian shRNA expressing control (co). Results are depicted as mean + SEM from 3 independent experiments. One representative blot is shown. Asterisks indicate significant changes vs. control determined by unpaired two-tailed student's t-test with Welch's correction. * (P<0.05), ** (P<0.01), *** (P<0.001).

Furthermore, knockdown of Rictor in HCT-116 cells led to a more fibroblastic phenotype of the cells (see App. Figure 7.7B). Acceptable knockdown efficiencies (>50%) were reached for most targets. However, the determination of Rictor knockdown efficiencies was difficult due to the pronounced cleavage of Rictor in both control cell lines (App. Figure 7.7A). Furthermore, knockdown of PKCζ yielded only a poor knockdown efficiency in both established cell lines (<40%) (Figure 4.19F, Figure 4.20F).

Surprisingly, knockdown of the mTOR kinase could not significantly induce 5-LO protein expression. The biological replicates showed a high variation of 5-LO expression compared to the respective control in both cell lines (Figure 4.19C, Figure 4.20C). Similar results were obtained from the analysis of HCT-116 Raptor KD cells (Figure 4.20B). In contrast, HT-29 Raptor KD cells showed no considerable change in 5-LO expression (Figure 4.19B). Contrary to this, knockdown of Rictor significantly induced 5-LO expression in both established cell lines (Figure 4.19A, Figure 4.20A). Surprisingly, knockdown of the catalytic subunit p110α of PI3K led to a significant downregulation of 5-LO protein expression in HT-29 and HCT-116 p110α KD cells (Figure 4.19D, Figure 4.20D). Knockdown of the other subunits *PI3KCB* and *PI3KCD* did not influence 5-LO expression in both cell lines (Figure 4.18A, B). However, knockdown of *PI3KCG* in HT-29 cells reduced 5-LO expression significantly as well (Figure 4.18C). HCT-116 cells generally showed no expression of this catalytic subunit (Figure 4.18C).

Knockdown of MEK-1 did not alter 5-LO expression in both established cell lines. Finally, the inefficient knockdown of PKCζ did not alter 5-LO expression in HCT-116 cells; however, a non-significant attenuation of 5-LO expression in the respective HT-29 cell line was detectable.

4.3.5 Investigations on the coherence between cell cycle regulation and 5-LO expression

As the results shown and described in the previous chapters indicated a coherence of the observed enhanced 5-LO expression with shifts towards the G0/G1 cell cycle phase, the expression of cell cycle regulated and regulating genes was investigated in several sample sets.

Therefore, the mRNA expression of several transcription factors which play central roles during cell cycle progression was examined. This group of transcription factors includes the forkhead box protein O (*FOXO*) 1 and 3, c-Myc (*MYC*), specificity protein 1 (*SP1*), as well as members of the DREAM (dimerization partner, RB-like, E2F, and multivulval class B) complex like E2F1-5 (*E2F*), c-Myb (*MYB*), and b-Myb (*MYBL2*). Initially, samples of cells treated with inhibitors of the PI3K/mTOR and MEK-1/ERK signaling were examined. As shown in Figure 4.11, treatment with those compounds led to elevated *ALOX5* mRNA expression in HT-29 and HCT-116 cells.

In HT-29 cells (Figure 4.21A), dual PI3K/mTOR inhibition using Dactolisib (3 µM, Dac) significantly induced the expression of *FOXO1* and *FOXO3*. In contrast, *E2F1-3* levels were significantly decreased. The expression of *MYC*, *SP1* (Figure 4.21A), *E2F4*, and *E2F5* (App. Figure 7.8) was unaffected. Treatment of HT-29 cells with Erlotinib (5 µM, Erlo) or LB42708 (1 µM, LB) did not lead to relevant changes in the expression of any tested gene. However, MEK/ERK inhibition using PD184352 (1 µM, PD), Cobimetinib (0.5 µM, Cobi), or SCH772984 (1 µM, SCH) led to a firm (Cobi, SCH) and significant induction of *FOXO3* expression, as well as to significantly elevated expression levels of *SP1* (Cobi, SCH). In contrast, expression of *MYC* and *E2F1* was significantly decreased after treatment with Cobimetinib or SCH772984 (Figure 4.21A).

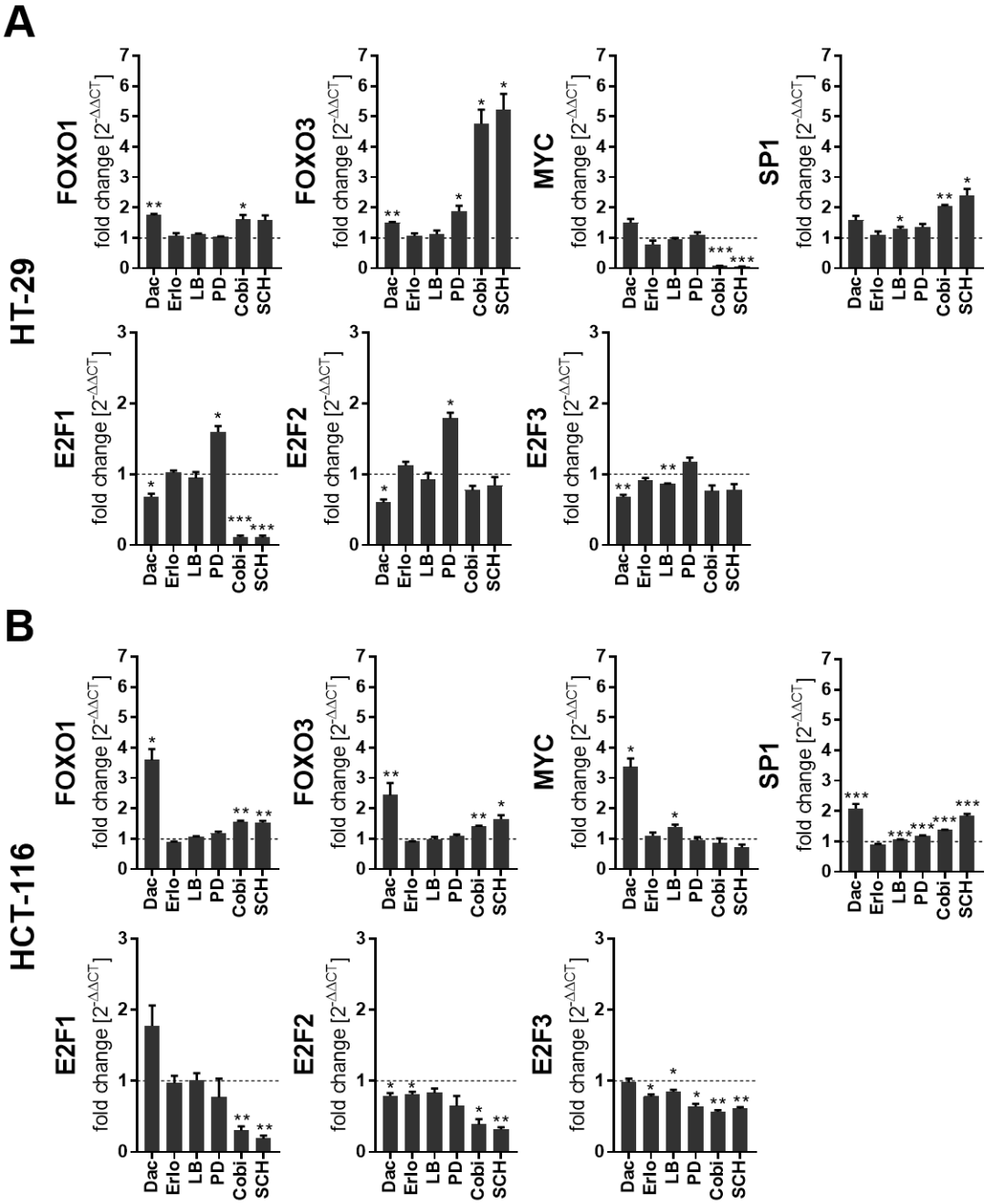

Figure 4.21: mRNA expression of cell cycle relevant transcription factors after 24 h of treatment with inhibitors of the PI3K/mTOR and MEK/ERK pathway in monolayer grown cells.
HT-29 (A) and HCT-116 (B) cells were seeded ($0.4x10^6$ cells/well, 6-well plate) and cell cycle was synchronized by serum starvation using RGM 22 h before treatment. Then, medium was changed to CGM for 2 h and cells were treated for 24 h with the indicated inhibitors Dactolisib (Dac) 3 µM, Erlotinib (Erlo) 5 µM; LB42708 (LB) 1 µM; PD184352 (PD) 1 µM; Cobimetinib (Cobi), 0.5 µM; SCH772984 (SCH) 1 µM. The vehicle control received DMSO instead. mRNA expression was determined via qPCR analysis. Expression was normalized to the housekeeping gene *ACTB* and the respective vehicle control ($2^{-\Delta\Delta CT}$ method). Results are depicted as mean + SEM from 3 independent experiments. Asterisks indicate significant changes vs. DMSO control determined by unpaired two-tailed student's t-test with Welch's correction. * (P<0.05), ** (P<0.01), *** (P<0.001).

As observed for HT-29 cells, treatment of HCT-116 cells using Dactolisib (3 µM) significantly induced the expression of *FOXO1* and *FOXO3* but was more pronounced (2.5-3.5-fold). Treatment of HCT-116 cells with Erlotinib (5 µM) or LB42708 (1 µM) did not lead to relevant changes in the expression of any tested gene; nevertheless, treatment sparsely but significantly

reduced the expression of *E2F2* (Erlo), *E2F3*, and *E2F4* (Figure 4.21B, App. Figure 7.8B). MEK/ERK inhibition by Cobimetinib or SCH772984 treatment led to a significant upregulation of *FOXO1* and *SP1* as well as a significant downregulation of *E2F1* in HCT-116 comparable to HT-29 cells. Furthermore, *FOXO3* was also significantly upregulated but to a lesser extent. While *E2F2* and *E2F3* expression levels were slightly decreased in HT-29 cells, effects were significant in HCT-116 cells. Interestingly, the treatment did not affect *MYC* expression in HCT-116 cells, although a strong downregulation was observed in HT-29 cells.

In addition, the mRNA expression of *MYB* and *MYBL2* was investigated (Figure 4.22). In HT-29 cells, *MYBL2* levels were significantly reduced following treatment with Dactolisib, Cobimetinib, and SCH772984, while Erlotinib, LB42708, and PD184352 treatment did not led to any significant changes in expression (Figure 4.22A). Interestingly, only treatment with Dactolisib was able to reduce *MYB* expression significantly. Treatment of HT-29 cells using MEK/ERK inhibitors even elevated the *MYB* expression. As seen for *MYBL2*, treatment using Erlotinib and LB42708 did not influence *MYB* expression (Figure 4.22A).

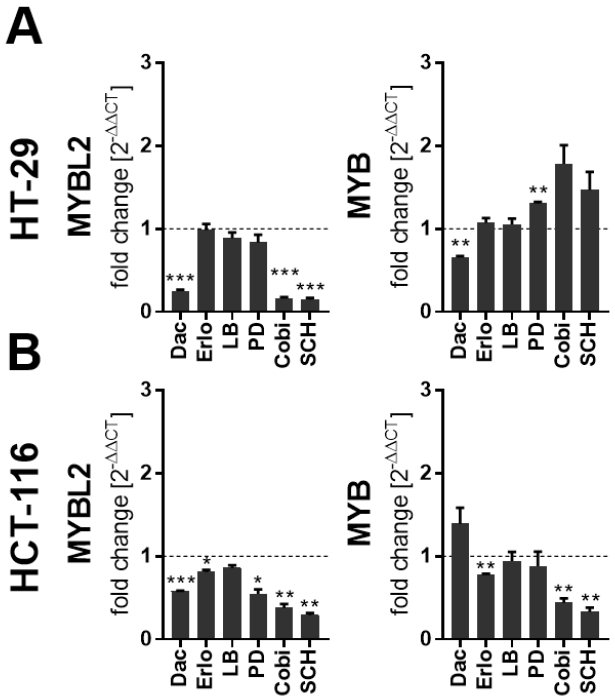

Figure 4.22: mRNA expression of *MYBL2* and *MYB* after 24 h of treatment with inhibitors of the PI3K/mTOR and MEK/ERK pathway in monolayer grown cells.
HT-29 (A) and HCT-116 (B) cells were seeded ($0.4x10^6$ cells/well, 6-well plate) and cell cycle was synchronized by serum starvation using RGM 22 h before treatment. Then, medium was changed to CGM for 2 h and cells were treated for 24 h with the indicated inhibitors Dactolisib (Dac) 3 µM; Erlotinib (Erlo) 5 µM; LB42708 (LB) 1 µM; PD184352 (PD) 1 µM; Cobimetinib (Cobi), 0.5 µM; SCH772984 (SCH) 1 µM. The vehicle control received DMSO instead. mRNA expression was determined via qPCR analysis. Expression was normalized to the housekeeping gene *ACTB* and the respective vehicle control ($2^{-\Delta\Delta CT}$ method). Results are depicted as mean + SEM from 3 independent experiments. Asterisks indicate significant changes vs. DMSO co determined by unpaired two-tailed student's t-test with Welch's correction. * ($P<0.05$), ** ($P<0.01$), *** ($P<0.001$).

In HCT-116 cells, all inhibitors but LB42708 led to significantly reduced mRNA expression of *MYBL2* but with more pronounced effects seen after treatment with PI3K/mTOR and MEK/ERK inhibitors (Figure 4.22B). While *MYBL2* expression levels were altered to a similar extent in both cell lines, *MYB* expression after treatment varied. In contrast to HT-29 cells, *MYB* expression was

increased in HCT-116 cells following Dactolisib treatment and significantly reduced after treatment with Erlotinib, Cobimetinib, and SCH772984. Treatment with LB42708 and PD184532 had no relevant effects (Figure 4.22B).

Since treatment with MEK/ERK inhibitors also led to an elevated *ALOX5* expression in HCT-116 p53 -/- cells (Figure 4.17B), expression of *E2F1*, *MYBL2*, *MYB*, and *SP1* was investigated as well. Compared to the parental cell line HCT-116, most inhibitor treatments failed to influence the expression of respective genes. However, treatment of HCT-116 p53 -/- cells with the ERK inhibitor SCH772984 (1 µM) led to comparable but less significant results as seen for HCT-116 wt cells (App. Figure 7.9).

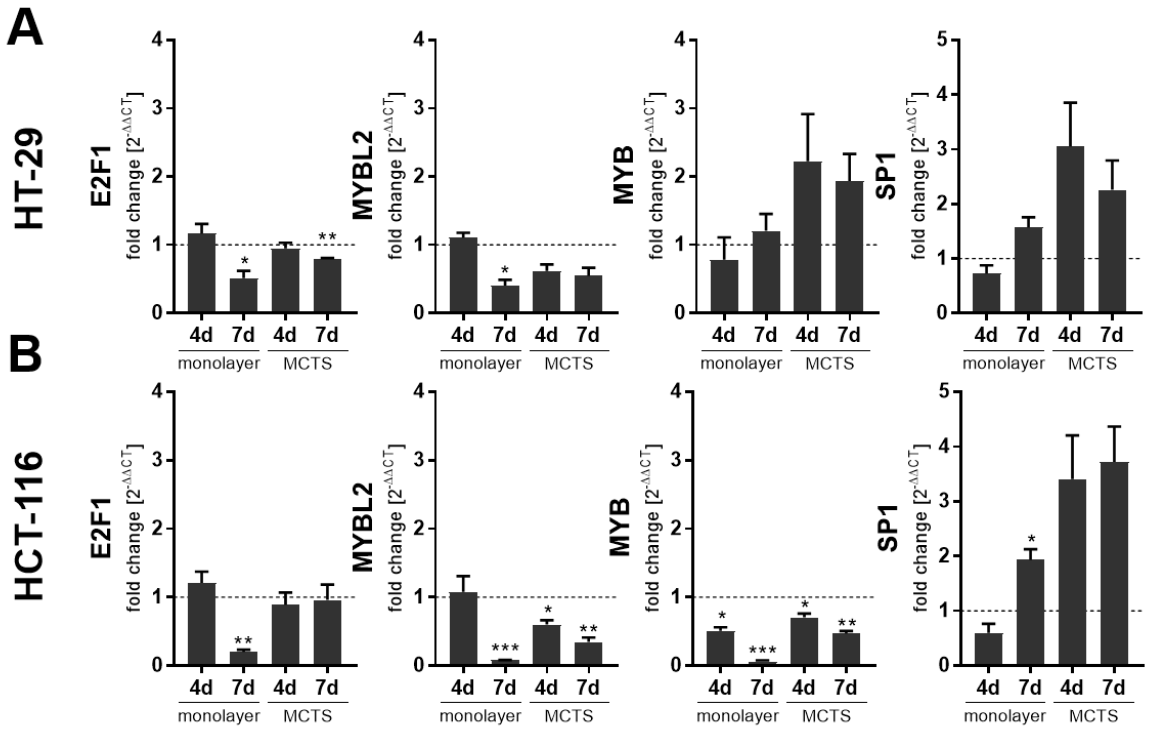

Figure 4.23: mRNA expression of *E2F1*, *MYBL2*, *MYB*, and *SP1* in MCTS.
MCTS were either grown for 4 or 7 days in 96-well low adherence plates. Respective monolayer controls were seeded in 12-well plates. Same cell amounts (0.05x10^6 cells/well) were used. The subconfluent monolayer controls (co) were seeded in 6-well plates (0.4x10^6 cells per well), received a medium change after 24 h, and were harvested after 48 h. Respective gene expression was determined via qPCR in HT-29 (A) and HCT-116 (B). Analysis was normalized to the housekeeping gene *ACTB* and the respective monolayer control ($2^{-\Delta\Delta CT}$ method). Results are depicted as mean + SEM from 3 independent experiments. Asterisks indicate significant changes vs. co determined by unpaired two-tailed student's t-test with Welch's correction. * (P<0.05), ** (P<0.01), *** (P<0.001).

Next, mRNA expression of selected transcription factors was investigated in MCTS of HT-29 and HCT-116 cells (Figure 4.23). *E2F1* expression was significantly reduced after 7 days of growth in MCTS and monolayer controls in HT-29 cells, whereas in HCT-116 cells only the 7-day monolayer controls were affected. A reduction in mRNA expression was also observable for *MYBL2* after 7 days of monolayer growth and in MCTS grown for 4 and 7 days in both cell lines. While the decrease in *MYBL2* expression was significant in HCT-116, mRNA levels in HT-29 cells were affected to a lesser extent and only significant for the 7-day monolayer control. Interestingly, *MYB* expression in HCT-116 was significantly downregulated under all conditions, whereas especially MCTS formation led to elevated *MYB* levels in HT-29 cells. Finally, *SP1* levels were slightly

reduced in 4-day monolayer controls of HT-29 and HCT-116 cells, but elevated in MCTS and 7-day monolayer controls.

A correlation of varying cellular seeding densities on the mRNA expression of *E2F1*, *MYBL2*, *MYB,* and *SP1* was also investigated, and the results are shown in Figure 4.24. *E2F1* and *MYBL2* expression levels indicated an inverse correlation with the seeding density in HT-29 and HCT-116 cells. Interestingly, lower seeding densities caused slightly elevated mRNA expression levels of *E2F1* and *MYBL2* compared to the low-density control ($0.04x10^6$ cells/cm^2). However, the reduced expression of both targets was only significant for the highest cellular seeding density in HCT-116 cells (Figure 4.24B). An opposite expression trend was observed for the expression of *SP1* in both cell lines. While the lowest seeding density only led to slightly increased mRNA expression levels in both cell lines, this effect was further enhanced with the cell number. In contrast to *E2F1*, *MYBL2,* and *SP1*, the expression of *MYB* was differently affected in each cell line, as already seen for other treatments and conditions. In HT-29 cells, *MYB* expression was not altered below a density of $0.21x10^6$ cells/cm^{2,} but increasing cell density led to an elevated *MYB* expression (Figure 4.24A). In HCT-116 cells, the *MYB* expression was generally reduced, but this reduction was more pronounced and only significant at the highest tested seeding density (Figure 4.24B).

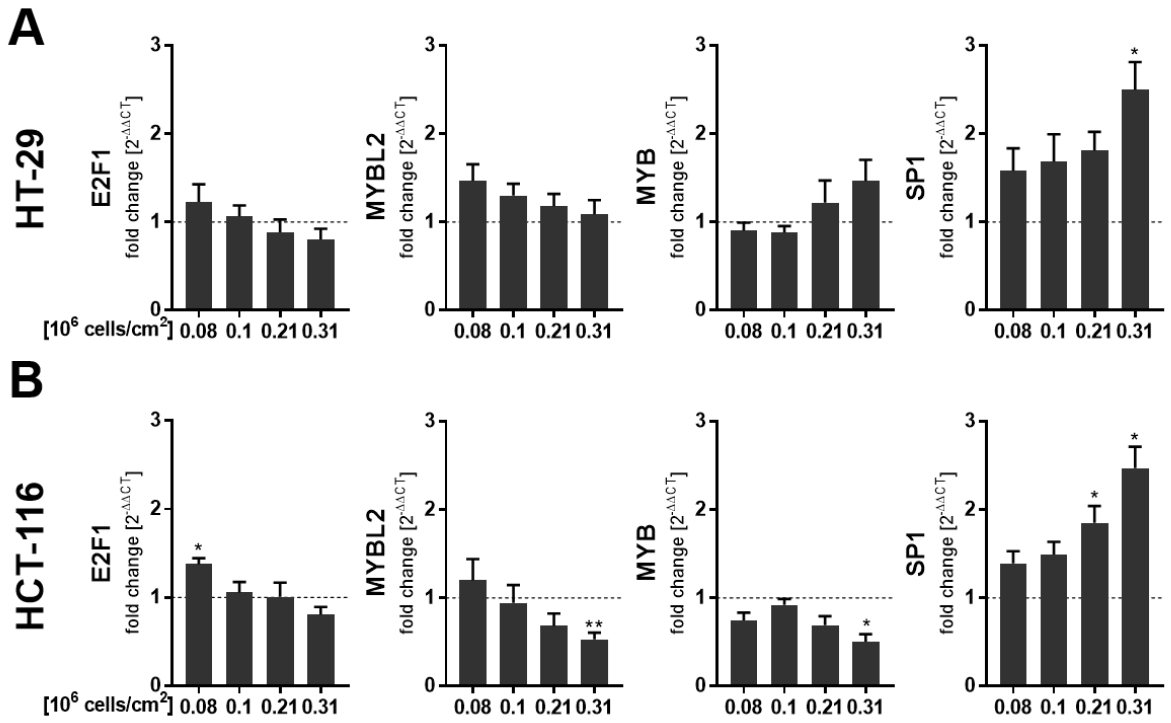

Figure 4.24: mRNA expression of *E2F1*, *MYBL2*, *MYB,* and *SP1* after growth in different cellular densities.
HT-29 (A) and HCT-116 (B) cells were seeded into 6-well plates using RGM in the indicated seeding densities. After 24 h medium was changed to CGM. Cells were harvested after another 24 h. mRNA expression was determined via qPCR analysis. Expression was normalized to the housekeeping gene *ACTB* and the respective 70-80% confluency control ($0.04x10^6$ cells/cm^2, $2^{-\Delta\Delta CT}$ method). Results are depicted as mean + SEM from 3 independent experiments. Asterisks indicate significant changes vs. $0.04x10^6$ cells/cm^2 co determined by unpaired two-tailed student's t-test with Welch's correction. * (P<0.05), ** (P<0.01), *** (P<0.001).

4.3.5.1 Influence of CDK1, CDK4/6 and E2F inhibition on 5-LO protein expression

Since the qPCR analysis of several sample sets revealed a downregulation of the transcription factors *E2F1* and *MYBL2* in both cell lines under conditions that were previously demonstrated to upregulate 5-LO expression, the influence of pharmacological cell cycle inhibition by CDK inhibitors on 5-LO expression was investigated next.

HT-29 and HCT-116 cells were treated with the CDK4/6 inhibitor Palbociclib (Palbo, 1 µM HT-29 cells, 10 µM HCT-116 cells) and the CDK1 inhibitor Ro-3306 (Ro, 10 µM). Cell cycle analysis was performed to verify sufficient cell cycle arrest. Treatment with Palbociclib induced a potent cell cycle arrest in the G0/G1 phase for HT-29 cells, while Ro-3306 triggered a potent arrest in the G2/M phase for both cell lines (Figure 4.25A).

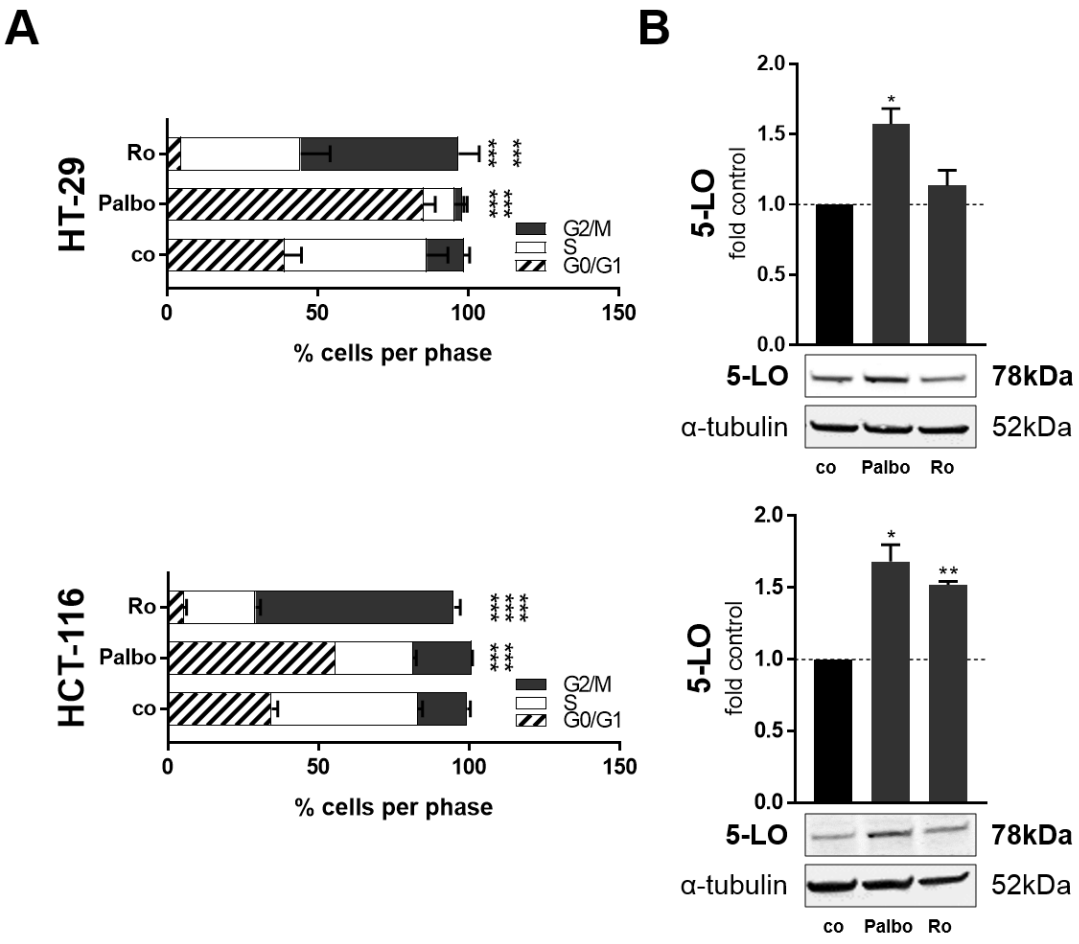

Figure 4.25: Cell cycle analysis and 5-LO protein expression after treatment with CDK1 and CDK4/6 inhibitors.
HT-29 and HCT-116 cells were seeded (3x10^6 cells/100 mm plate) and kept in RGM for 22 h to ensure cell cycle synchronization by serum starvation before treatment. Then, medium was changed to CGM for 2 h and cells were treated for 24 h with the indicated inhibitors Palbociclib (Palbo) and Ro-3306 (Ro). HT-29 cells were treated with 1 µM Palbolciclib or 10 µM Ro-3306, while HCT-116 cells were treated with 10 µM Palbocicib or 10 µM Ro-3306. The vehicle control (co) received DMSO instead. After 24 h cells were either harvested and prepared for cell cycle analysis (A) or Western blot analysis (B) to determine 5-LO protein expression. Densitometric values were determined and values were normalized to the loading control α-tubulin followed by normalization to the DMSO vehicle control (co). Results are depicted as mean + SEM from 4-6 independent experiments. Asterisks indicate significant changes vs. co determined by two-way ANOVA coupled with Dunnett's post-test for multiple comparisons. * (P<0.05), ** (P<0.01), *** (P<0.001). Respective inhibitor structures are displayed in App. Figure 7.10.

HCT-116 cells were less sensitive to treatment with Palbociclib and, therefore, treated with a higher concentration. However, CDK4/6 inhibition failed to induce complete cell cycle arrest in HCT-116 cells (Figure 4.25A). Although both cell lines were affected to a different extent by CDK4/6 inhibition, 5-LO expression on protein level (Figure 4.25B) was upregulated significantly in HT-29 and HCT-116 cells by 1.6- and 1.7-fold, respectively. G2/M arrest by CDK1 inhibition through Ro-3306 also led to a significant increase of 5-LO expression in HCT-116 cells, whereas the increase in HT-29 was only marginal.

As E2F1 expression was downregulated due to treatment or other tested conditions, the only commercially available pan-E2F inhibitor and its effect on 5-LO protein expression was tested. Therefore, HT-29 and HCT-116 cells were treated with HLM006474 (40 µM) for 24 h after cell cycle synchronization. Indeed, 5-LO protein expression was upregulated in both cell lines compared to the vehicle control (co) (Figure 4.26). However, the increase in 5-LO protein expression was minor and only significant for HCT-116 cells (Figure 4.26B).

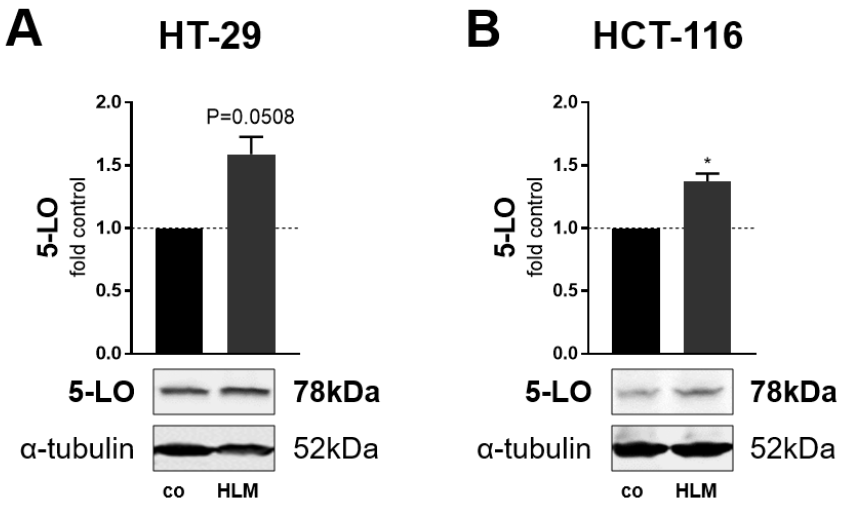

Figure 4.26: 5-LO protein expression after 24 h of treatment with an E2F inhibitor in monolayer grown cells.
HT-29 (A) and HCT-116 (B) cells were seeded ($3x10^6$ cells/100 mm plate) and cell cycle was synchronized by serum starvation using RGM 22 h before treatment. Then, medium was changed to CGM for 2 h and cells were treated for 24 h with the pan-E2F inhibitor HLM006474 (HLM) 40 µM. The vehicle control (co) received DMSO instead. Densitometric values were determined and values were normalized to the loading control α-tubulin followed by normalization to the DMSO vehicle control (co). Results are depicted as mean + SEM from 3 independent experiments. Asterisks indicate significant changes vs. DMSO vehicle control determined by unpaired two-tailed student's t-test with Welch's correction. * ($P<0.05$), ** ($P<0.01$), *** ($P<0.001$). The structure of HLM006474 is displayed in App. Figure 7.10.

4.3.5.2 5-LO localization in MCTS

As the previous results hint at a coherence between cell cycle regulation and 5-LO expression, the distribution of 5-LO expression in the MCTS was investigated and further related to proliferative and apoptotic regions in the spheroids.

For this, 14 µm cryosections of MCTS grown for 7 days were prepared and stained against the proliferation marker Ki67, the apoptosis marker (cleaved) Caspase 3 and 5-LO. After probing, samples were incubated with different secondary fluorophore-conjugated antibodies (Alexa Fluor™ Plus 488, Alexa Fluor™ Plus 647) for visualization employing a confocal laser scanning microscope. DAPI (4',6-diamidino-2-phenylindole) was used as a nuclear counterstain. MCTS cryosections generated from HT-29 and HCT-116 5-LO knockout cells served as controls to verify the specificity of the used primary 5-LO antibody (see (72) for KO generation and validation). Due to the size of the samples, tile scans were used to image a whole section of the respective HT-29 (3x3 tile scan) or HCT-116 (4x4 tile scan) MCTS. Total tile scans are displayed in App. Figure 7.11 and App. Figure 7.12. For better visibility, parts of those total tile scans are displayed in Figure 4.27 and Figure 4.28.

HT-29 MCTS displayed a dense coherent tissue mass which showed a distinct necrotic core. The necrotic core was characterized by a large mass of fragmented nuclei visualized by the DAPI staining (Figure 4.27C, Figure 4.28C, displayed as blue in the overlay Figure 4.27D, Figure 4.28D). In contrast, HCT-116 cells formed less coherent, sometimes even hollow MCTS. Staining of Ki67 was mainly concentrated towards the outer rim of the spheroid in both cell lines (Figure 4.27B, displayed as red in the overlay Figure 4.27D). Staining of cleaved Caspase 3 was primarily observed within the spheroid core or regions furthest from the rim regions (Figure 4.28B, displayed as red in the overlay Figure 4.28D).

Staining of 5-LO revealed a predominantly cytosolic location of the enzyme in cells within the MCTS of both cell lines (Figure 4.27E). HT-29 MCTS showed high 5-LO expression, mainly localized outside of the necrotic core region within the encasing viable mantle of cells. This region was also interspersed with highly proliferating cells. Notably, the Ki67-positive proliferating cells did not co-stain for 5-LO (Figure 4.27D, E). However, the cell mass within the necrotic core region also showed a positive 5-LO staining (Figure 4.28A, D). HCT-116 MCTS displayed an overall more diffuse 5-LO staining, concentrated on the viable outer rim of the MCTS structure, but 5-LO staining was also observed at the core rim (Figure 4.27D, Figure 4.28D). Of note, in HCT-116 MCTS the proliferating cells positive for Ki67 also showed a positive staining for 5-LO (Figure 4.27E).

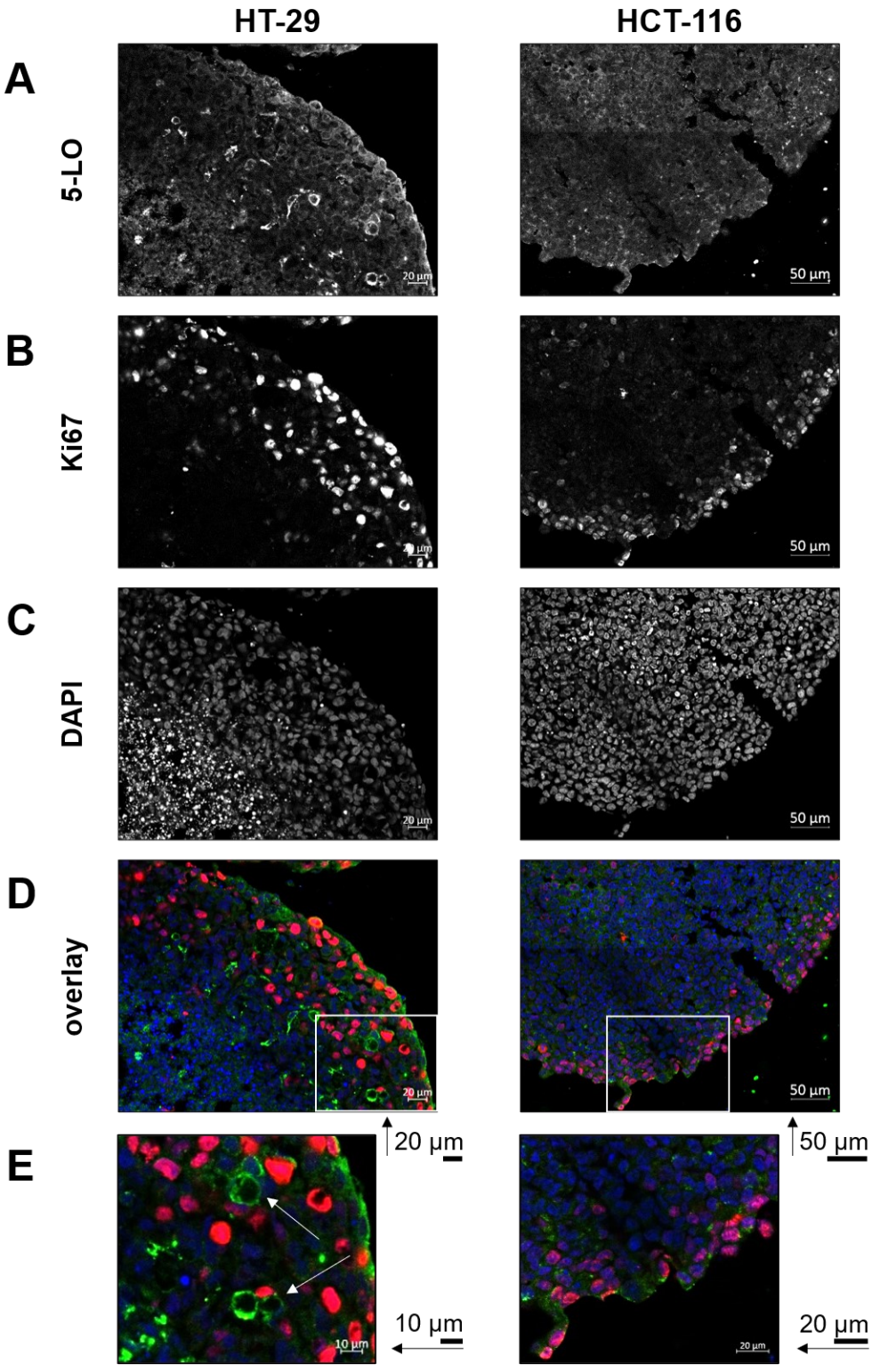

Figure 4.27: Confocal microscopy analysis of immunofluorescent stained MCTS cryosections.
MCTS ($0.05x10^6$ cells/well) were grown for 7 days in 96-well low adherence plates. 14 µM cryosections were co-stained with primary antibodies directed against 5-LO (A) and Ki67 (B). Afterwards, samples were probed with secondary fluorophore-conjugated antibodies (Alexa Fluor™ Plus 488, Alexa Fluor™ Plus 647). DAPI (C) was used for nuclear counterstaining. The sections were analyzed by confocal microscopy using 3x3 (HT-29) or 4x4 (HCT-116) tile scans. Displayed is a representative part of each digitally assembled scan. Single-channel fluorescence tile scan images (A-C) are displayed in black and white for better contrast, while channel overlay (D) is presented in color (Ki67 red, 5-LO green, DAPI blue). (E) shows an enlarged cut out of (D). Identical linear histogram adjustments were applied to each channel to adjust brightness and contrast. Scale bars are provided within the figure. Arrows indicate examples of cells expressing high amounts of 5-LO. One representative image of 3 independent experiments is shown.

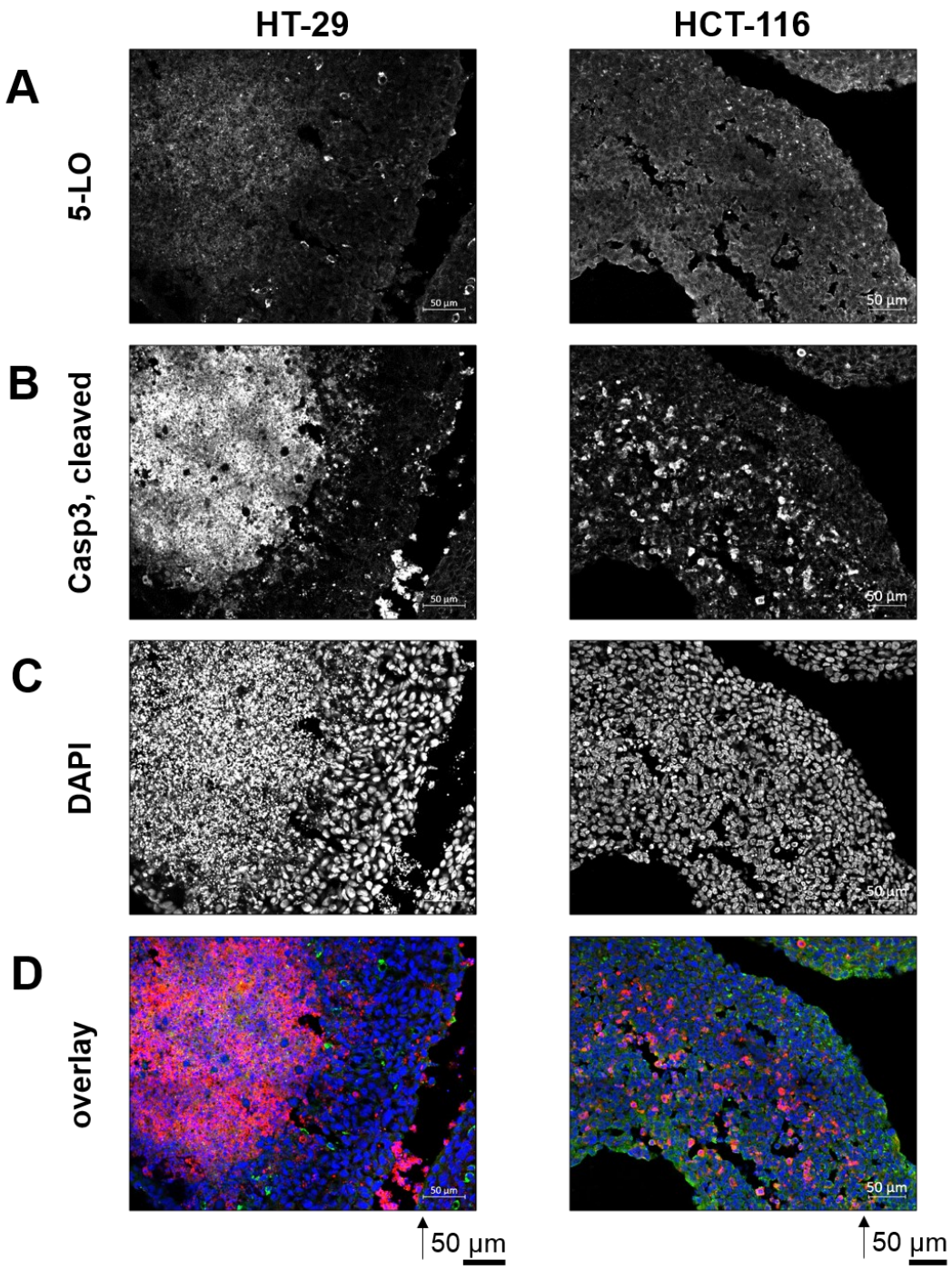

Figure 4.28: Confocal microscopy analysis of immunofluorescent stained MCTS cryosections.
MCTS ($0.05x10^6$ cells/well) were grown for 7 days in 96-well low adherence plates. 14 µM cryosections were co-stained with primary antibodies directed against 5-LO (A) and cleaved caspase 3 (B). Afterwards, samples were probed with secondary fluorophore-conjugated antibodies (Alexa Fluor™ Plus 488, Alexa Fluor™ Plus 647). DAPI (C) was used for nuclear counterstaining. The sections were analyzed by confocal microscopy using 3x3 (HT-29) or 4x4 (HCT-116) tile scans. Displayed is a representative part of each digitally assembled scan. Single-channel fluorescence tile scan images (A-C) are displayed in black and white for better contrast, while channel overlay (D) is presented in color (cleaved caspase 3 red, 5-LO green, DAPI blue). Identical linear histogram adjustments were applied to each channel to adjust brightness and contrast. Scale bars are provided within the figure. One representative image of 3 independent experiments is shown.

4.3.6 Influence of b-Myb expression on 5-LO expression

A number of genes were regulated in a similar way in HT-29 and HCT-116 cells after treatment with the different pathway inhibitors, MCTS formation as well as growth under high cellular density described in 4.3.5. These genes were *MYBL2*, *E2F1*, and *SP1*. Especially *MYBL2* and *E2F1* were significantly attenuated and negatively correlated with 5-LO expression. A *MYB* binding site upstream of the core promoter region (pN10) has already been characterized and identified to play a role in the repression of 5-LO expression in HL-60 cells (15, 355). In this context, the similarity in binding sites and the potential ability of b-Myb to bind at c-Myb binding sites were further discussed by Ponton et al. (355). Therefore, the potential role of b-Myb in the regulation of 5-LO in HT-29 and HCT-116 cells was further investigated within this study.

First, the influence of b-Myb overexpression on 5-LO expression was examined. Stably transfected HT-29 and HCT-116 cells constitutively overexpressing b-Myb (pSBbiGP_MYBL2) were designed and generated. Unfortunately, both cell lines quickly silenced the overexpressed transgene (App. Figure 7.13). Nevertheless, the constitutive b-Myb overexpression led to a significant downregulation of 5-LO expression in HCT-116 cells (App. Figure 7.13B).

To overcome the transgene silencing, HT-29 and HCT-116 cells carrying a Doxycycline-inducible variant of b-Myb (pSBtetGP_MYBL2) were designed and generated. After treatment with Doxycycline (400 ng/mL HT-29, 200 ng/mL HCT-116) for 24 and 48 h, b-Myb and 5-LO protein expression was analyzed. Compared to the control vector cell lines (CV), both HT-29 and HCT-116 cells induced b-Myb expression.

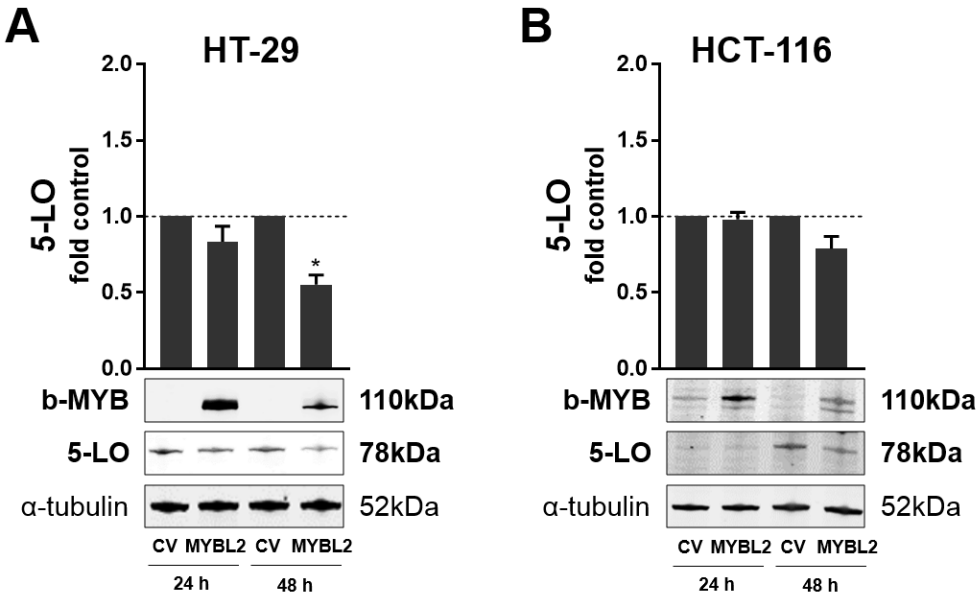

Figure 4.29: b-Myb and 5-LO protein expression in inducible b-Myb overexpressing cells after 24 and 48 h of Doxycycline treatment.
Inducible HT-29 (A) and HCT-116 (B) b-MYB overexpressing cells were seeded ($3x10^6$ cells/100 mm plate) and cell cycle was synchronized by serum starvation using RGM 22 h before treatment. Then, medium was changed to CGM for 2 h and cells were treated with either 400 ng/mL (A) or 200 ng/mL Doxycycline for 24 h or 48 h. The control vector cells (CV) received the same treatment. Densitometric values were determined and values were normalized to the loading control α-tubulin followed by normalization to the respective control vector cells (CV). Results are depicted as mean + SEM from 3 independent experiments. Asterisks indicate significant changes vs. DMSO vehicle control determined by unpaired two-tailed student's t-test with Welch's correction. * ($P<0.05$), ** ($P<0.01$), *** ($P<0.001$).

However, b-MYB expression was lower after 48 h of Doxycycline treatment compared to 24 h (Figure 4.29A, B). Nevertheless, 5-LO expression was significantly reduced (about 40%) in b-MYB overexpressing HT-29 cells after 48 h of Doxycycline treatment (Figure 4.29A). HCT-116 cells also showed a slight but not significant decrease (about 20%) in 5-LO expression.

Next, the influence of b-MYB overexpression on 5-LO expression during MCTS formation was investigated. Therefore, cells were seeded in CGM and treated with Doxycycline (400 ng/mL). After growth for 4 days, b-MYB and 5-LO protein expression were analyzed and compared with control vector cells (CV).

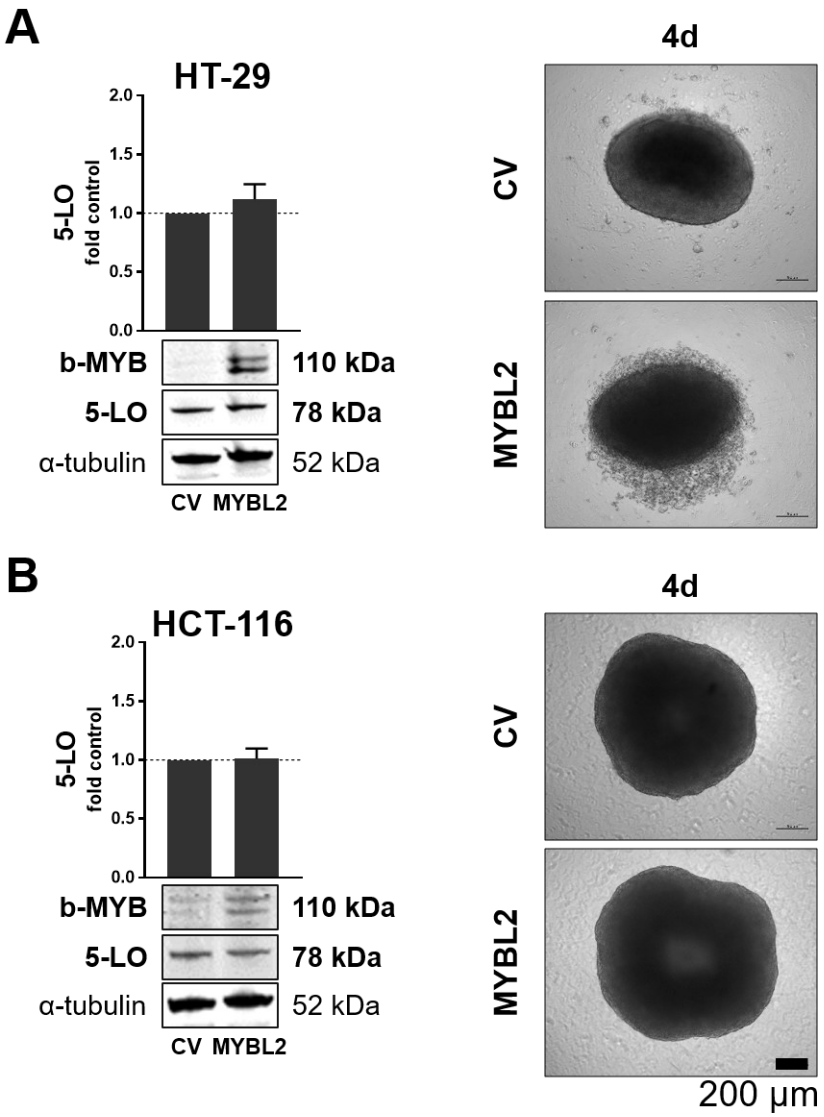

Figure 4.30: b-MYB and 5-LO protein expression in inducible b-Myb overexpressing cells after MCTS formation and Doxycycline treatment for 4 days.
Inducible HT-29 (A) and HCT-116 (B) b-MYB (pSBGP_MYBL2) overexpressing cells were seeded in 96-well low adherence plates ($0.05x10^6$ cells/well) using the respective CGM containing 400 ng/mL Doxycycline and were grown for 4 days. The control vector cells (CV) received the same treatment. Densitometric values were determined and values were normalized to the loading control α-tubulin followed by normalization to the respective control vector cells (CV). Results are depicted as mean + SEM from 3 independent experiments. Pictures were taken employing a light microscope (scale bar: 200 µm). One representative picture out of 3 is shown.

Neither HT-29 nor HCT-116 b-Myb overexpressing cells differentially expressed 5-LO compared to MCTS formed from control vector cells, which were also treated with Doxycycline (Figure 4.30). However, b-Myb expression influenced the spheroid formation of both cell lines. While HCT-116 b-Myb overexpressing cells formed bigger spheroids due to b-Myb overexpression, HT-29 b-Myb overexpressing cells formed spheroids with a loosened outer rim structure (Figure 4.30).

As the b-Myb overexpression experiments in HT-29 and HCT-116 monolayer-grown cells demonstrated a potential role of b-Myb in the regulation of 5-LO expression in those cells, additional reporter gene experiments were conducted. The *ALOX5* promoter region was investigated first.

To determine if the previously identified c-Myb binding site within the *ALOX5* promoter might play a role in the regulation of 5-LO expression in HT-29 and HCT-116 cells, stably transfected cells carrying reporter constructs containing the 5-LO core promoter (pN10LUC; -843 relative to the translation start (ATG)) or a larger promoter construct where the putative *MYB* response element is situated (pN6LUC; -2530 relative to translation start (ATG)), as well as a reporter construct carrying a promoter derivative that lacked the putative *MYB* binding site (pN6ΔMYBLUC) were generated (see Figure 1.3 for detailed sequences). Besides a firefly luciferase as the reporter, generated cell lines additionally constitutively expressed EGFP for easier verification of the efficacy of the antibiotic selection process. Furthermore, the EGFP signal was used for assay normalization since an in-house developed and produced substrate buffer system was applied (see 3.7 for substrate buffer composition and Figure 4.31E for schematic construct representation).

Parameters such as cell number, volumes, incubation times, pH, general assay procedure, and read-out were optimized and compared with Promega's commercially available Dual-Glo® substrate buffer. The generated cell lines were then tested under optimized conditions for their treatment response. Therefore, cells were treated with three different concentrations of the HDAC inhibitor Apicidin. As demonstrated for the pN10 cells in App. Figure 7.14, treatment of the pN10 carrying HT-29 and HCT-116 reporter cells with Apicidin led to a concentration-dependent increase of the firefly luciferase signal (App. Figure 7.14A) but did not significantly influence the EGFP signal (App. Figure 7.14B). After normalization, the results demonstrated a significant concentration-dependent increase of the firefly luciferase activity compared to the vehicle control (DMSO) and, therefore, suited reporter responsiveness of the generated cell lines (App. Figure 7.14C).

Analysis of the basal promoter activity in HT-29 and HCT-116 reporter cells showed a reduced relative firefly luciferase activity of the larger pN6 construct compared to the shorter pN10 construct in both cell lines, indicating the presence of an element that negatively regulates the *ALOX5* gene and is located upstream of the pN10 core promoter (Figure 4.31A, C). Mutation of the putative *MYB* binding site within the pN6 promoter construct led to different results for HT-29 and HCT-116 cells. Deleting the *MYB* binding site led to an activity loss of 83% in HT-29 cells, while the pN6 promoter activity was increased by about 34% in HCT-116 cells (Figure 4.31A, C).

After treatment with the pan-PI3K/mTOR inhibitor Dactolisib (Dac, 3 µM) and inhibitors of the MEK-1/ERK cascade (PD184352 (PD, 1 µM), Cobimetinib (Cobi, 0.5 µM), and SCH772984 (SCH, 1 µM)) a significant increase in relative firefly luciferase activity compared to vehicle

(DMSO) treated cells was detected in HT-29 and HCT-116 cells carrying the pN10 and pN6 reporter constructs (Figure 4.31B, D).

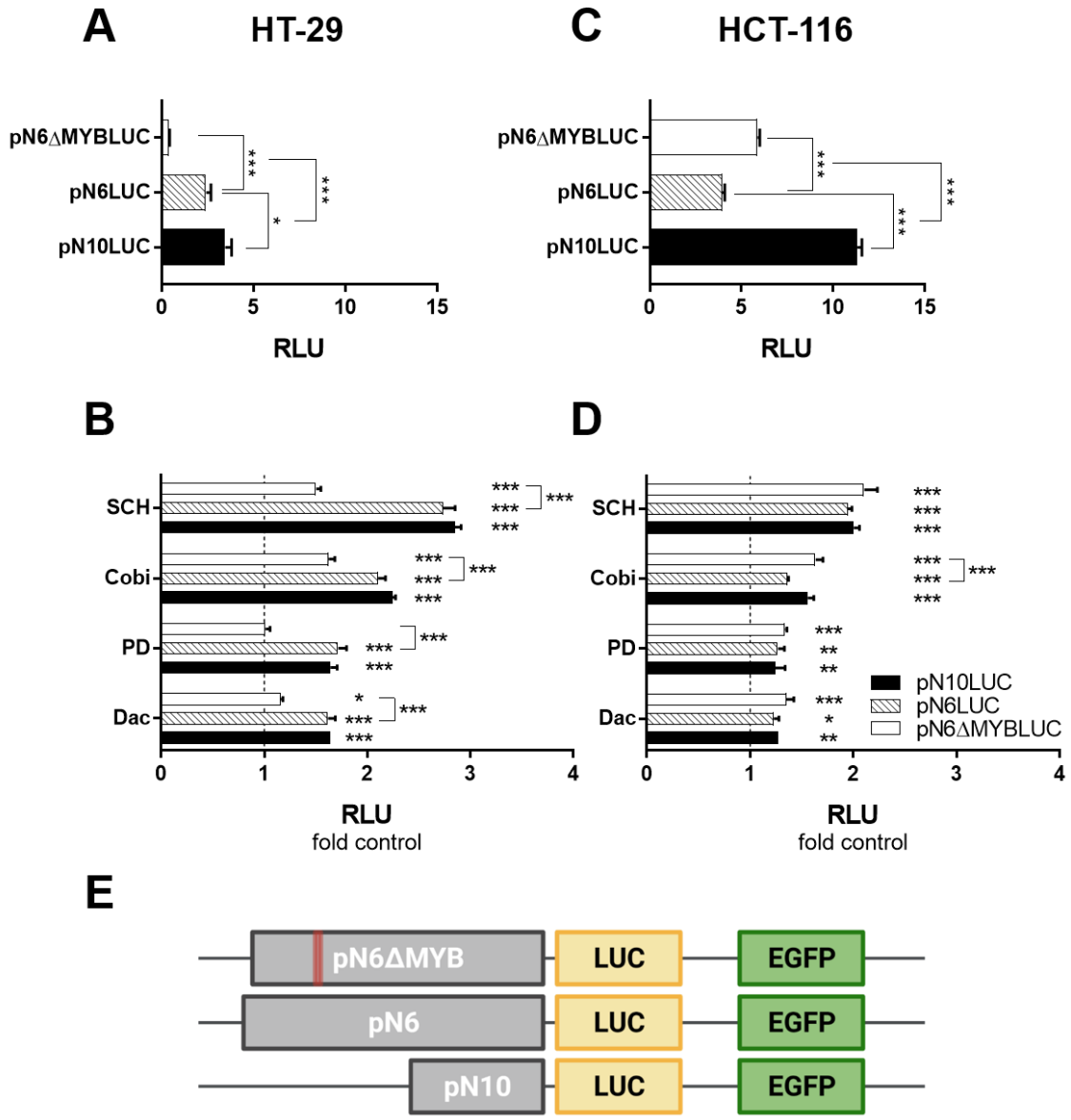

Figure 4.31: Firefly luciferase reporter gene assay to investigate different 5-LO promoter segments in stably transfected reporter cells.
Stably transfected (pSBGP_XLUC; X = promoter segment) HT-29 and HCT-116 reporter cells were seeded in black 96-well plates with a clear bottom ($0.03x10^6$ cells/well) and were cell cycle synchronized by serum starvation using RGM 22 h before further treatment. Then, medium was changed to CGM for 2 h and cells were treated for 24 h with the indicated inhibitors Dactolisib (Dac) 3 µM; PD184352 (PD) 1 µM; Cobimetinib (Cobi), 0.5 µM; SCH772984 (SCH) 1 µM. The vehicle control received DMSO instead. (A, C) Basal activity of luciferase (LUC) reporter constructs in HT-29 (A) and HCT-116 (C) reporter cells (pN10LUC; -843 relative to the translation start (ATG), pN6LUC; -2530 relative to translation start (ATG), pN6ΔMYBLUC missing the 7 bp MYB binding site; see Figure 1.2 for reference). Results are given as RLU (normalized to EGFP). (B, D) Reporter gene assay in HT-29 (B) and HCT-116 (D) reporter cells after treatment with inhibitors of the PI3K/mTOR and MEK/ERK axis for 24 h. Results are depicted as fold vehicle (DMSO) control. (E) Schematic representation of the luciferase constructs carrying different parts of the 5-LO promoter used for reporter gene experiments. Results are depicted as mean + SEM of 6 independent experiments. Asterisks indicate significant changes vs. co determined by two-way ANOVA coupled with Dunnett's post-test for multiple comparisons. * (P<0.05), ** (P<0.01), *** (P<0.001). Two-way ANOVA coupled with Tukey's post-test for multiple comparisons determined significant differences between constructs that received the same treatment. * (P<0.05), ** (P<0.01), *** (P<0.001).

HCT-116 carrying the pN6 construct with the deleted *MYB* binding site (pN6ΔMYB) showed the same results as obtained with the pN6 construct (Figure 4.31D). In contrast, deleting the *MYB* binding site of the pN6 construct (pN6ΔMYB) led to a significant decrease in luciferase activity in HT-29 cells compared with the pN6 reporter construct (Figure 4.31B).

In addition to the *ALOX5* promoter reporter constructs, constructs to investigate the role of a previously identified putative *MYB* binding site within the gene's coding sequence were generated, similar to Ringleb *et al.* (356). The constructs were designed to result in 5-LO cds fragment and firefly luciferase fusion proteins. A shortened 5-LO cds construct containing the putative *MYB* binding site should have been compared with a construct containing a mutated binding site (1600delmutMYB) and an even shorter construct not containing the putative *MYB* binding site (1699del) (see Figure 4.32C for schematic construct representation). Unfortunately, all constructs showed very low firefly luciferase activity in both cell lines, which was not significantly different from the control vector (SV40) (Figure 4.32A, B). Therefore, these constructs were not further evaluated.

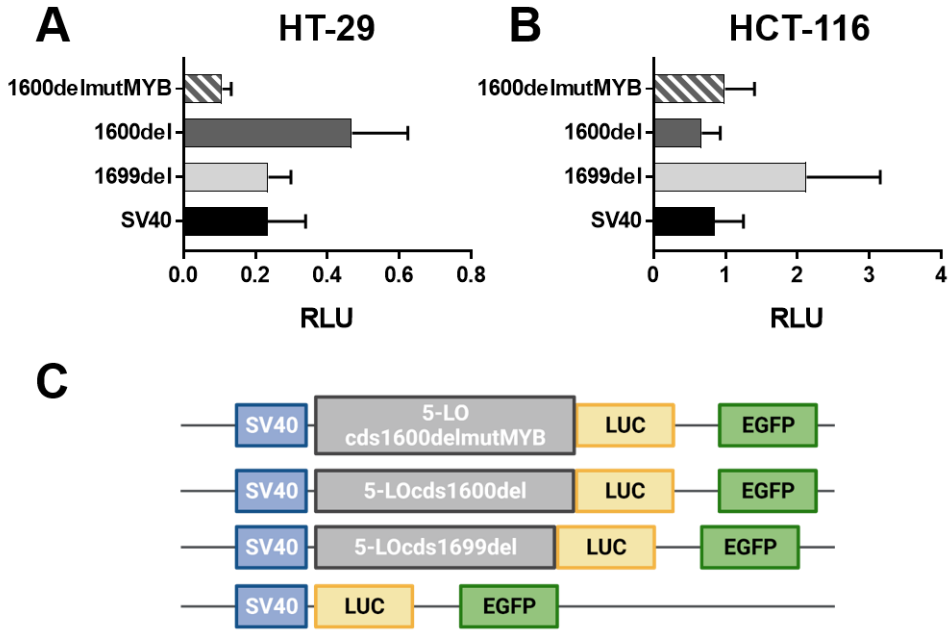

Figure 4.32: Firefly luciferase reporter gene assay to investigate different 5-LO coding sequence (cds) segments in stably transfected reporter cells.
Stably transfected (pSBGP_XLUC; X = cds segment) HT-29 and HCT-116 reporter cells were seeded in black 96-well plates with a clear bottom ($0.03x10^6$ cells/well) and were cell cycle synchronized by serum starvation using RGM for 22 h. Then, medium was changed to CGM and cells were incubated for 24 h. (A, B) Basal activity of luciferase (LUC) reporter constructs in HT-29 (A) and HCT-116 (B) reporter cells (SV40 control vector without cds; 1699del, +321 relative to the translation start (ATG); 1600del, +420 relative to the translation start (ATG) with a putative *MYB* binding site (CAAAGTTG); 1600delmutMYB, +420 relative to the translation start (ATG), with a mutated putative *MYB* binding site (TACATTCG)). Results are given as RLU (normalized to EGFP). (C) Schematic representation of the luciferase constructs carrying different segments of the 5-LO cds. Results are depicted as mean + SEM of 4 independent experiments.

4.3.7 Investigations on the applicability of 5-LO regulation by the PI3K/mTOR and MEK/ERK cascades in other cell lines

Elevated 5-LO expression is not restricted to colorectal malignancies and cell lines but has also frequently been found in other solid tumor specimens and cell lines of these tumors. Therefore, it was investigated if the previously identified regulation of 5-LO expression via the PI3K/mTOR and MEK-1/ERK signaling might be a mechanism that applies to other cancer cell lines as well.

To investigate the broader applicability of the findings obtained for HT-29 and HCT-116 cells, two other cell lines that show a substantial 5-LO expression (Capan-2, pancreas adenocarcinoma; U-2 OS, osteosarcoma, see Figure 2.1 for 5-LO expression compared to HT-29 and HCT-116 cells) and two cell lines which have inconsistent reports on their 5-LO expression status but are considered 5-LO negative under standard culture conditions, at least within the Steinhilber group, were selected (Caco-2, colon adenocarcinoma; MCF-7, mammary gland adenocarcinoma) (356–359).

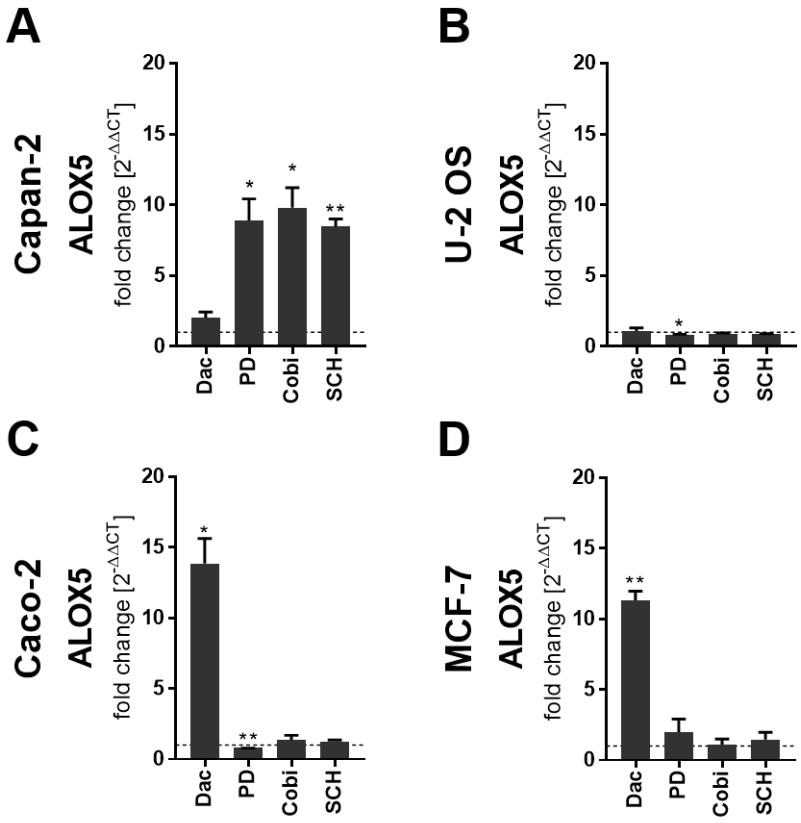

Figure 4.33: mRNA expression of ALOX5 after 24 h of treatment with inhibitors of the PI3K/mTOR and MEK/ERK pathway in monolayer grown cells.
Cell cycles of Capan-2 (A), U-2 OS (B), Caco-2 (C), and MCF-7 (D) cells were synchronized by serum starvation using RGM 22 h before treatment. Then, medium was changed to CGM for 2 h and cells were treated for 24 h with the indicated inhibitors Dactolisib (Dac) 3 µM; PD184352 (PD) 1 µM; Cobimetinib (Cobi), 0.5 µM; SCH772984 (SCH) 1 µM. The vehicle control received DMSO instead. *ALOX5* expression was determined via qPCR analysis. Expression was normalized to the housekeeping gene *ACTB* and the respective vehicle control ($2^{-\Delta\Delta CT}$ method). Results are depicted as mean + SEM from 3 independent experiments. Asterisks indicate significant changes vs. DMSO co determined by unpaired two-tailed student's t-test with Welch's correction. * (P<0.05), ** (P<0.01), *** (P<0.001).

Treatment of the respective cell lines with the pan-PI3K/mTOR inhibitor Dactolisib (Dac, 3 µM) and inhibitors of the MEK-1/ERK cascade (PD184352 (PD, 1 µM), Cobimetinib (Cobi, 0.5 µM), and SCH772984 (SCH, 1 µM)) for 24 h after cell cycle synchronization led to different results. While treatment of Capan-2 cells led to comparable results for *ALOX5* expression as previously shown for HT-29 and HCT-116 cells, U-2 OS cells showed no differential *ALOX5* expression due to the treatment (Figure 4.33A, B). *ALOX5* mRNA expression was significantly upregulated upon inhibition of MEK-1/ERK (8.5 - 9.8-fold, depending on the inhibitor), while dual inhibition of PI3K/mTOR only had a weak effect in Capan-2 cells. In contrast, Caco-2 and MCF-7 cells significantly induced *ALOX5* expression after treatment with Dactolisib (11.3 – 13.8-fold). But, treatment with MEK-1/ERK inhibitors did not upregulate *ALOX5* expression. Treatment of Caco-2 cells using PD184352 even reduced *ALOX5* expression. However, it is important to state that both cell lines only showed a very low basal *ALOX5* expression (CT values >33 for DMSO-treated cells). In Caco-2 cells, basal *ALOX5* expression was only detectable using 70 ng of cDNA template per PCR reaction instead of the usually used 20 ng.

Expression of *SP1* was upregulated in line with *ALOX5* expression. In U-2 OS cells, expression of *SP1* was not induced by any inhibitor, but treatment with Cobimetinib and SCH772984 reduced *SP1* expression significantly. *E2F1* expression was significantly downregulated in all tested cell lines due to Dactolisib treatment. Inhibition of MEK-1/ERK reduced *E2F1* expression significantly as well, but only in Capan-2 cells (Figure 4.34A). *MYBL2* expression was downregulated in all tested cell lines due to Dactolisib treatment as well, but only in a significant manner for U-2 OS, Caco-2, and MCF-7 cells. Treatment using MEK-1/ERK inhibitors did not reduce *MYBL2* expression in MCF-7 cells but led to a substantial and significant downregulation in Capan-2 cells (> 50%) (Figure 4.34A, D). Significant but minor downregulation was also observable in treated U-2 OS and Caco-2 cells. However, as shown in Figure 4.33, this was not accompanied by concurrent *ALOX5* upregulation. *MYB* expression was significantly downregulated in Capan-2, U-2 OS, and Caco-2 cells after treatment with Dactolisib. In contrast, this treatment led to a slightly elevated *MYB* expression in MCF-7 cells (Figure 4.34D). Treatment with the MEK/ERK inhibitors PD184352 and SCH772984 only significantly reduced *MYB* expression in Capan-2 cells (Figure 4.34A). Finally, treatment using Cobimetinib reduced the *MYB* expression in Capan-2 and U-2 OS cells but led to a slight but insignificant increase in Caco-2 cells (Figure 4.34A, B, C).

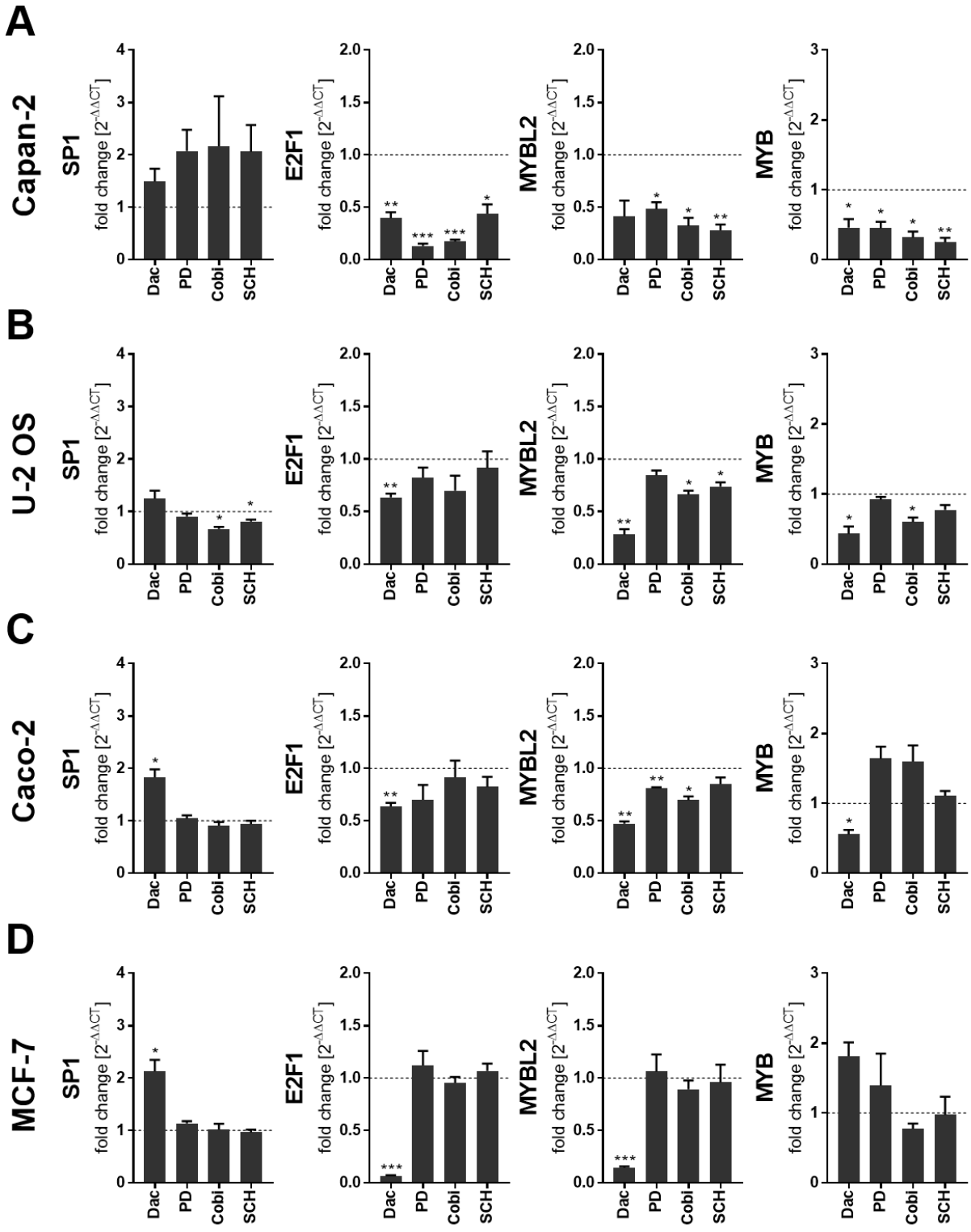

Figure 4.34: mRNA expression of cell cycle relevant transcription factors after 24 h of treatment with inhibitors of the PI3K/mTOR and MEK/ERK pathway in monolayer grown cells.
Capan-2 (A), U-2 OS (B), Caco-2 (C), and MCF-7 (D) cells were cell cycle synchronized by serum starvation using RGM 22 h before treatment. Then, medium was changed to CGM for 2 h and cells were treated for 24 h with the indicated inhibitors Dactolisib (Dac) 3 µM; PD184352 (PD) 1 µM; Cobimetinib (Cobi), 0.5 µM; SCH772984 (SCH) 1 µM. The vehicle control received DMSO instead. mRNA expression of *SP1*, *E2F1*, *MYBL2*, and *MYB* was determined via qPCR analysis. Expression was normalized to the housekeeping gene *ACTB* and the respective vehicle control ($2^{-\Delta\Delta CT}$ method). Results are depicted as mean + SEM from 3 independent experiments. Asterisks indicate significant changes vs. DMSO co determined by unpaired two-tailed student's t-test with Welch's correction. * ($P<0.05$), ** ($P<0.01$), *** ($P<0.001$).

4.4 Investigations on the impaired lipid mediator formation in HT-29 and HCT-116 cells

As demonstrated in Figure 2.1E published by Weisser *et al.*, the cell lines HT-29 and HCT-116, mainly investigated within this thesis, feature an impaired 5-LO activity in intact cells (72). In comparison to PMNL, the enzyme seemed inactive in those cell lines. However, the enzyme appears more active after the disruption of cellular integrity and segregation of membrane fractions via ultracentrifugation. Therefore, it was further investigated why the enzymes' activity is impaired in intact HT-29 and HCT-116 cells.

4.4.1 Lipid mediator formation and profile in HT-29 and HCT-116 cells

Due to the low 5-LO activity in intact HT-29 and HCT-116 cells compared to PMNL (Figure 2.1E), the differences between the basal and stimulated 5-LO activity were investigated first. For this purpose, $10x10^6$ cells per sample were prepared in ice-cold PBSG buffer. All samples were supplemented with 1 mM Ca^{2+} prior to the activity assay. Depending on the tested assay condition, cells were then either incubated for 10 min at 37°C or, prior to this, additionally stimulated with Ca^{2+} ionophore (A23187, 2.5 µM) or supplemented with a fatty acid mix (60 µM ARA, 60 µM DHA, 60 µM EPA), or stimulated and supplemented (A23187 2.5 µM, 60 µM ARA, 60 µM DHA, 60 µM EPA). An overview of the tested conditions is displayed in Figure 4.35A. After incubation, reactions were stopped by the addition of ice-cold MeOH. Samples were then aliquoted and stored at -80°C until further processing at the Fraunhofer-Institute for Translational Medicine and Pharmacology, Department of Clinical Research (Biomedical Analysis) by Carlo Angioni or Sandra Trautmann. Samples were analyzed towards the lipid mediator profile derived from lipoxygenase-mediated conversion of ARA, DHA, or EPA. The obtained lipid mediator concentrations were normalized according to 10^6 cells and corrected for non-enzymatic oxidation products determined in control samples without cells.

As shown in Figure 4.35B-F, the investigated cell lines did not produce any lipid mediators determined within this panel without supplementation of ARA, DHA, and EPA during the assay independent from the stimulation with Ca^{2+} ionophore (values <LLOQ). In the case of HT-29 cells, the stimulation using Ca^{2+} ionophore led to a significantly higher 5-LO-dependent 5-HETE and 5-HEPE formation (Figure 4.35B, C). Interestingly, the EPA-derived 5-HEPE amount was 2.5-fold higher than the formed ARA-derived 5-HETE amount (Figure 4.35C). Stimulation increased the formed LTB_4, but not significantly (Figure 4.35B). However, no differences in the formation of 7-HDHA were observed due to Ca^{2+} ionophore stimulation. The 15-LO-dependent formation of 17-HDHA and 15-HEPE was only minor and not significantly affected by stimulation with Ca^{2+} ionophore. Furthermore, both metabolites were formed in comparable amounts in HT-29 cells. In contrast, 15-HETE formation was 2-3-fold higher compared to 17-HDHA and 15-HEPE. Additionally, stimulation with Ca^{2+} ionophore increased 15-HETE formation significantly (Figure 4.35D). Interestingly, the formation of the 15-LO-1 metabolites 12-HETE, 14-HDHA, and 12-HEPE showed a different pattern. Here, the formation of 14-HDHA and 12-HEPE was preferred compared to the formation of 12-HETE. 14-HDHA and 12-HEPE formation was 2-3-fold higher compared to 12-HETE formation. Stimulation with Ca^{2+} ionophore failed to increase the formation of those metabolites significantly; however, an elevation was observed (Figure 4.35E).

Surprisingly, formation of the di-oxygenated metabolites 5,15-DiHETE and RvE4 derived from ARA and EPA, respectively, could also be detected in both cell lines. The panel also included the quantification of the DHA-dependent metabolite RvD5, but no quantifiable amounts were detected (<LLOQ). The formation of 5,15-DiHETE was 7.6-9.3-fold higher compared to RvE4 in HT-29 cells. Furthermore, no differences were observed for the formation of RvE4 after stimulation with Ca^{2+} ionophore. In contrast, this stimulation significantly induced the formation of 5,15-DiHETE. Notably, the formation of di-hydroxylated fatty acids was 25-80-fold lower compared to the formation of the mono-hydroxylated precursors in HT-29 cells.

In line with the already low 5-LO protein expression in HCT-116 cells (Figure 2.1), 5-LO-dependent lipid mediator formation was lower compared to HT-29 cells. Stimulation with Ca^{2+} ionophore did not significantly increase the formation of 5-HETE, but LTB_4 was only detectable in stimulated HCT-116 samples (Figure 4.35B). As already observed in HT-29 cells, 5-HEPE formation was 3-4-fold higher than 5-HETE formation. Furthermore, stimulation with Ca^{2+} ionophore increased 5-HEPE formation significantly. 7-HDHA formation was very low and not influenced by stimulation with Ca^{2+} ionophore (Figure 4.35C). In contrast to 5-LO metabolites, the formation of the 15-LO metabolites 15-HETE, 17-HDHA, and 15-HEPE was more pronounced in HCT-116 cells. However, no significant changes could be observed due to stimulation with Ca^{2+} ionophore. Compared to HT-29 cells, 15-HEPE formation was more pronounced in HCT-116 cells. The formation of 17-HDHA was comparable between both cell lines. Among the other 15-LO-1 metabolites, 12-HEPE was the most abundant and higher than in HT-29 cells. Again, as already seen in HT-29 cells, stimulation with Ca^{2+} ionophore did not significantly increase the formation of 12-HETE, 14-HDHA, and 12-HEPE. Finally, the formation of the di-hydroxylated fatty acids 5,15-DiHETE and RvE4 was lower compared to HT-29 cells, and formation was not influenced by stimulation with Ca^{2+} ionophore in HT-29 cells. As described for HT-29 cells, the formation of di-hydroxylated fatty acids was 40-170-fold lower than mono-hydroxylated precursors in HCT-116 cells.

Since *ALOX15* mRNA expression was relatively low compared to *ALOX5* expression, and *ALOX15B* expression could not be detected in HT-29 and HCT-116 cells, 15-LO-1 and 15-LO-2 protein expression was determined via Western blot (Figure 4.36A). By this, very low 15-LO-1 protein expression in both cell lines could be confirmed. Furthermore, no 15-LO-2 protein expression was detected (Figure 4.36A). Surprisingly, chiral 15-HETE and 17-HDHA analysis revealed significantly higher amounts of the respective *R*-enantiomers than the *S*-enantiomers in both cell lines. In HT-29 cells, the ratio of 15-*R/S*-HETE is distributed between 2.1-5, dependent on the assay condition. This ratio is lower (1.4-1.5) in HCT-116 cells. In comparison, the ratio of 17-*R/S*-HETE is distributed between 1.2-1.5 in HT-29 cells, while it is again lower (1.2-1.3) in HCT-116 cells. In HT-29 cells, the formation of 15-*R/S*-HETE and 17-*R/S*-HDHA was influenced by stimulation with Ca^{2+} ionophore but not significantly. This effect was only observed for the respective *S*-enantiomer in HCT-116 cells.

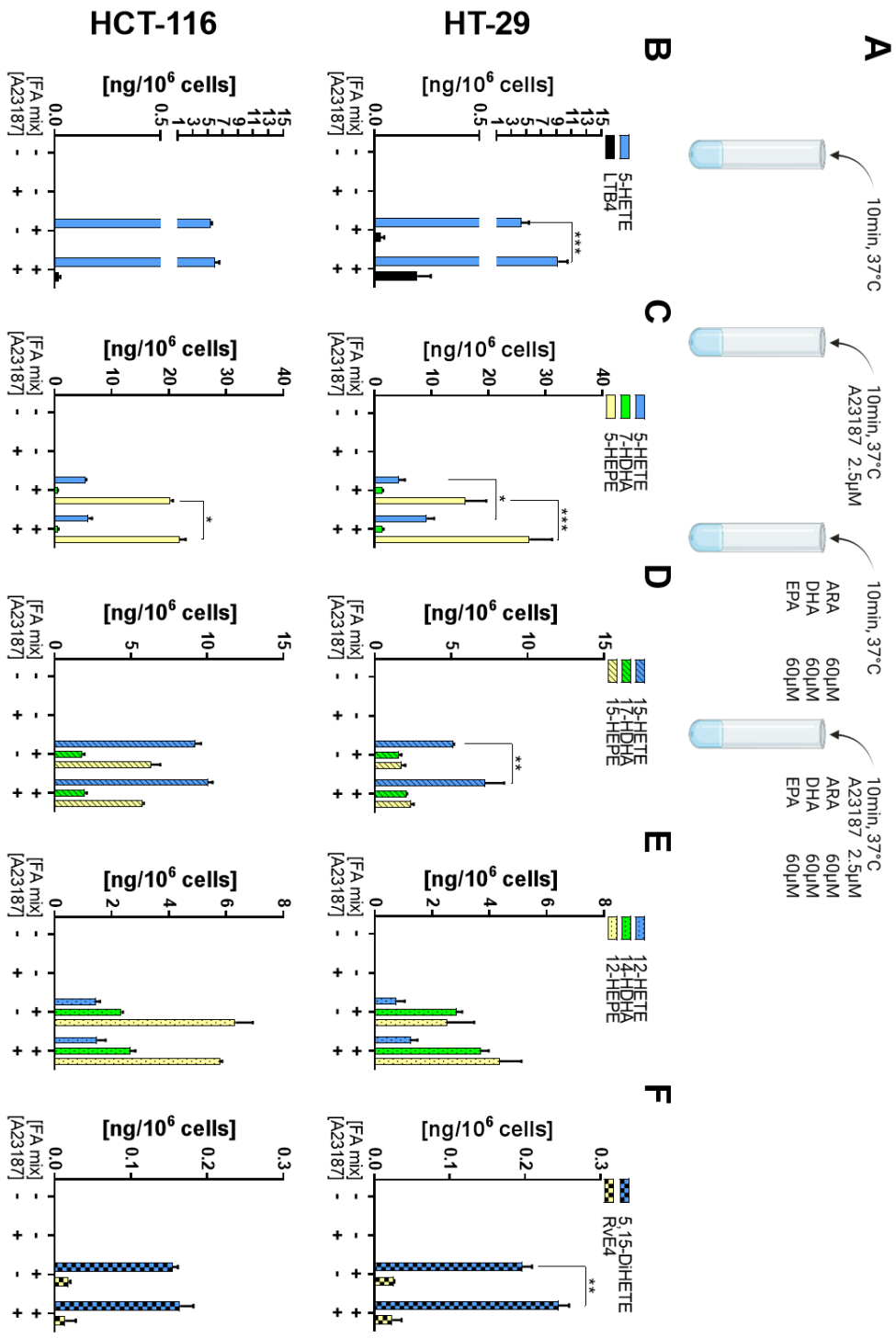

Figure 4.35: Lipid mediator profile in unstimulated and stimulated HT-29 and HCT-116 cells.
Comparison of the stimulated and unstimulated lipid mediator formation in intact HT-29 and HCT-116 cells (A). Cells were seeded (10x10^6 cells per 150 mm plate) in CGM and cultured for 48 h. Cells were harvested, counted and diluted according to 10x10^6 cells/mL in PBSG buffer prior to the assay. Intact cells (10x10^6 per sample) were stimulated with Ca^{2+} ionophore (A23187, 2.5 µM) and supplemented with 1 mM Ca^{2+} and a fatty assay mix (FA mix; 60 µM ARA, 60 µM DHA, and 60 µM EPA). Samples were incubated for 10 min at 37°C, then the reaction was terminated with 1 mL ice-cold MeOH and lipid mediator formation (5-HETE, LTB_4 (B); 5-HETE, 7-HDHA, 5-HEPE (C); 15-HETE, 17-HDHA, 15-HEPE (D); 12-HETE, 14-HDHA, 12-HEPE (E); 5,15-DiHETE, RvE_4 (F)) was analyzed via LC/MS-MS. Ascertained lipid mediator amounts were normalized to 10^6 cells and corrected for non-enzymatic oxidation products determined in control samples without cells. Results are depicted as mean + SEM from 3 independent experiments. Asterisks indicate significant changes between stimulated and unstimulated cells supplemented with fatty acid mix determined by two-way ANOVA coupled with Dunnett's post-test for multiple comparisons. * (P<0.05), ** (P<0.01), *** (P<0.001).

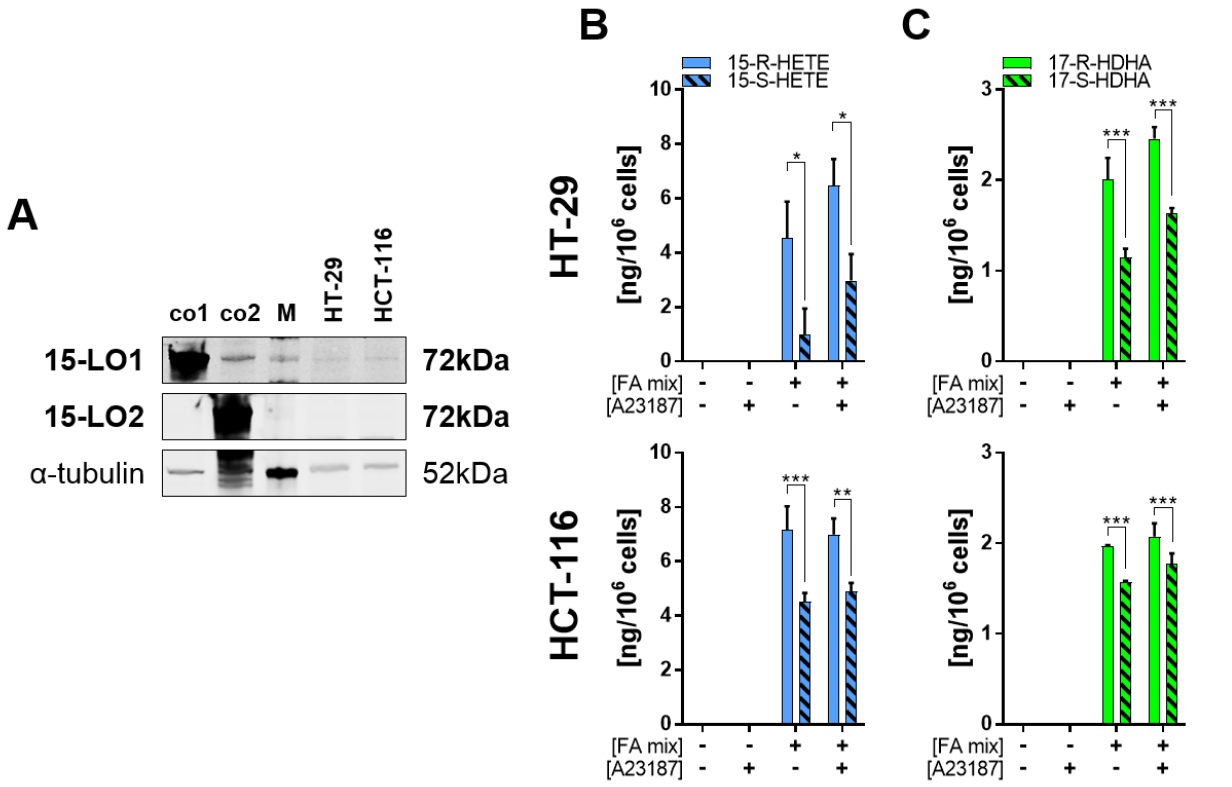

Figure 4.36: 15-LO expression and chiral 15-LO dependent lipid mediator formation in unstimulated and stimulated HT-29 and HCT-116 cells.
(A) 15-LO-1 and 15-LO-2 protein expression was analyzed via Western blot. Stably transfected HEK239T cells expressing either 15-LO-1 (co1) or 15-LO-2 (co2) and a size marker (M) served as controls. Displayed is one representative out of 3 independent blots. (B, C) Comparison of the stimulated and unstimulated 15-LO dependent 15*R/S*-HETE and 17*R/S*-HDHA formation in intact HT-29 and HCT-116 cells. Cells were seeded ($10x10^6$ cells per 150 mm plate) in CGM and cultured for 48 h. Cells were harvested, counted and diluted to $10x10^6$ cells/mL in PGC buffer prior to the assay. Intact cells ($10x10^6$ per sample) were stimulated with Ca^{2+} ionophore (A23187, 2.5 µM) and supplemented with 1 mM Ca^{2+} and a fatty acid mix (FA mix; 60 µM ARA, 60 µM DHA, and 60 µM EPA). Samples were incubated for 10 min at 37°C, then the reaction was terminated with 1 mL ice-cold MeOH, and lipid mediator formation was analyzed via LC/MS-MS. Ascertained lipid mediator amounts were normalized to 10^6 cells and corrected for non-enzymatic oxidation products determined in control samples without cells. Results are depicted as mean + SEM from 3 independent experiments. Asterisks indicate significant changes between stimulated and unstimulated cells supplemented with fatty acid mix determined by two-way ANOVA coupled with Bonferroni's post-test for multiple comparisons. * (P<0.05), ** (P<0.01), *** (P<0.001).

Since the general lipid mediator formation in both cell lines was relatively low, even though high fatty acid concentrations were used, substrate concentration dependent 5-HETE and LTB_4 formation was investigated (Figure 4.37). Indeed, the highest concentration of ARA (60 µM) led to the highest 5-HETE formation in both cell lines. However, doubling or tripling (10 µM vs. 20 µM, 20 µM vs. 60 µM) of the substrate concentration did not lead to doubling or tripling of formed 5-HETE. Instead, 3.8-fold less 5-HETE was formed using 20 µM ARA, 11-fold less using 10 µM ARA, and 57.6-fold less using 6 µM ARA compared to 60 µM ARA in HT-29 cells. In HCT-116 cells, 20 µM ARA led to 2-fold less 5-HETE, while 10 µM ARA led to 3-fold less 5-HETE, and 6 µM ARA led to 30-fold less 5-HETE compared to 60 µM ARA.

No LTB_4 formation could be detected in both cell lines using 6 µM ARA. Very low LTB_4 concentrations could be detected using 10 µM ARA in HT-29 cells (0.019 ng/10^6 cells, Figure 4.37A), while no LTB_4 formation could be detected in HCT-116 cells (Figure 4.37B). In comparison, the use of 60 µM ARA led to 0.21 ng/10^6 HT-29 cells and only 0.019 ng/10^6 HCT-116 cells. Therefore, using 6-fold less of the substrate (10 µM vs. 60 µM ARA) led to 11-fold less LTB_4 in HT-29 cells, the same ratio as seen for 5-HETE.

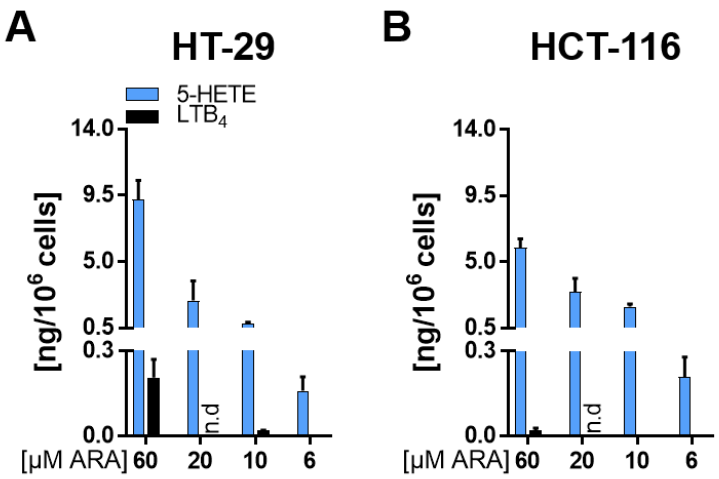

Figure 4.37: Substrate-dependent 5-LO activity in HT-29 and HCT-116 cells.
Comparison of the stimulated substrate concentration-dependent 5-LO activities in intact HT-29 and HCT-116 cells. Cells were harvested, counted and diluted according to 10x10^6 cells/mL in PGC buffer prior to the assay. Intact cells (10x10^6 per sample) were stimulated with Ca^{2+} ionophore (A23187, 2.5 µM) and supplemented with 1 mM Ca^{2+} and several ARA concentrations. Samples were incubated for 10 min at 37°C, then the reaction was terminated with 1 mL ice-cold MeOH, and lipid mediator formation was analyzed via LC/MS-MS. Ascertained lipid mediator amounts were normalized to 10^6 cells and corrected for non-enzymatic oxidation products determined in control samples without cells. Results are depicted as mean + SEM from 3 independent experiments. n.d = not determined.

4.4.2 Lipid mediator profile in HT-29 and HCT-116 cells compared to leukocytes

As 5-LO is primarily expressed in leukocytes, the activity of 5-LO in HT-29 and HCT-116 cells was compared to the enzymes' activity in PMNL, M1, and M2 macrophages. Furthermore, the lipid mediator formation was compared with the respective 5-LO and FLAP expression of the individual cells. For better comparability between the different cell types, the lipid mediator formation was, this time, normalized to the total protein amount of the cells assayed.

Samples were prepared in ice-cold PBSG buffer. All samples were supplemented with 1 mM Ca^{2+} prior to the activity assay. Cells were incubated for 10 min at 37°C and stimulated with Ca^{2+} ionophore (A23187, 2.5 µM) as well as supplemented with a fatty acid mix (60 µM ARA, 60 µM DHA, 60 µM EPA). As suspected, PMNL formed the highest amounts of 5-HETE (465.8 ng/mg total protein) and LTB_4 (110.6 ng/mg total protein) (Figure 4.38). Unfortunately, this does not align with the displayed 5-LO expression due to protein degradation (Figure 4.38A). In line with the higher 5-LO expression, M1 macrophages formed higher 5-HETE and LTB_4 amounts than M2 macrophages. Surprisingly, HT-29 (59 ng/mg total protein) and HCT-116 (46 ng/mg total protein) cells formed comparable amounts of 5-HETE to M2 macrophages (57 ng/mg total protein) (Figure 4.38). However, M2 macrophages formed higher amounts of LTB_4 (0.72 ng/mg total protein)

compared to HT-29 (0.43 ng/mg total protein) and HCT-116 (0.13 ng/mg total protein) cells (Figure 4.38B). Additionally, FLAP (upper band) expression was rather low in cells that formed only low amounts of LTB_4 (Figure 4.38A). Summarizing, 5-LO activity indicated by the formation of 5-HETE and LTB_4 was, compared to PMNL, 9.7-fold lower in HT-29 cells, 12.5-fold lower in HCT-116 cells, 4.9-fold lower in M1 macrophages, and 10-fold lower in M2 macrophages even though M1 and M2 macrophages showed much higher 5-LO protein expression than HT-29 and HCT-116 cells.

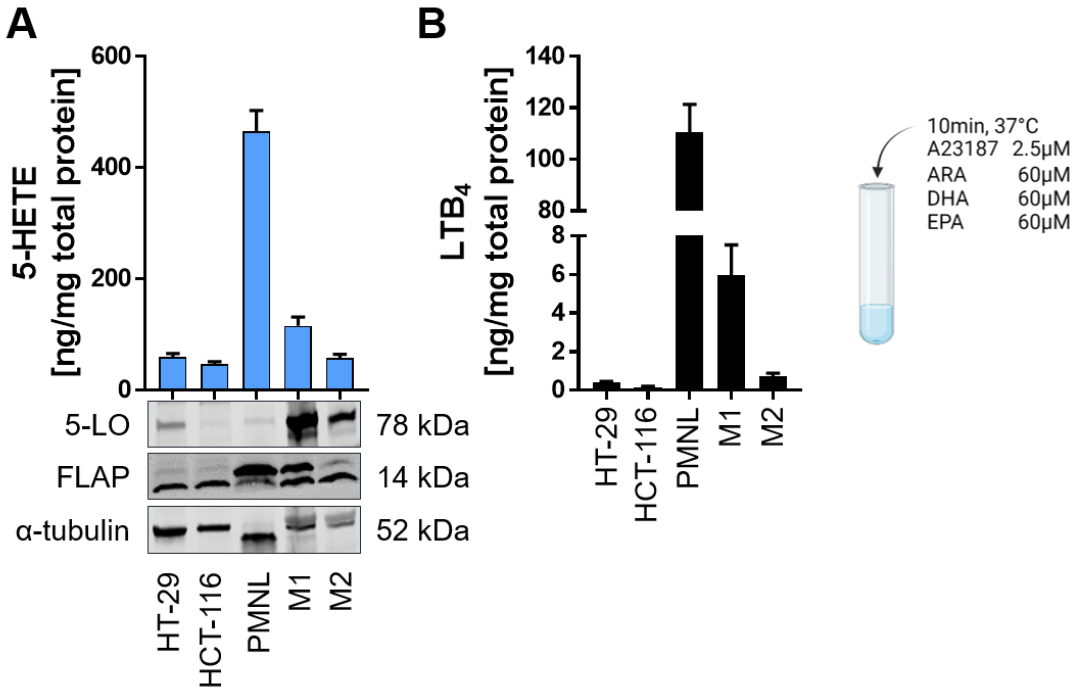

Figure 4.38: Comparison of 5-LO activity in tumor cells and leukocytes.
Comparison of the 5-LO activity with 5-LO and FLAP expression in intact HT-29 and HCT-116 cells, PMNL, M1 and M2 macrophages. Tumor cells were seeded ($10x10^6$ cells per 150 mm plate) in CGM and cultured for 48 h. PMNL and PBM were isolated from buffy coats via density centrifugation. Macrophages were differentiated from human PBM isolated via the adherence method (8x100 mm plates per patient). For this, cells were treated with 10 ng/mL GM-CSF (M1, 4 plates) or M-CSF (M2, 4 plates) for 7 days. Additionally, the cells received 10 ng/mL IFNγ (M1) or IL-4 (M2) during the final 48 h. Cells were harvested, counted (HT-29, HCT-116, and PMNL) and diluted according to $10x10^6$ cells/mL in PGC buffer prior to the assay. The 4 prepared M1 or M2 dishes of each donor were combined. Intact cells ($10x10^6$ cells, HT-29, HCT-116, PMNL, or M1/M2 cells combined from 4 dishes) were stimulated with Ca^{2+} ionophore (A23187, 2.5 µM) and supplemented with 1 mM Ca^{2+} and a fatty acid mix (FA mix; 60 µM ARA, 60 µM DHA, and 60 µM EPA). Samples were incubated for 10 min at 37°C, then the reaction was terminated with 1 mL ice-cold MeOH, and lipid mediator formation was analyzed via LC/MS-MS. Ascertained lipid mediator amounts were normalized to the determined total protein amounts and corrected for non-enzymatic oxidation products determined in control samples without cells. Results are depicted as mean + SEM from 3 (HT-29, HCT-116) or 6 (PMNL, M1, M2) independent experiments. 5-LO and FLAP expression was analyzed via Western blot. One representative out of 3 blots is shown.

Despite the fact that formed amounts of 5-HETE in PMNL were very high, the formation of 5-LO dependent 5-HEPE was even higher (465.8 ng/mg total protein vs. 642.7 ng/mg total protein) (Figure 4.39A). As already displayed in Figure 4.35C, 5-HEPE formation was also higher in HT-29 and HCT-116 cells compared to 5-HETE. This was also found for M1 and M2 macrophages. In comparison, the DHA metabolite 7-HDHA was formed only in low amounts in all cells tested (6.2-32.3 ng/mg total protein) (Figure 4.39A).

The 15-LO dependent 15-HETE formation was quite comparable among HT-29, HCT-116, PMNL, and M2 macrophages (47.3-73.4 ng/mg total protein). Unsurprisingly, M1 macrophages formed only minor amounts of 15-HETE and 17-HDHA as they do not express 15-LO-1 (Figure 4.39B) (42). Furthermore, no 15-HEPE formation was found in M1 macrophages. PMNL and M2 macrophages formed higher amounts of 17-HDHA than HT-29 and HCT-116 cells. However, the formation of 15-HEPE was quite comparable between HCT-116 cells and PMNL. In comparison, the other 15-LO-1 metabolites 12-HETE, 14-HDHA, and 12-HEPE were formed in equal amounts by PMNL (66-81.5 ng/mg total protein), while HT-29 and HCT-116 cells formed higher amounts of 12-HEPE and 14-HDHA compared to 12-HETE (Figure 4.39C). M2 macrophages formed comparable amounts of 14-HDHA like HT-29 and HCT-116 cells (20.1-22.6 ng/mg total protein) but lower amounts of 12-HEPE. Surprisingly, the formation of 12-HETE was higher in HT-29 and HCT-116 cells than in M2 macrophages (8.6 ng/mg total protein vs. 3.1 ng/mg total protein Figure 4.39C).

Finally, the formation of di-hydroxylated metabolites was compared. PMNL formed the highest amounts of 5,15-DiHETE, while M1 and M2 macrophages formed lower but surprisingly equal amounts. RvD5 was mainly formed by M2 macrophages but was also detected in M1 macrophages in very low amounts. PMNL formed RvD5 as well, while the formation was not detected in HT-29 and HCT-116 cells. Formation of RvE4 could be detected in all test cells, but only in very low amounts. However, RvE4 was preferably formed by PMNL and M2 macrophages compared to HT-29 cells, HCT-116 cells, and M1 macrophages.

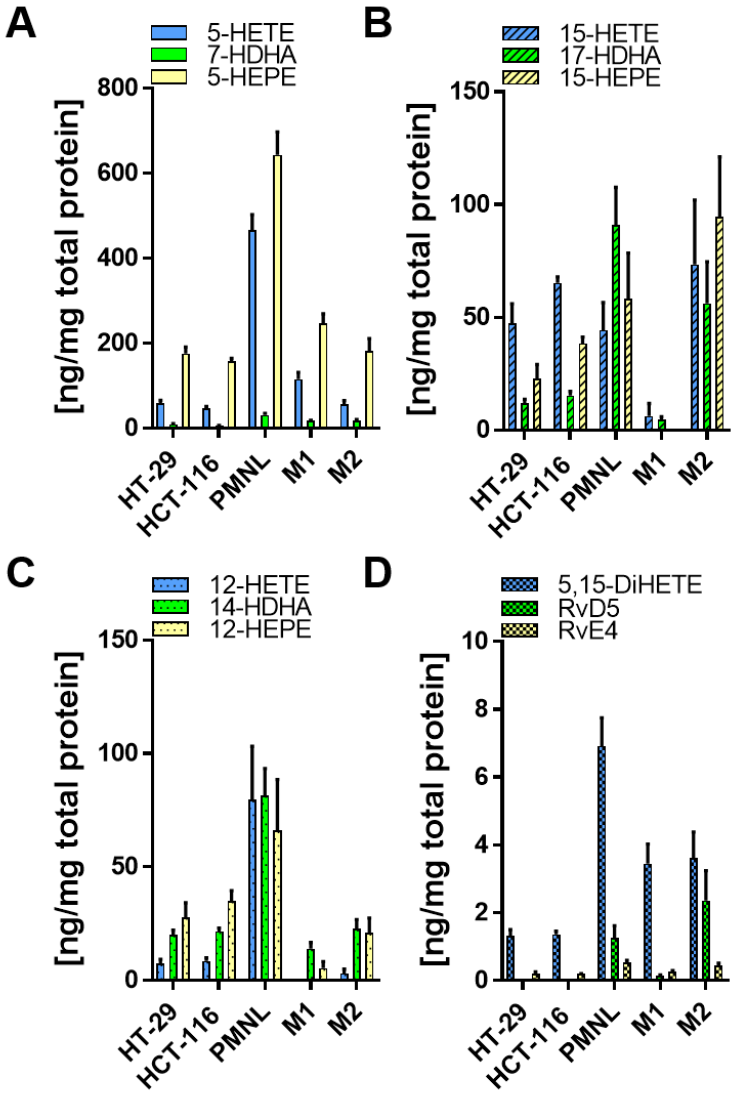

Figure 4.39: Comparison of the lipid mediator profile in tumor cells and leukocytes.
Comparison of the lipid mediator formation in intact HT-29 and HCT-116 cells, PMNL, M1 and M2 macrophages. Tumor cells were seeded ($10x10^6$ cells per 150 mm plate) in CGM and cultured for 48 h. PMNL and PBM were isolated from buffy coats via density centrifugation. Macrophages were differentiated from human PBM isolated via the adherence method (8x100 mm plates per patient). For this, cells were treated with 10 ng/mL GM-CSF (M1, 4 plates) or M-CSF (M2, 4 plates) for 7 days. Additionally, the cells received 10 ng/mL IFNγ (M1) or IL-4 (M2) during the final 48 h. Cells were harvested, counted (HT-29, HCT-116, and PMNL) and diluted according to $10x10^6$ cells/mL in PGC buffer prior to the assay. The 4 prepared M1 or M2 dishes of each donor were harvested using accutase and were combined. Intact cells ($10x10^6$ cells, HT-29, HCT-116, PMNL, or M1/M2 cells combined from 4 dishes) were stimulated with Ca^{2+} ionophore (A23187, 2.5 µM) and supplemented with 1 mM Ca^{2+} and a fatty acid mix (FA mix; 60 µM ARA, 60 µM DHA, and 60 µM EPA). Samples were then incubated for 10 min at 37°C, the reaction was terminated with 1 mL ice-cold MeOH and lipid mediator formation (5-HETE, 7-HDHA, 5-HEPE (A); 15-HETE, 17-HDHA, 15-HEPE (B); 12-HETE, 14-HDHA, 12-HEPE (C); 5,15-DiHETE, RvD5, RvE4 (D)) was analyzed via LC/MS-MS. Ascertained lipid mediator amounts were normalized to the determined total protein amounts and corrected for non-enzymatic oxidation products determined in control samples without cells. Results are depicted as mean + SEM from 3 (HT-29, HCT-116) or 6 (PMNL, M1, M2) independent experiments.

Next, co-incubations of PMNL, HT-29 cells, and HCT-116 cells were prepared. Since PMNL express high amounts of 5-LO but formed comparable amounts of 15-HETE to HT-29 and HCT-116 cells, it was of interest if the amount of di-hydroxylated metabolites would increase due to transcellular metabolism or if the lipid mediator profile in general, would change. Tumor cells and PMNL were coincubated in an equal ratio or an unequal ratio, where twice as many tumor cells compared to PMNL were used. Individual tumor cells and PMNL incubations served as controls, respectively. All samples were prepared in ice-cold PBSG buffer, and each sample was supplemented with 1 mM Ca^{2+} prior to the assay. Cells were stimulated with Ca^{2+} ionophore (A23187, 2.5 µM), supplemented with a fatty acid mix (10 µM ARA, 10 µM DHA), and incubated for 10 min at 37°C. After the incubation, reactions were stopped by adding ice-cold MeOH. After sonication (3x at the lowest pulse rate, MS72), samples were aliquoted and stored at -80°C until further processing at the Department of Food Chemistry (University Wuppertal) by Dr. Nadia Kampschulte from the group of Prof. Dr. Nils Helge Schebb. Samples were extracted and analyzed as described by Kutzner et al. (360). The complete measured panel for this assay can be found in App. Table 37 and App. Table 38. However, only lipoxygenase-dependent metabolites formed in tumor cells and PMNL are depicted in Figure 4.40 and Figure 4.41. As seen in other experiments, HT-29 cells alone produced only low amounts of ARA (5-HETE, LTB_4, 12-HETE, 15-HETE, and 5,15-DiHETE) and DHA (4-HDHA, 7-HDHA, 14-HDHA, 17-HDHA, and RvD5) metabolites. In contrast, PMNL formed especially high amounts of the ARA metabolites 5-HETE and 12-HETE (Figure 4.40A-E). 15-HETE and 5,15-DiHETE levels were also increased (Figure 4.40C, E) compared to HT-29 incubations, as well as the DHA metabolites (Figure 4.40B-E), but to a lesser extent. Surprisingly, co-incubation of HT-29 and PMNL formed product levels in concentrations between the HT-29 and PMNL single incubations instead of increased amounts. Beyond that, concentrations of 4-HDHA, 15-HETE, and 17-HDHA were even decreased in co-incubations compared to HT-29 single incubations (Figure 4.40B, C). This decrease seemed to depend on the total amount of cells since incubations with the highest amounts of cells resulted in the lowest amounts of those metabolites. The formation of 5-HETE, 15-HETE, and 17-HDHA was significantly decreased in co-incubations compared to the respective PMNL single incubations.

In addition, endogenous EPA metabolite levels of 5-HEPE, 12-HEPE, 15-HEPE, and 18-HEPE were determined since the cells were not stimulated with extracellular EPA (Figure 4.40F). In HT-29 cells, 5-HEPE levels were the lowest, while 18-HEPE was formed the most. In contrast, PMNL incubations only led to a relevant formation of 5-HEPE and 12-HEPE. Co-incubation resulted in 5-HEPE and 12-HEPE levels similar to PMNL incubations, while 15-HEPE and 18-HEPE levels were only slightly higher than the respective PMNL ones (Figure 4.40F).

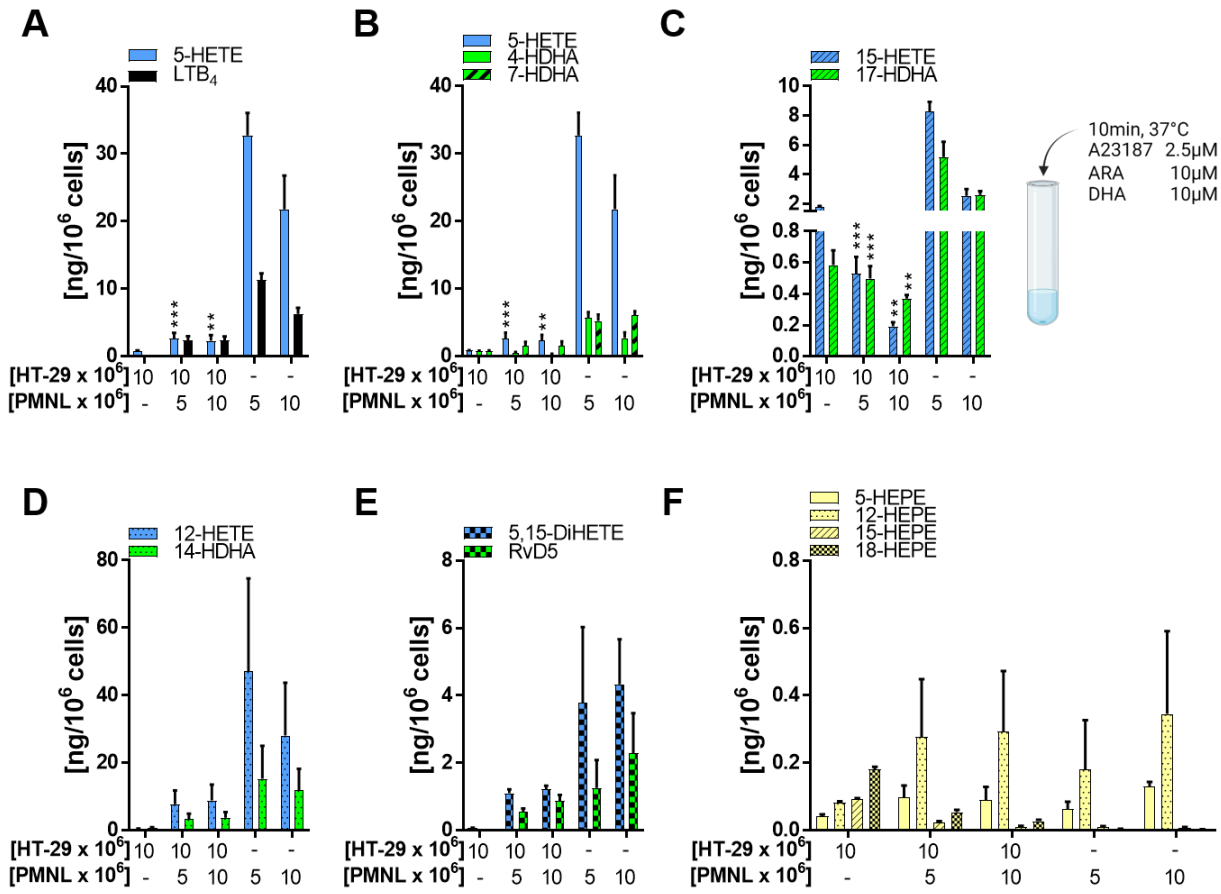

Figure 4.40: Lipid mediator formation in HT-29 and PMNL co-incubations.
Analysis of the lipid mediator formation in intact HT-29 cells in combination with freshly isolated PMNL. Tumor cells were cultured under standard conditions for 4 days. PMNL were isolated from buffy coats via density centrifugation. Cells were harvested, counted and diluted according to $10x10^6$ cells/mL in PGC buffer prior to the assay. Intact cells were stimulated with Ca^{2+} ionophore (A23187, 2.5 µM) and supplemented with 1 mM Ca^{2+} and a fatty acid mix (10 µM ARA, 10 µM DHA). Samples were then incubated for 10 min at 37°C, the reaction was terminated with 1 mL ice-cold MeOH, and lipid mediator formation (5-HETE, LTB_4 (A); 5-HETE, 7-HDHA, 5-HEPE (B); 15-HETE, 17-HDHA (C); 12-HETE, 14-HDHA (D); 5,15-DiHETE, RvD5 (E); 5-HEPE, 12-HEPE, 15-HEPE, 18-HEPE (F)) was analyzed via LC/MS-MS. Ascertained lipid mediator amounts were normalized to 10^6 cells and corrected for non-enzymatic oxidation products determined in control samples without cells. Results are depicted as mean + SEM from 3 independent experiments. Asterisks indicate significant changes vs. the respective PMNL single-cell incubations determined by two-way ANOVA coupled with Tukey's post-test for multiple comparisons. * ($P<0.05$), ** ($P<0.01$), *** ($P<0.001$).

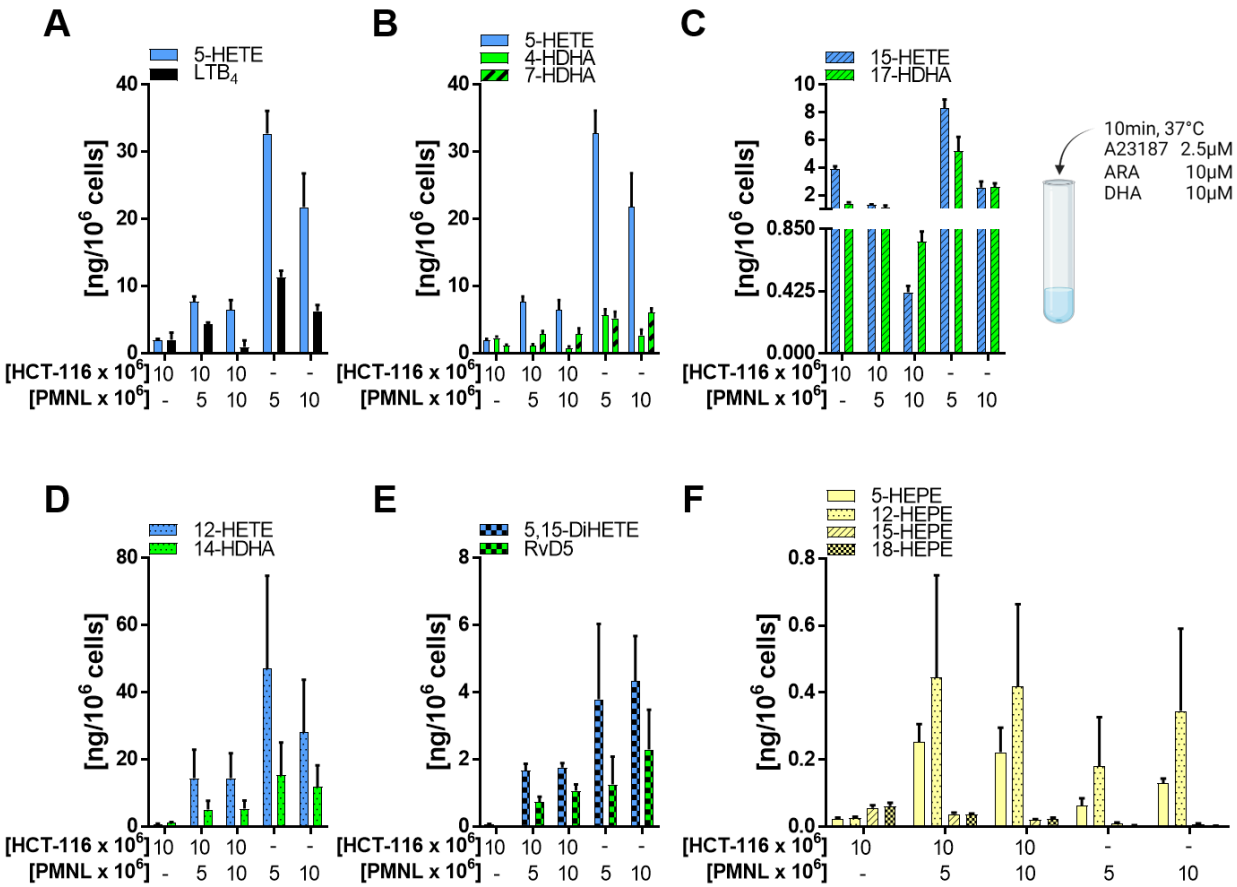

Figure 4.41: Lipid mediator formation in HCT-116 and PMNL co-incubations.
Analysis of the lipid mediator formation in intact HCT-116 cells in combination with freshly isolated PMNL. Tumor cells were cultured under standard conditions for 4 days. PMNL were isolated from buffy coats via density centrifugation. Cells were harvested, counted and diluted according to 10x10^6 cells/mL in PGC buffer prior to the assay. Intact cells were stimulated with Ca^{2+} ionophore (A23187, 2.5 µM) and supplemented with 1 mM Ca^{2+} and a fatty acid mix (10 µM ARA, 10 µM DHA). Samples were then incubated for 10 min at 37°C, the reaction was terminated with 1 mL ice-cold MeOH and lipid mediator formation (5-HETE, LTB_4 (A); 5-HETE, 7-HDHA, 5-HEPE (B); 15-HETE, 17-HDHA (C); 12-HETE, 14-HDHA (D); 5,15-DiHETE, RvD5 (E); 5-HEPE, 12-HEPE, 15-HEPE, 18-HEPE (F)) was analyzed via LC/MS-MS. Ascertained lipid mediator amounts were normalized to 10^6 cells and corrected for non-enzymatic oxidation products determined in control samples without cells. Results are depicted as mean + SEM from 3 independent experiments.

As seen for HT-29 cells, LO products were formed in minor amounts in HCT-116 single incubations. 15-HETE and 17-HDHA levels of PMNL were similar to those of HCT-116 cells, while 5,15-DiHETE and DHA-derived LO products were slightly higher in PMNL than in HCT-116 cells (Figure 4.41A-E). Co-incubations of HCT-116 and PMNL led to LO product levels between the respective single incubations except for 4-HDHA, 15-HETE, 17-HDHA, and LTB_4 (if equal amounts of cells were used). 4-HDHA and 15-HETE levels were slightly decreased if HCT-116 cells were incubated with $5x10^6$ PMNL, while 17-HDHA levels were unaffected. However, even 17-HDHA was decreased when the PMNL number was increased to $10x10^6$ cells. Interestingly, the other metabolites 5-HETE, 4-HDHA, 7-HDHA, 12-HETE, 14-HDHA, 5,15-DiHETE, and RvD5 were not affected by an increase in the PMNL/HCT-116 ratio from 0.5 to 1. Solely LTB_4 levels were affected by an increased ratio but were inversely correlated (Figure 4.41A). In addition to ARA- and DHA-derived LO products, endogenous EPA-derived metabolite levels of 5-HEPE, 12-HEPE, 15-HEPE, and 18-HEPE were analyzed (Figure 4.41F). In HCT-116 incubations, 5-HEPE and 12-HEPE were formed in equal amounts, which was also true for 15-HEPE and 18-HEPE, although the latter concentrations were slightly higher. In PMNL incubations, only 5-HEPE and 12-HEPE were formed in relevant amounts. Interestingly, co-incubations seemed to increase 5-HEPE and 12-HEPE formation and caused product levels that were even higher than those of PMNL single incubations. However, especially the large standard errors of 12-HEPE have to be considered.

4.4.3 Lipid mediator formation in cells with induced 5-LO expression

Since 5-LO expression was found inducible in HT-29 and HCT-116 cells due to treatment with the PI3K/mTOR inhibitor Dactolisib (Dac, 3 µM) or treatment with the MEK/ERK inhibitors PD184352 (PD, 1 µM), Cobimetinib (Cobi, 0.5 µM, and SCH772984 (SCH, 1 µM) it was investigated if the elevated protein expression would lead to elevated product formation.

Therefore, cells were treated identically to the respective Western blot experiments. After cell cycle synchronization via serum starvation, cells were incubated with the indicated inhibitors for 24 h. Then, cells were harvested using TE and counted for normalization. After sample preparation in ice-cold PBSG buffer, all samples were supplemented with 1 mM Ca^{2+} prior to the activity assay. Then, samples were stimulated with Ca^{2+} ionophore (A23187, 2.5 µM), supplemented with ARA (20µM), and incubated for 10 min at 37°C. After incubation, reactions were stopped by adding ice-cold MeOH. Samples were then aliquoted and stored at -80°C until further processing at the Fraunhofer-Institute for Translational Medicine and Pharmacology, Department of Clinical Research (Biomedical Analysis) by Carlo Angioni or Sandra Trautmann. There, samples were analyzed towards their 5-HETE and LTB_4 formation. Additionally, the concentration of free ARA was determined in each sample.

As suspected, the treatment with PI3K/mTOR and MEK/ERK inhibitors, previously shown to induce 5-LO expression, led to elevated 5-LO product formation in both cell lines. In HT-29 cells, treatment with Dactolisib led to 1.45-fold more 5-HETE formation but did not influence LTB_4 formation. The MEK/ERK inhibitors led to 1.95-fold (PD), 3.26-fold (Cobi), and 2.16-fold (SCH) higher 5-HETE formation but increased LTB_4 formation 3.64-fold (PB), 4.95-fold (Cobi), and 3.23-fold (SCH) (Figure 4.42A). In HCT-116 cells, no LTB_4 formation was detectable, and 5-HETE

formation in the vehicle control (co) was lower compared to HT-29 cells. However, treatment with Dactolisib increased the 5-HETE formation 5.96-fold, while MEK/ERK inhibitors led to a 2.58-fold (PD), 3.78-fold (Cobi), and 2.19-fold (SCH) increase in 5-HETE formation compared to the control, respectively (Figure 4.42B).

Notwithstanding the above, the overall 5-HETE and LTB_4 formation in those incubations was relatively low compared to those with the same substrate concentration presented before (Figure 4.37). Furthermore, analysis of free arachidonic acid in HT-29 incubations revealed a strongly reduced substrate concentration in the cell-less substrate control compared to the suspected ARA concentration of 20 µM (Figure 4.42C). Since the prepared samples were only analyzed towards selected metabolites, it was not possible to assess if the difference in ARA concentration between the cell-less control and the cell samples resulted due to product formation or other reasons.

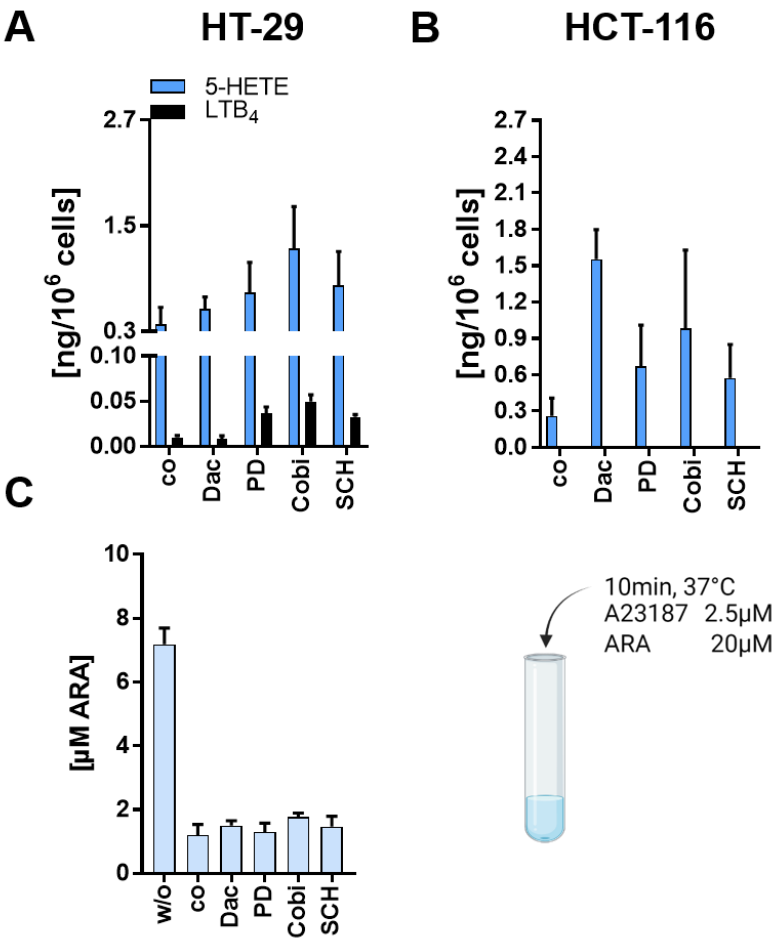

Figure 4.42: 5-LO product formation after 24 h of treatment with PI3K/mTOR and MEK/ERK pathway inhibitors.
HT-29 (A, C) and HCT-116 (B) cells were seeded ($3x10^6$ cells/100 mm dish, 2 dishes per sample) and cell cycle was synchronized by serum starvation using RGM 22 h before treatment. Then, medium was changed to CGM for 2 h and cells were treated for 24 h with the indicated inhibitors Dactolisib (Dac) 3 µM; PD184352 (PD) 1 µM; Cobimetinib (Cobi), 0.5 µM; SCH772984 (SCH) 1 µM. The vehicle control (co) received DMSO instead. Cells were harvested, counted and diluted in PBSG buffer prior to the assay. Intact cells were stimulated with Ca^{2+} ionophore (A23187, 2.5 µM) and supplemented with 1 mM Ca^{2+} and ARA (20 µM). Samples were incubated for 10 min at 37°C. Then, the reaction was terminated with 1 mL ice-cold MeOH and 5-LO product formation, as well as ARA concentrations were analyzed via LC/MS-MS. Ascertained lipid mediator amounts were normalized to 10^6 cells and corrected for non-enzymatic oxidation products determined in control samples without cells. Results are depicted as mean + SEM from 3 independent experiments.

4.4.4 4. Substrate availability in HT-29 and HCT-116 cells

As the analysis of free ARA in the control samples revealed a substantial concentration difference compared to cell incubations, it was investigated if the difference results from lipid mediator formation. Furthermore, it was examined if the difference in the measured fatty acid concentration compared to the intended concentration was due to an experimental error.

For this purpose, samples were prepared in ice-cold PBSG buffer and supplemented with 1 mM Ca^{2+} prior to the activity assay. Cells were incubated for 10 min at 37°C and stimulated with Ca^{2+} ionophore (A23187, 2.5 µM) as well as supplemented with a fatty acid mix (6 µM ARA, 6 µM DHA, 6 µM EPA). Samples were then aliquoted and stored at -80°C until further processing at the Fraunhofer-Institute for Translational Medicine and Pharmacology, Department of Clinical Research (Biomedical Analysis) by Carlo Angioni or Sandra Trautmann. There, samples were analyzed towards the formation of ARA, DHA, and EPA-dependent lipid mediators. The exact panel is listed in App. Table 32. Additionally, the concentration of free ARA, EPA, and DHA was determined in each sample.

Unfortunately, samples could not be quantified towards their DHA concentration since all control samples had concentrations above the upper limit of quantification (>ULOQ). Hence, Figure 4.43 only shows results for ARA and EPA. As seen previously, the measured ARA concentration differed widely from the intended concentration (1.99 µM vs. 6 µM, Figure 4.43A). However, the concentration of free ARA in samples containing cells was 4.95-fold lower than the determined concentration in the control samples. Surprisingly, analysis of the formed lipid mediators revealed that only a meager percentage of 0.4-0.9% of the substrate seems to be metabolized into analytes included in the panel (displayed in pink). A similar but yet higher turnover of 2.2-6.8% was found for EPA. HT-29 and HCT-116 cells metabolized more EPA, resulting in higher metabolite concentrations (displayed in green, Figure 4.43B). Surprisingly, the difference between measured and intended EPA concentration was even higher compared to ARA.

Analysis of both ARA and EPA revealed a vast difference in the respective free fatty acid concentration in preparations with cells compared to cell-free controls, which cannot be explained due to metabolite formation since the ARA and EPA-dependent lipid mediator formation in HT-29 and HCT-116 cells is very low compared to the substrate concentration (Figure 4.43 pink and green).

Since the determined and intended free fatty acid concentration differed strongly for two tested concentrations (6 µM, 20 µM), it was interesting to see if this might be the case for an even higher concentration and if measurement for EPA would show comparable results. Indeed, the analysis of 60 µM ARA or EPA in cell-free controls resulted in substantially reduced factual free fatty acid concentrations (Figure 4.44). Notably, the difference between intended and measured free fatty acid concentration was higher for EPA than ARA (Figure 4.44B). In detail, analysis of samples supplemented with the intended 60 µM of each free fatty acid exhibited 5.45-fold (ARA) and 9.48-fold (EPA) less concentration. Samples supplemented with the intended 20 µM of ARA exhibited 2.79-fold less in concentration. Finally, samples supplemented with the intended 6 µM of each free fatty acid exhibited 3-fold (ARA) and 5.83-fold (EPA) less in concentration.

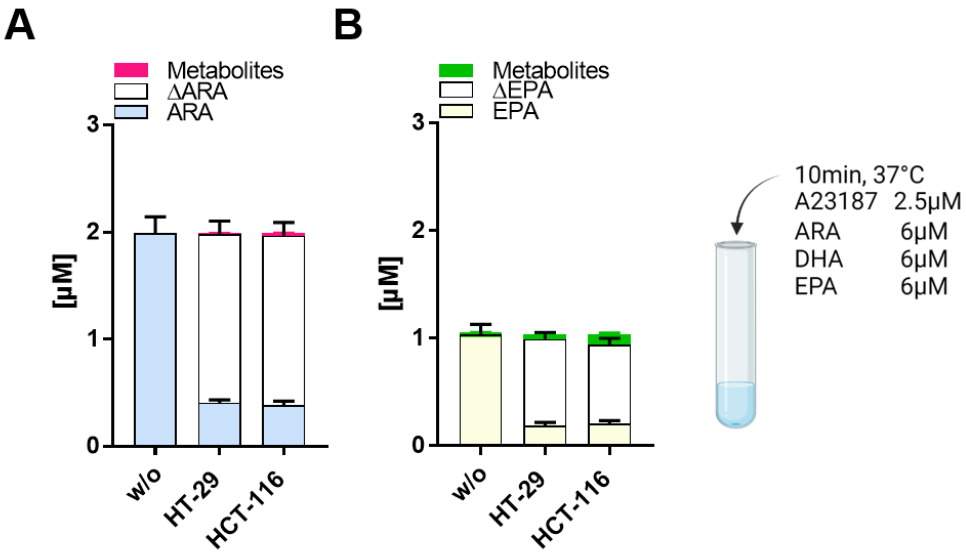

Figure 4.43: Free substrate and metabolite analysis in HT-29 and HCT-116 cells.
Cells were seeded ($10x10^6$ cells per 150 mm plate) in CGM and cultured for 48 h. Cells were harvested, counted and diluted according to $10x10^6$ cells/mL in PBSG buffer prior to the assay. Cells were stimulated with Ca^{2+} ionophore (A23187, 2.5 µM) and supplemented with 1 mM Ca^{2+} and a fatty assay mix (FA mix; 6 µM ARA, 6 µM DHA, and 6 µM EPA). Samples were incubated for 10 min at 37°C, then the reaction was terminated with 1 mL ice-cold MeOH, and lipid mediator formation (panel displayed in App. Table 32) was analyzed via LC/MS-MS. Ascertained lipid mediator and free fatty acid amounts in cell-less controls and cell-containing samples were calculated in µM for better comparison. ΔARA and ΔEPA were calculated by subtraction of ARA and its metabolites (blue and pink) or EPA and its metabolites (yellow and green) in cell-containing samples from respective control samples without cells (w/o). Quantifiable ARA metabolites (pink) include 5-HETE, 12-HETE, 15-HETE, 5(*S*),15(*S*)-DiHETE, PGD_2, TBX_2, and $PGF_{2\alpha}$. Quantifiable EPA metabolites include 5-HEPE, 12-HEPE, 15-HEPE, and 18-HEPE. LTB_4, 20-HETE, 8S,15S-DiHETE, LXA_4/15-epi-LXA_4, LXA_5, LXB_4, PGE_2, 11-dehydro-TXB_2, PGJ_2/Δ-12-PGJ_2, 6-keto-$PGF_{1\alpha}$, RvE1, and RvE4 were also part of the measured panel but not quantifiable. Determined metabolite values were corrected for non-enzymatic oxidation products determined in control samples without cells (w/o). Results are depicted as mean + SEM from 3 independent experiments.

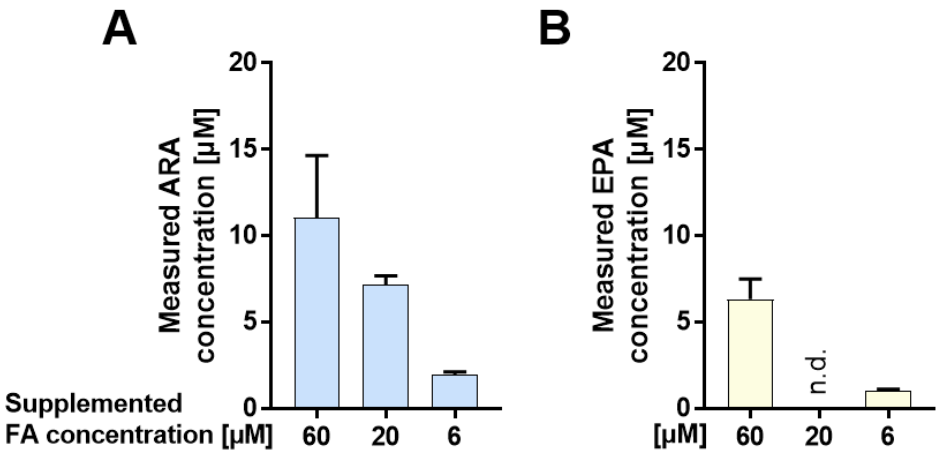

Figure 4.44: Comparison of intended and determined free FA concentrations in cell-free incubations.
PBSG buffer was spiked with Ca^{2+} ionophore (A23187, 2.5 µM), Ca^{2+} (1 mM), and a fatty assay mix containing the indicated concentration of each fatty acid (ARA, DHA, EPA). Samples were incubated for 10 min at 37°C, then the reaction was terminated with 1 mL ice-cold MeOH, and respective free fatty acid concentrations were analyzed and calculated. Results are depicted as mean + SEM from 3 independent experiments. n.d. = not determined.

5 Discussion

5.1 HT-29 and HCT-116 cells fine-tune 5-LO expression in response to environmental changes

In recent decades, non-physiological 5-LO expression was found frequently in various malignant neoplasms derived from different specimens. Several studies investigated the expression of 5-LO and the leukotriene cascade in several cancer cell lines and primary cells derived from different cancers (51, 72, 361–363). The presented study investigated the regulation of 5-LO expression and activity in HT-29 and HCT-116 colon carcinoma cells. Both cell lines express the enzyme of interest in different amounts together with the complete LT machinery, but its activity appears to be low as both cell lines only produce minor amounts of LTs and 5-HETE under conventional cell culture conditions (72). The two colon carcinoma cell lines carry different mutations in crucial oncogenic signaling pathways and were previously shown capable of forming MCTS (348, 364). Therefore, HT-29 and HCT-116 cells were selected as suitable cell lines for this study.

Most studies investigating 5-LO in tumor cell lines use conventional 2D culture models that provide controllable experimental parameters but do not display the *in vivo* characteristics of tumors. Therefore, it was of interest to investigate the expression of 5-LO and other enzymes of the leukotriene cascade in a 3D culture model, which provides a multitude of physicochemical factors such as cell-cell interactions and multiple gradients as, e.g., cell proliferation, viability, nutrients, catabolites, and oxygen which result in changes of the cellular signaling (293, 348, 365).

To investigate the expression of enzymes involved in the leukotriene cascade, MCTS grown for 4 and 7 days on special low adherence plates, without medium change, were compared to monolayer controls cultured under optimal cell culture conditions (incubation for 48 h, medium change after 24 h, 70-80% confluency). This comparison revealed that the protein expression of 5-LO and LTA_4H, as well as the mRNA expression of *LTC4S* were upregulated due to 3D growth (Figure 4.1 & Figure 4.2). Additionally, similar results were found for the expression of *ALOX15*, *PTGS1,* and *PTGS2* mRNA (Figure 4.2 & App. Figure 7.2). In contrast, expression of the $cPLA_{2\alpha}$ protein was downregulated due to MCTS formation (Figure 4.1). The results were verified using another MCTS model employing the liquid overlay technique, utilizing larger wells coated with ultra-pure agarose (1% in PBS) and higher volumes of media supernatant. Within the long incubation period, the medium surrounding the spheroids gets depleted of nutrients but accumulates catabolites and acidifies. Subsequently, many factors can influence the cells and act upon cellular signaling. However, a higher media volume (700 µL vs. 200 µL used on low adherence plates) did not influence the experimental outcome. Therefore, both spheroid formation methods provided comparable results. Additionally, both models formed similar MCTS in size and shape, even though the initial compacting of agarose-grown MCTS took longer (Figure 4.3 & Figure 4.4). The observed upregulation of 5-LO in MCTS of HT-29 and HCT-116 cells is in accordance with the reported elevation of LT release by human glioma spheroids (366). A study in MCF-7 breast cancer cells demonstrated the induced expression of *ALOX15* in MCF-7 spheroids compared to monolayer controls (367). Furthermore, MCTS-induced *PTGS2*

expression was previously demonstrated in DU145 prostate cancer cells and was reported to be dependent on necrosis (368).

An effective medium change during the spheroid formation period was difficult to handle and was therefore not performed. Since this leads to the accumulation of factors in the medium that can influence the cells as described above, additional controls were prepared. To better understand and further isolate the factors leading to the observed results in 3D culture, cells were seeded in 12-well plates employing the same cell numbers used for MCTS formation (per well). For a better comparison of monolayer-grown cells and spheroids, the medium was also not changed during the incubation periods of 4 or 7 days. Surprisingly, HT-29 and HCT-116 monolayers grown for 7 days showed comparable regulation for all investigated targets (with the exception of LTA_4H in HT-29 cells) compared to MCTS. Beyond this, similar results could also be observed for HCT-116 cells grown for 4 days.

The lengthy culture period of the additional control cells led to visible acidification of the medium and strong cellular overgrowth (Figure 4.3). An acidic environment is described as favorable for tumors. However, within the TME, tumor cells are adapted to extracellular acidity while maintaining a relatively stable intracellular pH (pH_i) (280). Therefore, studies show that an acidic extracellular pH (pH_e) can promote proliferation in cell cultures adapted to low pH conditions (369, 370). However, other studies demonstrate cell cycle inhibition of cancer cell lines exposed to low pH_e if previously cultured under physiological conditions (371, 372). Concerning cellular overgrowth, cancer cells feature no contact inhibition due to evading growth suppressors, but high cell density cultures can still lead to cell cycle arrest. A lack of nutrients, especially essential amino acids and glutamine, but also a lack of growth factors can induce growth arrest via mTOR (373–375). Therefore, cell cycle analysis of the control incubation experiments was performed. By this, a substantial accumulation of cells within the G0/G1 phase was observed for HT-29 and HCT-116 cells after 7 days compared to the controls cultured under optimal conditions (subconfluent growth, frequent media replenishment). Additionally, a shift towards the G0/G1 phase was observed for HCT-116 cells grown for 4 days, correlating with the higher cell density at this time point. This indicated a possible coherence between cell proliferation, culture density, and 5-LO expression.

Next, the influence of low pH_e was investigated in more detail. An acidic pH of 6.5 or 6.8 led to elevated *ALOX5* levels in both cell lines, with more pronounced effects in HT-29 cells (Figure 4.7). However, to investigate the *ALOX5* expression at defined non-physiological pH conditions, DMEM powder with a HEPES/PIPES buffer system had to be used, although HT-29 cells are usually cultured in McCoy's 5A medium as recommended by DSMZ. Unfortunately, this medium was unavailable as powder. Therefore, all pH experiments with HT-29 cells (including controls) were performed using the prepared DMEM medium, which might also influence the general signaling and protein expression due to deviations in nutrition (376, 377).

As the results of the pH experiments indeed showed an influence on *ALOX5* expression, but overall, only a low induction, additional experiments focusing on the effects of cellular density on 5-LO expression were performed. For this, increasing amounts of cells were incubated for 48 h, with a medium change after 24 h to minimize the effects of nutrient deprivation and acidification. The analysis revealed a cell density-dependent upregulation of 5-LO expression in both cell lines, which was more pronounced in HT-29 cells. Subsequent cell cycle analysis showed a cell density-

dependent increase of cells in the G0/G1 phase for HCT-116 cells but not for HT-29 cells. Proliferation-dependent 5-LO expression was already observed in BL41-E95-A cells (378). However, no cell cycle analysis was performed within this study.

HCT-116 cells generally show a higher proliferation rate but lower 5-LO expression than HT-29 cells (72, 379). Furthermore, both cell lines are classified in different consensus molecular status categories and transcriptional subtypes. While HT-29 cells are described to hold a MMS (microsatellite stability) molecular status and a more differentiated goblet-like transcriptional status, HCT-116 cells are described to hold a MSI molecular status and a less differentiated stem-like transcriptional status with higher metastatic potential (380–382). Therefore, pronounced 5-LO expression might be a feature of more differentiated cell lines since differentiation of, e.g., the colorectal cancer cell line Caco-2 or several leukemic cell lines induces 5-LO expression and activity significantly (20, 28, 29, 357).

5.2 5-LO expression is regulated in a mTORC-2- and MEK/ERK-dependent manner

Since CRC cells frequently show dysregulation in pathways that control cell growth, proliferation, survival, and metabolism, and 5-LO expression was induced by MCTS formation and high cellular density culture in HT-29 and HCT-116 cells, the potential involvement of the PI3K/mTOR and MEK/ERK pathway was investigated.

With the use of pharmacological inhibition of the PI3K/mTOR and MEK/ERK pathways, suppression of 5-LO expression was identified in proliferating cells (Figure 4.10). Especially inhibition of PI3K/mTOR using the dual PI3K/mTOR inhibitor Dactolisib and inhibition of MEK/ERK using the MEK-1 inhibitors PD184352, Cobimetinib, and the ERK inhibitor SCH772984 induced 5-LO expression significantly. Additionally, the PI3K inhibitor Wortmannin, the mTOR inhibitor Temsirolimus, the EGFR inhibitor Erlotinib, and the FTase inhibitor LB42708 were tested but failed to increase 5-LO expression as potently or at all compared to the other inhibitors. This was not too surprising. Dactolisib was shown to potently inhibit several PI3K class IA and IB isoforms, including common p110α mutations, as well as mTORC-1 and mTORC-2. In contrast, the effectiveness of the single target inhibitors Wortmannin (pan-PI3K) and the Rapalogue Temsirolimus (mTORC-1) is limited due to the negative feedback loop of PI3K and mTOR (272, 383). Furthermore, tumor cells frequently have mutations in the PI3K/mTOR and the MEK/ERK pathway, leading to overactivation (see Table 31 for an overview of mutations in the used cell lines) (384). For example, the three Ras genes *HRAS*, *KRAS*, and *NRAS* are common oncogenes in humans upstream of the PI3K/mTOR and MEK/ERK pathways. Especially *KRAS* is frequently mutated in colorectal, pancreatic, and non-small-cell lung carcinomas, while *HRAS* and *NRAS* are often mutated in papillary thyroid cancer or hepatocellular carcinoma, respectively (385–389). For activation, Ras proteins depend on prenylation, the addition of a lipid moiety that promotes the association with the plasma membrane (390). This prenylation is mediated via a farnesyltransferase (FTase) or a geranyl-geranyl transferase (GGTase) (391). However, H-Ras exclusively depends on FTase, while N-Ras and K-Ras can utilize GGTase-mediated prenylation as a bypass mechanism (392). HT-29 cells show an elevation in KRAS copy numbers but express the wt protein, while HCT-116 cells express the K-Ras p.G13D mutation (Table 31). Mutated Ras proteins lose the ability to cleave bound GTP to GDP and hence are permanently activated (393).

Due to the possible bypass prenylation of K-Ras and the overactivation in HCT-116 cells, it is not surprising that the FTase inhibitor LB42708 and the EGRF inhibitor Erlotinib failed to induce 5-LO expression in both cell lines, especially since downstream elements like Raf are frequently mutated in cancer cells as well (e.g., HT-29 BRAF V600E, Table 31).

Because data discussed in chapter 5.1 implicated a possible link between cell proliferation and 5-LO expression, cell cycle analysis and viability/cytotoxicity assays of inhibitor-treated cells were performed. Additionally, it was validated that the reversible short-term cell synchronization via serum deprivation did not influence 5-LO expression (App. Figure 7.4). Interestingly, cell synchronization using serum deprivation accumulates cells in the transition stage between G0 quiescence and the early G1 phase (394, 395). Treatment with Dactolisib, PD184352, Cobimetinib, and SCH772984, which mediated upregulation of 5-LO expression, also induced G0/G1 cell cycle arrest in HT-29 and HCT-116 cells (Figure 4.10, Figure 4.13). Those inhibitors were previously shown to mediate G0/G1 cell cycle arrest in similar concentrations. As Dactolisib, PD184352, Cobimetinib, and SCH772984 were also shown to promote a decrease in viability proliferation and provoke cytotoxic effects in different cancer cells, WST-1 and LDH assays were performed as well (396–399). However, only treatment with Dactolisib and Cobimetinib decreased the cell viability, probably by reducing the overall cell number due to a reduction in cell proliferation, but did not promote a pronounced cytotoxicity (Figure 4.12).

Riedl et al. recently reported that 3D cultures of HT-29 and HCT-116 cells diminished PI3K/mTOR and MEK/ERK signaling and induced a shift towards the G0/G1 phase (348). Since this supported the hypothesis that 5-LO might be regulated by pro-proliferative pathways in a cell cycle dependent manner in HT-29 and HCT-116 cells, Western blot analysis of p-p70S6K/p70S6K and pERK/ERK in HT-29 and HCT-116 MCTS was performed (Figure 4.14). Surprisingly, MCTS formation and high-density monolayer culture did not reduce but induce ERK phosphorylation in HCT-116 cells. Additionally, phosphorylation of p70S6K downstream of mTOR was elevated in HCT-116 MCTS and high-density monolayers as well. In contrast, MCTS formation potently reduced ERK phosphorylation in HT-29 cells. Especially the obtained findings for HCT-116 MCTS differed strongly from the reported findings by Riedl et al. However, this might be explainable by differences in the experimental setup. Riedl et al. incubated $3x10^3$ cells for 24 h in reduced serum-containing medium (5%) with 0.3% methylcellulose for 2D monolayers and MCTS formation. But for this thesis, $5x10^4$ cells were incubated in their respective complete growth medium for 4 or 7 days. Therefore, the results are hard to compare, and culture of 2D monolayers under reduced serum conditions might influence cellular signaling. In addition, phosphorylation of p70S6K is mediated via mTORC-1 but not mTORC-2 (400). Furthermore, p-p70S6K was previously reported to inhibit the mTORC-2 core component Rictor (via Thr-1135) and thus inhibit mTORC-2-mediated ATK activation (401, 402). Inhibition of mTORC-2 was also previously shown to induce G0/G1 cell cycle arrest in hepatocellular carcinoma cell lines (403). Related to the inhibitor-based findings, a possible signaling route across mTORC-2 resulting in 5-LO upregulation seems plausible. As described above, Dactolisib is reported to inhibit both mTORC-1 and mTORC-2, while Temsirolimus, which did not induce 5-LO expression in HT-29 and HCT-116 cells, is described to inhibit mTORC-1 but not mTORC-2 (383). Therefore, the hypothesis was adapted and further investigated if MEK/ERK and PI3K/mTORC-2 inhibition might be responsible for the seen upregulation of 5-LO. Additionally, it was considered that the observed 5-LO regulation might

be slightly different in both cell lines with differently preferred routes dependent on the respective mutational profile of the cells.

Since pharmacological inhibition using small molecules is well known to promote both off-target effects and bypass mechanisms by activating other pathways than the intended, RNAi technology was used to validate and further investigate the previous results. Surprisingly, the knockdown of the PI3K isoforms PIK3CA and PIK3CG led to a significant downregulation of 5-LO expression in HT-29 (PIK3CA, PIK3CG) and HCT-116 cell (PI3KCA)(Figure 4.18, Figure 4.19, Figure 4.20). The consequences of PI3K knockdown on 5-LO expression have not been investigated in other cell lines yet. However, it has been reported that overexpression of 5-LO in bladder cancer cells (HT1376, J82) leads to elevated PI3K and AKT phosphorylation. In line with this, knockdown and pharmacological inhibition of 5-LO in the HER2-positive breast cancer cell line SKBR3 led to decreased PI3K and AKT phosphorylation (404). Knockdown of 5-LO in an $Apc^{min/x}$ mouse model also decreased PI3K and AKT phosphorylation (405). Therefore, the existence of a regulatory feedback loop seems possible. Treatment of pancreatic cancer cell lines (Panc-1, AsPC-1) using LTB_4 increased AKT phosphorylation (406). Both 5-LO overexpression and treatment with exogenous LTB_4 or 5-HETE have been shown to induce cell proliferation in several cell lines (308, 407). Cancer cells might upregulate 5-LO during cell stress conditions, inhibiting cell growth to produce LTB_4 to reactivate pro-proliferation pathways. Additionally, PI3K might have another role in 5-LO regulation besides its part in the PI3K/mTOR cascade.

Contrary to PI3K, the knockdown of the mTORC-2 core component RICTOR significantly increased 5-LO expression in both cell lines. This supports the theory that 5-LO expression might be regulated via mTORC-2. Knockdown of mTOR itself elevated 5-LO expression, but only non-significantly in both cell lines. In contrast, the knockdown of RAPTOR, the core component of mTORC-1, led to opposing results in both cell lines, again in a non-significant manner. Contrary to the results obtained by using MEK/ERK inhibitors, the knockdown of MAP2K1 (MEK-1) did not influence 5-LO expression in HT-29 cells but led to an elevated, non-significant 5-LO expression in HCT-116 cells. Knockdown of MAP2K1 (MEK-1) did not display the results obtained using pharmacological inhibition of MEK-1 and ERK. However, the MEK-1 inhibitors PD184352 and Cobimetinib were shown to inhibit both ERK-1 and ERK-2 phosphorylation. Therefore, knockdown of MEK-1 alone might not be able to mimic the results obtained using pharmacological inhibition. As discussed for the PI3K/mTOR pathway, MEK/ERK signaling can be activated via 5-LO-dependent products. Furthermore, 5-LO inhibition also decreased ERK phosphorylation (408). In turn, 5-LO activity can be stimulated by phosphorylation via a PKC/MEK-1/ERK axis in ionophore-treated MM6 cells and differentiated Daidzein-treated THP-1 cells (82, 409). However, some publications show 5-LO downregulation after inhibition of the MEK/ERK axis or 5-LO upregulation with parallel ERK activation (408, 410, 411). As this is contrary to the results presented in this thesis, it should be mentioned that most of the studies used very high inhibitor or compound concentrations (e.g., You et al. 2009, 50 µM PD98059, MCF-7 cells) and used cells (MCF-7) which only showed *ALOX5* expression on mRNA level within our group (32, 408). Additionally, publications that tested very high inhibitor or compound concentrations mainly provided no information on cytotoxicity testing (408, 411). And, as discussed before, different cell lines might regulate 5-LO expression differently, depending on their respective mutational profile. It can also be speculated that cells are heavily dependent on pro-proliferative oxylipins, which

downregulate energy-expensive pro-proliferative pathways when growth conditions are suboptimal, thereby triggering cell cycle arrest.

Finally, knockdown of PRKCZ (PKCζ), a known downstream target of mTORC-2 and a known kinase for $cPLA_{2\alpha}$ which stabilizes the enzyme, led to no effects on 5-LO expression in HT-29 cells but to a recognizable downregulation in HCT-116 cells. Knockdown of PRKCZ was investigated since it was recently shown that constitutive activation of the PI3K p100α catalytic subunit reprograms breast cancer cells towards an oxylipin-dependent phenotype. They showed that these cells are enriched in certain fatty acids, particularly palmitoleate and ARA, due to an elevated *de novo* lipogenesis and increased FA uptake. Constitutive activation of PI3K downstream pathways leads to the stabilization of $cPLA_{2\alpha}$ by an mTORC-2/PKCζ-dependent axis and constantly elevated intracellular Ca^{2+} levels, which activate $cPLA_{2\alpha}$ resulting in the continuous release of ARA-derived oxylipins with growth stimulating properties (412). Interestingly, HT-29 and HCT-116 cells also carry a mutated, constitutively active PI3KCA (see Table 31). It seemed possible that the knockdown of PRKCZ might, therefore, influence 5-LO expression. Even though this was not the case, at least for HT-29 cells, the described regulation via mTORC-2/PKCζ might explain the downregulation of $cPLA_{2\alpha}$ during 3D growth.

As conditions inhibiting the investigated pathways triggered cell cycle arrest and elevated 5-LO expression, it was also investigated if the observed 5-LO upregulation is independent of p53. This possible dependency was investigated using HCT-116 cells since they express wt p53 (Table 31) and HCT-116 p53 -/- cells. Treatment of both cell lines using Dactolisib, PD184352, Cobimetinib, and SCH772984 induced *ALOX5* mRNA expression and led to a shift towards the G0/G1 phase in both cell lines (Figure 4.11A, Figure 4.17B, C). A p53-independent G0/G1 arrest induction was already observed in HCT-116 cells using Cobimetinib (397). However, the observed *ALOX5* mRNA induction in HCT-116 53 -/- did not translate into 5-LO protein, and basal 5-LO protein expression was potently suppressed (Figure 4.17A). It is indeed known that p53 can influence several targets on the transcriptional level by regulation factors that control translation initiation (413). *ALOX5* was previously described as a direct p53 target gene, and it has already been established that 5-LO is upregulated upon genotoxic stress induced by UV irradiation, oxidative agents, or treatment with cytostatic drugs in several cancer cell lines together with p53. However, the observed upregulation was initially described as independent of p53 since cells that carried a p53 frameshift mutation also upregulated 5-LO upon these stimuli by Catalano et al. (88). In contrast, the 5-LO upregulation after treatment with Etoposide and Actinomycin D was described as p53-dependent by another study (32). The presented results might explain the putative discrepancies between both studies: 5-LO is a direct p53 target gene, but as shown in the present study, pro-proliferative signaling pathways can simultaneously suppress its gene expression. Upon p53 activation, cell cycle arrest is triggered by p21. This triggers most probably the inhibition of the transcriptional repression of 5-LO by pro-proliferative pathways in a synergistic way. Alternatively, *ALOX5* transcription can also be upregulated by cell cycle arrest independent of p53 by exclusive attenuation of PI3K/mTOR and MEK-1/ERK-dependent signaling pathways, as shown in this thesis. In line with this, it has been reported that oncogenic RasV12 is known to induce 5-LO expression in fibroblasts and a number of other cell lines. This was accompanied by an activation of p53 by 5-LO-derived ROS, which induced cell cycle arrest by elevation of p53 and, thus, p21 (414). Furthermore, the interplay of p53 and 5-LO in HT-29 cells that express the R273H p53 mutation that lost its DNA binding capacity is less clear since the expression of 5-LO

is per se p53-independent. Therefore, 5-LO translation may be independent of p53 in cancer cells carrying a p53 gain of function mutation.

Table 31: MS status, transcriptional subtype, and mutational status overview of investigated cell lines.
Information about entries marked with * was obtained using the COSMIC database (https://cancer.sanger.ac.uk) as other sources were not available (415).

Cell line	**HT-29**	**HCT-116**	**Capan-2**	**U-2 OS**	**Caco-2**	**MCF-7**
Mutation						
MS status (380)	MSS (380)	MSI (380)	MSS* (415)	MSS* (415)	MSS (380)	MSS (416)
CRC transcriptional subtype (380)	goblet	stem	-	-	stem	-
PIK3CA	p.P449T (417)	p.H1047R (417)	wt* (415)	wt (418)	wt (419)	p.E545K (420)
KRAS	wt (421)	p.G13D (421)	p.G12C (422)	wt (423)	wt (421)	wt (424)
BRAF	p.V600E (425) p.T119S (421)	wt (425)	wt* (415)	wt (426)	wt (425)	wt (427)
TP53	p.R273H (428)	wt (428)	p.R273H (428)	wt (429)	p.E204X (421)	wt (428)

In addition to p53, further transcription factors involved in cell cycle regulation, such as *FOXO1* and *3*, *SP1*, *MYC,* and members of the DREAM complex (*E2F1-5*, *MYB,* and *MYBL2*), were investigated in monolayer grown cells. Interestingly, MEK/ERK inhibition revealed differences between the respective inhibitors. While treatment with Cobimetinib and SCH772984 resulted in similar effects for all transcription factors the effects of PD184352 differed. This was unexpected as Cobimetinib and PD184352 are both non-ATP competitive allosteric inhibitors of MEK1. However, results obtained using Cobimetinib, an optimized structural analog of PD184352 in terms of metabolic stability, indicate that side products might cause the observed effects of PD184352 due to extensive oxidative metabolism (430, 431).

Inhibition of the MEK/ERK or PI3K/mTOR pathway resulted in a similar regulation of *MYBL2*, *E2F1,* and *SP1*. As these findings supported the hypothesis that 5-LO upregulation is at least partially mediated by the reduced MEK/ERK and PI3K/mTOR signaling in HT-29 and HCT-116 cells, MCTS were analyzed next (Figure 4.23). Again, the transcription factors were regulated mostly similar to MEK/ERK or PI3K/mTOR inhibition in monolayer grown cells, although some effects were less pronounced. Nevertheless, these findings are in accordance with the previous report of Riedl et al. confirming the restriction of PI3K/mTOR and MEK/ERK signaling in HT-29 and HCT-116 cells (348).

As already discussed in chapter 5.1, an increase in cellular density leads to enhanced *ALOX5* expression in the tested cell lines. Thus, the influence of cellular density on *E2F1*, *MYBL2*, *MYB*, and *SP1* was analyzed next (Figure 4.24). *E2F1* and *MYBL2* expression slightly decreased with higher density, whereas *SP1* levels were increased in both cell lines. *MYB* expression, however, led to mixed results. As the data indicate transcriptional repression of *ALOX5* mRNA via *E2F1*, a pan-E2F inhibitor (HLM006474) was used to confirm this correlation on protein level. Indeed, 5-LO expression was significantly upregulated in HCT-116 cells, whereas the increase in 5-LO protein was similar but not significant in HT-29 cells (Figure 4.26). As a selective *E2F1* inhibitor was commercially not available, a pan-E2F inhibitor also inhibiting *E2F4* had to be used (432). This might explain why the induction of 5-LO was only minor. Furthermore, the data also indicate that b-Myb (*MYBL2*) is involved in transcriptional repression of *ALOX5,* although regulation of *ALOX5* has only been described for c-Myb (*MYB*) in myeloid cells (355, 356, 433). However, both transcription factors share their DNA consensus sequence, so a similar function seems reasonable. b-Myb overexpressing cell lines derived from HT-29 and HCT-116 cells were prepared to investigate this effect further. Unfortunately, constitutive overexpression of b-Myb was silenced within a few passages, so doxycycline-inducible cell lines had to be used instead. Here, b-Myb expression resulted in a decreased 5-LO expression in both cell lines after 48 h of Doxycycline treatment, although data were only significant in HT-29 cells (Figure 4.29). However, in MCTS of these inducible cell lines, 5-LO expression was not affected. Instead, b-Myb overexpression resulted in larger MCTS of HCT-116 cells and MCTS with a loosened outer rim structure in HT-29 cells (Figure 4.30). It is important to note that MCTS were seeded and kept in a Doxycycline-containing medium for 4 days, whereas the monolayer-grown cells were only treated for 48 h at max. Thus, it could not be excluded that the cell lines somehow adapted to the Doxycycline treatment, leading to normalized 5-LO levels. In addition, MCTS are characterized by gradients of nutrients or oxygen deprivation as the inner core region is cut off from the surrounding medium (280, 281). Therefore, it might also be that the inner cells of the MCTS received less or no Doxycycline at all, which consequently led to reduced b-Myb and, thus, unaltered 5-LO expression.

To gain more information on the b-Myb interaction, reporter gene experiments were conducted. So far, two c-Myb binding sites have been identified in the *ALOX5* gene. The first is located upstream of the core promoter region, whereas the second is located within the coding region (356). Therefore, *ALOX5* promoter constructs with varying lengths were prepared in order to identify the site responsible for *ALOX5* repression. Indeed, the larger (pN6) construct resulted in a decreased luciferase signal for both cell lines, indicating a regulatory element upstream of the core promoter region (pN10) (Figure 4.31A). However, deletion of the putative b-Myb binding site (pN6ΔMYB) led to inconclusive results. In HCT-116 cells, the luciferase signal was increased again, whereas the signal in HT-29 cells was further reduced. When treated with the MEK/ERK and PI3K/mTOR inhibitors, the signals of the pN6ΔMYB constructs were significantly decreased compared to pN6 and pN10 in HT-29 cells (Figure 4.31C), whereas the results in HCT-116 cells did not differ from the control (Figure 4.31D). In addition, the *MYB* binding site within the *ALOX5* coding region was investigated using constructs that contained a mutated binding site (Figure 4.32), according to Ringleb et al. (356). However, only low signals were observed for these constructs, so this approach was not further pursued. The low signals were presumably caused by the design of these constructs. To investigate the putative b-Myb binding site within the coding

sequence of *ALOX5*, a fusion protein of the N-terminal 5-LO sequence and the luciferase gene was used for the read-out. The combination of both protein parts was not tested in advance, so the low signals are most likely the result of a misfolded fusion protein. Although only the investigation of the putative binding site upstream of the core promoter led to sufficient results, the analysis indicated that *ALOX5* is indeed transcriptionally repressed by b-MYB. However, the underlying mechanism, or at least the responsible binding site, seems to differ in HT-29 and HCT-116 cells.

As MEK/ERK and PI3K/mTOR inhibition was shown to affect the cell cycle (Figure 4.13), HT-29 and HCT-116 cells were treated with inhibitors of cell-cycle promoting factors. CDK4/6 inhibition by Palbociclib resulted in a strong G0/G1 arrest in HT-29 cells (Figure 4.25A), accompanied by a significant increase in 5-LO expression (Figure 4.25B). Treatment with Ro-3306 (CDK1 inhibitor) resulted in a G2/M arrest in HT-29 cells, but 5-LO expression was nearly unchanged. HCT-116 cells were similarly affected, but CDK4/6 inhibition resulted in a less pronounced G0/G1 arrest, although the concentration of Palbociclib was 10-fold increased (10 µM) compared to HT-29 cells. Nevertheless, 5-LO expression was significantly increased following both treatments in HCT-116 cells. Overall, 5-LO expression was more responsive to cell-cycle manipulation in HCT-116 cells than in HT-29 cells, probably due to the already higher basal expression of HT-29 cells (72).

MCTS contain several zones, including a necrotic inner core region, a proliferative outer rim, and a quiescent viable zone in between (280, 281). Therefore, it was of interest which cells actually express 5-LO. For this purpose, confocal microscopy images of MCTS cryosections were prepared and stained for the proliferation marker Ki67, the apoptosis marker caspase-3 (cleaved), and 5-LO. As expected, Ki67 was predominantly expressed in the outer proliferative zone (Figure 4.27), whereas caspase-3 cleavage was found in the inner core region or the region farthest away from the outer rim as HCT-116 cells tend to form hollow structures (Figure 4.28). A solid 5-LO expression was found within the proliferative outer rim, which fits previous reports describing a correlation between 5-LO inhibition and cell proliferation in human pancreatic cancer cells (434–436). Co-staining of 5-LO and Ki67 was not observed in MCTS of HT-29 cells. Instead, 5-LO-positive cells were found to be intermixed with Ki67-positive cells. In contrast, HCT-116 cells in the outer rim were found to be co-stained for both proteins. Interestingly, 5-LO-positive cells with increased expression levels were also found in the inner necrotic core region of HT-29 spheroids.

Increased 5-LO expression is not exclusively found in CRC but also in other tumor entities. Thus, cell lines derived from other solid tumors were investigated regarding their *ALOX5*, *SP1*, *E2F1*, *MYBL2,* and *MYB* expression. For this purpose, the 5-LO-positive cell lines Capan-2 (pancreas adenocarcinoma), U-2 OS (osteosarcoma), as well as 5-LO-negative Caco-2 (colon adenocarcinoma) and MCF-7 (mammary gland adenocarcinoma) cells were treated with PI3K/mTOR (Dactolisib) and MEK/ERK (PD184352, Cobimetinib and SCH772984) inhibitors. It is important to note that the literature on 5-LO expression in Caco-2 and MCF-7 cells is inconsistent; however, within the Steinhilber group, these cell lines are considered 5-LO negative under standard culture conditions (356–359). MEK/ERK inhibition strongly increased *ALOX5* levels in Capan-2 cells (Figure 4.37A) but did not lead to relevant changes in U-2 OS, Caco-2, and MCF-7 cells (Figure 4.37B-D). In contrast, treatment with Dactolisib induced *ALOX5* expression in Caco-2 (Figure 4.37C) and MCF-7 (Figure 4.37D) cells but not in Capan-2 (Figure 4.37A) and U-2 OS (Figure 4.37B) cells. These results indicate that *ALOX5* expression is inhibited by PI3K/mTOR in Caco-2 and MCF-7 cells under standard conditions, whereas the MEK/ERK

pathway seems to regulate *ALOX5* expression in Capan-2 cells. Interestingly, either treatment did not affect the osteosarcoma cell line U-2 OS. Since U-2 OS cells carry a mutation in the *RICTOR* gene, which is part of mTORC-2, this might be an explanation for the poor responsiveness to MEK/ERK and PI3K/mTOR inhibition and also for the high basal 5-LO expression in these cells (415). Even though *ALOX5* expression in Caco-2, Capan-2, and MCF-7 cells was only sensitive to either MEK/ERK or PI3K/mTOR inhibition, the respective treatment resulted in an increased *SP1* and reduced *E2F1* and *MYBL2* expression that was in accordance with the findings in HCT-116 and HT-29 cells. Taken together, these results indicate that *ALOX5* expression might also be upregulated in other solid tumor specimens as a result of MEK/ERK and/or PI3K/mTOR inhibition.

5.3 5-LO activity of HT-29 and HCT-116 cells is comparable to M2 macrophages and strongly dependent on substrate availability

Myeloid cells express high amounts of 5-LO and its enzymatic activity is well investigated in these leukocyte subsets. 5-LO activity is very low in 5-LO-expressing tumor cells (see Figure 2.1), and factors triggering 5-LO expression and controlling its activity in solid malignant neoplasms are still poorly understood (72). However, many studies provided evidence that 5-LO product formation would benefit tumor cells, as LTB_4 and 5-HETE were shown to induce cell proliferation (308, 437). High 5-LO activity represents a potential threat to healthy cells due to the accumulation of reactive oxygen species during the enzymatic reaction and the formation of highly reactive 5-LO products like LTA_4 and FA hydroperoxides. It is indeed known that these products can trigger ferroptosis and form DNA adducts (438–442). Therefore, it is unsurprising that high 5-LO activity is primarily found in short-lived cells such as granulocytes. Based on previously shown results (Figure 2.1), it was investigated how 5-LO enzyme activity is potentially repressed in HT-29 and HCT-116 cells. Additionally, their lipid mediator profile and the amount of lipid mediators released were compared to 5-LO-expressing immune cells.

As the results in Figure 2.1 show, 5-LO activity is impaired in intact HT-29 and HCT-116 cells, and increases after cell disruption and segregation of membrane fractions via ultracentrifugation. Therefore, it was considered that substrate availability might be an inhibiting factor. The differences between the basal and stimulated 5-LO activity were investigated using a highly concentrated fatty acid mix (intended 60 µM assay concentration for each FA) consisting of ARA, DHA, and EPA. Product formation increased by stimulation using calcium ionophore (A23187, 2.5 µM), but only in a significant manner for 5-HETE, 5-HEPE, 15-HETE, and 5,15-DiHETE. Both cell lines showed no 5-LO activity without addition of exogenous substrates (Figure 4.35). Surprisingly, both cell lines formed higher amounts of 5-HEPE compared to 5-HETE. The formation of LTB_5 was not determined, but LTB_4 formation was quantified in both cell lines. The 5-HEPE formation was significantly increased using calcium ionophore in both cell lines. Contrary to the elevated 5-HEPE formation, ARA is described as the preferred substrate for 5-LO (33). However, the formation of EPA over ARA products was previously described for differentiated and polarized human macrophages, 5-LO purified from peritoneal guinea pig PMNL, and *ex vivo* lung preparations from rabbits (42, 144, 443, 444). In contrast, calcium ionophore-stimulated human PMNL incubations show higher concentrations of 5-LO products derived from ARA (69). It is known that granulocytes can mobilize high amounts of ARA upon activation, exceeding the

intended ARA assay concentration and resulting in higher ARA-derived oxylipin concentrations (445). Additionally, ARA is more abundant in membranes than DHA and EPA (446). Therefore, ARA products are more likely formed within the physiological context. Furthermore, only a few studies investigated the product formation profile in samples with substrate competition. Nevertheless, this competition aspect is important since it was shown that EPA and LTB_5 can inhibit LTB_4 formation in rat alveolar macrophages and, by this, influence the lipid mediator profile (447, 448).

In contrast to 5-LO products, the 15-LO product 15-HETE was preferably formed over 15-HEPE and 17-HDHA (Figure 4.35D). This is in line with the literature where the poor conversion of DHA compared to ARA and EPA is already described, e.g., for PMNL and M1 macrophages (42, 185, 449). However, a preferred turnover of DHA was recently described for human recombinant 15-LO-1 compared to ARA and EPA (450). 15-LO-1 and 15-LO-2 expression was determined in both cell lines (Figure 4.36A), but only 15-LO-1 was expressed in very low amounts. As a result, the 15-HETE to 12-HETE ratio was 6.4-7.6:1 in HT-29 and HCT-116 cells (Figure 4.39B, C), which is in line with the observed ratios between 4-13:1 in literature, depending on the composition of the supplemented FA mix (10, 450, 451). Surprisingly, the (*R*)-enantiomers of 15-HETE and 17-HDHA were preferentially formed in both cell lines (Figure 4.36B, C). This was unexpected, as 15-LO-1 is known to predominantly produce the respective (*S*)-enantiomer (452). A possible explanation might be, e.g., the conversion of 15-(*S*)-HETE to other metabolites (e.g., 5,15-DiHETE, 15-KETE), resulting in a reduced ratio between both enantiomers. Additionally, it is known that 15-(*S*)-HETE is rapidly esterified into membrane phospholipids, which also would result in a reduced enantiomer ratio. However, this does not identify the 15-(*R*)-HETE source in both cell lines. 15-(*R*)-HETE is known to be formed by either acetylated COX-2, COX-1, or CYP450 enzymes (170, 453). However, COX-1 was also shown to produce 15-(*S*)-HETE (453). Preliminary tests using ASA and other COX-1 and COX-2 inhibitors did not reduce the formation of 15-HETE in HT-29 and HCT-116 cells (data not shown). Furthermore, cells were also treated with high concentrations of the pan CYP450 inhibitors Ketoconazole (100 µM) (Master's Thesis Marius Mathes, 2019) and Cimetidine (100 µM). This resulted in elevated 15-(*R/S*)-HETE formation using Ketoconazole, while the use of Cimetidine did not influence the 15-HETE formation. 15-(*R*)-HETE was previously detected in, e.g., clotted human whole blood samples where concentrations were higher than those of 15-(*S*)-HETE. Treatment with high concentrations of the COX-1 inhibitor ASA (300 µM) increased 15-(*R*)-HETE formation instead of inhibiting it. It is essential to mention that clotted whole blood samples do not express COX-2. Also, HCA7 cells showed 15-(*R*)-HETE formation, which was increasable by ASA treatment (1 mM), but those effects were only detectable in combination with supplementation of very high exogenous ARA concentrations (100 µM). The formation of 15-(*R*)-HETE in HCA7 cells was attributed to unacetylated COX-2 and dependent on high ARA concentrations (454). As the expression of both COX enzymes was only investigated on mRNA level (*PTGS1* and *PTGS2*, App. Figure 7.2), it is unclear whether the formation of 15-(*R*)-HETE in HT-29 and HCT-116 cells (Figure 4.36B) is mediated by unacetylated COX-2 protein. Nevertheless, it would be important to investigate the exact source of 15-(*R*)-HETE and 17-(*R*)-HDHA in HT-29 and HCT-116 cells.

Interestingly, the dihydroxylated ARA and EPA metabolites 5,15-DiHETE and RvE_4 were also quantifiable in both cell lines, but again only after supplementation with the FA mix. Stimulation with calcium ionophore only increased the amount of 5,15-DiHETE. Furthermore, the formation

of those di-hydroxylated derivatives was 25-80-fold (HT-29) and 40-170-fold (HCT-116) lower compared to their mono-hydroxylated precursors (Figure 4.35F). This observation is not unique to cancer cell lines. Several publications showed very low formation of di-hydroxylated oxylipins derived from ARA, DHA, and EPA in calcium ionophore-stimulated PMNL and macrophages supplemented with respective fatty acids or macrophages exposed to pathogenic *E. coli.* Additionally, tri-hydroxylated oxylipin concentrations are even lower (42, 69, 455, 456).

Due to the very low 5-LO product formation after supplementation with high concentrations of exogenous fatty acids, even after calcium ionophore stimulation, one might assume that the formation of 5-HETE and 15-HETE, particularly, might be driven by non-enzymatic oxidation. Indeed, non-enzymatic product formation was observed (e.g., 8-HETE, data not shown). However, cell-free non-enzymatic oxidation controls were prepared for each sample set, and results were subtracted from respective samples. Furthermore, additional pre-tests using NAC (N-acetylcysteine, 1 mM) as a ROS scavenger did not reduce lipid mediator formation in HT-29 and HCT-116 cells (data not shown). Finally, the formation of LTB_4, albeit in low amounts, and the elevated product formation after the segregation of membrane fractions (Figure 2.1) indicated 5-LO enzyme activity. Even though the treatment of HT-29 homogenates using the 5-LO inhibitor NDGA was previously shown to abolish 5-LO product formation, partial non-enzymatic formation of mono-hydroxylated products should be considered and further investigated in the future using pharmacological 5-LO inhibition and 5-LO knockout cells (457).

As the use of very high substrate concentrations might lead to substrate inhibition, as already shown for 5-LO and ARA, 5-LO activity determined by 5-HETE and LTB_4 formation was investigated using lower concentrations (Figure 4.37) (458). However, the use of lower ARA concentrations led to less 5-HETE formation. In the case of HCT-116 cells, LTB_4 formation was only observed using 60 µM ARA (20 µM was not determined), while HT-29 cells could form low concentrations of LTB_4 with only 10 µM ARA. Nevertheless, LTB_4 formation was not detectable using only 6 µM ARA, indicating a strong dependency on substrate availability.

Besides substrate availability, 5-LO activity/LT formation is known to be regulated by several other factors within the cellular context, among them the intracellular location of the enzyme, its phosphorylation status, alternative splicing, and the presence of FLAP. As shown in Figure 2.1, 5-LO is primarily localized within the cytosol of resting HT-29 and HCT-116 cells. It was not investigated if the stimulation using calcium ionophore properly translocates the enzyme towards the nuclear membrane in those cells. However, the association of 5-LO with the nuclear membrane is very important for the intracellular 5-LO activity (459). Additionally, phosphorylation of 5-LO at Ser523 was shown to inhibit the enzyme's activity, probably by preventing the association with the nuclear membrane or nuclear import (77). Unfortunately, it was not possible to analyze this phosphorylation within this work since the respective antibody directed against the phosphorylation of Ser523 detected a protein similar in size to 5-LO in HT-29 and HCT-116 5-LO knockout cells as well as in HEK293T cells, which do not express 5-LO (data not shown). The expression of *ALOX5* splice variants was not investigated within this work. But, since there are several 5-LO isoforms known today, including some that were reported to negatively regulate 5-LO activity (34, 37), mRNA splice-variants represent another interesting research topic for future investigations.

Last but not least, 5-LO activity strongly depends on FLAP in intact cells which is thought to transfer the lipid substrates to 5-LO (460). Both HT-29 and HCT-116 cells express only very low amounts of FLAP (Figure 4.1). However, after the disruption of cellular integrity and segregation of membrane fractions via ultracentrifugation, 5-LO product formation was elevated in both cell lines (Figure 2.1). This fits existing literature, where 5-LO was shown to gain activity in broken cell preparations when exogenous ARA is freely available to the enzyme in solution, even in the absence of FLAP (116).

With regard to the low FLAP expression in HT-29 and HCT-116 cells, lipid mediator formation profiles, 5-LO, and FLAP expression were compared to PMNL, M1, and M2 macrophages. As expected, PMNL formed very high amounts of 5-HETE and LTB_4 after stimulation with calcium ionophore (2.5 µM) and supplementation with a FA mix (ARA, DHA, EPA, intended assay concentration of 60 µM for each FA), while M1 macrophages formed moderate but significantly lower amounts. Surprisingly, 5-LO product formation (5-HETE, 7-HDHA, 5-HEPE, LTB_4) per mg protein was comparable between M2 macrophages and tumor cells (Figure 4.38). Interestingly, 5-LO expression was low in HT-29 and HCT-116 cells compared to M1 macrophages. Due to massive protein degradation in PMNL lysates, 5-LO expression was not appropriately depictable for these cells. The excessive protein degradation due to abundant neutral proteases in PMNL is well-known and described (461). However, several protocol adaptions did not lead to appropriate results. FLAP was not degraded in the lysates, most probably due to its transmembrane character that limits the access of proteolytic enzymes. FLAP was strongly expressed in PMNL and M1 macrophages, while it was significantly reduced in M2 macrophages. Again, this is already well documented in the literature. However, the observed low FLAP expression in both tumor cell lines and M2 macrophages might also explain the low formation of 5-HETE and LTB_4.

Interestingly, analysis of di-hydroxylated products revealed that 5,15-DiHETE was the preferentially formed product in each cell line (Figure 4.39D), although 5-HEPE was formed over 5-HETE. Notably, di-hydroxylated products may also be formed by subsequent reactions of 15-LO and 5-LO; however, this reaction is less efficient and slower (462). As the levels of di-hydroxylated products were remarkably lower (<8 ng/mg total protein) compared to mono-oxygenated PUFAs such as 5-HEPE, which reached up to 600 ng/mg total protein (PMNL), co-incubation experiments were performed to investigate the influence of a transcellular metabolism. Co-incubations of HCT-116 cells and PMNL revealed mostly similar results as co-incubations of HT-29 cells and PMNL. However, an enhanced product formation was not observed. Furthermore, the results indicate that PMNL take up endogenous substrates of neighboring cells.

In addition to the upregulation of 5-LO on mRNA and protein level, inhibition of the MEK/ERK (PD184352, Cobimetinib, SCH772984) and/or PI3K/mTOR (Dactolisib) pathways led to an increased 5-HETE formation in HT-29 and HCT-116 cells (Figure 4.42). However, product levels were lower than expected from previous experiments, which was presumably caused by a lack of substrate. Indeed, even control experiments showed 2-5 times less substrate (ARA and EPA) than expected (Figure 4.42C). Taken together, the difference between the determined ARA/EPA levels and the amount of formed metabolites in intact cells might be caused by the esterification of the substrates into cellular membranes since supernatants were used for the analysis. Alternatively, the substrates might stick to the cells simply by hydrophobic interactions. Nevertheless, this does not explain the fact that substrate levels in cell-free controls were manifold

lower than intended. To further investigate this issue, varying concentrations of ARA and EPA were prepared and analyzed. Again, the determined concentrations were substantially lower, with approx. 11 µM, 7.2 µM and 2 µM ARA instead of 60 µM, 20 µM and 6 µM, respectively (Figure 4.44A). As it was seen before, EPA values were again lower, with 6.3 µM and 1 µM instead of 60 µM and 6 µM, respectively (Figure 4.44B). These findings confirm the previous observations and indicate that a considerable amount of substrate does not even reach the cells. Hartung et al. recently evaluated concentrations in certified and non-certified oxylipin standards (463). They found enormous variations for non-certified 15-HETE and 17-HDHA standards with concentrations lower than 50% of the declared concentration. A difference between intended and found compound concentrations has also been shown for commercially obtained 15-HETE, 17-HDHA, and 18-HEPE by Mainka et al. (69). When they analyzed 10 µM preparations, more than 12 µM of 15-HETE and approx. 11 µM 18-HEPE were found. However, in samples with 17S- and 17R-HDHA, only 7.7 µM and 5.7 µM were found, respectively. This indicates that some obtained substrates indeed contain concentrations close to the desired amounts, while some do not. Therefore, careful evaluation has to be taken in future investigations as it is unclear what causes these variations. A possible explanation might either be hydrophobic interactions with test tubes or pipette tips but also inaccurate concentration details on commercially available products. As ARA and EPA levels were decreased even stronger in this work compared to the monooxygenated substrates of Mainka et al., it seems reasonable that at least part of the substrate is lost due to hydrophobic interactions. Nevertheless, future studies should definitely include cell-free control determinations to ensure reliable results.

5.4 Conclusion and perspective

This work summarizes the results and findings obtained while investigating the regulation and activity of 5-LO in two colorectal cancer cell lines. 3D culture revealed the upregulation of 5-LO along other oxygenases and members of the leukotriene cascade. The observed up-regulation of 5-LO was inversely correlated with cell proliferation and activation of PI3K/mTORC-2– and MEK/ERK-dependent pathways in monolayer cultures. Further analysis revealed the involvement of E2F and its target gene *MYBL2* in the repression of 5-LO during cell proliferation. Additionally, the PI3K/mTORC-2- and MEK/ERK-dependent suppression of 5-LO was also observed in other cancer cells lines. Therefore, a wider variety of cancer cells derived from solid malignant neoplasms might tightly regulate 5-LO expression by suppressing the enzyme during proliferation via pro-proliferative signaling pathways while up-regulating its expression upon cell stress conditions.

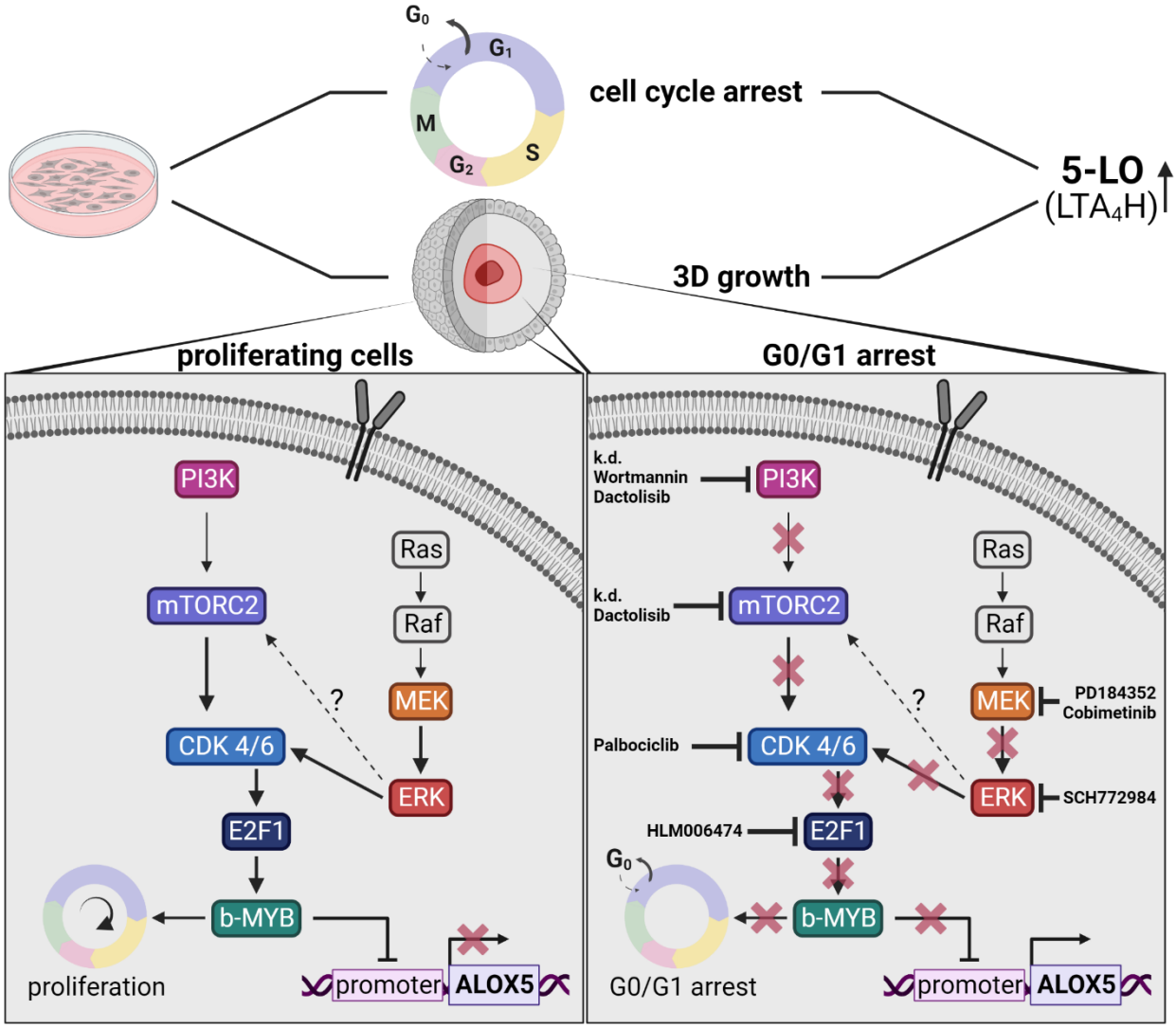

Figure 5.1: Summary of the signaling pathways that control 5-LO expression in solid cancer cell lines identified in the present thesis.
The Figure is adapted from (464).

In addition, activity analysis of both colorectal cancer cell lines revealed that LO product formation was not detectable in the absence of exogenous substrates. Supplementation with exogenous substrates, however, resulted in low product formation that was further enhanced by inhibition of the MEK/ERK or PI3K/mTOR pathway. This thigh regulation of 5-LO expression and activity in tumor cells underlines the assumed role of 5-LO in carcinogenesis.

Even though this work identified the involvement of pro-proliferative pathways in 5-LO expression and, therefore, LT formation, several questions remain unanswered. Further research on the regulation and activity of 5-LO and the leukotrienes cascade in cancer cells should, therefore, address the following questions:

- Which additional factors control 5-LO expression in tumor cells?
- What leads to 5-LO upregulation downstream of PI3K/mTORC-2, MEK/ERK, and upstream of *E2F1* and *MYBL2*?
- Do the additional tested cell lines also upregulate 5-LO after spheroid formation?
- Is the observed 5-LO upregulation in spheroids rather tied to necrosis and/or apoptosis?
- Why is 5-LO expression effectively suppressed under stress-free conditions in some cell lines while other cells permanently overexpress 5-LO on a basal level?
- Are tumor cells suppressing substrate availability and oxylipin synthesis by esterifying ARA, DHA, and EPA into the cell membrane?
- Which enzyme produces 15(*R*)-HETE in HT-29 and HCT-116 cells?

6 Zusammenfassung

Die vorliegende Arbeit beschäftigt sich mit der Regulation und Aktivität der 5-Lipoxygenase (5-LO), dem Schlüsselenzym der Leukotrienbiosynthese, in den beiden kolorektalen Krebszelllinien HT-29 und HCT-116. Obwohl die Leukotrienbiosynthese positiv mit dem Fortschreiten solider Tumorerkrankungen korreliert ist, ist bisher nur wenig über die Rolle der 5-LO bzw. deren Regulierung in Tumorzellen bekannt. So konnte in Vorarbeiten bereits gezeigt werden, dass viele Tumorzelllinien 5-LO exprimieren, obwohl dies im gesunden Gewebe nicht der Fall ist. Allerdings zeigte sich hier auch, dass die Expression der 5-LO zwar vorhanden, aber eingeschränkt zu sein scheint, da nur eine geringe Leukotrienproduktion festgestellt wurde. Zudem konnte bereits gezeigt werden, dass die 5-LO auch an der Regulation verschiedener Gene in Tumorzelllinien beteiligt ist. Da viele Ergebnisse bisheriger Studien aus 2-dimensionalen (2D) Zellkulturexperimenten stammen, diese das Tumormikromilieu (engl. t*umor microenvironment*, TME) aber nur unzureichend abbilden können, wurden bereits 3-dimensionale (3D) Ansätze getestet. Hierbei zeigte sich, dass die Bildung von 3D Sphären aus Tumorzellen zu einer erhöhten Expression der 5-LO führt. Daher konzentriert sich die vorliegende Arbeit auf die Untersuchung der Aktivität und Regulierung der 5-LO und untersucht die Mechanismen und Bedingungen, welche zur erhöhten 5-LO-Expression, insbesondere in 3D-Sphären, führen.

Zunächst wurde sichergestellt, dass die verwendeten Zelllinien, HT-29 und HCT-116, alle Komponenten der Leukotrienkaskade exprimierten. Untersuchungen auf mRNA und Proteinebene zeigten, dass alle relevanten Enzyme exprimiert wurden. Zudem bestätigte die Untersuchung nicht nur eine erhöhte Expression der 5-LO in 3D-Zellkulturen, sondern zeigte auch, dass LTA_4H, *LTC₄S*, *ALOX15*, *PTGS1* und *PTGS2* ebenfalls verstärkt exprimiert wurden. Nur die Expression von $cPLA_2$ war im Vergleich zur 2D-Zellkultur verringert. Mit Hilfe einer alternativen Technik zur Erzeugung dreidimensionaler Sphären wurde zudem sichergestellt, dass die Ergebnisse nicht von der Methode beeinflusst wurden. Da ein Mediumswechsel während der Bildung der Sphären nicht ohne weiteres möglich war, wurden die Zellen bis zu 7 Tage im selben Medium gehalten. Dabei zeigte eine Gelbfärbung des im Medium enthaltenen Indikators mit zunehmender Inkubationsdauer eine Azidifizierung an. Ein extrazellulärer saurer pH-Wert ist in der Literatur einerseits mit einem vorteilhaften Effekt auf die Tumorzellproliferation assoziiert, gleichzeitig wird jedoch eine Inhibierung des Zellzyklus beschrieben, wenn zuvor physiologische Bedingungen vorherrschten. Eine erste Analyse des Zellzyklus zeigte sowohl für HT-29 wie auch für HCT-116-Zellen eine Anreicherung der Zellpopulation in der G0/G1 Phase im Vergleich zu Zellen, die unter optimalen Bedingungen kultiviert wurden. Um den Einfluss des sauren Mediums besser zu verstehen, wurden Inkubationen in Medien mit definierten pH-Werten (6.6 und 6.8) durchgeführt. Dabei zeigte sich, dass die Expression des 5-LO-Gens (*ALOX5*), teilweise signifikant, erhöht war. Da mit einer zunehmenden Inkubationsdauer auch die Zelldichte zunimmt, wurde zudem der Einfluss einer erhöhten Zellzahl auf die *ALOX5*-Expression untersucht. Auch hier konnte ein erhöhter *ALOX5*-Spiegel in beiden Zelllinien festgestellt werden. Dieser Effekt war in HT-29-Zellen stärker ausgeprägt als in HCT-116-Zellen. Bei der anschließenden Zellzyklusanalyse zeigte sich zudem, dass ein G0/G1 Arrest nur in HCT-116-Zellen beobachtet werden konnte. Während HT-29-Zellen bereits unter Standardbedingungen hohe 5-LO-Spiegel aufweisen, zeichnen sich HCT-116-Zellen durch eine geringere 5-LO-Expression, aber eine höhere Proliferationsrate aus. Da HCT-116-Zellen, im Vergleich zu HT-29-Zellen, zudem als

weniger differenziert und eher stammzellähnlich gelten, könnte dies ein Indiz dafür sein, dass die Expression der 5-LO mit dem Differenzierungsstatus der Zellen zusammenhängt.

Kolorektale Krebszelllinien zeigen häufig eine Störung hinsichtlich Zellwachstum, Zellteilung, Überleben und ihrem Metabolismus. Diese Funktionen hängen typischerweise eng mit dem Status des Zellzyklus der Zellen zusammen. Da die ersten Untersuchungen bereits zeigten, dass der Zellzyklus einen Einfluss auf die Expression der 5-LO zu haben scheint, wurden im Folgenden die beiden Zellzyklus-regulierenden Signalwege MEK/ERK und PI3K/mTOR näher untersucht. Dazu wurden zunächst Inhibitoren der beiden Signalwege hinsichtlich ihres Effektes auf die Expression der 5-LO untersucht. Dabei zeigte sich, dass die Expression der 5-LO nach Behandlung mit dem dualen PI3K/mTOR-Inhibitor Dactolisib, den MEK-1-Inhibitoren PD184352 und Cobimetinib, sowie dem ERK-Inhibitor SCH772984 signifikant erhöht war. Im Gegensatz hierzu führte die Behandlung mit dem mTOR-Inhibitor Temsirolismus, dem PI3K-Inhibitor Wortmannin, dem EGFR-Inhibitor Erlotinib und dem FTase-Inhibitor LB42708, wenn überhaupt, nur zu einer leichten Erhöhung der 5-LO-Expression. Zusätzlich zur signifikant erhöhten 5-LO-Expression nach Behandlung mit den Inhibitoren Dactolisib, PD184352, Cobimetinib und SCH772984 konnte hier ebenfalls ein G0/G1-Arrest festgestellt werden. Um auszuschließen, dass die beobachteten Effekte durch die Toxizität der Inhibitoren verursacht wurden, wurden entsprechende Viabilitätsuntersuchungen durchgeführt. Für die Inhibitoren Dactolisib und Cobimetinib konnte zwar eine verringerte Zellviabilität beobachtet werden, jedoch war keine nennenswerte Zytotoxizität feststellbar. Da somit gezeigt werden konnte, dass die Inhibierung des PI3K/mTOR- bzw. des MEK/ERK-Signalweges einen Einfluss auf die Expression der 5-LO und den Zellzyklus hat, wurde eine Untersuchung des Phospholylierungsstatus der Proteinkinasen ERK und p70S6K in 3D-Sphären durchgeführt. Wie erwartet konnte in HT-29-Sphären eine verringerte Phosphorylierung von ERK feststellt werden. Der Phosphorylierungsstatus der p70S6K hingegen konnte nicht ermittelt werden, da der verwendete Antikörper kein reproduzierbares Signal in HT-29-Zellen ergab. Im Gegensatz dazu konnte in HCT-116-Sphären eine verstärkte Phosphorylierung beider Kinasen festgestellt werden. Erneut zeigte sich somit ein Unterschied zwischen den beiden kolorektalen Krebszelllinien.

Da frühere Untersuchungen bereits zeigen konnten, dass die Behandlung von verschiedenen Krebszelllinien mit gentoxischen Substanzen zu einer p53-abhängigen Regulation des *ALOX5*-Gens führt, sollte überprüft werden, ob dies auch hier der Fall ist. Zusätzlich zum p53-Gen (*TP53*) wurde dabei auch das *BAX*-Gen untersucht, welches ebenfalls durch p53 reguliert wird. Die folgende qPCR-Analyse ergab, dass, mit Ausnahme von Erlotinib, alle Inhibitoren zu einer erhöhten Expression von *TP53* führten, wogegen ein Effekt auf die *BAX*-Expression nicht festgestellt werden konnte. Da trotz eines erhöhten *TP53*-Spiegels kein Einfluss auf die *BAX*-Expression zu beobachten war, wurden die Zellen mit Pifthrin-α, einem p53-Inhibitor, und NSC 66811, einem MDM2-Antagonisten, behandelt. Eine Regulierung der 5-LO-Expression konnte jedoch auch hier nicht festgestellt werden. Um sicherzustellen, dass die verwendeten Inhibitoren Pifithrin-α und NSC 66811 nicht ebenfalls die 5-LO-Expression unterdrücken, wurden weitere Untersuchungen in p53-Knock-out-Zellen (HCT-116 p53 -/-) durchgeführt. Da diese von sich aus eine verringerte 5-LO-Expression aufwiesen, konnte eine Zunahme der Expression nach Inhibierung der MEK/ERK-Achse nur auf mRNA-Ebene festgestellt werden. Dennoch war eine erhöhte Zellpolulation in der G0/G1-Phase zu beobachten. Allerdings war der Effekt in HCT-116 p53 -/- Zellen schwächer ausgeprägt als in HCT-116 wt p53 Zellen.

Da die Inhibierung von MEK/ERK bzw. PI3K/mTOR auch in p53-Knock-out-Zellen zu einer Verschiebung des Zellzyklus führte und zumindest auf mRNA-Ebene teilweise eine verstärkte *ALOX5*-Expression beobachtet werden konnte, wurden die beiden Signalwege genauer untersucht. Hierzu wurde der shRNA-vermittelte Knock-down verschiedener Proteine der beiden Signalwege im Hinblick auf die *ALOX5*- bzw. 5-LO-Expression untersucht. Wie sich zeigte, führte der Knock-down der PI3K-Untereinheiten p110α und p110γ zu einer verringerten 5-LO Expression. Im Gegenteil dazu zeigte der Knock-down von mTOR wie erwartet eine leichte, jedoch nicht signifikante, Erhöhung der 5-LO-Expression. Zudem zeigte der Knock-down von RICTOR, der Hauptkomponente der mTOR Untereinheit mTORC-2, eine signifikant erhöhte 5-LO-Expression in beiden Zelllinien, während Knock-down von RAPTOR, der Hauptkomponente der mTOR-Untereinheit mTORC-1, zu unterschiedlichen aber nicht signifikanten Ergebnissen führte. Da somit mTORC-2 für die beobachteten Effekte durch Inhibierung des PI3K/mTOR-Signalweges auf die Expression der 5-LO mitverantwortlich sein dürfte, wurde *PRKCZ*, ein bekanntes nachgeschaltetes Protein von mTORC-2 untersucht. Jedoch zeigte sich, dass der Knock-down von *PRKCZ* keinen Einfluss auf die Expression der 5-LO in HT-29-Zellen hatte und in HCT-116-Zellen sogar zu einer verringerten Expression führte. Als Nächstes wurde der MEK/ERK-Signalweg untersucht. Hier zeigte sich jedoch, dass die Knock-down-Experimente die beobachteten Inhibitoreffekte nicht abbilden konnten. So führte der Knock-down von MAP2K1, auch als MEK-1 bekannt, zu einer leicht erhöhten 5-LO-Expression in HCT-116-Zellen, wogegen die Expression in HT-29-Zellen nicht beeinflusst wurde.

Um weiter zu untersuchen, über welchen Mechanismus die 5-LO Expression gesteuert wird, wurden weitere Transkriptionsfaktoren, die in Verbindung zur Regulation des Zellzyklus oder dem DREAM-Komplex stehen, näher betrachtet. Zunächst wurden hierbei die beiden Zelllinien, in einem Zellrasenexperiment, erneut mit den bereits verwendeten Inhibitoren behandelt und die Expression der Transkriptionsfaktoren auf mRNA-Ebene analysiert. Wie bereits für die Expression der 5-LO beobachtet werden konnte, zeigte sich auch hier, dass die Inhibierung von EGFR mit Erlotinib und FTase durch LB42708 keinen nennenswerten Einfluss auf die Transkriptionsfaktoren hatte. Bei der Behandlung mit den MEK/ERK-Inhibitoren zeigte sich, dass Cobimetinib und SCH772984 zu vergleichbaren Effekten bei allen Transkriptionsfaktoren führten, während der Effekt des dritten MEK/ERK-Inhibitors, PD184352, abwich. Nach Behandlung mit Cobimetinib und SCH772984 wurden erhöhte Werte von *SP1*, *FOXO1* und *FOXO3* sowie verringerte Mengen an *MYBL2* und *E2F1* in beiden Zelllinien gefunden. Darüber hinaus war die Expression von *E2F1/2* und *MYB* in HCT-116-Zellen und *MYC* in HT-29-Zellen verringert. Bei der Inhibierung des PI3K/mTOR-Signalweges durch Dactolisib konnte ein sehr ähnliches Expressionsmuster festgestellt werden, mit Ausnahme von *MYC*, *E2F1* und *MYB*. Basierend auf den erhaltenen Ergebnissen, wurde die Expression von *E2F1*, *MYBL2*, *MYB* und *SP1* in 3D-Sphären der beiden Zelllinien weiter untersucht. In HT-29-Zellen wurden vergleichbare Ergebnisse zur MEK/ERK-Inhibierung mittels Cobimetinib/SCH772984 beobachtet, obwohl die Effekte auf *E2F1* und *SP1* weniger stark ausgeprägt waren. Auch die Ergebnisse der PI3K/mTOR-Inhibierung waren insgesamt recht ähnlich, auch wenn hier eine leicht erhöhte *MYB*-Expression anstatt einer Verringerung festgestellt wurde. Grundsätzlich lieferten auch die 3D-Sphären der HCT-116-Zellen ein ähnliches Bild. So wichen nach Inhibierung des PI3K/mTOR-Signalweges nur die Expression von *E2F1* und *MYB*, sowie nach Inhibierung des MEK/ERK-Signalweges die Expression von *E2F1* ab.

Da zuvor bereits beobachtet werden konnte, dass eine höhere Zelldichte mit einer erhöhten Expression der 5-LO einhergeht, wurde der Effekt auf *E2F1*, *MYB*, *MYBL2* und *SP1* ebenfalls untersucht. Dabei zeigte sich, dass die Expression von *E2F1* und *MYB* verringert war. Um den Zusammenhang zwischen *E2F1* und 5-LO auch auf Proteinebene zu verifizieren, wurde der pan-E2F-Inhibitor HLM006474 verwendet. Dieser führte in beiden Zelllinien zu einer Erhöhung der 5-LO-Expression, auch wenn diese nur in HCT-116-Zellen signifikant war. Um den Effekt von *MYB* weiter zu untersuchen, wurden durch Doxycyclin induzierbare, stabil transfizierte b-Myb (*MYB*) Überexpressionszelllinien erstellt. Hier zeigte sich, dass 48 h nach Induktion der b-Myb-Expression, durch Doxycyclin, eine verringerte 5-LO-Expression vorlag, auch wenn die Daten nur in HT-29-Zellen signifikant waren. In 3D-Sphären war dieser Effekt jedoch nicht zu beobachten. Hier führte die Überexpression von b-Myb stattdessen zu einer veränderten Sphären-Morphologie. Um dennoch zu untersuchen, ob b-Myb mit der Regulierung der 5-LO in Tumorzellsphären zusammenhängt, wurden Reportergenexperimente durchgeführt. Da bereits bekannt ist, dass sowohl die Promotorsequenz wie auch die kodierende Sequenz der 5-LO eine c-Myb-Bindestelle enthalten und zudem bereits gezeigt werden konnte, dass b-Myb und c-Myb an dieselben DNA-Konsensussequenzen binden, wurden die beiden Bereiche näher analysiert. Dabei zeigte sich, dass ein verkürzter Promotor in beiden Zelllinien zu einem verringerten Luciferasesignal führte. Die Entfernung der vermeintlichen b-Myb-Bindestelle im Promotor lieferte dagegen jedoch zelllinienabhängige Ergebnisse. In HCT-116-Zellen wurde eine erhöhte Luciferaselumineszenz festgestellt, während HT-29-Zellen ein verringertes Signal aufwiesen. Bei der Analyse der vermeintlichen b-Myb-Bindestelle der kodierenden Sequenz wurden hingegen nur sehr schwache Signale erhalten, weshalb eine genauere Auswertung nicht möglich war.

Da die bisherigen Untersuchungen zeigten, dass eine erhöhte Expression der 5-LO zusammen mit einer Zunahme an Zellen in der G0/G1-Phase auftritt, wurden Experimente mit Zellzyklusinhibitoren durchgeführt. In der Tat bewirkte der CDK4/6-Inhibitor Palbociclib einen starken Arrest in der G0/G-Phase sowie eine erhöhte 5-LO-Expression, während der CDK1-Inhibitor Ro-3306 zu einer Verschiebung der Zellpopulation in die G2/M-Phase führte und keinen nennenswerten Einfluss auf die 5-LO Expression zeigte. Insgesamt zeigten beide Zelllinien eine vergleichbare Reaktion auf die Manipulation des Zellzyklus.

3D-Zellkultursphären lassen sich in unterschiedliche Bereiche wie dem nekrotischen inneren Kern, dem proliferierenden äußeren Rand sowie einem Bereich aus gesunden Zellen in der Mitte aufteilen. Daher wurde als nächstes untersucht, in welchem Bereich die Expression der 5-LO auftritt. Wie erwartet, zeigten Konfokalmikroskopiebilder eine verstärkte Expression im proliferierenden äußeren Bereich. Allerdings konnten auch einige Zellen mit erhöhter 5-LO-Expression im nekrotischen Kern beobachtet werden. Interessanterweise zeigten sich jedoch Unterschiede zwischen den beiden Zelllinien. Während in HCT-116-Zellen eine Co-Lokalisation der 5-LO-Expression und dem Proliferationsmarker Ki67 beobachtet werden konnte, bestand der äußere Rand der HT-29-Sphären aus einer Mischung an Zellen, die jeweils nur die Expression eines der beiden Proteine zeigten.

Da eine erhöhte Expression der 5-LO in soliden Tumoren nicht auf Kolonkarzinome beschränkt ist, wurden die 5-LO-positiven Zelllinien Capan-2 (Pankreaskarzinom) und U-2 OS (Osteosarkom) sowie die 5-LO-negativen Zelllinien MCF-7 (Mammakarzinom) und Caco-2 (Kolonkarzinom) ebenfalls untersucht. Dazu wurden die Zelllinien ebenfalls mit den Inhibitoren des PI3K/mTOR- bzw. MEK/ERK-Signalweges behandelt und der Effekt auf die *ALOX5*-

Expression analysiert. Hierbei zeigte sich, dass die Inhibierung des MEK/ERK-Signalweges nur in Capan-2-Zellen zu einer stark erhöhten *ALOX5*-Expression führte. Die Inhibierung des PI3K/mTOR-Signalweges hingegen führte zu einer erhöhten *ALOX5*-Expression in den Zelllinien Caco-2 und MCF-7. Interessanterweise führte jedoch keine der Behandlungen zu einer Änderung der *ALOX5*-Expression in U-2 OS-Zellen.

Nach den Untersuchungen zur Regulation der *ALOX5*-, bzw. 5-LO-Expression wurde die Aktivität des Enzyms näher betrachtet. Da Vorarbeiten bereits zeigen konnten, dass die Aktivität der 5-LO nach Störung der zellulären Integrität erhöht ist, wurde ein Problem mit der Substratverfügbarkeit untersucht. In der Tat zeigte sich, dass die Zelllinien nur nach Zugabe von exogenem Substrat (60 µM Mix an Arachidonsäure (ARA), Eicosapentaensäure (EPA) und Docosahexaensäure (DHA)) in der Lage waren entsprechende Produkte zu bilden. Die Produktbildung war allerdings vergleichsweise gering, ließ sich jedoch durch zusätzliche Inkubation mit Calciumionophor A23187 teilweise erhöhen. Neben den monohydroxylierten Produkten von ARA und EPA, 5-HETE und 5-HEPE, konnten auch die dihydroxylierten Produkte 5,15-DiHETE und RvE_4 detektiert werden. Allerdings lag die Produktbildung der dihydroxlierten Verbindungen in HT-29-Zellen um das 25-80-fache und in HCT-116-Zellen um 40-170-fache unter der der monohydroxylierten Produkte. Um eine Substratinhibition der 5-LO ausschließen zu können, wurden die Inkubationen mit einem geringer konzentrierten Substratmix wiederholt. Es zeigte sich jedoch, dass eine geringere Substratkonzentration auch mit einer verringerten Produktbildung einherging. Da die Aktivität der 5-LO ebenfalls mit der Expression des 5-LO-aktivierenden Proteins, kurz FLAP, korreliert, wurden das Lipidprofil sowie die Expressionslevel von 5-LO und FLAP der beiden Zelllinien HT-29 und HCT-116 bestimmt und mit denen von M1- und M2-Makrophagen sowie polymorphonukleären Leukozyten (PMNL) verglichen. Wie erwartet zeigten PMNL eine starke FLAP-Expression und die höchste Lipidmediatorbildung. M1-Makrophagen zeigten ebenfalls eine moderate Produktbildung, die jedoch deutlich unter der der PMNL lag, während die Bildung von 5-LO-Produkten (5-HETE, 5-HEPE und 7-HDHA) in M2-Makrophagen vergleichbar mit denen der Tumorzelllinien war. Wie erwartet zeigten M1-Makrophagen eine starke 5-LO- und FLAP-Expression, während M2-Makrophagen deutlich weniger exprimierten. Wie bereits in der Literatur beschrieben ist, neigen PMNL dazu, 5-LO abzubauen, weshalb eine Bestimmung des Expressionlevels der 5-LO hier nicht durchgeführt werden konnte. Der Vergleich der Lipidmediatorprofile zeigte in allen Zellen, dass das 5-LO-Produkt 5-HEPE bevorzugt gebildet wurde. Während 5-HETE, gebildet aus ARA, ebenfalls in deutlichen Mengen gebildet wurde, konnten nur Spuren des DHA-Produktes 7-HDHA gefunden werden. Bei den 15-LO-Produkten 15-HETE, 15-HEPE und 17-HDHA war hingegen kein klarer Trend erkennbar. Während die Tumorzelllinien HT-29 und HCT-116 bevorzugt 15-HETE bildeten, war in PMNL die Bildung von 17-HDHA am höchsten. Dagegen bildeten M2-Makrophagen präferiert 15-HEPE und in M1-Makrophagen war keine nennenswerte Produktbildung festzustellen. Trotz der unterschiedlichen Substratpräferenzen bei monohydroxylierten Produkten, war 5,15-DiHETE das bevorzugte dihydroxylierte Produkt in sämtlichen Zellen. Da Tumorzellen dafür bekannt sind, einen transzellulären Metabolismus mit benachbarten Zellen zu vollziehen, wurden Co-Inkubationsexperimente mit PMNL und jeweils einer der beiden Tumorzelllinien durchgeführt. Dabei konnte eine Steigerung an hydroxlierten Produkten durch Co-Inkubation jedoch nicht festgestellt werden.

Um zu untersuchen, ob die Inhibierung des PI3K/mTOR- bzw. MEK/ERK-Signalweges auch mit einer erhöhten 5-LO-Aktivität einhergeht, wurden die beiden Herangehensweisen kombiniert. Tatsächlich zeigte die Inhibierung des MEK/ERK-Signalweges in HT-29-Zellen eine erhöhte Produktbildung an 5-HETE und LTB_4, während die Inhibierung von PI3K/mTOR lediglich die 5-HETE-Bildung steigerte. Zwar konnte in HCT-116-Zellen keine LTB_4-Bildung festgestellt werden, die Bildung von 5-HETE war jedoch unter allen Bedingungen erhöht.

Zusammenfassend zeigen die Ergebnisse der vorliegenden Dissertation, dass die Expression und Aktivität der 5-LO in den kolorektalen Tumorzellinien HT-29 und HCT-116 streng reguliert sind. Während der Zellproliferation scheinen die Expression und Aktivität der 5-LO unterdrückt zu sein, während zellulärer Stress zu einer Hochregulierung führt. Die 5-LO könnte somit eine Rolle bei der Entwicklung oder Unterstützung eines tumorfördernden Mikromilieus spielen.

7 Appendix

7.1 App. Results

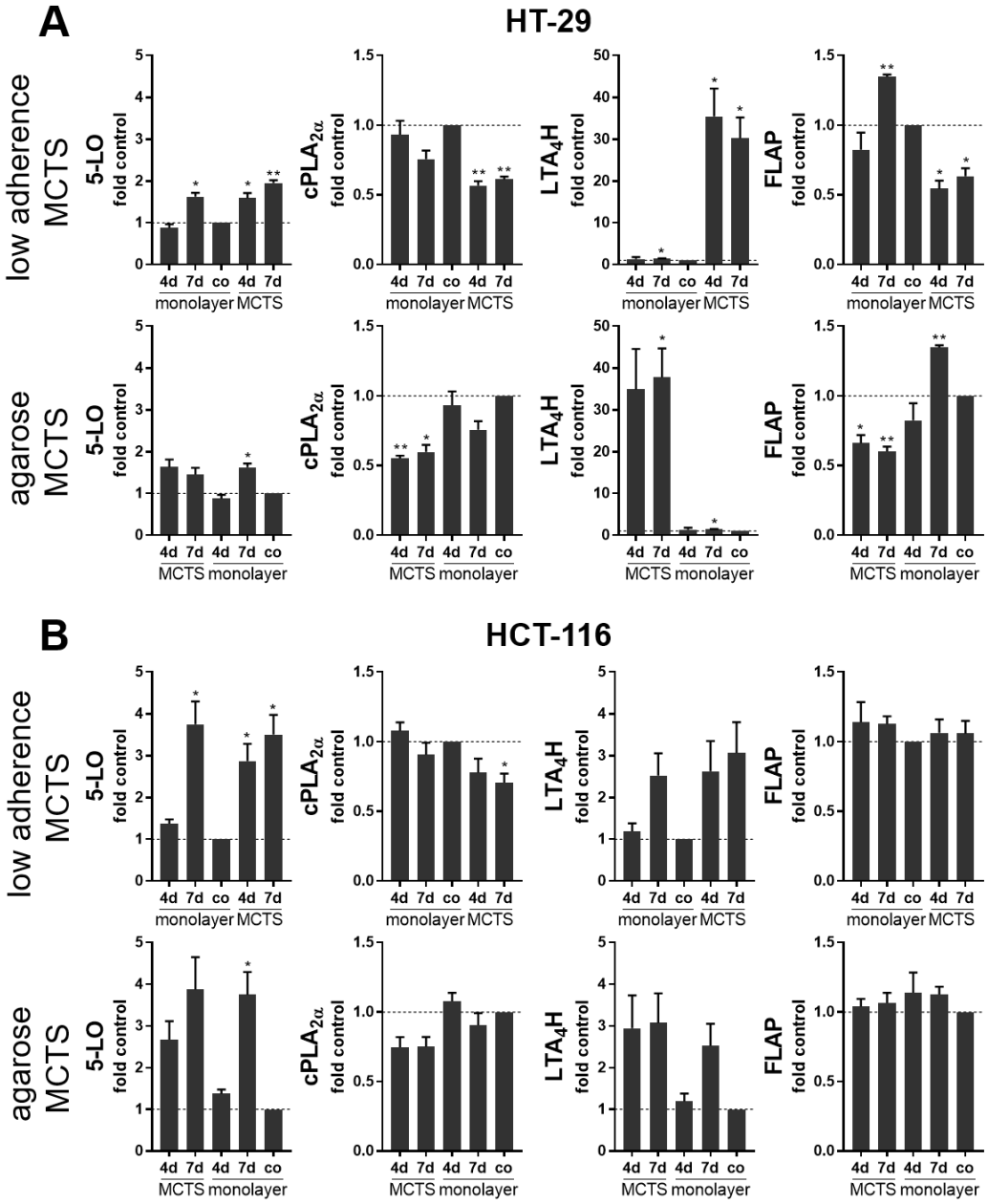

App. Figure 7.1: Densitometric analysis of the protein expression of 5-LO and other members of the LT cascade in MCTS.

Protein expression of 5-LO, cPLA2α, LTA4H, and FLAP in HT-29 (A) and HCT-116 (B) cells analyzed via Western blot. MCTS were either grown for 4 or 7 days in 96-well low adherence plates or 24-well plates coated with ultra-pure agarose (1%). Respective monolayer controls were seeded in 12-well plates. Identical cell amounts ($0.05x10^6$ cells/well) were used. The subconfluent monolayer controls (co) were seeded in 100 mm dishes ($3x10^6$ per dish), received a medium change after 24 h, and were harvested after 48 h. Densitometric values were determined using the Image Studio Software (V 5.2). Densitometric values were normalized to the loading control α-tubulin followed by normalization to the DMSO vehicle control (co). Results are depicted as mean + SEM from 3 independent experiments. Asterisks indicate significant changes vs. DMSO vehicle control determined by student's t-test with Welch's correction * ($P<0.05$), ** ($P<0.01$), *** ($P<0.001$).

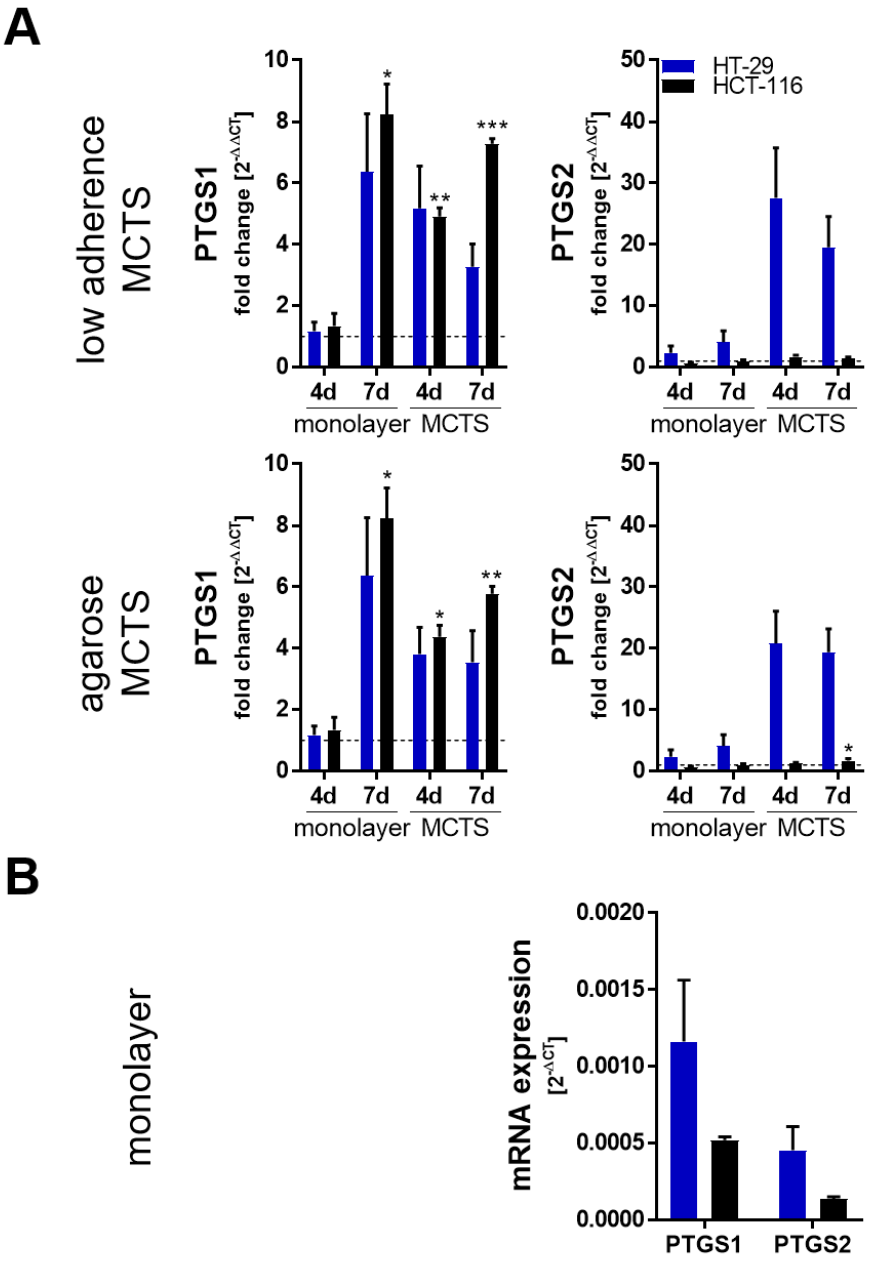

App. Figure 7.2: mRNA expression of PTGS1 and PTGS2 in MCTS.
MCTS were either grown for 4 or 7 days in 96-well low adherence plates or 24-well plates coated with ultra-pure agarose (1%). Respective monolayer controls were seeded in 12-well plates. Same cell amounts ($0.05x10^6$ cells/well) were used. The subconfluent monolayer controls (co) were seeded in 6-well plates ($0.4x10^6$ cells per well), received a medium change after 24 h, and were harvested after 48 h. (A) Gene expression determined via qPCR analysis was normalized to the housekeeping gene ACTB and the respective monolayer control ($2^{-\Delta\Delta CT}$ method). (B) Comparison of monolayer gene expression normalized to ACTB ($2^{-\Delta CT}$). Results are depicted as mean + SEM from 3 independent experiments. Asterisks indicate significant changes vs. co determined by student's t-test with Welch's correction. * ($P<0.05$), ** ($P<0.01$), *** ($P<0.001$).

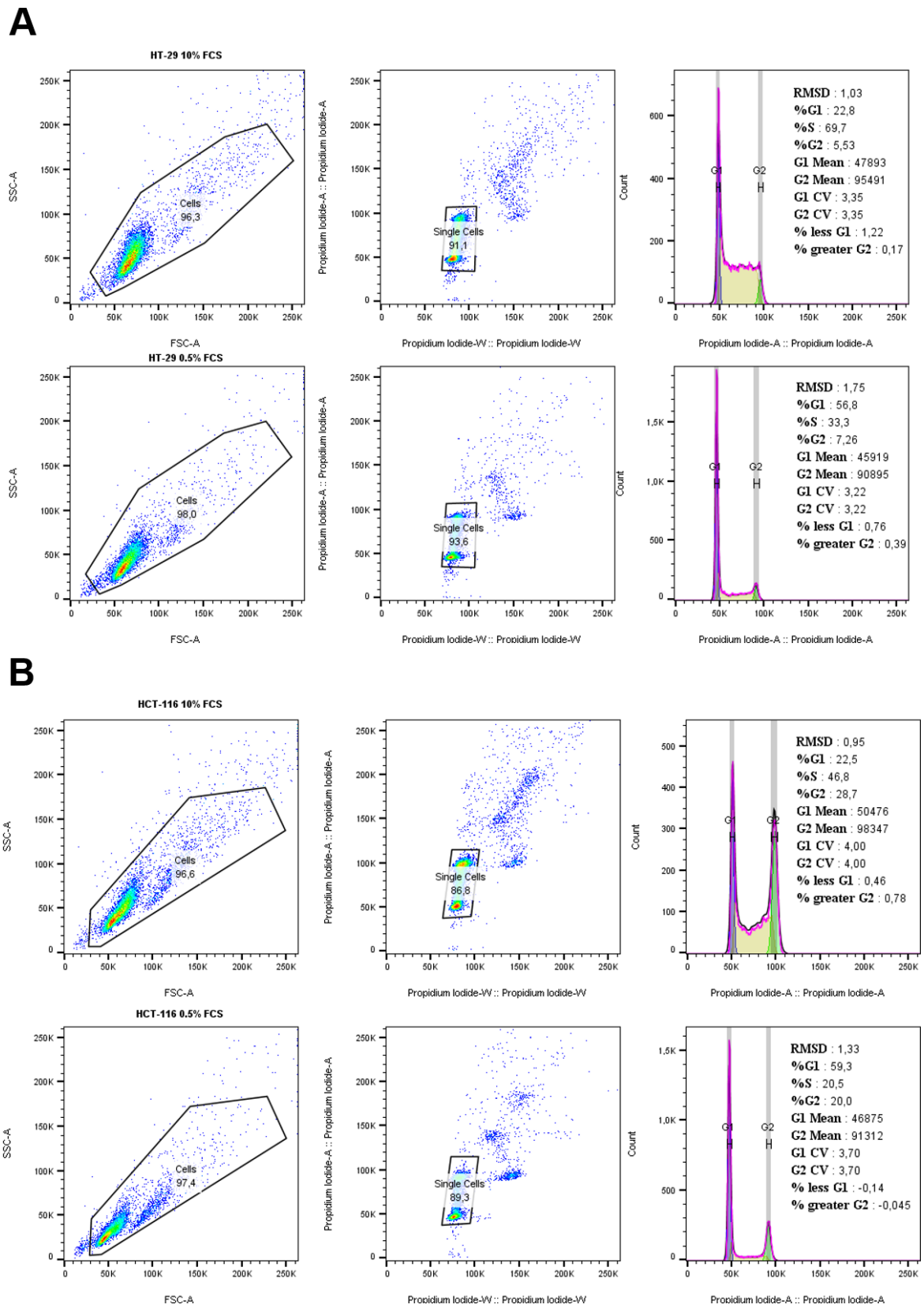

App. Figure 7.3: Representative plots of the gating strategy for cell cycle analysis and respective histograms resulting from cell cycle analysis.
Values are percentages of the parent population. Doublets are excluded before cell cycle analysis by plotting PI-A against PI-W. Gating and cell cycle analysis was performed using FlowJo V10, and the Watson Pragmatic algorithm was applied.

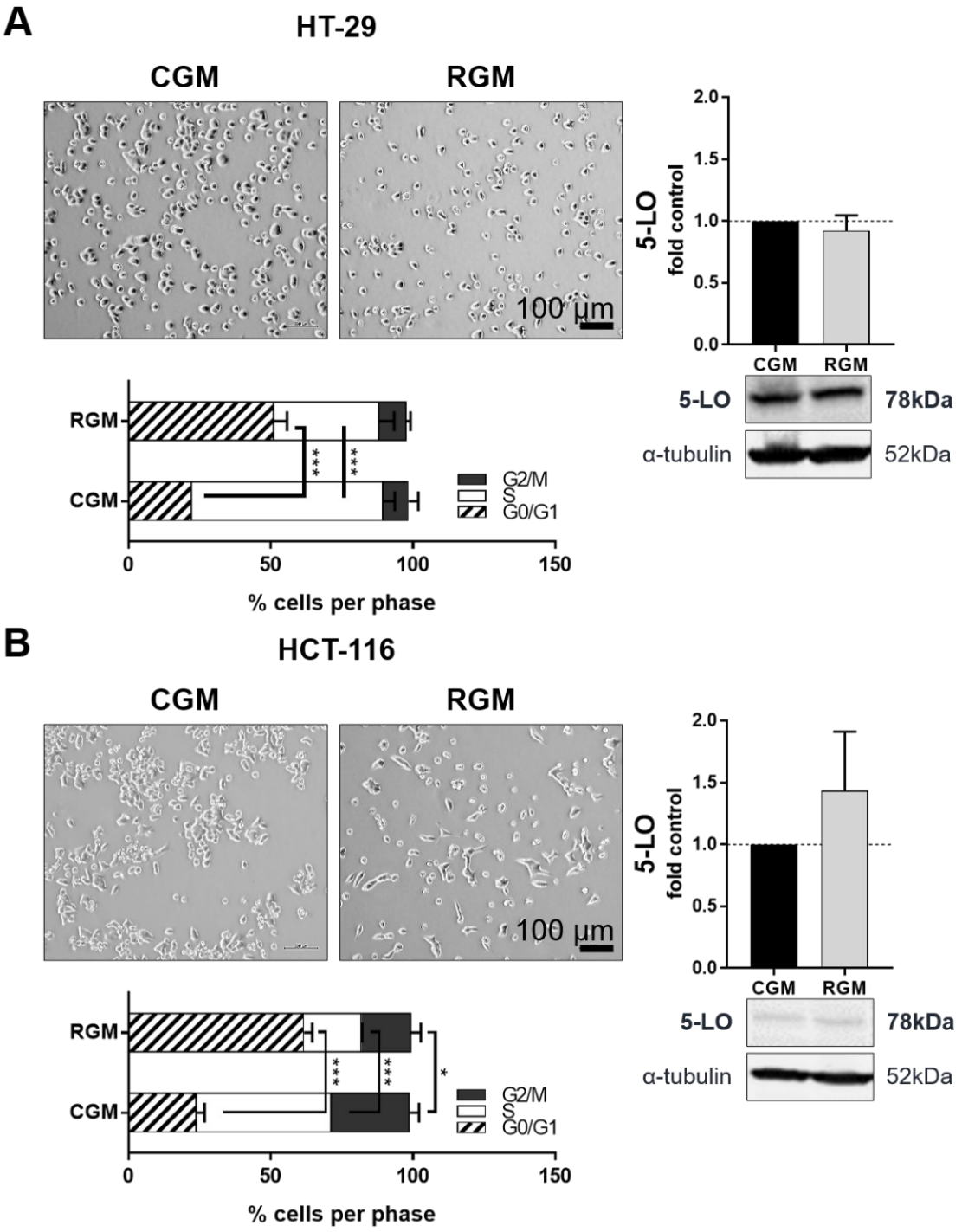

App. Figure 7.4: Reversible cell cycle synchronization via serum deprivation.
HT-29 cells (A) or and HCT-116 cells (B) were seeded in their respective CGM or RGM. Pictures were taken employing a light microscope. One representative picture out of 3 independent experiments is shown. Cells were analyzed via flow cytometry, and cell cycle analysis was performed using FlowJo software 10. Results are depicted as mean + SEM from 3 independent experiments. Asterisks indicate significant changes vs. co determined by two-way ANOVA coupled with Dunnett's post-test for multiple comparisons. * ($P<0.05$), ** ($P<0.01$), *** ($P<0.001$). 5-LO expression was analyzed via Western blot. One representative out of 3 blots is shown. Results are depicted as mean + SEM from 3 independent experiments.

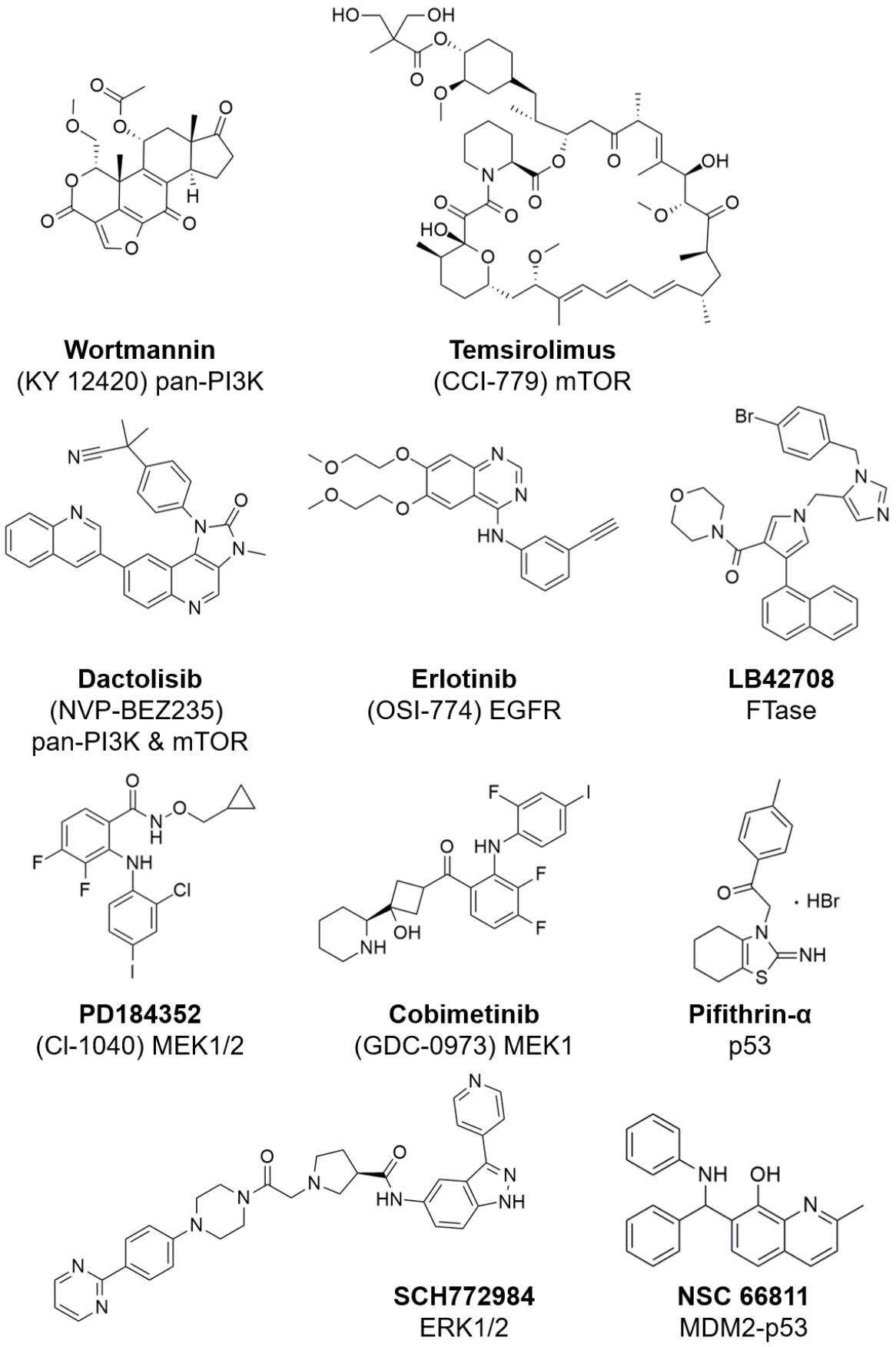

App. Figure 7.5: Structural overview of compounds used for the inhibition of various targets of the PI3K/mTOR, MEK/ERK, and p53 signaling.

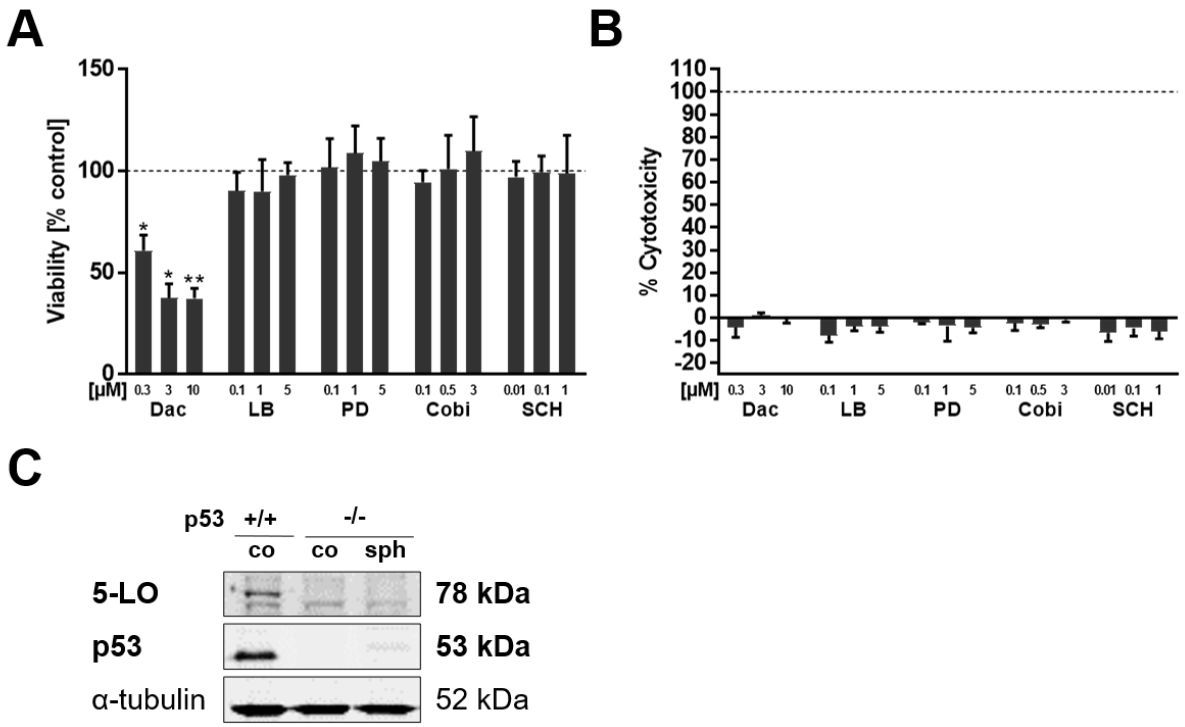

App. Figure 7.6: 5-LO expression after MCTS of HCT-116 p53 -/ cells and cell viability and cytotoxicity after 24 h of treatment with inhibitors of the PI3K/mTOR and MEK/ERK in monolayer grown HCT-116 p53 -/- cells.
Cells were cell cycle synchronized by serum starvation using RGM 22 h before treatment. Then, the medium was changed to CGM for 2 h and cells were treated for 24 h with the indicated inhibitors Dactolisib (Dac) 3 µM; LB42708 (LB) 1 µM; PD184352 (PD) 1 µM; Cobimetinib (Cobi), 0.5 µM; SCH772984 (SCH) 1 µM. The vehicle control (co) received DMSO instead. Cell viability was determined using a WST-1 assay (A). Results were normalized to the respective DMSO control (100%). Compound cytotoxicity was determined using an LDH assay (B). To determine the percentage of cytotoxicity, average absorbance of the respective background control was subtracted from each sample. Then, samples were normalized to the Triton-X-100 control (100%) and the respective DMSO control (0%). 5-LO and p53 protein expression of HCT-116 p53 -/- cells cultured in 24-well plates coated with ultra-pure agarose (1%) for 7 days for MCTS formation. Monolayer-cultured HCT-116 p53 -/- and HCT-116 p53 wt cells served as controls (co). Results shown in are depicted as mean + SEM from 3 independent experiments. Asterisks indicate significant changes vs. control determined by unpaired two-tailed student's t-test with Welch's correction * ($P<0.05$), ** ($P<0.01$), *** ($P<0.001$).

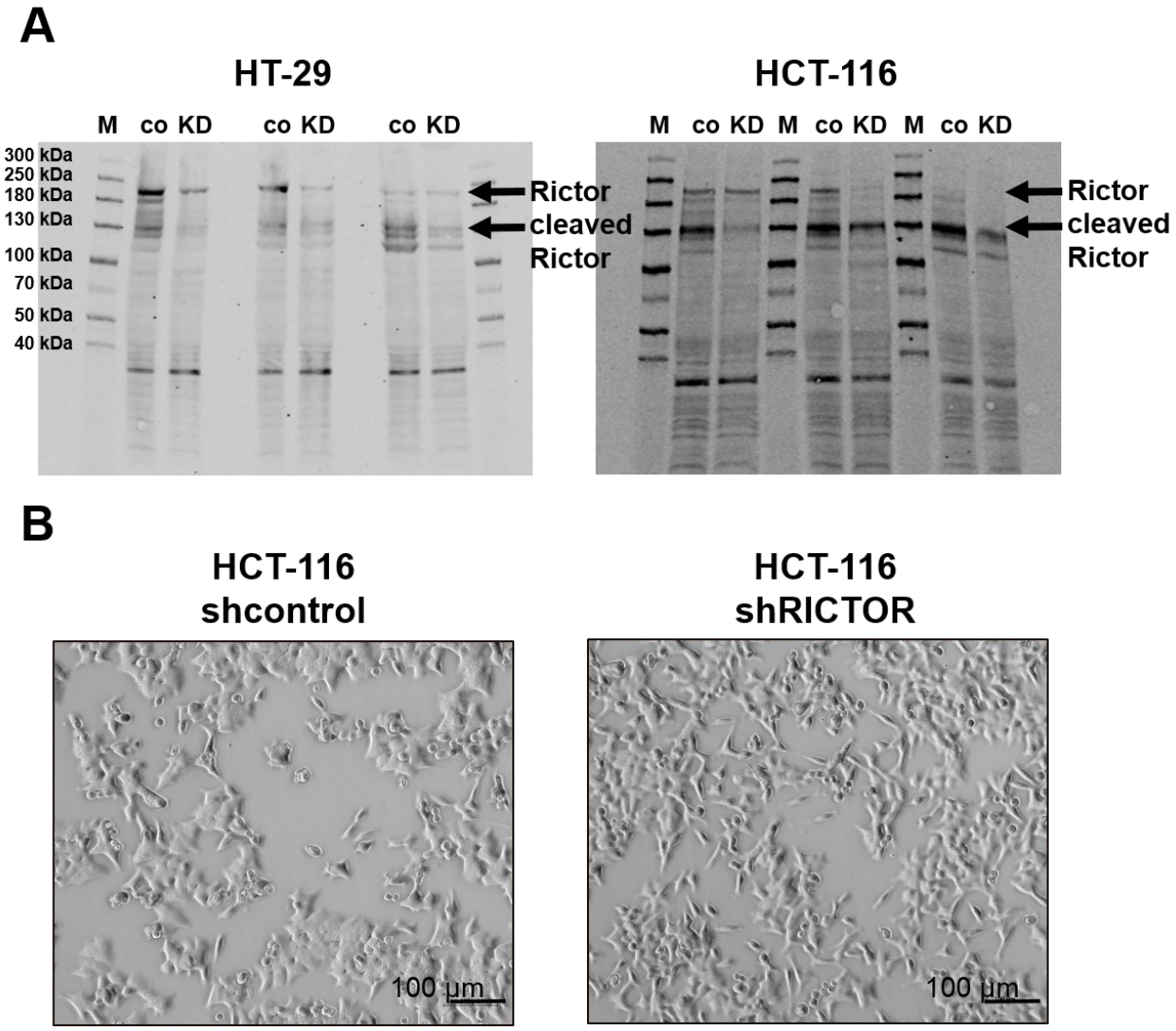

App. Figure 7.7: Rictor protein cleavage and cellular morphology of stable HT-29 and HCT-116 RICTOR knockdown and non-mammalian shRNA control cells.
(A) Rictor expression in stable knockdown (KD) HT-29 and HCT-116 cells determined via Western blot. Respective non-mammalian shRNA expressing control cells are indicated as co. Shown are samples of 3 different passages. Arrows indicate the respective full-length Rictor size and the assumed cleaved variant. (B) Pictures of HCT-116 Rictor knockdown cells and the respective non-mammalian shRNA expressing control cells were taken employing a light microscope (scale bar: 100 µm). One representative picture out of 3 is shown.

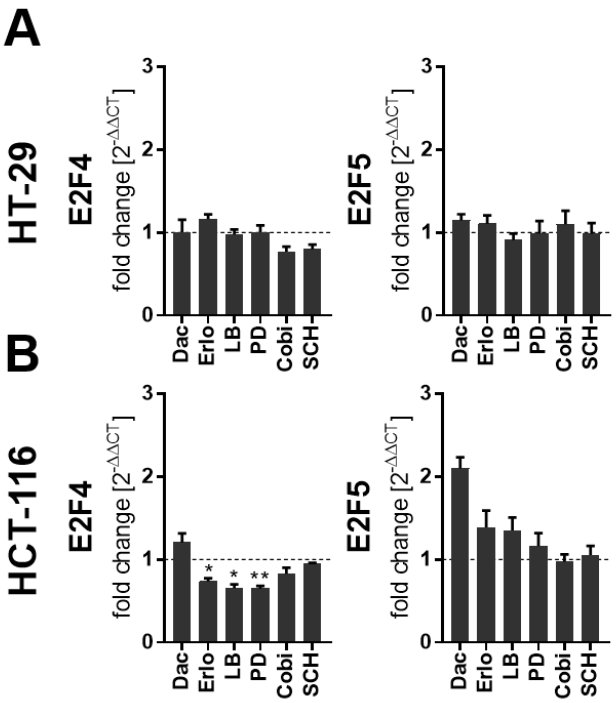

App. Figure 7.8: mRNA expression of *E2F4* and *E2F5* after 24 h of treatment with inhibitors of the PI3K/mTOR and MEK/ERK pathway in monolayer grown cells.
HT-29 (A) and HCT-116 (B) cells were cell cycle synchronized by serum starvation using RGM 22 h before treatment. Then medium was changed to CGM for 2 h and cells were treated for 24 h with the indicated inhibitors Dactolisib (Dac) 3 µM; Erlotinib (Erlo) 5 µM; LB42708 (LB) 1 µM; PD184352 (PD) 1 µM; Cobimetinib (Cobi), 0.5 µM; SCH772984 (SCH) 1 µM. The vehicle control received DMSO instead. mRNA expression was determined via qPCR analysis. Expression was normalized to the housekeeping gene *ACTB* and the respective vehicle control ($2^{-\Delta\Delta CT}$ method). Results are depicted as mean + SEM from 3 independent experiments. Asterisks indicate significant changes vs. DMSO co determined by unpaired two-tailed student's t-test with Welch's correction. * (P<0.05), ** (P<0.01), *** (P<0.001).

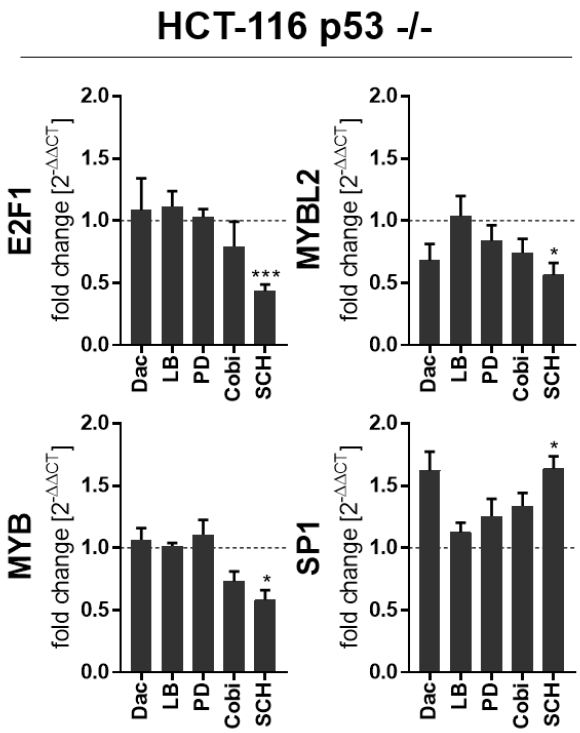

App. Figure 7.9: mRNA expression of *E2F1*, *MYBL2*, *MYB*, and *SP1* after 24 h of treatment with inhibitors of the PI3K/mTOR and MEK/ERK pathway in monolayer grown cells.
HCT-116 p53 -/- cells were seeded ($0.4x10^6$ cells/well, 6-well plate) and cell cycle synchronized by serum starvation using RGM 22 h before treatment. Then, the medium was changed to CGM for 2 h and cells were treated for 24 h with the indicated inhibitors Dactolisib (Dac) 3 µM; LB42708 (LB) 1 µM; PD184352 (PD) 1 µM; Cobimetinib (Cobi), 0.5 µM; SCH772984 (SCH) 1 µM. The vehicle control received DMSO instead. mRNA expression was determined via qPCR analysis. Expression was normalized to the housekeeping gene *ACTB* and the respective vehicle control ($2^{-\Delta\Delta CT}$ method). Results are depicted as mean + SEM from 3 independent experiments. Asterisks indicate significant changes vs. DMSO control determined by unpaired two-tailed student's t-test with Welch's correction. * (P<0.05), ** (P<0.01), *** (P<0.001).

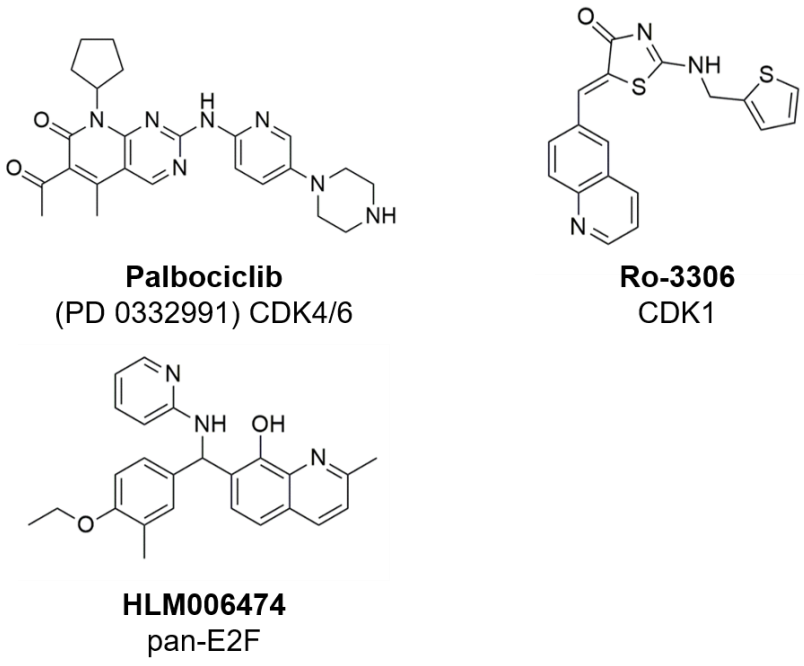

App. Figure 7.10: Structural overview of compounds used for the inhibition of CDK1, CDK4/6, and E2Fs.

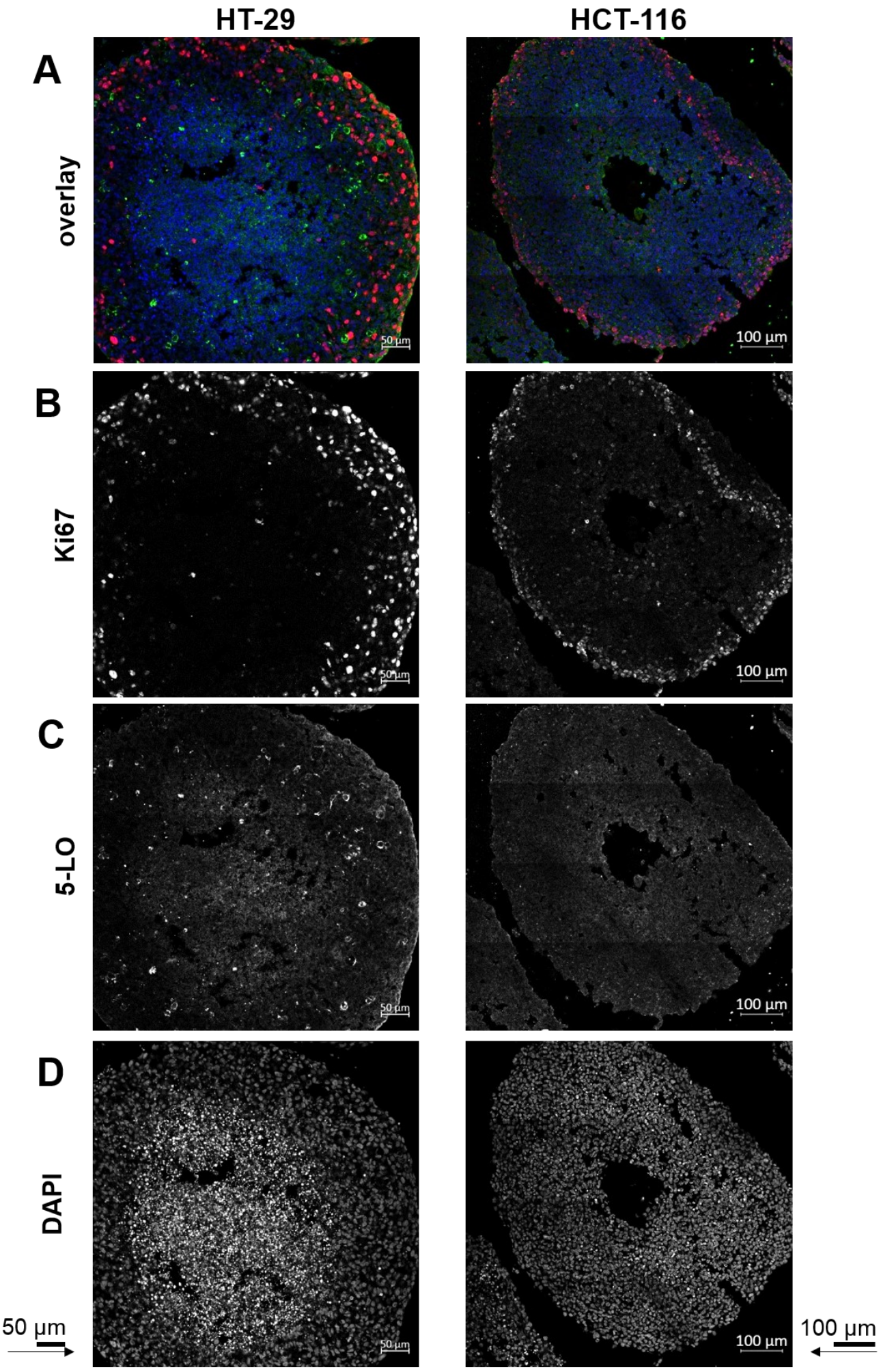
HT-29
HCT-116
A
overlay
B
Ki67
C
5-LO
D
DAPI
50 µm
100 µm
50 µm
100 µm

App. Figure 7.11: MCTS confocal microscopy tile scan overview.
MCTS were grown for 7 days in 96-well low adherence plates. 14 µM cryosections were co-stained with primary antibodies directed against Ki67 (B) and 5-LO (C). Afterwards, samples were probed with secondary fluorophore-conjugated antibodies (Alexa Fluor™ Plus 488, Alexa Fluor™ Plus 647). DAPI (D) was used for nuclear counterstaining. The sections were analyzed by confocal microscopy using 3x3 (HT-29) or 4x4 (HCT-116) tile scans. Single-channel fluorescence tile scan images (B-D) are displayed in black and white for better contrast, while channel overlay (A) is presented in color (Ki67 red, 5-LO green, DAPI blue). Identical linear histogram adjustments were applied to each channel to adjust brightness and contrast. Scale bars are provided within the figure. One representative of 3 independent experiments is shown.

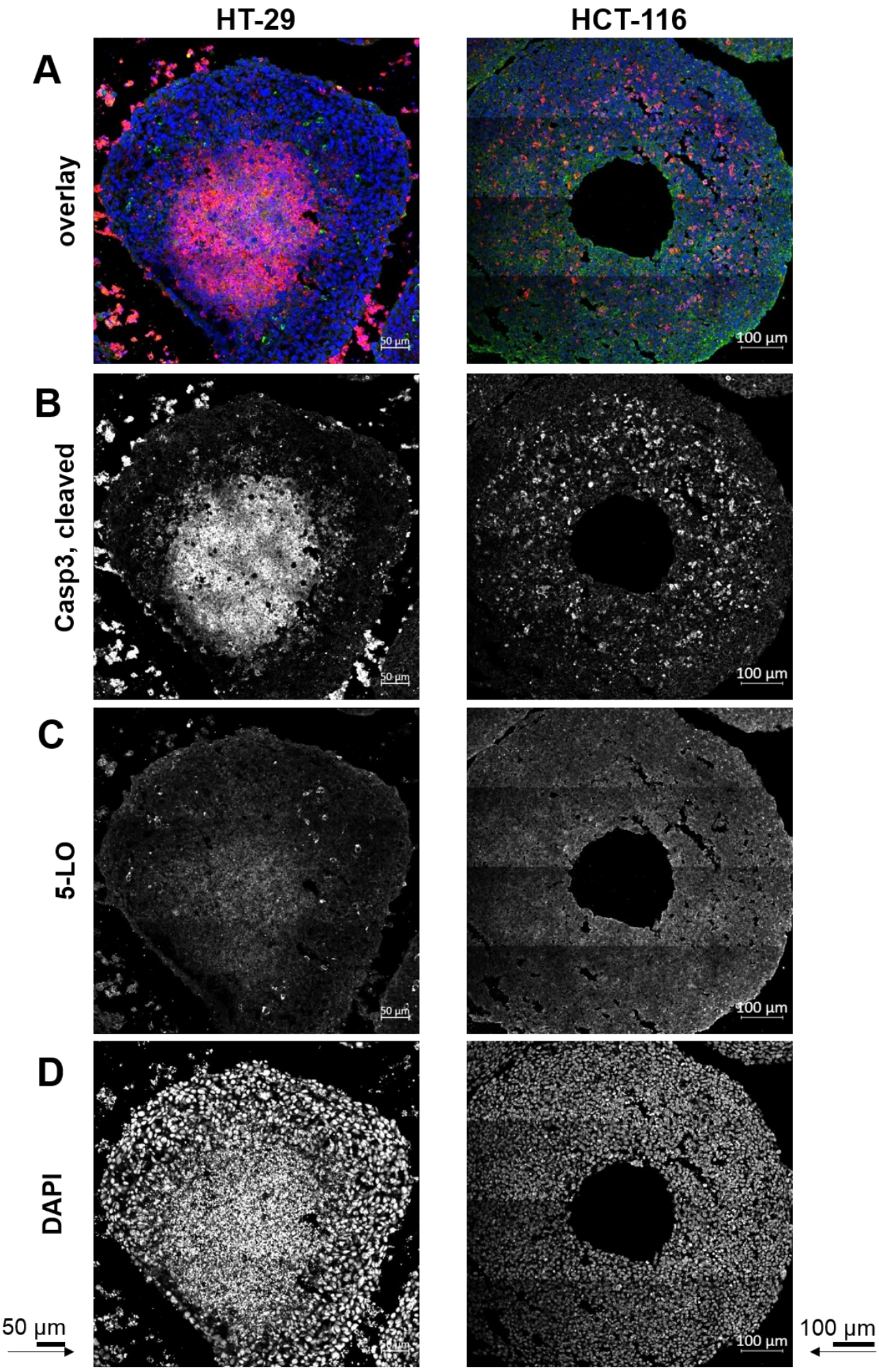
HT-29
HCT-116
A
overlay
B
Casp3, cleaved
C
5-LO
D
DAPI
50 µm
100 µm
50 µm
100 µm

App. Figure 7.12: MCTS confocal microscopy tile scan overview.
MCTS were grown for 7 days in 96-well low adherence plates. 14 µM cryosections were co-stained with primary antibodies directed against cleaved caspase 3 (B) and 5-LO (C). Afterwards, samples were probed with secondary fluorophore-conjugated antibodies (Alexa Fluor™ Plus 488, Alexa Fluor™ Plus 647). DAPI (D) was used for nuclear counterstaining. The sections were analyzed by confocal microscopy using 3x3 (HT-29) or 4x4 (HCT-116) tile scans. Single-channel fluorescence tile scan images (B-D) are displayed in black and white for better contrast, while channel overlay (A) is presented in color (cleaved caspase 3 red, 5-LO green, DAPI blue). Identical linear histogram adjustments were applied to each channel to adjust brightness and contrast. Scale bars are provided within the figure. One representative of 3 independent experiments is shown.

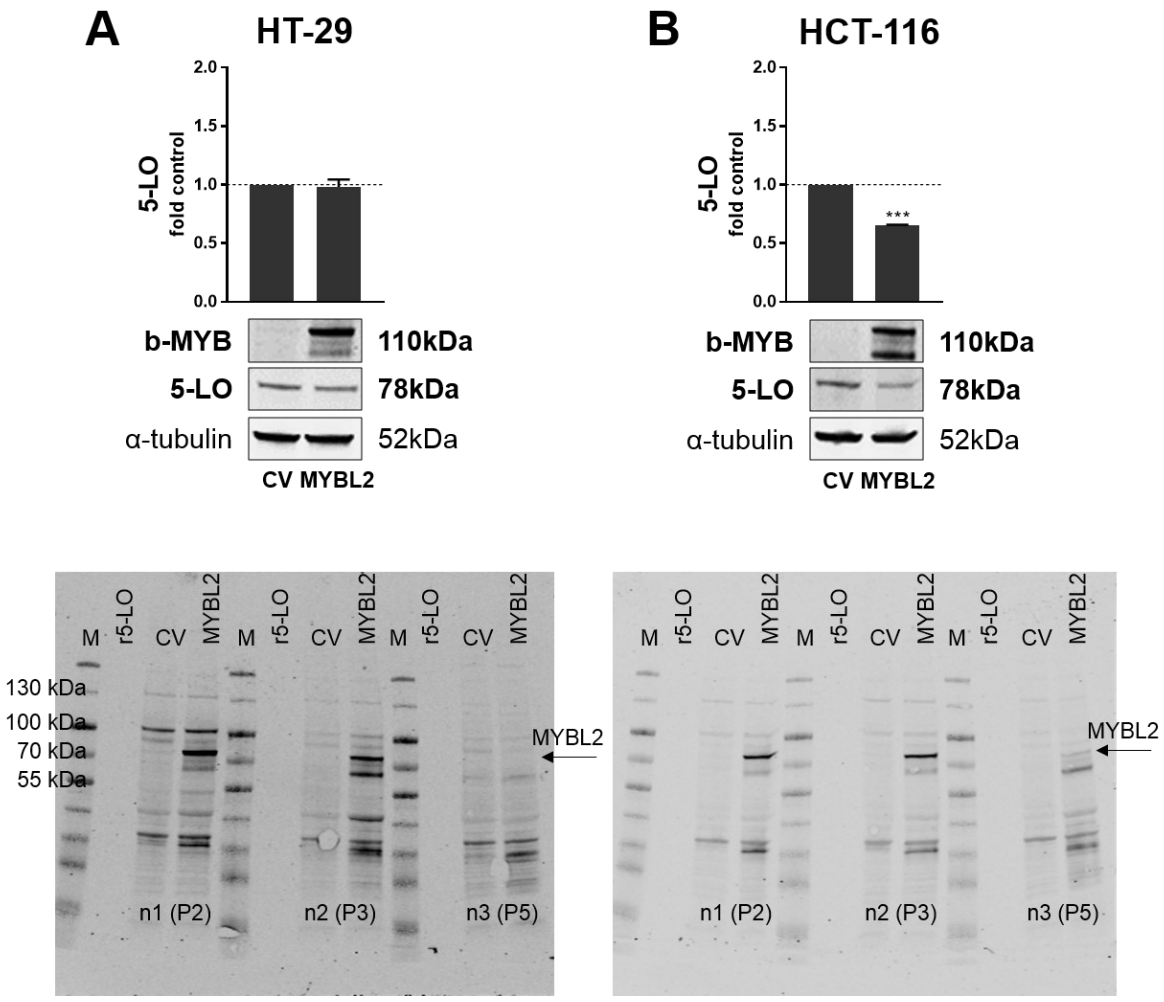

App. Figure 7.13: b-Myb and 5-LO protein expression in b-Myb overexpressing cells.
Samples of stable transfected (pSBbiGP_MYBL2) HT-29 (A) and HCT-116 (A) and respective control (CV) cultures from several passages (P2, P3, P5) were analyzed via Western blot. Densitometric values of 5-LO expression were determined and values were normalized to the loading control α-tubulin followed by normalization to the respective control vector cells (CV). Recombinant purified 5-LO (r5-LO) served as a control. Results are depicted as mean + SEM from 3 independent experiments. Asterisks indicate significant changes vs. DMSO vehicle control determined by unpaired two-tailed student's t-test with Welch's correction * (P<0.05), ** (P<0.01), *** (P<0.001).

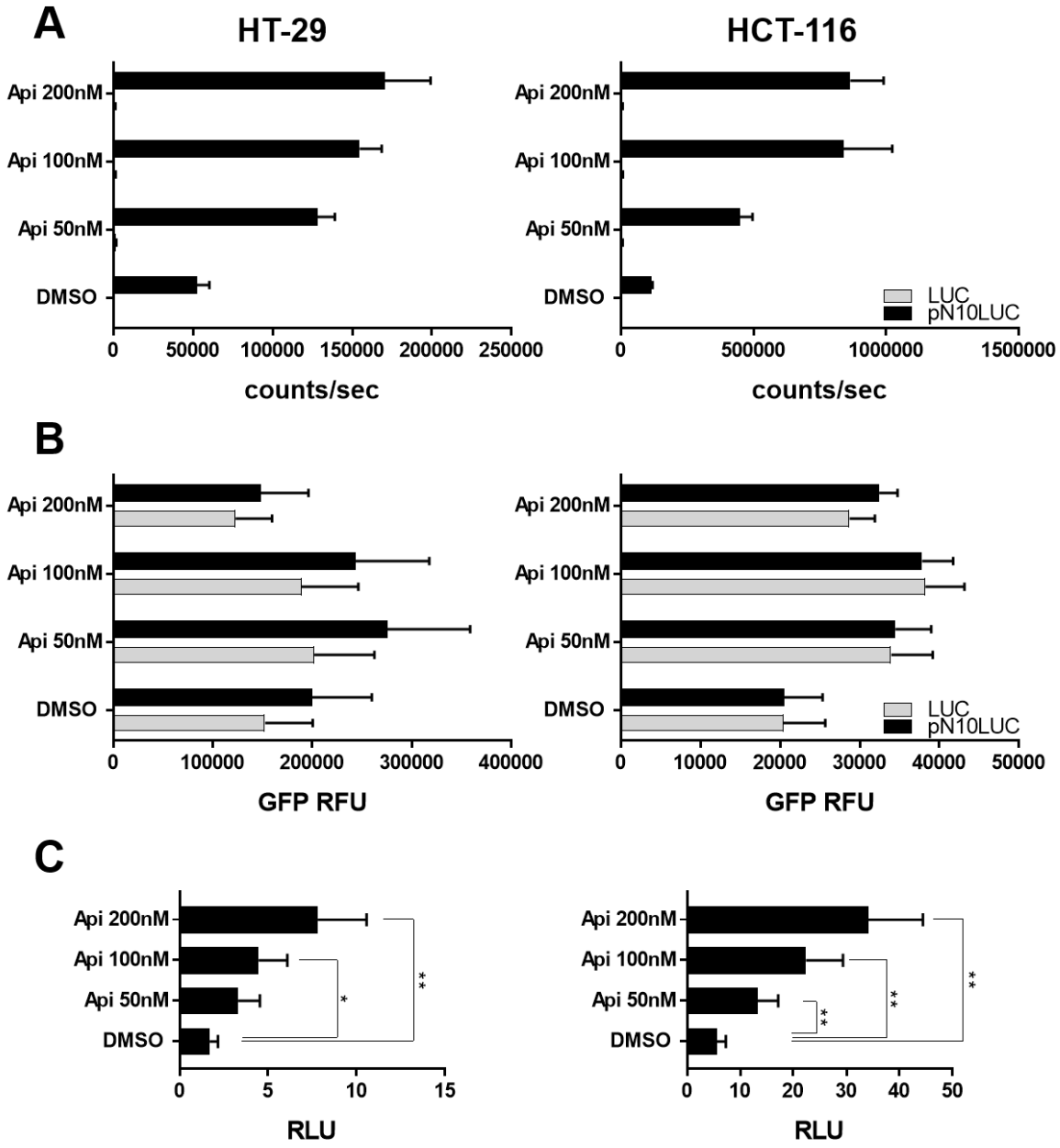

App. Figure 7.14: Firefly luciferase reporter gene assay response testing in stably transfected reporter cells.
Stable transfected (pSBGP_pN10LUC) HT-29 and HCT-116 reporter cells were seeded in black 96-well plates with a clear bottom ($0.03x10^6$ cells/well) and were cell cycle synchronized by serum starvation using RGM 22 h before further treatment. Then, the medium was changed to CGM for 2 h, and cells were treated for 24 h with Apicidin in the indicated concentrations. The vehicle control received DMSO instead. (A) Unnormalized firefly luciferase activity (counts/sec) in HT-29 and HCT-116 cells stably transfected with the pN10 (pN10LUC; -843 relative to the translation start (ATG)) reporter and a control vector (LUC). (B) GFP signal in stably transfected HT-29 and HCT-116 cells (pSBGP_pN10LUC; pSBGB_LUC) given in relative fluorescence units (RFU). (C) Normalized reporter gene results given as relative light units (RLU) obtained by dividing the unnormalized firefly activity signal with the GFP signal. Results are depicted as mean + SEM of 4 independent experiments. Asterisks indicate significant changes vs. co-determined by unpaired two-tailed student's t-test. * (P<0.05), ** (P<0.01), *** (P<0.001).

7.2 App. Methods

LC-MS/MS parameters Frankfurt

All provided parameters were developed and validated by the Fraunhofer Institute for Translational Medicine and Pharmacology, Department of Clinical Research (Biomedical Analysis) Frankfurt am Main (LC-MS/MS unit).

App. Table 32:Calibration ranges of all quantified analytes

Analyte	Concentration
11-dehydro-TXB2	8 – 2400 pg
12-HEPE	8 – 2400 pg
12-HETE	8 – 2400 pg
14-HDHA	16 – 4800 pg
15-HEPE	8 – 2400 pg
15-HETE	8 – 2400 pg
15R-HETE	100 – 20000 pg
15S-HETE	100 – 20000 pg
16-HDHA	16 – 4800 pg
17-HDHA	16 – 4800 pg
17R-HDHA	20 – 4000 pg
17S-HDHA	20 – 4000 pg
18-HEPE	8 – 2400 pg
20-HETE	40 – 2400 pg
5-HETE	8 – 2400 pg
5S,15S-DiHETE	4 – 1200 pg
5S-HEPE	16 – 2400 pg
6-epi-LXA4	8 – 2400 pg
6-keto-PGF1alpha	16 – 4800 pg
7-HDHA	16 – 4800 pg
8S,15S-DiHETE	20 - 1200 pg
LTB4	16 – 4800 pg
LXA4 /15-epi-LXA4	8 – 2400 pg
LXA5	4 – 1200 pg
LXB4	-
Mar1	8 – 2400 pg
PD1	16 – 4800 pg

Analyte	Concentration
PDX	16 – 4800 pg
PGD2	4 – 1200 pg
PGE2	4-1200 pg
PGF2alpha	8 – 2400 pg
PGJ2 / delta-12-PGJ2	4 – 1200 pg
RvD1 / AT-RvD1	20 - 1200 pg
RvD2	8 - 1200 pg
RvD5	4 – 1200 pg
RvE1	8 - 1200 pg
RvE4	4 – 1200 pg
TXB2	8 – 2400 pg

Reversed phase analysis

App. Table 33: LC gradient parameters for reversed phase lipid mediator analysis

Time (min)	A%	B%	Flow (mL/min)
0.00	75	25	0.4
0.50	75	25	0.4
9.00	15	85	0.4
10.00	15	85	0.4
10.01	75	25	0.4
12.00	75	25	0.4

App. Table 34: MS parameters for reversed phase analysis

Parameter	Value
Curtain gas	40
Collision gas	medium
IonSpray voltage	-4500
Temperature	500
Ion source gas 1	50
Ion source gas 2	70

App. Table 35: MRM settings
1 = Quantifier, 2 and 3 = Qualifier, Q1 = precursor ion, Q3 = product ion, declustering potential (DP), entrance potential (EP), collision energy (CE), collision cell exit potential (CXP).

Analyte	Q1	Q3	DP	EP	CE	CXP
PGE2 1	351.2	315	-40	-10	-16	-21
PGE2 2	351.2	271.1	-40	-10	-26	-13
PGD2 1	351.2	189	-40	-10	-26	-17
PGD2 2	351.2	233	-40	-10	-14	-21
PGF2alpha 1	353.1	193	-85	-10	-34	-13
PGF2alpha 2	353.1	309.2	-85	-10	-26	-13
PGJ2/delta-12-PGJ2 1	333.2	233.1	-50	-10	-14	-15
PGJ2/delta-12-PGJ2 2	333.2	271.1	-50	-10	-20	-13
6-keto-PGF1alpha 1	369.2	163	-40	-10	-36	-17
6-keto-PGF1alpha 2	369.2	245.1	-40	-10	-34	-25
TXB2 1	369.2	169.1	-55	-10	-24	-13
TXB2 2	369.2	195	-55	-10	-20	-11
11-dehydro-TXB2 1	367.2	305.2	-55	-10	-22	-17
11-dehydro-TXB2 2	367.2	161	-55	-10	-26	-15
LTB4 1	335.2	195.2	-50	-10	-22	-14
LTB4 2	335.2	129.1	-50	-10	-28	-16
5-HETE 1	319.2	115	-50	-10	-20	-11
5-HETE 2	319.2	257.2	-50	-10	-20	-13
12-HETE 1	319.2	179.1	-50	-10	-20	-7
12-HETE 2	319.2	208.1	-50	-10	-20	-15
15-HETE 1	319.2	175.1	-50	-10	-20	-13
15-HETE 2	319.2	257.2	-50	-10	-20	-13
20-HETE 1	319.2	289.1	-50	-10	-26	-21
20-HETE 2	319.2	245.1	-50	-10	-22	-21
5-HEPE 1	317.2	115	-60	-10	-16	-12
5-HEPE 2	317.2	255	-50	-10	-16	-21
12-HEPE 1	317.2	179	-70	-10	-18	-15
12-HEPE 2	317.2	255	-50	-10	-16	-21
15-HEPE 1	317.2	219	-50	-10	-16	-15

Analyte	Q1	Q3	DP	EP	CE	CXP
15-HEPE 2	317.2	255	-50	-10	-16	-21
18-HEPE 1	317.2	215.3	-50	-10	-20	-11
18-HEPE 2	317.2	255	-50	-10	-16	-21
5S,15S-DiHETE 1	335.2	115	-50	-10	-16	-11
8S,15S-DiHETE 1	335.2	155	-50	-10	-20	-12
8S,15S-DiHETE 2	335.2	235	-50	-10	-20	-19
7-HDHA 1	343.2	281.3	-65	-10	-16	-23
7-HDHA 2	343.2	141	-65	-10	-16	-9
14-HDHA 1	343.2	161.2	-50	-10	-22	-8
14-HDHA 2	343.2	281.3	-50	-10	-20	-13
16-HDHA 1	343.2	233.2	-70	-10	-18	-15
16-HDHA 2	343.2	189.2	-70	-10	-22	-15
17-HDHA 1	343.2	201	-50	-10	-19	-10
17-HDHA 2	343.2	245	-50	-10	-16	-12
LXA4/15-epi-LXA4 1	351.2	235.1	-60	-10	-18	-11
LXA4/15-epi-LXA4 2	351.2	58.9	-60	-10	-46	-7
LXA4/15-epi-LXA4 3	351.2	115	-60	-10	-20	-15
6-epi-LXA4 1	351.2	115	-60	-10	-20	-15
6-epi-LXA4 2	351.2	58.9	-60	-10	-46	-7
6-epi-LXA4 3	351.2	235.1	-60	-10	-18	-11
LXA5 1	349.2	114.9	-25	-10	-20	-13
LXA5 2	349.2	215	-25	-10	-18	-15
LXB4 1	351.2	129.1	-50	-10	-28	-10
LXB4 2	351.2	221.2	-50	-10	-23	-11
RvD1/AT-RvD1 1	375.2	215	-35	-10	-26	-10
RvD1/AT-RvD1 2	375.2	141	-35	-10	-20	-8
RvD2 1	375.2	277.1	-70	-10	-19	-15
RvD2 2	375.2	175	-70	-10	-31	-15
RvE1 1	349.2	195.1	-80	-10	-21	-15
RvE1 2	349.2	161	-80	-10	-24	-15

Analyte	Q1	Q3	DP	EP	CE	CXP
RvE4 1	333.2	115	-40	-10	-16	-11
RvE4 2	333.2	173	-40	-10	-18	-15
RvD5 1	359.2	199.1	-60	-10	-20	-15
RvD5 2	359.2	141	-60	-10	-18	-12
Mar1 1	359.2	177.1	-35	-10	-23	-14
Mar1 2	359.2	123.1	-35	-10	-23	-10
PD1 1	359.2	206	-50	-10	-22	-10
PD1 2	359.2	153.1	-30	-10	-22	-11
PDX 1	359.2	206	-50	-10	-22	-10
PDX 2	359.2	153.1	-30	-10	-22	-11
PGE2-d4 1	355.2	319.1	-40	-10	-16	-33
PGE2-d4 2	355.2	275.1	-40	-10	-24	-19
PGD2-d4 1	355.2	319.1	-40	-10	-16	-33
PGD2-d4 2	355.2	275.1	-40	-10	-24	-19
TXB2-d4 1	373.2	173	-55	-10	-28	-9
TXB2-d4 2	373.2	199	-55	-10	-22	-17
11-dehydro-TXB2-d4 1	371.2	309.2	-55	-10	-24	-19
11-dehydro-TXB2-d4 2	371.2	353.1	-55	-10	-20	-17
PGF2alpha-d4 1	357.1	313.2	-85	-10	-28	-11
PGF2alpha-d4 2	357.1	197	-85	-10	-36	-25
6-keto-PGF1alpha-d4 1	373.2	167.3	-40	-10	-37	-8
6-keto-PGF1alpha-d4 2	373.2	249.4	-40	-10	-39	-10
LTB4-d4 1	339.1	197	-50	-10	-24	-9
LTB4-d4 2	339.1	59.1	-50	-10	-46	-5
5-HETE-d8 1	327.2	116	-50	-10	-20	-7
5-HETE-d8 2	327.2	309.3	-50	-10	-16	-15
12-HETE-d8 1	327.2	184.2	-50	-10	-22	-17
12-HETE-d8 2	327.2	214.1	-50	-10	-20	-13
15-HETE-d8 1	327.2	226.2	-50	-10	-18	-3
15-HETE-d8 2	327.2	182	-50	-10	-22	-25

Analyte	Q1	Q3	DP	EP	CE	CXP
20-HETE-d6 1	325.2	281.1	-50	-10	-22	-25
20-HETE-d6 2	325.2	251.3	-50	-10	-24	-11
15-HEPE-d5 1	322.2	168	-50	-10	-15	-12
15-HEPE-d5 2	322.2	180	-50	-10	-19	-15
17-HDHA-d5 1	348.2	201	-50	-10	-19	-10
17-HDHA-d5 2	348.2	286	-50	-10	-17	-12
LXA4-d5 1	356.2	114.9	-60	-10	-20	-11
LXA4-d5 2	356.2	58.8	-60	-10	-50	-33
AT-RvD1-d5 1	380.2	220.2	-35	-10	-28	-15
AT-RvD1-d5 2	380.2	141.1	-35	-10	-30	-15
RvD2-d5 1	380.2	175.2	-70	-10	-30	-15
RvD2-d5 2	380.2	141.1	-35	-10	-30	-15
Mar1-d5 1	364.2	177.1	-35	-10	-23	-14
Mar1-d5 2	364.2	123.1	-35	-10	-23	-10

Chiral analysis

App. Table 36: LC gradient parameters for chiral reversed phase lipid mediator analysis

Time (min)	A%	B%	Flow (mL/min)
0.00	85	15	0.7
1.00	85	15	0.7
1.50	65	35	0.7
2.50	65	35	0.7
4.00	40	60	0.7
6.50	40	60	0.7
9.00	25	75	0.7
9.01	25	75	1.0
11.50	25	75	1.0
16.50	5	95	1.0
20.50	5	95	1.0
20.51	5	95	0.7
21.00	85	15	0.7
25.00	85	15	0.7

Lipid mediator panel Wuppertal

Following oxylipins were analyzed but not detected in any samples presented in Figure 4.40 and Figure 4.41:

App. Table 37: Analytes assessed within the oxylipin panel at Wuppertal.
Analytes were analyzed, but values were <LOD

Analytes		
17(18)-EpETE	7,17-DiHDPA	2,3-dinor-TxB2
14(15)-EpETE	LTB3	TxB3
8(9)-EpETE	17-HETE	13,14-dihydro-15-keto-tetranor-PGE2
15,16-DiHODE	RvE1	RvE3
9,10-DiHODE	RvD3	11,12-DiHETE
12,13-DiHODE	LxA5	PGD3
9(10)-EpODE	7-epi-MaR1	PGE3
12(13)-EpODE	MaR1	
17(RS)-RvD4	20-OH-PGE2	
10,17-diH-n3DPA	2,3-dinor-TxB1	

The following oxilipins were analyzed and quantified in all of the samples presented in Figure 4.40 and Figure 4.41.

App. Table 38: Analytes assessed within the oxylipin panel at Wuppertal with respective LOD and LLOQ values per analyte.

Analyte	LOD (nM)	LLOQ (nM)
5-HETE	0.000875	0.00175
8-HETE	0.00468	0.0117
9-HETE	0.01325	0.019875
11-HETE	0.0010925	0.002185
12-HETE	0.005	0.0125
15-HETE	0.0055	0.011
16-HETE	0.005	0.0125
18-HETE	0.005	0.0125
19-HETE	0.05	0.125
20-HETE	0.0125	0.025
5(S),15(S)-DiHETE	0.0025	0.005
8(S),15(S)-DiHETE	0.02525	0.063125
5(S),6(R)-DiHETE	0.000975	0.00195
5(S),6(S)-DiHETE	0.001115	0.00223
LxA4	0.025	0.05
LxB4	0.025	0.05

Analyte	LOD (nM)	LLOQ (nM)
8(9)-EpETrE	0.0125	0.025
11(12)-EpETrE	0.0025	0.005
14(15)-EpETrE	0.005	0.0125
5,6-DiHETrE	0.0025	0.005
8,9-DiHETrE	0.0017	0.0034
11,12-DiHETrE	0.0016	0.0032
14,15-DiHETrE	0.0005	0.00125
PGD2	0.025	0.05
PGE2	0.005	0.0125
PGF2	0.0125	0.025
5-HEPE	0.001475	0.00295
8-HEPE	0.0015	0.003
9-HEPE	0.005	0.0125
11-HEPE	0.00155	0.0031
12-HEPE	0.0025	0.005
15-HEPE	0.0025	0.005
18-HEPE	0.0025	0.005
20-HEPE	0.05	0.1
LTB5	0.0125	0.025
14,15-DiHETE	0.00125	0.0025
17,18-DiHETE	0.004125	0.0055
4-HDHA	0,0025	0.005
7-HDHA	0,0025	0.005
8-HDHA	0,0019	0.00475
10-HDHA	0,00125	0.0025
11-HDHA	0,005	0.0125
13-HDHA	0.0025	0.005
14-HDHA	0.00275	0.006875
16-HDHA	0.005	0.0125
17-HDHA	0.017	0.0425
20-HDHA	0.005	0.0125
RvD5	0.005	0.0125
7(8)-EpDPE	0.021775	0.0326625
10(11)-EpDPE	0.0005	0.00125
13(14)-EpDPE	0.0025	0.005

Analyte	LOD (nM)	LLOQ (nM)
16(17)-EpDPE	0.005	0.0125
19(20)-EpDPE	0.0125	0.025
7,8-DiHDPE	0.0125	0.025
10,11-DiHDPE	0.0025	0.005
13,14-DiHDPE	0.0025	0.005
16,17-DiHDPE	0.0025	0.005
19,20-DiHDPE	0.0125	0.025

Primer sequences, combinations, and used templates

Table 39: Primer names and sequences used for cloning

Primer name	5´-3´
TG001	GCG GAA AGA TCG CCG TGT AAG GCC TGT CAG GCC AAG CTT C
TG002	GTG GGC TTG TAC TCG GTC ATG GGG CCA GGA TTC TCC TCG A
TG003	ATG ACC GAG TAC AAG CCC AC
TG004	ATG TTT TTG GCG TCT TCC ATG TCT AGA TAG CGG ACC CCT T
TG005	ATG GAA GAC GCC AAA AAC ATA AAG
TG006	TTA CAC GGC GAT CTT TCC GC
TG007	GTG GAG AAG GTT TCG CGC CGT CTA GAT AGC GGA CCC CTT AC
TG008	GTA CTG TTG GTA AAG CCA CCA TGG AAG ACG CCA AAA ACA TAA AGA
TG009	GGC GCG AAA CCT TCT CCA
TG010	GGT GGC TTT ACC AAC AGT ACC
TG011	GGC GGT CCA GGT GTC CGC ATG TCT AGA TAG CGG ACC CCT TAC
TG012	ATG CGG ACA CCT GGA CCG
TG013	CAG TCT GGA ATT CCC GTA CCG TCT AGA TAG CGG ACC CCT T
TG014	GGT ACG GGA ATT CCA GAC TGC
TG017	GAA CTT AGT GTA TGT AAA CTT C
TG026	GAA TGC GGC GAT GTT TCG GTA AGG GGT CCG CTA TCT AGA CAT GCC CTC CTA CAC GGT C
TG024	GAA GTT TAC ATA CAC TAA GTT CGG TGT GGA AAG TCC CCA G
TG025	CTT TAT GTT TTT GGC GTC TTC CAT TTG CCG TGT TTC CAG TTC
TG027	CCG AAA CAT CGC CGC ATT CTG CAG AGG AGT CTA GCT CAG AGG CAG AGG
TG028	GAA GAC GCC AAA AAC ATA AAG
TG029	GAA TTT GGT CAT CTC GGG CCG AAT GTA CGC GTC CAT CCC TCA G
TG030	GCC CGA GAT GAC CAA ATT CAC ATT CTC AAG CAA CAC CGA CGT AAA GAA CTG GAA ACA CGG CAA ATG GAA GAC GCC AAA AAC ATA AAG
TG031u	CTT TAT GTT TTT GGC GTC TTC CAT ATC GCC GGT GAT CCA GC
TG035	GAT CAA GGT ACC GGT GTG GAA AGT CCC CAG
TG036	GTT CTT CTC GAG TAG CTC AGA GGC AGA GG
TG037	GTC TAG ATA GCG GAC CCC
TG038	AGA TCT GCG ATC TAA GTA AGC
TG039	CTT ACT TAG ATC GCA GAT CTC TCG AGG GAG CAG CGA GC
TG040	CAA TGT CCA GGT TTA TAA TGA ATT ACT TTT TAA TAA GGT GTC AAG ACA ACG C
TG041	CAT TAT AAA CCT GGA CAT TGA TTC TAG TCC
TG042	AAG GGG TCC GCT ATC TAG ACC TGG GTG TTC ACC TCT TG
TG043	GAG TTT AAA TGT ATT TGG CTA AG

Primer name	5´-3´
TG044	CAT TTT TAT TAT ACT TCA AGT TCT AGG GGT ACC CAA TTT TAA CAA AAT ATT AAC GCT TAC
TG045	GGC CTC TGA GGC CAC CAT GGA TGT CTC GGC GGA CGC G
TG046	AGA ATT GAT CCC CAA GCT TTC AGG ACA AGA TGA GGG TCC G
TG050	CTT TGA ACA TCT TTT CAC ATG CTT GTT G
TG051	GCG GTT AGC TCC TTC GGT C

Table 40: Summary of plasmid preparations

Cloned Plasmid	Primers & Enzymes	Template	Used for
pSBbiGP_MYBL2	TG045 + TG046	human cDNA clone of b-Myb	MYBL2 insert
	NcoI + HindIII-HF	pSBbiGP	open backbone
pSBGP_BaxLUC	TG008 + TG013	pSBGP_LUC	linear backbone
	TG010 + TG014	pGL3B_BAX-Luc	Bax promoter
pSBGP_LUC	TG001 + TG002	pSBtetGP	backbone part 1
	TG003 + TG004	pSBtetGP	backbone part 2
	TG005 + TG006	pGL3B_pN10	firefly LUC insert
pSBGP_p53LUC	TG010 + TG012	pGL3B_pN10_IntG	p53 promoter
	TG008 + TG011	pSBGP_LUC	linear backbone
pSBGP_pN0LUC	KpnI/XhoI	pGL3Basic_pN0	pN0 promoter
	XhoI/BamHI	pSBGP_pN10LUC	backbone part 1
	TG043+TG044 & BamHI/KpnI	PCR + Digest with pSBGP_pN10LUC	backbone part 2
pSBGP_pN10LUC	TG007 + TG008	pSBGP_LUC	linear backbone
	TG009 + TG010	pGL3B_pN10	pN10 promoter
pSBGP_pN10p53LUC	TG009 + TG010	pN10_IntG	pN10 promoter with p53 RE
	TG007 + TG008	pSBGP_LUC	linear backbone
pSBGP_pN6LUC	TG042 + TG039	pGL3Basic_pN0	pN6 promoter
	TG038 + TG037	pSBGP_pN10LUC	linear backbone
pSBGP_pN6ΔMYBLUC	EcoRV-HF/PvuI-HF	pSBGP_pN6LUC	open backbone
	TG041 + TG051	pSPGP_pN6LUC	pN6 promoter part 1
	TG040 + TG050	pSBGP_pN6LUC	pN6 promoter part 1
pSBGP_SV40_5LOcds	TG024 + TG027	pcGlobin2_SB100X	SV40 promoter
1600delLUC	TG025 + TG026	pcDNA3.1_5LO	5LOcds1600del
	TG017 + TG028	pSBGP_pN10LUC	linear backbone

Cloned Plasmid	Primers & Enzymes	Template	Used for
pSBGP_SV40_5LOcds	TG024 + TG027	pcGlobin2_SB100X	SV40 promoter
1600delmutMYBLUC	TG017 + TG028	pSBGP_pN10LUC	Backbone
	TG026 + TG029	pcDNA3.1_5LO	5LOcds part 1
		bought as oligo = TG030	5LOcds part 2
pSBGP_SV40_5LOcds	TG024 + TG027	pcGlobin2_SB100X	SV40 promoter
1699delLUC	TG026 + TG031	pcDNA3.1_5LO	5LOcds1699del
	TG017 + TG028	pSBGP_pN10LUC	Linear backbone
pSBGP_SV40_LUC	TG035 + TG036 & KpnI/XhoI	pcGlobin2_SB100X	SV40 promoter
	XhoI/BamHI	pSBGP_pN10LUC	backbone part 1
	TG043+TG044 & BamHI/KpnI	PCR + Digest with pSBGP_pN10LUC	backbone part 2
pSBtetGP_LV	NcoI/HindIII-HF	pSBbiGP	Empty MCS
	NcoI/HindIII-HF	pSBtetGP	Open backbone
pSBtetGP_MYBL2	TG045 + TG046	human cDNA clone of b-Myb	PCR insert MYBL2
	NcoI + HindIII-HF	pSBtet_LV	Open backbone

Plasmid Maps

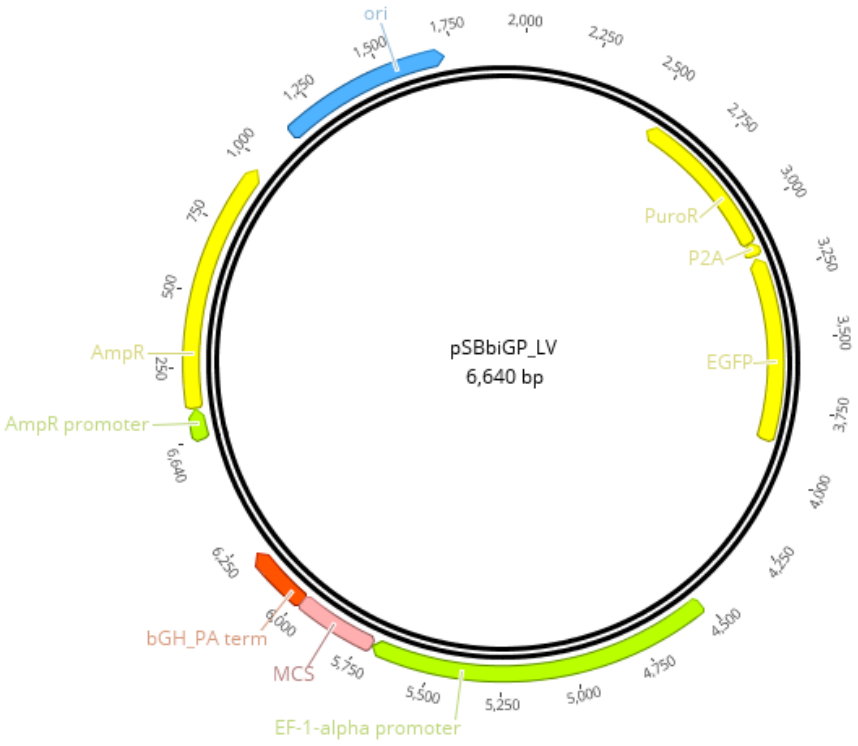

App. Figure 7.15: pSBbiGP_LV construct map.

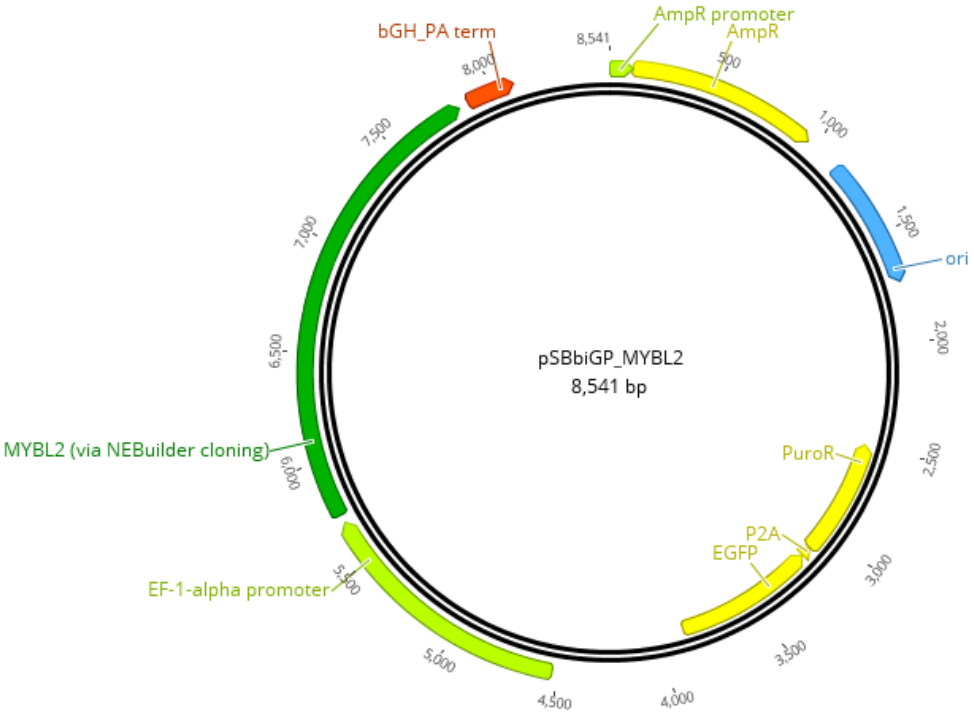

App. Figure 7.16: pSBbiGP_MYBL2 construct map.

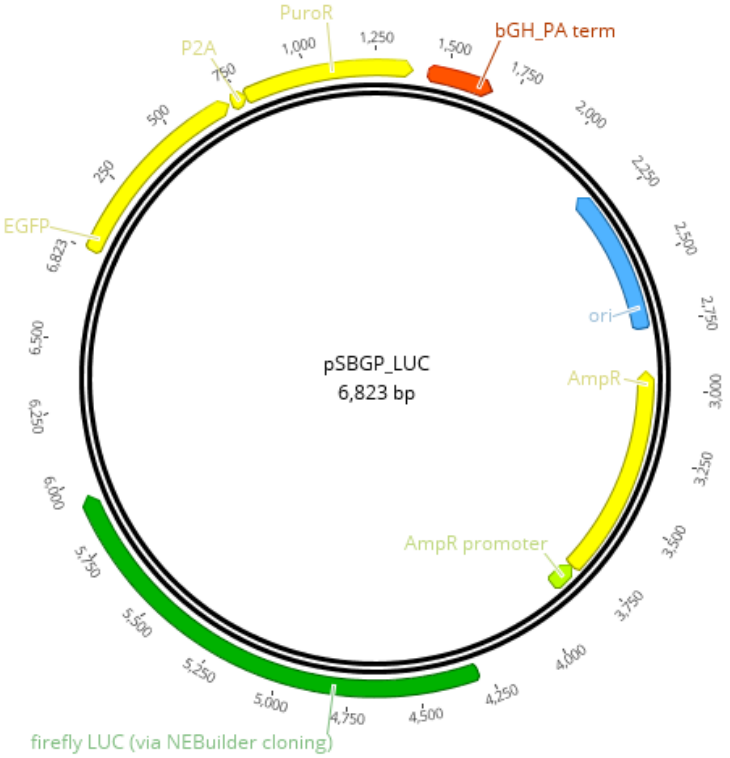

App. Figure 7.17: pSBGP_LUC construct map.

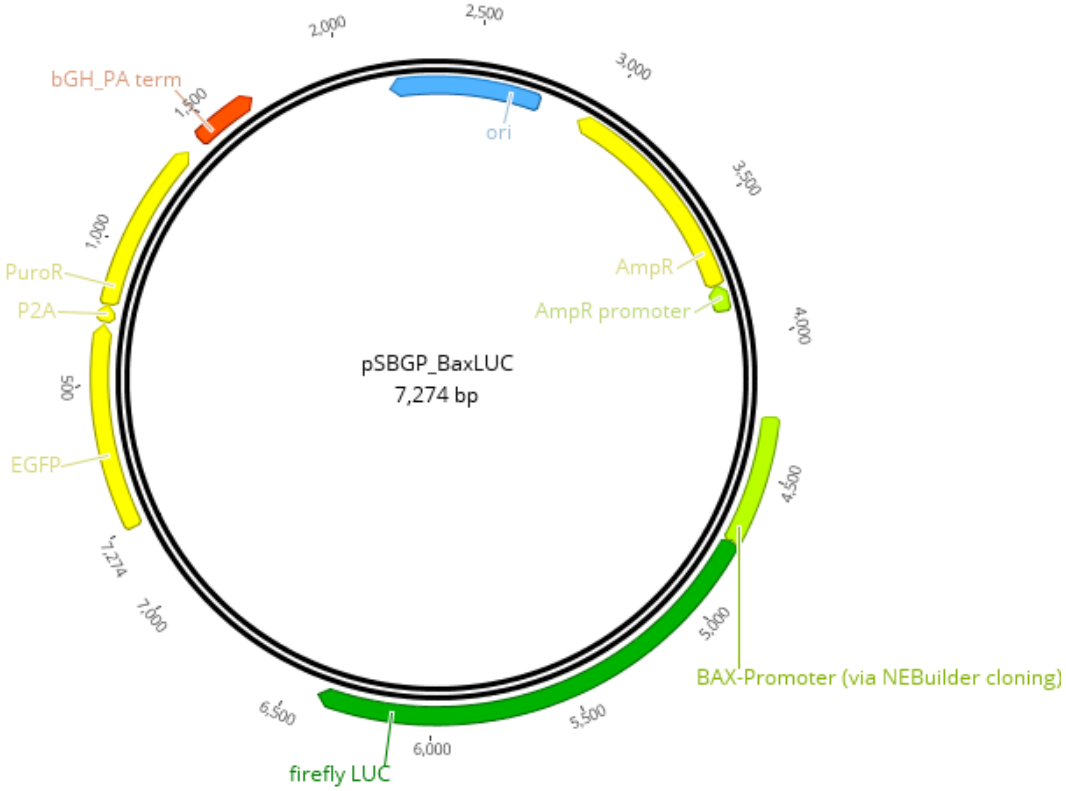

App. Figure 7.18: pSBGP_BaxLUC construct map.
This construct was cloned and transfected during this work but not further tested.

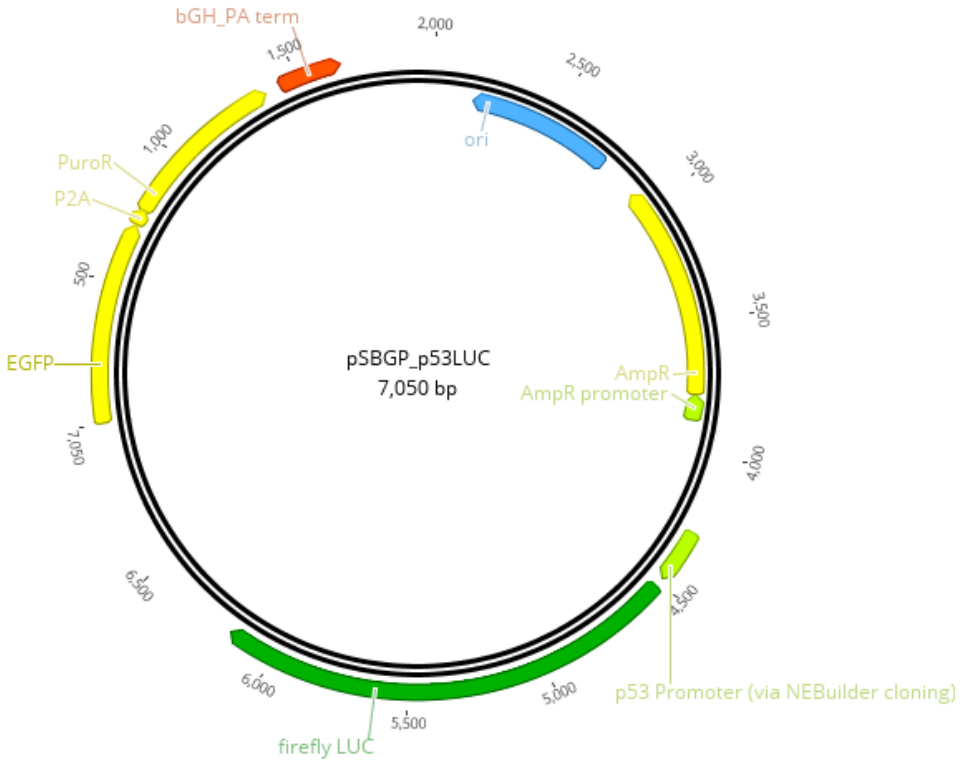

App. Figure 7.19: pSBGP_p53LUC construct map.
This construct was cloned and transfected during this work but not further tested.

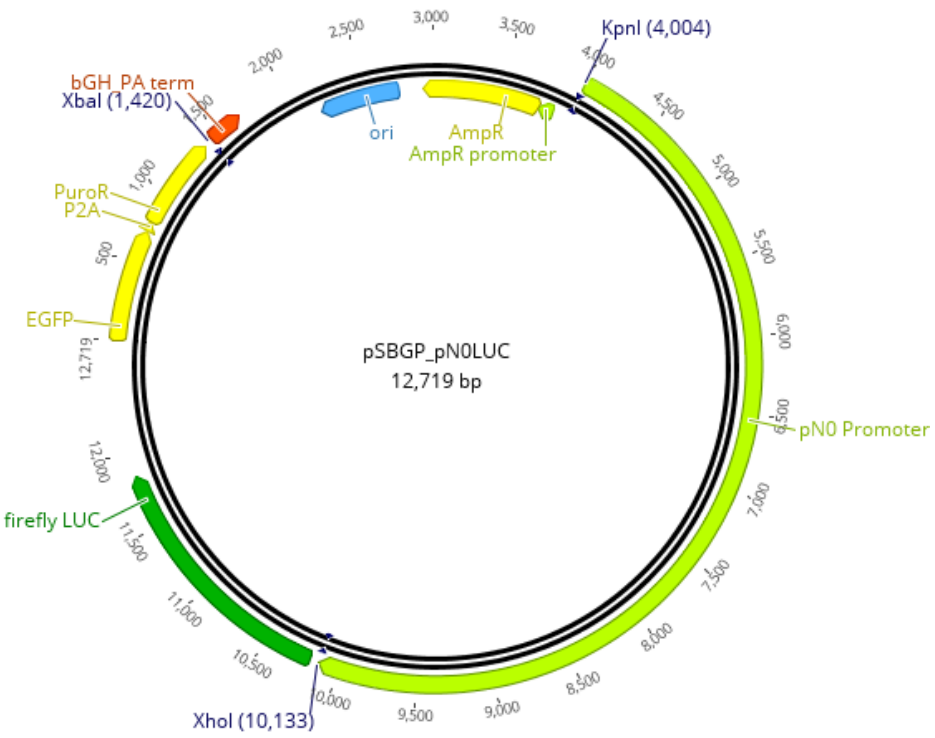

App. Figure 7.20: pSBGP_pN0LUC construct map.
This construct was cloned and transfected during this work but not further tested.

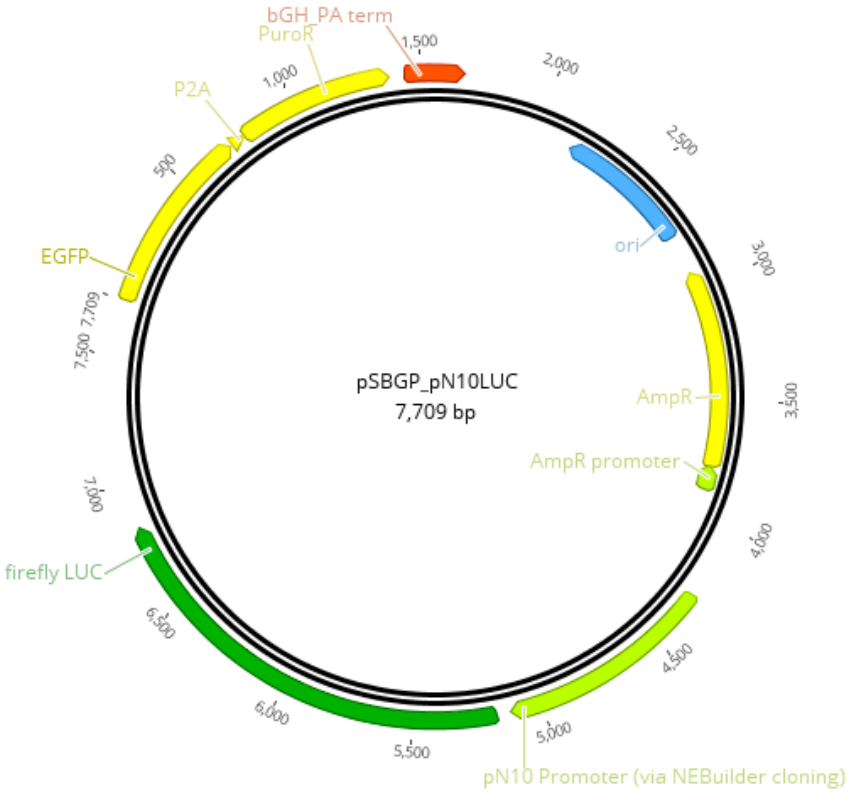

App. Figure 7.21: pSBGP_pN10LUC construct map.

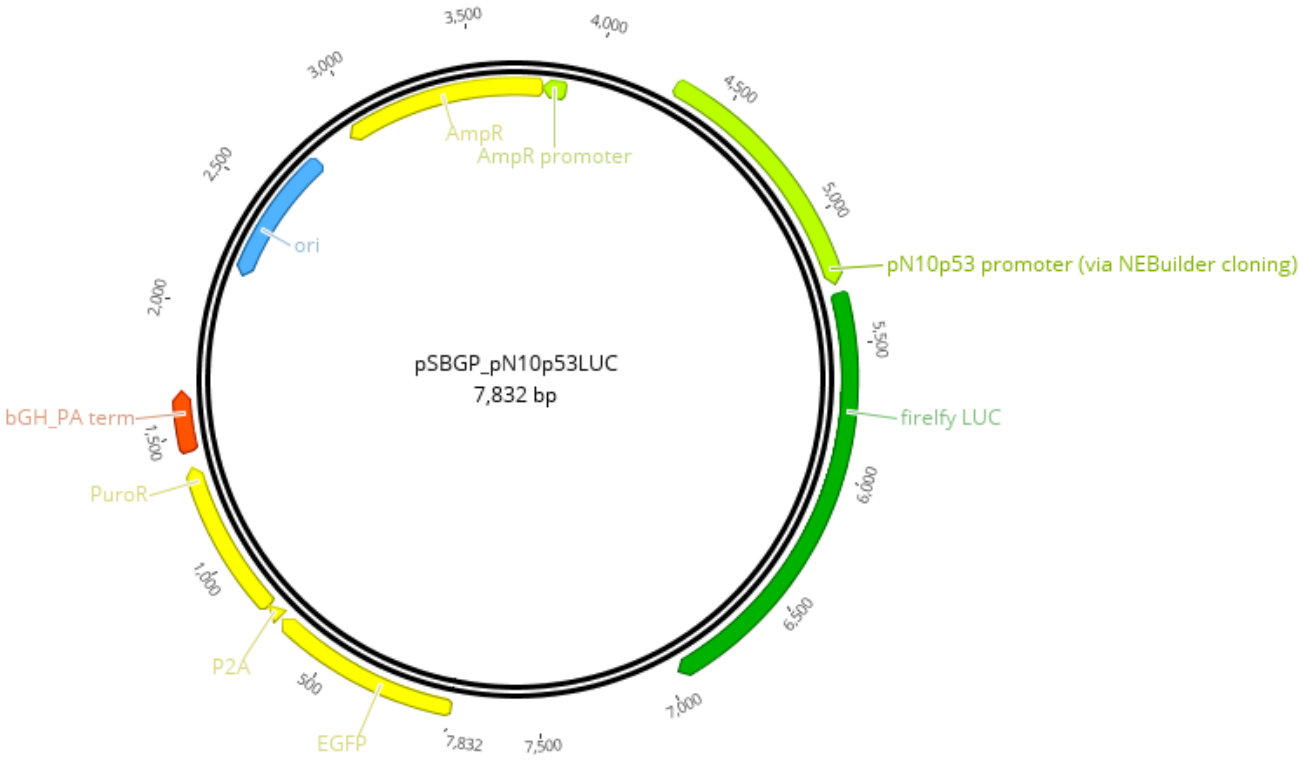

App. Figure 7.22: pSBGP_pN10p53LUC construct map.
This construct was cloned and transfected during this work but not further tested.

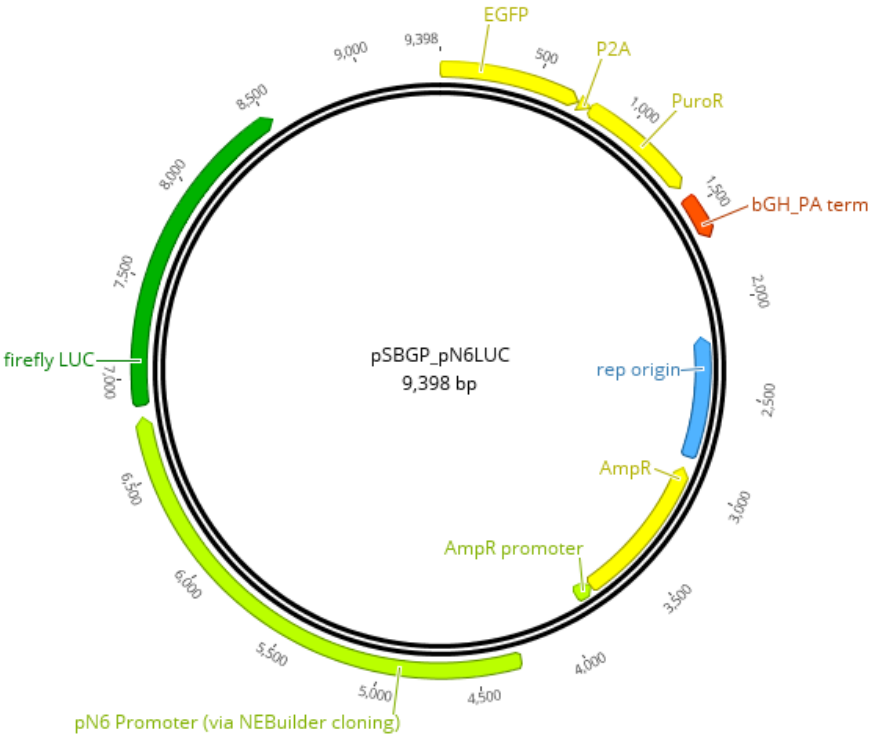

App. Figure 7.23: pSBGP_pN6LUC construct map.

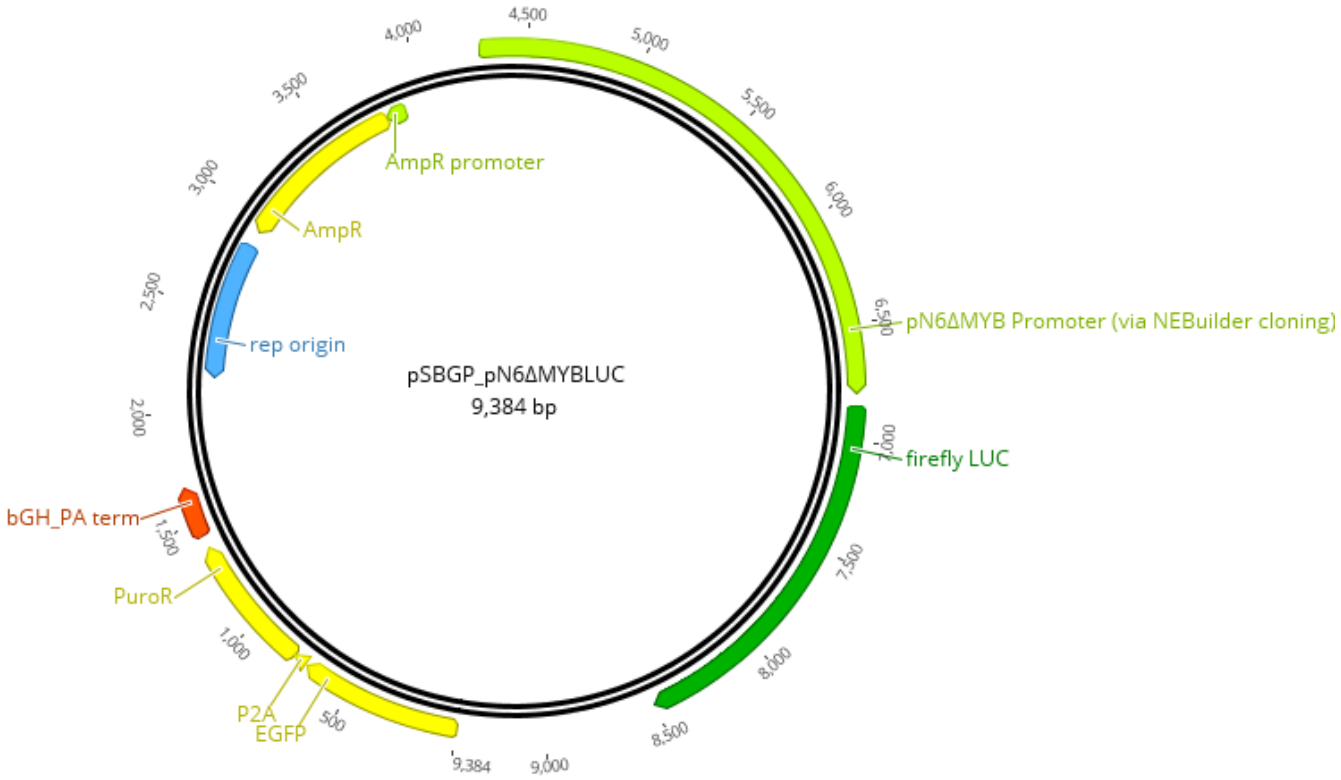

App. Figure 7.24: pSBGP_pN6ΔMYBLUC construct map.

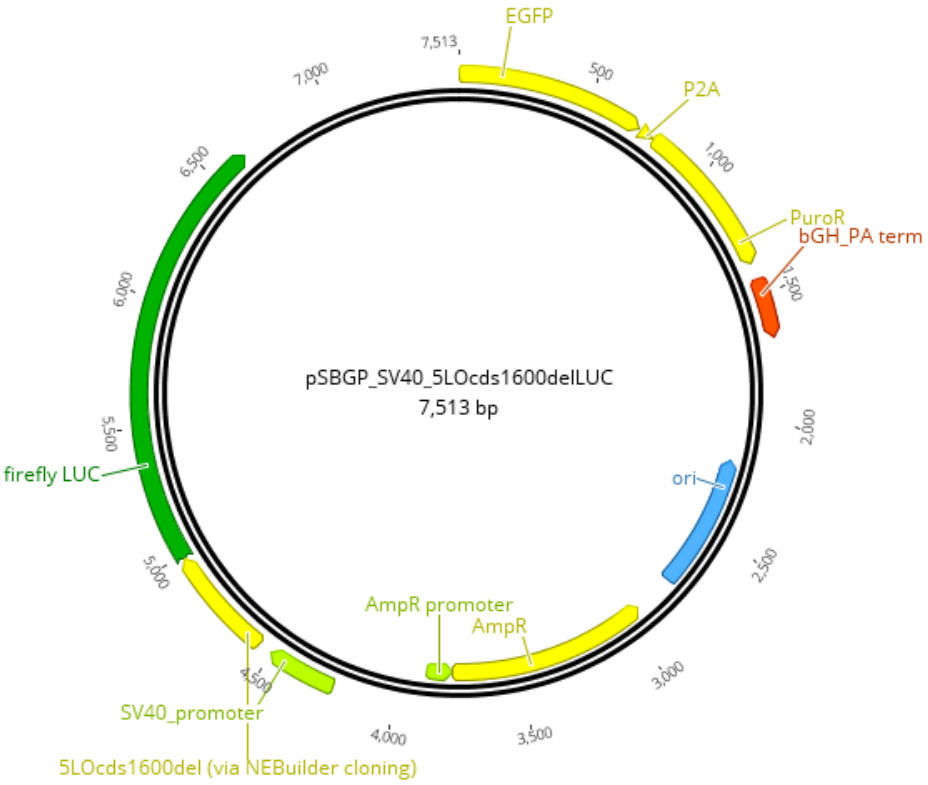

App. Figure 7.25: pSBGP_SV40_5LOcds1600delLUC construct map.

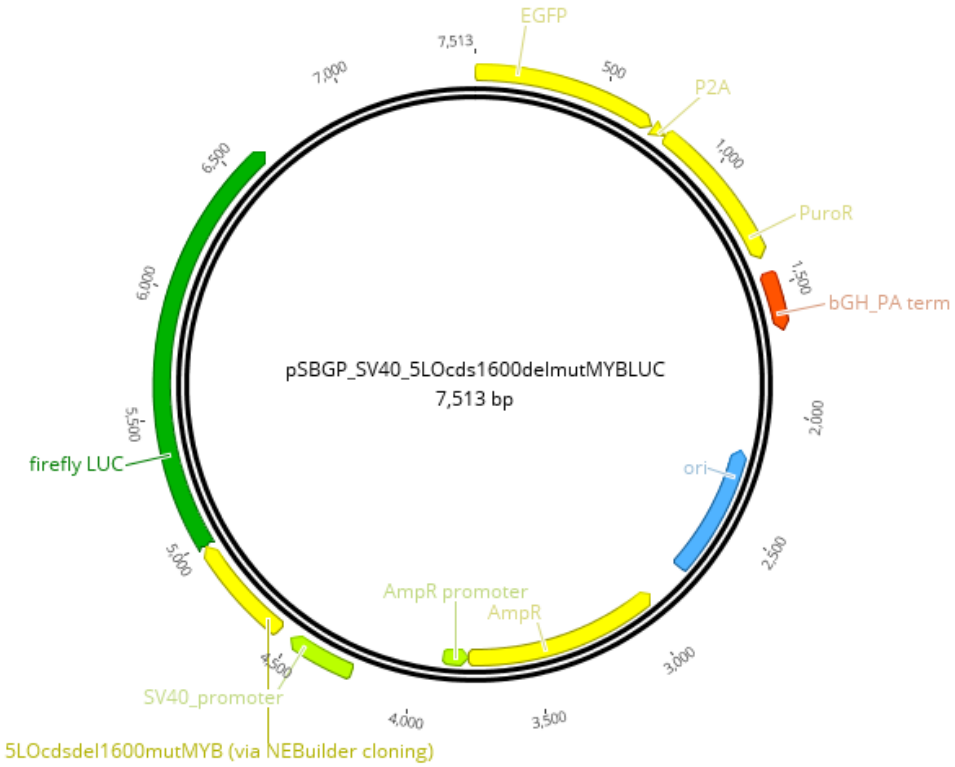

App. Figure 7.26: pSBGP_SV40_5LOcds1600delmutMYBLUC construct map.

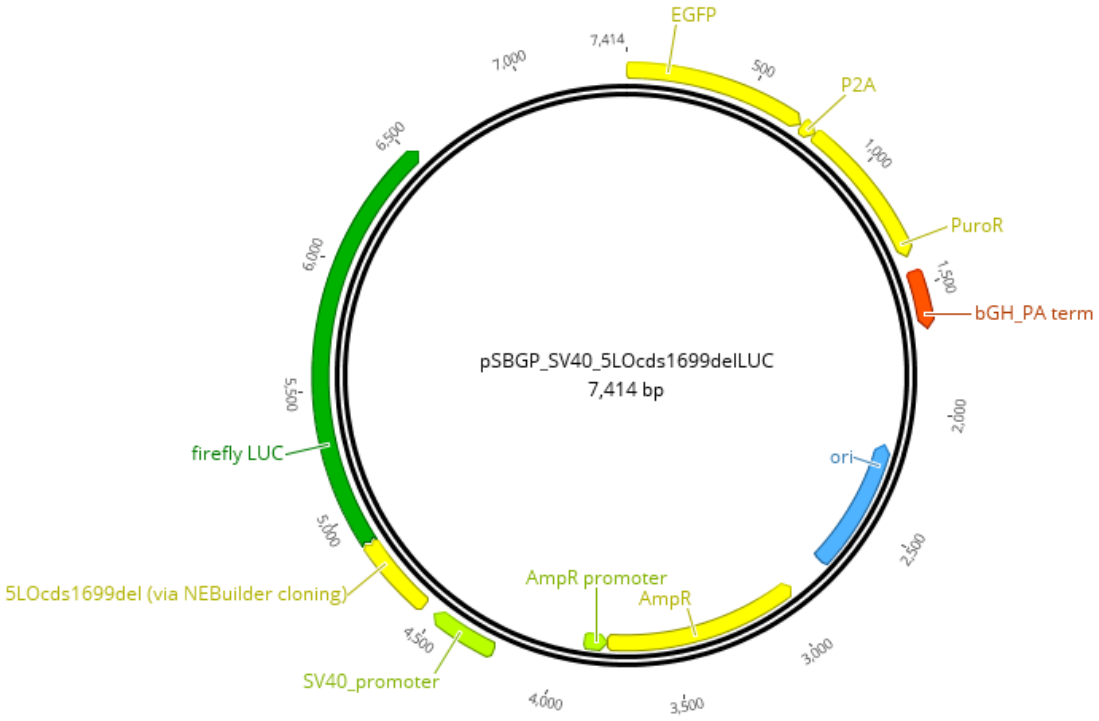

App. Figure 7.27: pSBGP_SV40_5LOcds1699delLUC construct map.

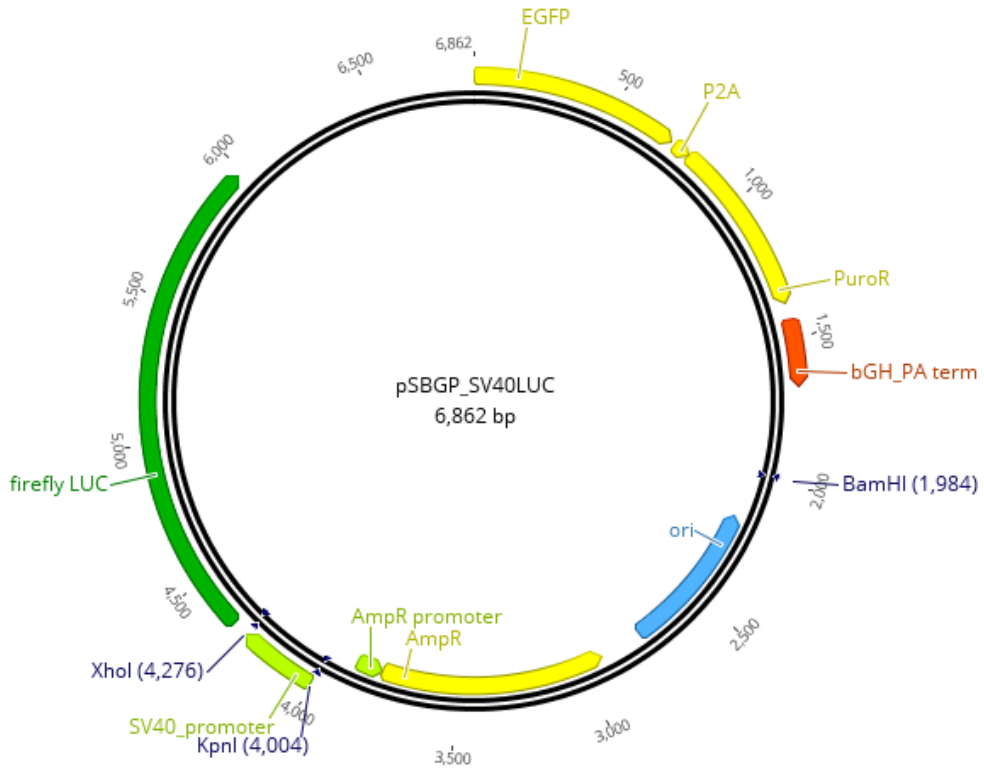

App. Figure 7.28: pSBGP_SV40LUC construct map.

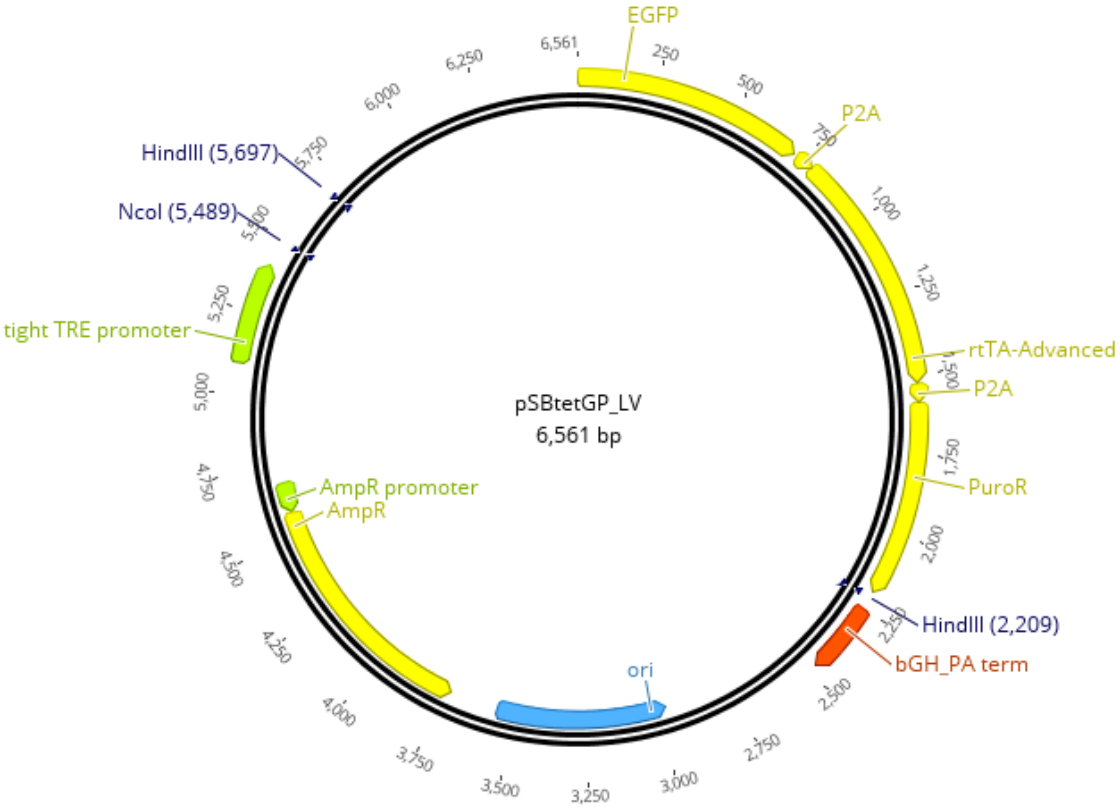

App. Figure 7.29: pSBtetGP_LV construct map.

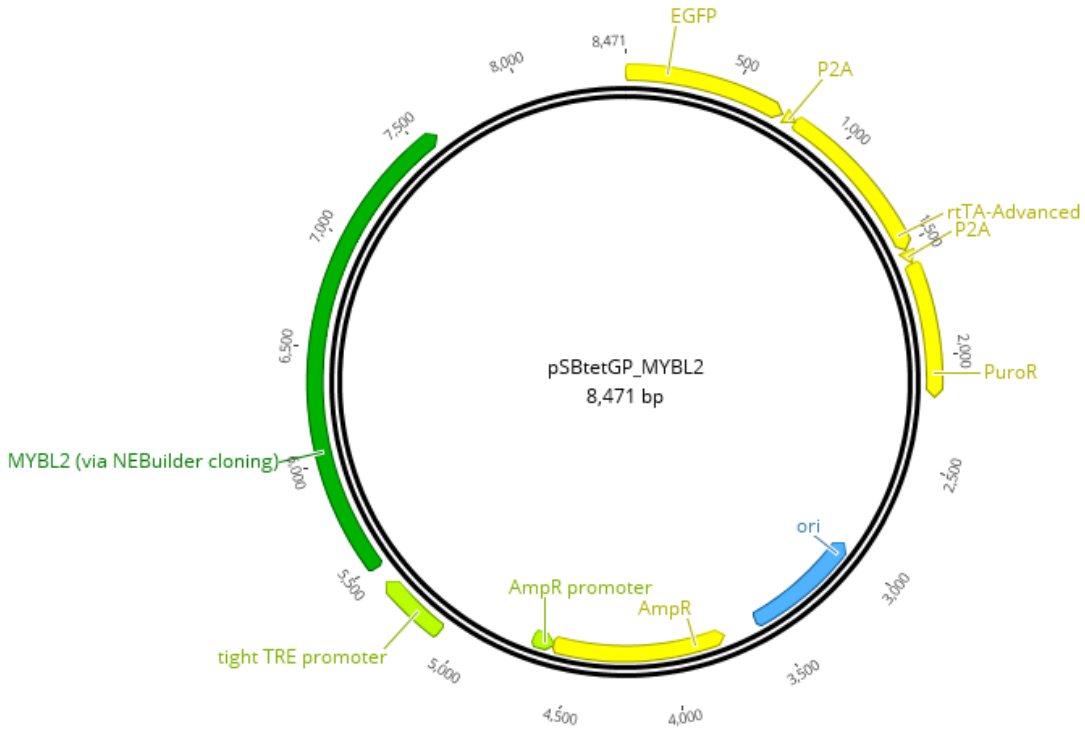

App. Figure 7.30: pSBtetGP_MYBL2 construct map.

8 References

1. Chan, H. W. (1973) Soya-bean lipoxygenase: an iron-containing dioxygenase. *Biochim. Biophys. Acta* 327, 32–35
2. Hamberg, M. and Samuelsson, B. (1967) On the specificity of the oxygenation of unsaturated fatty acids catalyzed by soybean lipoxidase. *J. Biol. Chem.* 242, 5329–5335
3. Dolev, A., Rohwedder, W. K., Mounts, T. L., et al. (1967) Mechanism of lipoxidase reaction. II. Origin of the oxygen incorporated into linoleate hydroperoxide. *Lipids* 2, 33–36
4. Funk, C. D., Chen, X.-S., Johnson, E. N., et al. (2002) Lipoxygenase genes and their targeted disruption. *Prostaglandins Other Lipid Mediat.* 68–69, 303–312
5. Kuhn, H., Banthiya, S., and van Leyen, K. (2015) Mammalian lipoxygenases and their biological relevance. *Biochim. Biophys. Acta* 1851, 308–330
6. Newcomer, M. E. and Brash, A. R. (2015) The structural basis for specificity in lipoxygenase catalysis. *Protein Sci.* 24, 298–309
7. Ivanov, I., Heydeck, D., Hofheinz, K., et al. (2010) Molecular enzymology of lipoxygenases. *Arch. Biochem. Biophys.* 503, 161–174
8. Ivanov, I., Kakularam, K. R., Shmendel, E. V, et al. (2021) Oxygenation of endocannabinoids by mammalian lipoxygenase isoforms. *Biochim. Biophys. acta. Mol. cell Biol. lipids* 1866, 158918
9. O'Donnell, V. B. and Murphy, R. C. (2012) New families of bioactive oxidized phospholipids generated by immune cells: identification and signaling actions. *Blood* 120, 1985–1992
10. Snodgrass, R. G. and Brüne, B. (2019) Regulation and Functions of 15-Lipoxygenases in Human Macrophages. *Front. Pharmacol.* 10, 719
11. Hajeyah, A. A., Griffiths, W. J., Wang, Y., et al. (2020) The Biosynthesis of Enzymatically Oxidized Lipids. *Front. Endocrinol. (Lausanne).* 11, 591819
12. Lehnert, N. and Solomon, E. I. (2003) Density-functional investigation on the mechanism of H-atom abstraction by lipoxygenase. *J. Biol. Inorg. Chem.* 8, 294–305
13. Haeggström, J. Z. and Funk, C. D. (2011) Lipoxygenase and leukotriene pathways: biochemistry, biology, and roles in disease. *Chem. Rev.* 111, 5866–5898
14. Funk, C. D., Hoshiko, S., Matsumoto, T., et al. (1989) Characterization of the human 5-lipoxygenase gene. *Proc. Natl. Acad. Sci. U. S. A.* 86, 2587–2591
15. Samuelsson, B., Hoshiko, S., and Rådmark, O. (1991) Characterization of the promoter of the human 5-lipoxygenase gene. *Adv. Prostaglandin. Thromboxane. Leukot. Res.* 21A, 1–8
16. Sorg, B. L., Klan, N., Seuter, S., et al. (2006) Analysis of the 5-lipoxygenase promoter and characterization of a vitamin D receptor binding site. *Biochim. Biophys. Acta* 1761, 686–697
17. Silverman, E. S., Du, J., De Sanctis, G. T., et al. (1998) Egr-1 and Sp1 interact functionally with the 5-lipoxygenase promoter and its naturally occurring mutants. *Am. J. Respir. Cell Mol. Biol.* 19, 316–323
18. Dishart, D., Schnur, N., Klan, N., et al. (2005) GC-rich sequences in the 5-lipoxygenase gene promoter are required for expression in Mono Mac 6 cells, characterization of a novel Sp1 binding site. *Biochim. Biophys. Acta* 1738, 37–47
19. Rådmark, O., Werz, O., Steinhilber, D., et al. (2007) 5-Lipoxygenase: regulation of expression and enzyme activity. *Trends Biochem. Sci.* 32, 332–341
20. Schlag, K., Steinhilber, D., Karas, M., et al. (2020) Analysis of proximal ALOX5 promoter

binding proteins by quantitative proteomics. *FEBS J.* 287, 4481–4499

21. Katryniok, C., Schnur, N., Gillis, A., et al. (2010) Role of DNA methylation and methyl-DNA binding proteins in the repression of 5-lipoxygenase promoter activity. *Biochim. Biophys. Acta* 1801, 49–57
22. Uhl, J., Klan, N., Rose, M., et al. (2002) The 5-lipoxygenase promoter is regulated by DNA methylation. *J. Biol. Chem.* 277, 4374–4379
23. Klan, N., Seuter, S., Schnur, N., et al. (2003) Trichostatin A and structurally related histone deacetylase inhibitors induce 5-lipoxygenase promoter activity. *Biol. Chem.* 384, 777–785
24. Schnur, N., Seuter, S., Katryniok, C., et al. (2007) The histone deacetylase inhibitor trichostatin A mediates upregulation of 5-lipoxygenase promoter activity by recruitment of Sp1 to distinct GC-boxes. *Biochim. Biophys. Acta* 1771, 1271–1282
25. Ahmad, K., Katryniok, C., Scholz, B., et al. (2014) Inhibition of class I HDACs abrogates the dominant effect of MLL-AF4 by activation of wild-type MLL. *Oncogenesis* 3, e127
26. Silverman, E. S. and Drazen, J. M. (2000) Genetic variations in the 5-lipoxygenase core promoter. Description and functional implications. *Am. J. Respir. Crit. Care Med.* 161, S77-80
27. In, K. H., Asano, K., Beier, D., et al. (1997) Naturally occurring mutations in the human 5-lipoxygenase gene promoter that modify transcription factor binding and reporter gene transcription. *J. Clin. Invest.* 99, 1130–1137
28. Brungs, M., Rådmark, O., Samuelsson, B., et al. (1995) Sequential induction of 5-lipoxygenase gene expression and activity in Mono Mac 6 cells by transforming growth factor beta and 1,25-dihydroxyvitamin D3. *Proc. Natl. Acad. Sci.* 92, 107–111
29. Brungs, M., Radmark, O., Samuelsson, B., et al. (1994) On the Induction of 5-Lipoxygenase Expression and Activity in HL-60 Cells: Effects of Vitamin D3, Retinoic Acid, DMSO and TGFβ. *Biochem. Biophys. Res. Commun.* 205, 1572–1580
30. Seuter, S., Sorg, B. L., and Steinhilber, D. (2006) The coding sequence mediates induction of 5-lipoxygenase expression by Smads3/4. *Biochem. Biophys. Res. Commun.* 348, 1403–1410
31. Seuter, S., Väisänen, S., Rådmark, O., et al. (2007) Functional characterization of vitamin D responding regions in the human 5-Lipoxygenase gene. *Biochim. Biophys. Acta - Mol. Cell Biol. Lipids* 1771, 864–872
32. Gilbert, B., Ahmad, K., Roos, J., et al. (2015) 5-Lipoxygenase is a direct p53 target gene in humans. *Biochim. Biophys. Acta* 1849, 1003–1016
33. Häfner, A.-K., Kahnt, A. S., and Steinhilber, D. (2019) Beyond leukotriene formation-The noncanonical functions of 5-lipoxygenase. *Prostaglandins Other Lipid Mediat.* 142, 24–32
34. Ochs, M. J., Suess, B., and Steinhilber, D. (2014) 5-Lipoxygenase mRNA and Protein Isoforms. *Basic Clin. Pharmacol. Toxicol.* 114, 78–82
35. Häfner, A.-K., Beilstein, K., Graab, P., et al. (2016) Identification and Characterization of a New Protein Isoform of Human 5-Lipoxygenase. *PLoS One* 11, e0166591
36. Boudreau, L. H., Bertin, J., Robichaud, P. P., et al. (2011) Novel 5-lipoxygenase isoforms affect the biosynthesis of 5-lipoxygenase products. *FASEB J.* 25, 1097–1105
37. Ball, A.-K., Beilstein, K., Wittmann, S., et al. (2017) Characterization and cellular localization of human 5-lipoxygenase and its protein isoforms 5-LOΔ13, 5-LOΔ4 and 5-LOp12. *Biochim. Biophys. acta. Mol. cell Biol. lipids* 1862, 561–571
38. Allain, E. P., Boudreau, L. H., Flamand, N., et al. (2015) The Intracellular Localisation and Phosphorylation Profile of the Human 5-Lipoxygenase Δ13 Isoform Differs from That of Its Full Length Counterpart. *PLoS One* 10, e0132607

39. Mahshid, Y., Lisy, M.-R., Wang, X., et al. (2009) High expression of 5-lipoxygenase in normal and malignant mantle zone B lymphocytes. *BMC Immunol.* 10, 2

40. Jakobsson, P. J., Steinhilber, D., Odlander, B., et al. (1992) On the expression and regulation of 5-lipoxygenase in human lymphocytes. *Proc. Natl. Acad. Sci. U. S. A.* 89, 3521–3525

41. Busch, S., Auth, E., Scholl, F., et al. (2015) 5-Lipoxygenase Is a Direct Target of miR-19a-3p and miR-125b-5p. *J. Immunol.* 194, 1646–1653

42. Ebert, R., Cumbana, R., Lehmann, C., et al. (2020) Long-term stimulation of toll-like receptor-2 and -4 upregulates 5-LO and 15-LO-2 expression thereby inducing a lipid mediator shift in human monocyte-derived macrophages. *Biochim. Biophys. acta. Mol. cell Biol. lipids* 1865, 158702

43. Cook-Moreau, J. M., El-Makhour Hojeij, Y., Barrière, G., et al. (2007) Expression of 5-lipoxygenase (5-LOX) in T lymphocytes. *Immunology* 122, 157–166

44. von Knethen, A., Sha, L. K., Kuchler, L., et al. (2013) 5-Lipoxygenase contributes to PPARγ activation in macrophages in response to apoptotic cells. *Cell. Signal.* 25, 2762–2768

45. Nagashima, T., Ichimiya, S., Kikuchi, T., et al. (2011) Arachidonate 5-lipoxygenase establishes adaptive humoral immunity by controlling primary B cells and their cognate T-cell help. *Am. J. Pathol.* 178, 222–232

46. El Makhour-Hojeij, Y., Baclet, M. C., Chable-Rabinovitch, H., et al. (1994) Expression of 5-lipoxygenase in lymphoblastoid B and T cells. *Prostaglandins* 48, 21–29

47. Mahshid, Y., Markoutsa, S., Dincbas-Renqvist, V., et al. (2015) Phosphorylation of serine 523 on 5-lipoxygenase in human B lymphocytes. *Prostaglandins. Leukot. Essent. Fatty Acids* 100, 33–40

48. Werz, O., Tretiakova, I., Michel, A., et al. (2005) Caspase-mediated degradation of human 5-lipoxygenase in B lymphocytic cells. *Proc. Natl. Acad. Sci. U. S. A.* 102, 13164–13169

49. Chen, X., Sood, S., Yang, C. S., et al. (2006) Five-lipoxygenase pathway of arachidonic acid metabolism in carcino-genesis and cancer chemoprevention. *Curr. Cancer Drug Targets* 6, 613–622

50. Matsuyama, M., Yoshimura, R., Mitsuhashi, M., et al. (2004) Expression of lipoxygenase in human prostate cancer and growth reduction by its inhibitors. *Int. J. Oncol.* 24, 821–827

51. Gupta, S., Srivastava, M., Ahmad, N., et al. (2001) Lipoxygenase-5 is overexpressed in prostate adenocarcinoma. *Cancer* 91, 737–743

52. Xingfu, W., Lifeng, Z., Yupeng, C., et al. (2015) Cytoplasmic 5-Lipoxygenase Staining Is a Highly Sensitive Marker of Human Tumors of the Choroid Plexus. *Am. J. Clin. Pathol.* 144, 295–304

53. Barresi, V., Grosso, M., Vitarelli, E., et al. (2007) 5-Lipoxygenase is coexpressed with Cox-2 in sporadic colorectal cancer: a correlation with advanced stage. *Dis. Colon Rectum* 50, 1576–1584

54. Häfner, A.-K., Cernescu, M., Hofmann, B., et al. (2011) Dimerization of human 5-lipoxygenase. *Biol. Chem.* 392, 1097–1111

55. VanderNoot, V. A. and Fitzpatrick, F. A. (1995) Competitive binding assay of src homology domain 3 interactions between 5-lipoxygenase and growth factor receptor binding protein 2. *Anal. Biochem.* 230, 108–114

56. Hemak, J., Gale, D., and Brock, T. G. (2002) Structural characterization of the catalytic domain of the human 5-lipoxygenase enzyme. *J. Mol. Model.* 8, 102–112

57. Hanaka, H., Shimizu, T., and Izumi, T. (2005) Stress-induced nuclear export of 5-lipoxygenase. *Biochem. Biophys. Res. Commun.* 338, 111–116

58. Zhang, Y. Y., Hammarberg, T., Radmark, O., et al. (2000) Analysis of a nucleotide-binding site of 5-lipoxygenase by affinity labelling: binding characteristics and amino acid sequences. *Biochem. J.* 351 Pt 3, 697–707

59. Provost, P., Samuelsson, B., and Rådmark, O. (1999) Interaction of 5-lipoxygenase with cellular proteins. *Proc. Natl. Acad. Sci. U. S. A.* 96, 1881–1885

60. Hammarberg, T., Provost, P., Persson, B., et al. (2000) The N-terminal domain of 5-lipoxygenase binds calcium and mediates calcium stimulation of enzyme activity. *J. Biol. Chem.* 275, 38787–38793

61. Hörnig, C., Albert, D., Fischer, L., et al. (2005) 1-Oleoyl-2-acetylglycerol stimulates 5-lipoxygenase activity via a putative (phospho)lipid binding site within the N-terminal C2-like domain. *J. Biol. Chem.* 280, 26913–26921

62. Noguchi, M., Miyano, M., Matsumoto, T., et al. (1994) Human 5-lipoxygenase associates with phosphatidylcholine liposomes and modulates LTA4 synthetase activity. *Biochim. Biophys. Acta* 1215, 300–306

63. Gilbert, N. C., Bartlett, S. G., Waight, M. T., et al. (2011) The structure of human 5-lipoxygenase. *Science* 331, 217–219

64. Neau, D. B., Gilbert, N. C., Bartlett, S. G., et al. (2009) The 1.85 Å Structure of an 8 R -Lipoxygenase Suggests a General Model for Lipoxygenase Product Specificity. *Biochemistry* 48, 7906–7915

65. Sloane, D. L., Browner, M. F., Dauter, Z., et al. (1990) Purification and crystallization of 15-lipoxygenase from rabbit reticulocytes. *Biochem. Biophys. Res. Commun.* 173, 507–513

66. Mitra, S., Bartlett, S. G., and Newcomer, M. E. (2015) Identification of the Substrate Access Portal of 5-Lipoxygenase. *Biochemistry* 54, 6333–6342

67. Gilbert, N. C., Gerstmeier, J., Schexnaydre, E. E., et al. (2020) Structural and mechanistic insights into 5-lipoxygenase inhibition by natural products. *Nat. Chem. Biol.* 16, 783–790

68. Woods, J. W., Coffey, M. J., Brock, T. G., et al. (1995) 5-Lipoxygenase is located in the euchromatin of the nucleus in resting human alveolar macrophages and translocates to the nuclear envelope upon cell activation. *J. Clin. Invest.* 95, 2035–2046

69. Mainka, M., George, S., Angioni, C., et al. (2022) On the biosynthesis of specialized pro-resolving mediators in human neutrophils and the influence of cell integrity. *Biochim. Biophys. acta. Mol. cell Biol. lipids* 1867, 159093

70. Brock, T. G., Paine, R., and Peters-Golden, M. (1994) Localization of 5-lipoxygenase to the nucleus of unstimulated rat basophilic leukemia cells. *J. Biol. Chem.* 269, 22059–22066

71. Jakobsson, P. J., Shaskin, P., Larsson, P., et al. (1995) Studies on the regulation and localization of 5-lipoxygenase in human B-lymphocytes. *Eur. J. Biochem.* 232, 37–46

72. Weisser, H., Göbel, T., Melissa Krishnathas, G., et al. (2022) Knock-out of 5-lipoxygenase in overexpressing tumor cells-consequences on gene expression and cellular function. *Cancer Gene Ther.* 30, 108–123

73. Jones, S. M., Luo, M., Healy, A. M., et al. (2002) Structural and functional criteria reveal a new nuclear import sequence on the 5-lipoxygenase protein. *J. Biol. Chem.* 277, 38550–38556

74. Luo, M., Pang, C. W. M., Gerken, A. E., et al. (2004) Multiple nuclear localization sequences allow modulation of 5-lipoxygenase nuclear import. *Traffic* 5, 847–854

75. Woods, J. W., Evans, J. F., Ethier, D., et al. (1993) 5-lipoxygenase and 5-lipoxygenase-activating protein are localized in the nuclear envelope of activated human leukocytes. *J. Exp. Med.* 178, 1935–1946

76. Schmider, A. B., Bauer, N. C., Sunwoo, H., et al. (2020) Two- and three-color STORM

analysis reveals higher-order assembly of leukotriene synthetic complexes on the nuclear envelope of murine neutrophils. *J. Biol. Chem.* 295, 5761–5770

77. Luo, M., Jones, S. M., Phare, S. M., et al. (2004) Protein kinase A inhibits leukotriene synthesis by phosphorylation of 5-lipoxygenase on serine 523. *J. Biol. Chem.* 279, 41512–41520

78. Luo, M., Jones, S. M., Flamand, N., et al. (2005) Phosphorylation by protein kinase a inhibits nuclear import of 5-lipoxygenase. *J. Biol. Chem.* 280, 40609–40616

79. Markoutsa, S., Sürün, D., Karas, M., et al. (2014) Analysis of 5-lipoxygenase phosphorylation on molecular level by MALDI-MS. *FEBS J.* 281, 1931–1947

80. Flamand, N., Luo, M., Peters-Golden, M., et al. (2009) Phosphorylation of serine 271 on 5-lipoxygenase and its role in nuclear export. *J. Biol. Chem.* 284, 306–313

81. Werz, O., Szellas, D., Steinhilber, D., et al. (2002) Arachidonic acid promotes phosphorylation of 5-lipoxygenase at Ser-271 by MAPK-activated protein kinase 2 (MK2). *J. Biol. Chem.* 277, 14793–14800

82. Werz, O., Bürkert, E., Fischer, L., et al. (2002) Extracellular signal-regulated kinases phosphorylate 5-lipoxygenase and stimulate 5-lipoxygenase product formation in leukocytes. *FASEB J.* 16, 1441–1443

83. Mehrabian, M., Schulthess, F. T., Nebohacova, M., et al. (2008) Identification of ALOX5 as a gene regulating adiposity and pancreatic function. *Diabetologia* 51, 978–988

84. Müller-Tidow, C., Steffen, B., Cauvet, T., et al. (2004) Translocation products in acute myeloid leukemia activate the Wnt signaling pathway in hematopoietic cells. *Mol. Cell. Biol.* 24, 2890–2904

85. Roos, J., Oancea, C., Heinssmann, M., et al. (2014) 5-Lipoxygenase Is a Candidate Target for Therapeutic Management of Stem Cell–like Cells in Acute Myeloid Leukemia. *Cancer Res.* 74, 5244–5255

86. Xie, S., Chen, M., Fang, W., et al. (2022) Diminished arachidonate 5-lipoxygenase perturbs phase separation and transcriptional response of Runx2 to reverse pathological ventricular remodeling. *eBioMedicine* 86, 104359

87. Kreiß, M., Oberlis, J. H., Seuter, S., et al. (2022) Human 5-lipoxygenase regulates transcription by association to euchromatin. *Biochem. Pharmacol.* 203, 115187

88. Catalano, A., Caprari, P., Soddu, S., et al. (2004) 5-lipoxygenase antagonizes genotoxic stress-induced apoptosis by altering p53 nuclear trafficking. *FASEB J.* 18, 1740–1742

89. Uebbing, S., Kreiß, M., Scholl, F., et al. (2021) Modulation of microRNA processing by 5-lipoxygenase. *FASEB J.* 35, e21193

90. Dincbas-Renqvist, V., Pépin, G., Rakonjac, M., et al. (2009) Human Dicer C-terminus functions as a 5-lipoxygenase binding domain. *Biochim. Biophys. Acta* 1789, 99–108

91. Liu, Y. W., Arakawa, T., Yamamoto, S., et al. (1997) Transcriptional activation of human 12-lipoxygenase gene promoter is mediated through Sp1 consensus sites in A431 cells. *Biochem. J.* 324 (Pt 1, 133–140

92. Ivanov, I., Kuhn, H., and Heydeck, D. (2015) Structural and functional biology of arachidonic acid 15-lipoxygenase-1 (ALOX15). *Gene* 573, 1–32

93. Zheng, Z., Li, Y., Jin, G., et al. (2020) The biological role of arachidonic acid 12-lipoxygenase (ALOX12) in various human diseases. *Biomed. Pharmacother.* 129, 110354

94. Yamamoto, S., Suzuki, H., and Ueda, N. (1997) Arachidonate 12-lipoxygenases. *Prog. Lipid Res.* 36, 23–41

95. Tsai, W.-C., Aleem, A. M., Whittington, C., et al. (2021) Mutagenesis, Hydrogen-Deuterium Exchange, and Molecular Docking Investigations Establish the Dimeric Interface of Human

Platelet-Type 12-Lipoxygenase. *Biochemistry* 60, 802–812

96. Boeglin, W. E., Kim, R. B., and Brash, A. R. (1998) A 12R-lipoxygenase in human skin: mechanistic evidence, molecular cloning, and expression. *Proc. Natl. Acad. Sci. U. S. A.* 95, 6744–6749

97. Conrad, D. J. (1999) The arachidonate 12/15 lipoxygenases. A review of tissue expression and biologic function. *Clin. Rev. Allergy Immunol.* 17, 71–89

98. Benatzy, Y., Palmer, M. A., and Brüne, B. (2022) Arachidonate 15-lipoxygenase type B: Regulation, function, and its role in pathophysiology. *Front. Pharmacol.* 13, 1042420

99. Klil-Drori, A. J. and Ariel, A. (2013) 15-Lipoxygenases in cancer: a double-edged sword? *Prostaglandins Other Lipid Mediat.* 106, 16–22

100. Contursi, A., Tacconelli, S., Hofling, U., et al. (2022) Biology and pharmacology of platelet-type 12-lipoxygenase in platelets, cancer cells, and their crosstalk. *Biochem. Pharmacol.* 205, 115252

101. CLAESSON, H.-E. and HAEGGSTROM, J. (1988) Human endothelial cells stimulate leukotriene synthesis and convert granulocyte released leukotriene A4 into leukotrienes B4, C4, D4 and E4. *Eur. J. Biochem.* 173, 93–100

102. Edenius, C., Heidvall, K., and Lindgren, J. A. (1988) Novel transcellular interaction: conversion of granulocyte-derived leukotriene A4 to cysteinyl-containing leukotrienes by human platelets. *Eur. J. Biochem.* 178, 81–86

103. McGee, J. E. and Fitzpatrick, F. A. (1986) Erythrocyte-neutrophil interactions: formation of leukotriene B4 by transcellular biosynthesis. *Proc. Natl. Acad. Sci. U. S. A.* 83, 1349–1353

104. Capra, V., Rovati, G. E., Mangano, P., et al. (2015) Transcellular biosynthesis of eicosanoid lipid mediators. *Biochim. Biophys. Acta* 1851, 377–382

105. Dennis, E. A., Cao, J., Hsu, Y.-H., et al. (2011) Phospholipase A2 enzymes: physical structure, biological function, disease implication, chemical inhibition, and therapeutic intervention. *Chem. Rev.* 111, 6130–6185

106. Burke, J. E. and Dennis, E. A. (2009) Phospholipase A2 biochemistry. *Cardiovasc. drugs Ther.* 23, 49–59

107. Schaloske, R. H. and Dennis, E. A. (2006) The phospholipase A2 superfamily and its group numbering system. *Biochim. Biophys. Acta* 1761, 1246–1259

108. Evans, J. H., Spencer, D. M., Zweifach, A., et al. (2001) Intracellular calcium signals regulating cytosolic phospholipase A2 translocation to internal membranes. *J. Biol. Chem.* 276, 30150–30160

109. Lin, L. L., Wartmann, M., Lin, A. Y., et al. (1993) cPLA2 is phosphorylated and activated by MAP kinase. *Cell* 72, 269–278

110. Hayashi, D., Mouchlis, V. D., and Dennis, E. A. (2021) Omega-3 versus Omega-6 fatty acid availability is controlled by hydrophobic site geometries of phospholipase A2s. *J. Lipid Res.* 62, 100113

111. Evans, J. F., Ferguson, A. D., Mosley, R. T., et al. (2008) What's all the FLAP about?: 5-lipoxygenase-activating protein inhibitors for inflammatory diseases. *Trends Pharmacol. Sci.* 29, 72–78

112. Ferguson, A. D., McKeever, B. M., Xu, S., et al. (2007) Crystal structure of inhibitor-bound human 5-lipoxygenase-activating protein. *Science* 317, 510–512

113. Mandal, A. K., Skoch, J., Bacskai, B. J., et al. (2004) The membrane organization of leukotriene synthesis. *Proc. Natl. Acad. Sci. U. S. A.* 101, 6587–6592

114. Mancini, J. A., Abramovitz, M., Cox, M. E., et al. (1993) 5-lipoxygenase-activating protein is an arachidonate binding protein. *FEBS Lett.* 318, 277–281

115. Häfner, A.-K., Gerstmeier, J., Hörnig, M., et al. (2015) Characterization of the interaction of human 5-lipoxygenase with its activating protein FLAP. *Biochim. Biophys. Acta* 1851, 1465–1472

116. Hill, E., Maclouf, J., Murphy, R. C., et al. (1992) Reversible membrane association of neutrophil 5-lipoxygenase is accompanied by retention of activity and a change in substrate specificity. *J. Biol. Chem.* 267, 22048–22053

117. Rouzer, C. A. and Samuelsson, B. (1985) On the nature of the 5-lipoxygenase reaction in human leukocytes: enzyme purification and requirement for multiple stimulatory factors. *Proc. Natl. Acad. Sci. U. S. A.* 82, 6040–6044

118. Abramovitz, M., Wong, E., Cox, M. E., et al. (1993) 5-lipoxygenase-activating protein stimulates the utilization of arachidonic acid by 5-lipoxygenase. *Eur. J. Biochem.* 215, 105–111

119. Christmas, P., Weber, B. M., McKee, M., et al. (2002) Membrane Localization and Topology of Leukotriene C4 Synthase. *J. Biol. Chem.* 277, 28902–28908

120. Brock, T. G., Maydanski, E., McNish, R. W., et al. (2001) Co-localization of Leukotriene A4Hydrolase with 5-Lipoxygenase in Nuclei of Alveolar Macrophages and Rat Basophilic Leukemia Cells but Not Neutrophils. *J. Biol. Chem.* 276, 35071–35077

121. Lehmann, C., Homann, J., Ball, A.-K., et al. (2015) Lipoxin and resolvin biosynthesis is dependent on 5-lipoxygenase activating protein. *FASEB J.* 29, 5029–5043

122. Haeggström, J. Z. and Wetterholm, A. (2002) Enzymes and receptors in the leukotriene cascade. *Cell. Mol. Life Sci.* 59, 742–753

123. Haeggström, J. Z., Wetterholm, A., Shapiro, R., et al. (1990) Leukotriene A4 hydrolase: a zinc metalloenzyme. *Biochem. Biophys. Res. Commun.* 172, 965–970

124. Wan, M., Tang, X., Stsiapanava, A., et al. (2017) Biosynthesis of leukotriene B4. *Semin. Immunol.* 33, 3–15

125. Snelgrove, R. J., Jackson, P. L., Hardison, M. T., et al. (2010) A critical role for LTA4H in limiting chronic pulmonary neutrophilic inflammation. *Science* 330, 90–94

126. Haeggström, J. Z. (2018) Leukotriene biosynthetic enzymes as therapeutic targets. *J. Clin. Invest.* 128, 2680–2690

127. Evans, J. F., Nathaniel, D. J., Zamboni, R. J., et al. (1985) Leukotriene A3. A poor substrate but a potent inhibitor of rat and human neutrophil leukotriene A4 hydrolase. *J. Biol. Chem.* 260, 10966–10970

128. Ohishi, N., Izumi, T., Minami, M., et al. (1987) Leukotriene A4 hydrolase in the human lung. Inactivation of the enzyme with leukotriene A4 isomers. *J. Biol. Chem.* 262, 10200–10205

129. Ago, H., Kanaoka, Y., Irikura, D., et al. (2007) Crystal structure of a human membrane protein involved in cysteinyl leukotriene biosynthesis. *Nature* 448, 609–612

130. Lam, B. K. and Austen, K. F. (2002) Leukotriene C4 synthase: a pivotal enzyme in cellular biosynthesis of the cysteinyl leukotrienes. *Prostaglandins Other Lipid Mediat.* 68–69, 511–520

131. Söderström, M., Mannervik, B., Garkov, V., et al. (1992) On the nature of leukotriene C4 synthase in human platelets. *Arch. Biochem. Biophys.* 294, 70–74

132. Hevko, J. M. and Murphy, R. C. (2002) Formation of murine macrophage-derived 5-oxo-7-glutathionyl-8,11,14-eicosatrienoic acid (FOG7) is catalyzed by leukotriene C4 synthase. *J. Biol. Chem.* 277, 7037–7043

133. Esser, J., Gehrmann, U., Salvado, M. D., et al. (2011) Zymosan suppresses leukotriene C_4 synthase activity in differentiating monocytes: antagonism by aspirin and protein kinase inhibitors. *FASEB J.* 25, 1417–1427

134. Ahmad, S., Ytterberg, A. J., Thulasingam, M., et al. (2016) Phosphorylation of Leukotriene C4 Synthase at Serine 36 Impairs Catalytic Activity. *J. Biol. Chem.* 291, 18410–18418

135. Aharony, D. and Stein, R. L. (1986) Kinetic mechanism of guinea pig neutrophil 5-lipoxygenase. *J. Biol. Chem.* 261, 11512–11519

136. Hammarberg, T. and Rådmark, O. (1999) 5-lipoxygenase binds calcium. *Biochemistry* 38, 4441–4447

137. Reddy, K. V, Hammarberg, T., and Rådmark, O. (2000) Mg2+ activates 5-lipoxygenase in vitro: dependency on concentrations of phosphatidylcholine and arachidonic acid. *Biochemistry* 39, 1840–1848

138. Werz, O., Bürkert, E., Samuelsson, B., et al. (2002) Activation of 5-lipoxygenase by cell stress is calcium independent in human polymorphonuclear leukocytes. *Blood* 99, 1044–1052

139. Wong, A., Cook, M. N., Foley, J. J., et al. (1991) Influx of extracellular calcium is required for the membrane translocation of 5-lipoxygenase and leukotriene synthesis. *Biochemistry* 30, 9346–9354

140. Borgeat, P. and Samuelsson, B. (1979) Arachidonic acid metabolism in polymorphonuclear leukocytes: effects of ionophore A23187. *Proc. Natl. Acad. Sci. U. S. A.* 76, 2148–2152

141. Salari, H., Braquet, P., Naccache, P., et al. (1985) Characterization of effect of N-formyl-methionyl-leucyl-phenylalanine on leukotriene synthesis in human polymorphonuclear leukocytes. *Inflammation* 9, 127–138

142. McDonald, P. P., McColl, S. R., Naccache, P. H., et al. (1992) Activation of the human neutrophil 5-lipoxygenase by leukotriene B4. *Br. J. Pharmacol.* 107, 226–232

143. Schröder, J. M. (1989) The monocyte-derived neutrophil activating peptide (NAP/interleukin 8) stimulates human neutrophil arachidonate-5-lipoxygenase, but not the release of cellular arachidonate. *J. Exp. Med.* 170, 847–863

144. Ochi, K., Yoshimoto, T., Yamamoto, S., et al. (1983) Arachidonate 5-lipoxygenase of guinea pig peritoneal polymorphonuclear leukocytes. Activation by adenosine 5'-triphosphate. *J. Biol. Chem.* 258, 5754–5758

145. Skorey, K. I. and Gresser, M. J. (1998) Calcium is not required for 5-lipoxygenase activity at high phosphatidyl choline vesicle concentrations. *Biochemistry* 37, 8027–8034

146. Noguchi, M., Miyano, M., and Matsumoto, T. (1996) Physiochemical characterization of ATP binding to human 5-lipoxygenase. *Lipids* 31, 367–371

147. Smyrniotis, C. J., Barbour, S. R., Xia, Z., et al. (2014) ATP allosterically activates the human 5-lipoxygenase molecular mechanism of arachidonic acid and 5(S)-hydroperoxy-6(E),8(Z),11(Z),14(Z)-eicosatetraenoic acid. *Biochemistry* 53, 4407–4419

148. Gilbert, N. C., Rui, Z., Neau, D. B., et al. (2012) Conversion of human 5-lipoxygenase to a 15-lipoxygenase by a point mutation to mimic phosphorylation at Serine-663. *FASEB J.* 26, 3222–3229

149. Adel, S., Hofheinz, K., Heydeck, D., et al. (2014) Phosphorylation mimicking mutations of ALOX5 orthologs of different vertebrates do not alter reaction specificities of the enzymes. *Biochim. Biophys. Acta - Mol. Cell Biol. Lipids* 1841, 1460–1466

150. Rådmark, O., Werz, O., Steinhilber, D., et al. (2015) 5-Lipoxygenase, a key enzyme for leukotriene biosynthesis in health and disease. *Biochim. Biophys. Acta* 1851, 331–339

151. Provost, P., Doucet, J., Stock, A., et al. (2001) Coactosin-like protein, a human F-actin-binding protein: critical role of lysine-75. *Biochem. J.* 359, 255–263

152. Rakonjac, M., Fischer, L., Provost, P., et al. (2006) Coactosin-like protein supports 5-lipoxygenase enzyme activity and up-regulates leukotriene A4 production. *Proc. Natl.*

Acad. Sci. U. S. A. 103, 13150–13155

153. Esser, J., Rakonjac, M., Hofmann, B., et al. (2009) Coactosin-like protein functions as a stabilizing chaperone for 5-lipoxygenase: role of tryptophan 102. *Biochem. J.* 425, 265–274

154. Provost, P., Doucet, J., Hammarberg, T., et al. (2001) 5-Lipoxygenase interacts with coactosin-like protein. *J. Biol. Chem.* 276, 16520–16527

155. Feisst, C., Pergola, C., Rakonjac, M., et al. (2009) Hyperforin is a novel type of 5-lipoxygenase inhibitor with high efficacy in vivo. *Cell. Mol. Life Sci.* 66, 2759–2771

156. Rådmark, O. and Samuelsson, B. (2010) Regulation of the activity of 5-lipoxygenase, a key enzyme in leukotriene biosynthesis. *Biochem. Biophys. Res. Commun.* 396, 105–110

157. Hammarberg, T., Kuprin, S., Rådmark, O., et al. (2001) EPR investigation of the active site of recombinant human 5-lipoxygenase: inhibition by selenide. *Biochemistry* 40, 6371–6378

158. Riendeau, D., Denis, D., Choo, L. Y., et al. (1989) Stimulation of 5-lipoxygenase activity under conditions which promote lipid peroxidation. *Biochem. J.* 263, 565–572

159. Rouzer, C. A. and Samuelsson, B. (1986) The importance of hydroperoxide activation for the detection and assay of mammalian 5-lipoxygenase. *FEBS Lett.* 204, 293–296

160. Aharony, D., Redkar-Brown, D. G., Hubbs, S. J., et al. (1987) Kinetic studies on the inactivation of 5-lipoxygenase by 5(S)-hydroperoxyeicosatetraenoic acid. *Prostaglandins* 33, 85–100

161. Werz, O., Szellas, D., and Steinhilber, D. (2000) Reactive oxygen species released from granulocytes stimulate 5-lipoxygenase activity in a B-lymphocytic cell line. *Eur. J. Biochem.* 267, 1263–1269

162. Huang, H. S., Chen, C. J., Lu, H. S., et al. (1998) Identification of a lipoxygenase inhibitor in A431 cells as a phospholipid hydroperoxide glutathione peroxidase. *FEBS Lett.* 424, 22–26

163. Bürkert, E., Arnold, C., Hammarberg, T., et al. (2003) The C2-like beta-barrel domain mediates the Ca2+-dependent resistance of 5-lipoxygenase activity against inhibition by glutathione peroxidase-1. *J. Biol. Chem.* 278, 42846–42853

164. Puustinen, T., Scheffer, M. M., and Samuelsson, B. (1988) Regulation of the human leukocyte 5-lipoxygenase: stimulation by micromolar Ca2+ levels and phosphatidylcholine vesicles. *Biochim. Biophys. Acta* 960, 261–267

165. Albert, D., Buerkert, E., Steinhilber, D., et al. (2003) Induction of 5-lipoxygenase activation in polymorphonuclear leukocytes by 1-oleoyl-2-acetylglycerol. *Biochim. Biophys. Acta* 1631, 85–93

166. Albert, D., Pergola, C., Koeberle, A., et al. (2008) The role of diacylglyceride generation by phospholipase D and phosphatidic acid phosphatase in the activation of 5-lipoxygenase in polymorphonuclear leukocytes. *J. Leukoc. Biol.* 83, 1019–1027

167. Romano, M. (2010) Lipoxin and aspirin-triggered lipoxins. *ScientificWorldJournal.* 10, 1048–1064

168. Schebb, N. H., Kühn, H., Kahnt, A. S., et al. (2022) Formation, Signaling and Occurrence of Specialized Pro-Resolving Lipid Mediators-What is the Evidence so far? *Front. Pharmacol.* 13, 838782

169. Serhan, C. N., Hamberg, M., Samuelsson, B., et al. (1986) On the stereochemistry and biosynthesis of lipoxin B. *Proc. Natl. Acad. Sci. U. S. A.* 83, 1983–1987

170. Clària, J., Lee, M. H., and Serhan, C. N. (1996) Aspirin-triggered lipoxins (15-epi-LX) are generated by the human lung adenocarcinoma cell line (A549)-neutrophil interactions and are potent inhibitors of cell proliferation. *Mol. Med.* 2, 583–596

171. Giménez-Bastida, J. A., Boeglin, W. E., Boutaud, O., et al. (2019) Residual cyclooxygenase activity of aspirin-acetylated COX-2 forms 15 R-prostaglandins that inhibit platelet aggregation. *FASEB J.* 33, 1033–1041

172. Birnbaum, Y., Ye, Y., Lin, Y., et al. (2006) Augmentation of myocardial production of 15-epi-lipoxin-a4 by pioglitazone and atorvastatin in the rat. *Circulation* 114, 929–935

173. Serhan, C. N., Yang, R., Martinod, K., et al. (2009) Maresins: novel macrophage mediators with potent antiinflammatory and proresolving actions. *J. Exp. Med.* 206, 15–23

174. Serhan, C. N. and Levy, B. D. (2018) Resolvins in inflammation: emergence of the pro-resolving superfamily of mediators. *J. Clin. Invest.* 128, 2657–2669

175. Hong, S., Gronert, K., Devchand, P. R., et al. (2003) Novel docosatrienes and 17S-resolvins generated from docosahexaenoic acid in murine brain, human blood, and glial cells. Autacoids in anti-inflammation. *J. Biol. Chem.* 278, 14677–14687

176. Serhan, C. N., Hong, S., Gronert, K., et al. (2002) Resolvins: a family of bioactive products of omega-3 fatty acid transformation circuits initiated by aspirin treatment that counter proinflammation signals. *J. Exp. Med.* 196, 1025–1037

177. Deng, B., Wang, C.-W., Arnardottir, H. H., et al. (2014) Maresin biosynthesis and identification of maresin 2, a new anti-inflammatory and pro-resolving mediator from human macrophages. *PLoS One* 9, e102362

178. Mukherjee, P. K., Marcheselli, V. L., Serhan, C. N., et al. (2004) Neuroprotectin D1: a docosahexaenoic acid-derived docosatriene protects human retinal pigment epithelial cells from oxidative stress. *Proc. Natl. Acad. Sci. U. S. A.* 101, 8491–8496

179. Lam, B. K. and Wong, P. Y. (1988) Biosynthesis and biological activities of lipoxin A5 and B5 from eicosapentaenoic acid. *Adv. Exp. Med. Biol.* 229, 51–59

180. Libreros, S., Shay, A. E., Nshimiyimana, R., et al. (2020) A New E-Series Resolvin: RvE4 Stereochemistry and Function in Efferocytosis of Inflammation-Resolution. *Front. Immunol.* 11, 631319

181. Serhan, C. N., Clish, C. B., Brannon, J., et al. (2000) Novel functional sets of lipid-derived mediators with antiinflammatory actions generated from omega-3 fatty acids via cyclooxygenase 2-nonsteroidal antiinflammatory drugs and transcellular processing. *J. Exp. Med.* 192, 1197–1204

182. Isobe, Y., Arita, M., Matsueda, S., et al. (2012) Identification and structure determination of novel anti-inflammatory mediator resolvin E3, 17,18-dihydroxyeicosapentaenoic acid. *J. Biol. Chem.* 287, 10525–10534

183. Kutzner, L., Goloshchapova, K., Rund, K. M., et al. (2020) Human lipoxygenase isoforms form complex patterns of double and triple oxygenated compounds from eicosapentaenoic acid. *Biochim. Biophys. Acta - Mol. Cell Biol. Lipids* 1865, 158806

184. Romano, M., Cianci, E., Simiele, F., et al. (2015) Lipoxins and aspirin-triggered lipoxins in resolution of inflammation. *Eur. J. Pharmacol.* 760, 49–63

185. Kahnt, A. S., Schebb, N. H., and Steinhilber, D. (2023) Formation of Lipoxins and Resolvins in Human Leukocytes. *Prostaglandins Other Lipid Mediat.* 106726

186. Guichardant, M., Chen, P., Liu, M., et al. (2011) Functional lipidomics of oxidized products from polyunsaturated fatty acids. *Chem. Phys. Lipids* 164, 544–548

187. Serhan, C. N., Chiang, N., and Van Dyke, T. E. (2008) Resolving inflammation: dual anti-inflammatory and pro-resolution lipid mediators. *Nat. Rev. Immunol.* 8, 349–361

188. Dyall, S. C., Balas, L., Bazan, N. G., et al. (2022) Polyunsaturated fatty acids and fatty acid-derived lipid mediators: Recent advances in the understanding of their biosynthesis, structures, and functions. *Prog. Lipid Res.* 86, 101165

189. Yokomizo, T., Nakamura, M., and Shimizu, T. (2018) Leukotriene receptors as potential therapeutic targets. *J. Clin. Invest.* 128, 2691–2701

190. Serhan, C. N., Chiang, N., Dalli, J., et al. (2014) Lipid mediators in the resolution of inflammation. *Cold Spring Harb. Perspect. Biol.* 7, a016311

191. Ortega-Gómez, A., Perretti, M., and Soehnlein, O. (2013) Resolution of inflammation: an integrated view. *EMBO Mol. Med.* 5, 661–674

192. Medzhitov, R. (2008) Origin and physiological roles of inflammation. *Nature* 454, 428–435

193. Hafstrom, I., Palmblad, J., Malmsten, C. L., et al. (1981) Leukotriene B4--a stereospecific stimulator for release of lysosomal enzymes from neutrophils. *FEBS Lett.* 130, 146–148

194. Rae, S. A. and Smith, M. J. (1981) The stimulation of lysosomal enzyme secretion from human polymorphonuclear leucocytes by leukotriene B4. *J. Pharm. Pharmacol.* 33, 616–617

195. Steiner, D. R., Gonzalez, N. C., and Wood, J. G. (2001) Leukotriene B(4) promotes reactive oxidant generation and leukocyte adherence during acute hypoxia. *J. Appl. Physiol.* 91, 1160–1167

196. Palmer, R. M., Stepney, R. J., Higgs, G. A., et al. (1980) Chemokinetic activity of arachidonic and lipoxygenase products on leuocyctes of different species. *Prostaglandins* 20, 411–418

197. Yamaoka, K. A., Dugas, B., Paul-Eugene, N., et al. (1994) Leukotriene B4 enhances IL-4-induced IgE production from normal human lymphocytes. *Cell. Immunol.* 156, 124–134

198. Yamaoka, K. A., Claésson, H. E., and Rosén, A. (1989) Leukotriene B4 enhances activation, proliferation, and differentiation of human B lymphocytes. *J. Immunol.* 143, 1996–2000

199. He, R., Chen, Y., and Cai, Q. (2020) The role of the LTB4-BLT1 axis in health and disease. *Pharmacol. Res.* 158, 104857

200. Owman, C., Nilsson, C., and Lolait, S. J. (1996) Cloning of cDNA encoding a putative chemoattractant receptor. *Genomics* 37, 187–194

201. Yokomizo, T., Kato, K., Hagiya, H., et al. (2001) Hydroxyeicosanoids bind to and activate the low affinity leukotriene B4 receptor, BLT2. *J. Biol. Chem.* 276, 12454–12459

202. Okuno, T., Iizuka, Y., Okazaki, H., et al. (2008) 12(S)-Hydroxyheptadeca-5Z, 8E, 10E-trienoic acid is a natural ligand for leukotriene B4 receptor 2. *J. Exp. Med.* 205, 759–766

203. Yokomizo, T., Kato, K., Terawaki, K., et al. (2000) A second leukotriene B(4) receptor, BLT2. A new therapeutic target in inflammation and immunological disorders. *J. Exp. Med.* 192, 421–432

204. Okuno, T. and Yokomizo, T. (2018) Biological functions of 12(S)-hydroxyheptadecatrienoic acid as a ligand of leukotriene B4 receptor 2. *Inflamm. Regen.* 38, 29

205. Iizuka, Y., Okuno, T., Saeki, K., et al. (2010) Protective role of the leukotriene B4 receptor BLT2 in murine inflammatory colitis. *FASEB J.* 24, 4678–4690

206. Matsunaga, Y., Fukuyama, S., Okuno, T., et al. (2013) Leukotriene B4 receptor BLT2 negatively regulates allergic airway eosinophilia. *FASEB J.* 27, 3306–3314

207. Zinn, S., Sisignano, M., Kern, K., et al. (2017) The leukotriene B4 receptors BLT1 and BLT2 form an antagonistic sensitizing system in peripheral sensory neurons. *J. Biol. Chem.* 292, 6123–6134

208. Narala, V. R., Adapala, R. K., Suresh, M. V, et al. (2010) Leukotriene B4 is a physiologically relevant endogenous peroxisome proliferator-activated receptor-alpha agonist. *J. Biol. Chem.* 285, 22067–22074

209. Varga, T., Czimmerer, Z., and Nagy, L. (2011) PPARs are a unique set of fatty acid regulated transcription factors controlling both lipid metabolism and inflammation. *Biochim. Biophys. Acta* 1812, 1007–1022

210. Peters-Golden, M. and Henderson, W. R. (2007) Leukotrienes. *N. Engl. J. Med.* 357, 1841–1854

211. Watkins, P. B., Dube, L. M., Walton-Bowen, K., et al. (2007) Clinical pattern of zileuton-associated liver injury: results of a 12-month study in patients with chronic asthma. *Drug Saf.* 30, 805–815

212. Singh, R. K., Gupta, S., Dastidar, S., et al. (2010) Cysteinyl leukotrienes and their receptors: molecular and functional characteristics. *Pharmacology* 85, 336–349

213. Rovati, G. E. and Capra, V. (2007) Cysteinyl-leukotriene receptors and cellular signals. *ScientificWorldJournal.* 7, 1375–1392

214. Kelloway, J. S. (1997) Zafirlukast: the first leukotriene-receptor antagonist approved for the treatment of asthma. *Ann. Pharmacother.* 31, 1012–1021

215. Clarridge, K., Chin, S., Eworuke, E., et al. (2021) A Boxed Warning for Montelukast: The FDA Perspective. *J. allergy Clin. Immunol. Pract.* 9, 2638–2641

216. Hoxha, M., Rovati, G. E., and Cavanillas, A. B. (2017) The leukotriene receptor antagonist montelukast and its possible role in the cardiovascular field. *Eur. J. Clin. Pharmacol.* 73, 799–809

217. Fredman, G., Li, Y., Dalli, J., et al. (2012) Self-limited versus delayed resolution of acute inflammation: temporal regulation of pro-resolving mediators and microRNA. *Sci. Rep.* 2, 639

218. Serhan, C. N. (2010) Novel lipid mediators and resolution mechanisms in acute inflammation: to resolve or not? *Am. J. Pathol.* 177, 1576–1591

219. Serhan, C. N. (2014) Pro-resolving lipid mediators are leads for resolution physiology. *Nature* 510, 92–101

220. Yang, M., Lippestad, M., Hodges, R. R., et al. (2020) RvE1 uses the LTB4 receptor BLT1 to increase [Ca2+]i and stimulate mucin secretion in cultured rat and human conjunctival goblet cells. *Ocul. Surf.* 18, 470–482

221. Arita, M., Ohira, T., Sun, Y.-P., et al. (2007) Resolvin E1 selectively interacts with leukotriene B4 receptor BLT1 and ChemR23 to regulate inflammation. *J. Immunol.* 178, 3912–3917

222. Lee, S. A., Kim, H. J., Chang, K. C., et al. (2009) DHA and EPA Down-regulate COX-2 Expression through Suppression of NF-kappaB Activity in LPS-treated Human Umbilical Vein Endothelial Cells. *Korean J. Physiol. Pharmacol.* 13, 301–307

223. Gao, Y., Zhang, H., Luo, L., et al. (2017) Resolvin D1 Improves the Resolution of Inflammation via Activating NF-κB p50/p50-Mediated Cyclooxygenase-2 Expression in Acute Respiratory Distress Syndrome. *J. Immunol.* 199, 2043–2054

224. Zhang, J., Li, Z., Fan, M., et al. (2022) Lipoxins in the Nervous System: Brighter Prospects for Neuroprotection. *Front. Pharmacol.* 13, 781889

225. Ungaro, F., D'Alessio, S., and Danese, S. (2020) The Role of Pro-Resolving Lipid Mediators in Colorectal Cancer-Associated Inflammation: Implications for Therapeutic Strategies. *Cancers (Basel).* 12, 2060

226. Zhang, Q., Zhu, B., and Li, Y. (2017) Resolution of Cancer-Promoting Inflammation: A New Approach for Anticancer Therapy. *Front. Immunol.* 8

227. Hanson, J., Ferreirós, N., Pirotte, B., et al. (2013) Heterologously expressed formyl peptide receptor 2 (FPR2/ALX) does not respond to lipoxin A_4. *Biochem. Pharmacol.* 85, 1795–

1802

228. Hodges, R. R., Li, D., Shatos, M. A., et al. (2017) Lipoxin A4 activates ALX/FPR2 receptor to regulate conjunctival goblet cell secretion. *Mucosal Immunol.* 10, 46–57

229. Fattori, V., Zaninelli, T. H., Rasquel-Oliveira, F. S., et al. (2020) Specialized pro-resolving lipid mediators: A new class of non-immunosuppressive and non-opioid analgesic drugs. *Pharmacol. Res.* 151, 104549

230. Giera, M., Ioan-Facsinay, A., Toes, R., et al. (2012) Lipid and lipid mediator profiling of human synovial fluid in rheumatoid arthritis patients by means of LC-MS/MS. *Biochim. Biophys. Acta* 1821, 1415–1424

231. Ramsden, C. E., Faurot, K. R., Zamora, D., et al. (2015) Targeted alterations in dietary n-3 and n-6 fatty acids improve life functioning and reduce psychological distress among patients with chronic headache: a secondary analysis of a randomized trial. *Pain* 156, 587–596

232. Durán, A. M., Salto, L. M., Câmara, J., et al. (2019) Effects of omega-3 polyunsaturated fatty-acid supplementation on neuropathic pain symptoms and sphingosine levels in Mexican-Americans with type 2 diabetes. *Diabetes. Metab. Syndr. Obes.* 12, 109–120

233. Caturla, N., Funes, L., Pérez-Fons, L., et al. (2011) A randomized, double-blinded, placebo-controlled study of the effect of a combination of lemon verbena extract and fish oil omega-3 fatty acid on joint management. *J. Altern. Complement. Med.* 17, 1051–1063

234. Mas, E., Croft, K. D., Zahra, P., et al. (2012) Resolvins D1, D2, and other mediators of self-limited resolution of inflammation in human blood following n-3 fatty acid supplementation. *Clin. Chem.* 58, 1476–1484

235. Barden, A., Mas, E., Croft, K. D., et al. (2014) Short-term n-3 fatty acid supplementation but not aspirin increases plasma proresolving mediators of inflammation. *J. Lipid Res.* 55, 2401–2407

236. See, V. H. L., Mas, E., Prescott, S. L., et al. (2017) Effects of postnatal omega-3 fatty acid supplementation on offspring pro-resolving mediators of inflammation at 6 months and 5 years of age: A double blind, randomized controlled clinical trial. *Prostaglandins. Leukot. Essent. Fatty Acids* 126, 126–132

237. Schebb, N. H. and Steinhilber, D. (2022) What Mediates the Inflammation Resolution? *Function* 4

238. O'Donnell, V., Schebb, N. H., Milne, G. L., et al. (2021) Failure to apply standard limit-of-detection or limit-of-quantitation criteria to specialized pro-resolving mediator analysis incorrectly characterizes their presence in biological samples. Preprint, 10.5281/ZENODO.5766267

239. Carbone, A. (2020) Cancer Classification at the Crossroads. *Cancers (Basel).* 12, 980

240. Weinberg, R. A. (2013) The Biology of Cancer. W.W. Norton & Company, New York

241. Vardiman, J. W., Thiele, J., Arber, D. A., et al. (2009) The 2008 revision of the World Health Organization (WHO) classification of myeloid neoplasms and acute leukemia: rationale and important changes. *Blood* 114, 937–951

242. Armitage, J. O., Gascoyne, R. D., Lunning, M. A., et al. (2017) Non-Hodgkin lymphoma. *Lancet (London, England)* 390, 298–310

243. WHO. (2022) International Classification of Diseases for Oncology, 3rd Edition (ICD-O-3).

244. Sung, H., Ferlay, J., Siegel, R. L., et al. (2021) Global Cancer Statistics 2020: GLOBOCAN Estimates of Incidence and Mortality Worldwide for 36 Cancers in 185 Countries. *CA. Cancer J. Clin.* 71, 209–249

245. Hanahan, D. and Weinberg, R. A. (2000) The hallmarks of cancer. *Cell* 100, 57–70

246. Hanahan, D. and Weinberg, R. A. (2011) Hallmarks of cancer: the next generation. *Cell* 144, 646–674

247. Hanahan, D. (2022) Hallmarks of Cancer: New Dimensions. *Cancer Discov.* 12, 31–46

248. Simon, K. (2016) Colorectal cancer development and advances in screening. *Clin. Interv. Aging* 11, 967–976

249. Müller, M. F., Ibrahim, A. E. K., and Arends, M. J. (2016) Molecular pathological classification of colorectal cancer. *Virchows Arch.* 469, 125–134

250. Kasi, A., Handa, S., Bhatti, S., et al. (2020) Molecular Pathogenesis and Classification of Colorectal Carcinoma. *Curr. Colorectal Cancer Rep.* 16, 97–106

251. Li, J., Ma, X., Chakravarti, D., et al. (2021) Genetic and biological hallmarks of colorectal cancer. *Genes Dev.* 35, 787–820

252. Nair, A., Chauhan, P., Saha, B., et al. (2019) Conceptual Evolution of Cell Signaling. *Int. J. Mol. Sci.* 20

253. Lindemann, L. and Hoener, M. C. (2005) A renaissance in trace amines inspired by a novel GPCR family. *Trends Pharmacol. Sci.* 26, 274–281

254. Paudel, S., Wu, G., and Wang, X. (2021) Amino Acids in Cell Signaling: Regulation and Function. *Adv. Exp. Med. Biol.* 1332, 17–33

255. Leonard, W. J. and Lin, J. X. (2000) Cytokine receptor signaling pathways. *J. Allergy Clin. Immunol.* 105, 877–888

256. Parker, R. B. and Kohler, J. J. (2010) Regulation of intracellular signaling by extracellular glycan remodeling. *ACS Chem. Biol.* 5, 35–46

257. Kihara, Y. (2020) Introduction: Druggable Lipid Signaling Pathways. *Adv. Exp. Med. Biol.* 1274, 1–4

258. Qi, W., Man, L., Suguro, S., et al. (2022) Endocrine effects of three common gas signaling molecules in humans: A literature review. *Front. Endocrinol. (Lausanne).* 13, 1074638

259. Ubersax, J. A. and Ferrell, J. E. (2007) Mechanisms of specificity in protein phosphorylation. *Nat. Rev. Mol. Cell Biol.* 8, 530–541

260. Torry, D. S. and Cooper, G. M. (1991) Proto-oncogenes in development and cancer. *Am. J. Reprod. Immunol.* 25, 129–132

261. Lynch, D. H. (1987) Oncogenes and cancer. *Am. J. Reprod. Immunol. Microbiol.* 15, 24–28

262. Zheng, J. (2013) Oncogenic chromosomal translocations and human cancer (review). *Oncol. Rep.* 30, 2011–2019

263. Fröhling, S. and Döhner, H. (2008) Chromosomal Abnormalities in Cancer. *N. Engl. J. Med.* 359, 722–734

264. Lee, E. Y. H. P. and Muller, W. J. (2010) Oncogenes and tumor suppressor genes. *Cold Spring Harb. Perspect. Biol.* 2, a003236

265. Pećina-Šlaus, N., Kafka, A., Salamon, I., et al. (2020) Mismatch Repair Pathway, Genome Stability and Cancer. *Front. Mol. Biosci.* 7, 122

266. Jones, C. L. A. and Kane, M. A. (1996) Oncogenic signaling. *Curr. Opin. Oncol.* 8, 54–59

267. Martini, M., De Santis, M. C., Braccini, L., et al. (2014) PI3K/AKT signaling pathway and cancer: an updated review. *Ann. Med.* 46, 372–383

268. Downward, J. (2003) Targeting RAS signalling pathways in cancer therapy. *Nat. Rev. Cancer* 3, 11–22

269. Ullah, R., Yin, Q., Snell, A. H., et al. (2022) RAF-MEK-ERK pathway in cancer evolution

and treatment. *Semin. Cancer Biol.* 85, 123–154

270. Sanchez-Vega, F., Mina, M., Armenia, J., et al. (2018) Oncogenic Signaling Pathways in The Cancer Genome Atlas. *Cell* 173, 321-337.e10
271. Dienstmann, R., Rodon, J., Serra, V., et al. (2014) Picking the point of inhibition: a comparative review of PI3K/AKT/mTOR pathway inhibitors. *Mol. Cancer Ther.* 13, 1021–1031
272. Rozengurt, E., Soares, H. P., and Sinnet-Smith, J. (2014) Suppression of feedback loops mediated by PI3K/mTOR induces multiple overactivation of compensatory pathways: an unintended consequence leading to drug resistance. *Mol. Cancer Ther.* 13, 2477–2488
273. McCubrey, J. A., Steelman, L. S., Chappell, W. H., et al. (2007) Roles of the Raf/MEK/ERK pathway in cell growth, malignant transformation and drug resistance. *Biochim. Biophys. Acta* 1773, 1263–1284
274. Labani-Motlagh, A., Ashja-Mahdavi, M., and Loskog, A. (2020) The Tumor Microenvironment: A Milieu Hindering and Obstructing Antitumor Immune Responses. *Front. Immunol.* 11, 940
275. Anderson, N. M. and Simon, M. C. (2020) The tumor microenvironment. *Curr. Biol.* 30, R921–R925
276. Cox, T. R. (2021) The matrix in cancer. *Nat. Rev. Cancer* 21, 217–238
277. Theocharis, A. D., Skandalis, S. S., Gialeli, C., et al. (2016) Extracellular matrix structure. *Adv. Drug Deliv. Rev.* 97, 4–27
278. Winkler, J., Abisoye-Ogunniyan, A., Metcalf, K. J., et al. (2020) Concepts of extracellular matrix remodelling in tumour progression and metastasis. *Nat. Commun.* 11, 5120
279. Mohan, V., Das, A., and Sagi, I. (2020) Emerging roles of ECM remodeling processes in cancer. *Semin. Cancer Biol.* 62, 192–200
280. Boedtkjer, E. and Pedersen, S. F. (2020) The Acidic Tumor Microenvironment as a Driver of Cancer. *Annu. Rev. Physiol.* 82, 103–126
281. Roma-Rodrigues, C., Mendes, R., Baptista, P. V, et al. (2019) Targeting Tumor Microenvironment for Cancer Therapy. *Int. J. Mol. Sci.* 20
282. Marshall, J. S., Warrington, R., Watson, W., et al. (2018) An introduction to immunology and immunopathology. *Allergy Asthma. Clin. Immunol.* 14, 49
283. Shapouri-Moghaddam, A., Mohammadian, S., Vazini, H., et al. (2018) Macrophage plasticity, polarization, and function in health and disease. *J. Cell. Physiol.* 233, 6425–6440
284. Martinez, F. O. and Gordon, S. (2014) The M1 and M2 paradigm of macrophage activation: time for reassessment. *F1000Prime Rep.* 6, 13
285. Greten, F. R. and Grivennikov, S. I. (2019) Inflammation and Cancer: Triggers, Mechanisms, and Consequences. *Immunity* 51, 27–41
286. Zhou, J., Tang, Z., Gao, S., et al. (2020) Tumor-Associated Macrophages: Recent Insights and Therapies. *Front. Oncol.* 10, 188
287. Shen, M., Hu, P., Donskov, F., et al. (2014) Tumor-associated neutrophils as a new prognostic factor in cancer: a systematic review and meta-analysis. *PLoS One* 9, e98259
288. Farc, O. and Cristea, V. (2021) An overview of the tumor microenvironment, from cells to complex networks (Review). *Exp. Ther. Med.* 21, 96
289. Yang, Y., Li, C., Liu, T., et al. (2020) Myeloid-Derived Suppressor Cells in Tumors: From Mechanisms to Antigen Specificity and Microenvironmental Regulation. *Front. Immunol.* 11, 1371
290. Jensen, C. and Teng, Y. (2020) Is It Time to Start Transitioning From 2D to 3D Cell Culture?

Front. Mol. Biosci. 7, 33

291. Badr-Eldin, S. M., Aldawsari, H. M., Kotta, S., et al. (2022) Three-Dimensional In Vitro Cell Culture Models for Efficient Drug Discovery: Progress So Far and Future Prospects. *Pharmaceuticals (Basel).* 15
292. Langhans, S. A. (2018) Three-Dimensional in Vitro Cell Culture Models in Drug Discovery and Drug Repositioning. *Front. Pharmacol.* 9, 6
293. Weiswald, L.-B., Bellet, D., and Dangles-Marie, V. (2015) Spherical cancer models in tumor biology. *Neoplasia* 17, 1–15
294. Friedrich, J., Seidel, C., Ebner, R., et al. (2009) Spheroid-based drug screen: considerations and practical approach. *Nat. Protoc.* 4, 309–324
295. Sutherland, R. M. (1988) Cell and environment interactions in tumor microregions: the multicell spheroid model. *Science* 240, 177–184
296. Nederman, T., Norling, B., Glimelius, B., et al. (1984) Demonstration of an extracellular matrix in multicellular tumor spheroids. *Cancer Res.* 44, 3090–3097
297. Timmins, N. E., Dietmair, S., and Nielsen, L. K. (2004) Hanging-drop multicellular spheroids as a model of tumour angiogenesis. *Angiogenesis* 7, 97–103
298. Uhlen, M., Zhang, C., Lee, S., et al. (2017) A pathology atlas of the human cancer transcriptome. *Science* 357
299. Uhlén, M., Fagerberg, L., Hallström, B. M., et al. (2015) Tissue-based map of the human proteome. *Science* 347
300. Uhlén, M., Björling, E., Agaton, C., et al. (2005) A Human Protein Atlas for Normal and Cancer Tissues Based on Antibody Proteomics. *Mol. Cell. Proteomics* 4, 1920–1932
301. Steinhilber, D., Fischer, A. S., Metzner, J., et al. (2010) 5-Lipoxygenase: Underappreciated Role of a Pro-Inflammatory Enzyme in Tumorigenesis. *Front. Pharmacol.* 1
302. Barresi, V., Vitarelli, E., Tuccari, G., et al. (2008) Correlative Study of Microvessel Density and 5-Lipoxygenase Expression in Human Sporadic Colorectal Cancer. *Arch. Pathol. Lab. Med.* 132, 1807–1812
303. Merchant, N., Bhaskar, L. V. K. S., Momin, S., et al. (2018) 5-Lipoxygenase: Its involvement in gastrointestinal malignancies. *Crit. Rev. Oncol. Hematol.* 127, 50–55
304. Xingfu, W., Lifeng, Z., Yupeng, C., et al. (2015) Cytoplasmic 5-Lipoxygenase Staining Is a Highly Sensitive Marker of Human Tumors of the Choroid Plexus. *Am. J. Clin. Pathol.* 144, 295–304
305. Kumar, R., Singh, A. K., Kumar, M., et al. (2016) Serum 5-LOX: a progressive protein marker for breast cancer and new approach for therapeutic target. *Carcinogenesis* 37, 912–917
306. Bai, C.-Y., Zhang, J.-Y., Shi, T.-W., et al. (2018) Association between 5-lipoxygenase expression, and malignant behaviors and poor prognosis in esophageal squamous cell carcinoma. *Oncol. Lett.* 15, 9353–9360
307. Wang, X., Chen, Y., Zhang, S., et al. (2015) Co-expression of COX-2 and 5-LO in primary glioblastoma is associated with poor prognosis. *J. Neurooncol.* 125, 277–285
308. Tong, W.-G., Ding, X.-Z., Talamonti, M. S., et al. (2005) LTB4 stimulates growth of human pancreatic cancer cells via MAPK and PI-3 kinase pathways. *Biochem. Biophys. Res. Commun.* 335, 949–956
309. Ding, X.-Z., Tong, W.-G., and Adrian, T. E. (2003) Multiple Signal Pathways Are Involved in the Mitogenic Effect of 5(S)-HETE in Human Pancreatic Cancer. *Oncology* 65, 285–294
310. Hu, N., Li, Y., Zhao, Y., et al. (2011) A novel positive feedback loop involving FASN/p-

ERK1/2/5-LOX/LTB4/FASN sustains high growth of breast cancer cells. *Acta Pharmacol. Sin.* 32, 921–929

311. Tang, J., Zhang, C., Lin, J., et al. (2021) ALOX5-5-HETE promotes gastric cancer growth and alleviates chemotherapy toxicity via MEK/ERK activation. *Cancer Med.* 10, 5246–5255

312. Bortuzzo, C., Hanif, R., Kashfi, K., et al. (1996) The effect of leukotrienes B and selected HETEs on the proliferation of colon cancer cells. *Biochim. Biophys. Acta - Lipids Lipid Metab.* 1300, 240–246

313. Romano, M., Catalano, A., Nutini, M., et al. (2001) 5-lipoxygenase regulates malignant mesothelial cell survival: involvement of vascular endothelial growth factor. *FASEB J.* 15, 2326–2336

314. Tsai, M.-J., Chang, W.-A., Chuang, C.-H., et al. (2021) Cysteinyl Leukotriene Pathway and Cancer. *Int. J. Mol. Sci.* 23, 120

315. Paruchuri, S., Hallberg, B., Juhas, M., et al. (2002) Leukotriene D4 activates MAPK through a Ras-independent but PKCε-dependent pathway in intestinal epithelial cells. *J. Cell Sci.* 115, 1883–1893

316. Ghosh, J. and Myers, C. E. (1997) Arachidonic Acid Stimulates Prostate Cancer Cell Growth: Critical Role of 5-Lipoxygenase. *Biochem. Biophys. Res. Commun.* 235, 418–423

317. Hammamieh, R., Sumaida, D., Zhang, X., et al. (2007) Control of the growth of human breast cancer cells in culture by manipulation of arachidonate metabolism. *BMC Cancer* 7, 138

318. Ihara, A., Wada, K., Yoneda, M., et al. (2007) Blockade of Leukotriene B4 Signaling Pathway Induces Apoptosis and Suppresses Cell Proliferation in Colon Cancer. *J. Pharmacol. Sci.* 103, 24–32

319. Hoque, A. (2005) Increased 5-lipoxygenase expression and induction of apoptosis by its inhibitors in esophageal cancer: a potential target for prevention. *Carcinogenesis* 26, 785–791

320. HAYASHI, T., NISHIYAMA, K., and SHIRAHAMA, T. (2006) Inhibition of 5-lipoxygenase pathway suppresses the growth of bladder cancer cells. *Int. J. Urol.* 13, 1086–1091

321. Tsukada, T., Nakashima, K., and Shirakawa, S. (1986) Arachidonate 5-lipoxygenase inhibitors show potent antiproliferative effects on human leukemia cell lines. *Biochem. Biophys. Res. Commun.* 140, 832–836

322. Ghosh, J. and Myers, C. E. (1998) Inhibition of arachidonate 5-lipoxygenase triggers massive apoptosis in human prostate cancer cells. *Proc. Natl. Acad. Sci.* 95, 13182–13187

323. Huang, J.-K., Huang, C.-C., Lu, T., et al. (2009) Effect of MK-886 on Ca 2+ Level and Viability in PC3 Human Prostate Cancer Cells. *Basic Clin. Pharmacol. Toxicol.* 104, 441–447

324. FAN, X. M., TU, S. P., LAM, S. K., et al. (2004) Five-lipoxygenase-activating protein inhibitor MK-886 induces apoptosis in gastric cancer through upregulation of p27 kip1 and bax. *J. Gastroenterol. Hepatol.* 19, 31–37

325. ZHOU, G.-X., DING, X.-L., WU, S.-B., et al. (2015) Inhibition of 5-lipoxygenase triggers apoptosis in pancreatic cancer cells. *Oncol. Rep.* 33, 661–668

326. Li, L., Xiao, Y., Xu, Z., et al. (2021) Zileuton inhibits arachidonate-5-lipoxygenase to exert antitumor effects in preclinical cervical cancer models. *Cancer Chemother. Pharmacol.* 88, 953–960

327. Lim, Park, Um, et al. (2019) Zileuton, a 5-Lipoxygenase Inhibitor, Exerts Anti-Angiogenic Effect by Inducing Apoptosis of HUVEC via BK Channel Activation. *Cells* 8, 1182

328. Gener, P., Montero, S., Xandri-Monje, H., et al. (2020) Zileuton™ loaded in polymer

micelles effectively reduce breast cancer circulating tumor cells and intratumoral cancer stem cells. *Nanomedicine* 24, 102106

329. Fischer, A., Metzner, J., Steinbrink, S., et al. (2010) 5-Lipoxygenase inhibitors induce potent anti-proliferative and cytotoxic effects in human tumour cells independently of suppression of 5-lipoxygenase activity. *Br. J. Pharmacol.* 161, 936–949

330. Friedlander, T. (2011) A phase II study of insulin-like growth factor receptor inhibition with nordihydroguaiaretic acid in men with non-metastatic hormone-sensitive prostate cancer. *Oncol. Rep.*

331. Bishayee, K. and Khuda-Bukhsh, A. R. (2013) 5-Lipoxygenase Antagonist therapy: a new approach towards targeted cancer chemotherapy. *Acta Biochim. Biophys. Sin. (Shanghai).* 45, 709–719

332. Jänne, P. A., Paz-Ares, L., Oh, Y., et al. (2014) Randomized, Double-Blind, Phase II Trial Comparing Gemcitabine-Cisplatin plus the LTB4 Antagonist LY293111 versus Gemcitabine-Cisplatin plus Placebo in First-Line Non–Small-Cell Lung Cancer. *J. Thorac. Oncol.* 9, 126–131

333. Saif, M. W., Oettle, H., Vervenne, W. L., et al. (2009) Randomized Double-Blind Phase II Trial Comparing Gemcitabine Plus LY293111 Versus Gemcitabine Plus Placebo in Advanced Adenocarcinoma of the Pancreas. *Cancer J.* 15, 339–343

334. Kim, T. Y., Kim, J., Choo, H.-Y. P., et al. (2016) Inhibition of 5-lipoxygenase suppresses vascular endothelial growth factor-induced angiogenesis in endothelial cells. *Biochem. Biophys. Res. Commun.* 478, 1117–1122

335. Ding, X., Zhou, X., Zhang, H., et al. (2012) Triptolide augments the effects of 5-lipoxygenase RNA interference in suppressing pancreatic tumor growth in a xenograft mouse model. *Cancer Chemother. Pharmacol.* 69, 253–261

336. Ding, X., Zhou, X., Zhang, H., et al. (2012) Triptolide augments the effects of 5-lipoxygenase RNA interference in suppressing pancreatic tumor growth in a xenograft mouse model. *Cancer Chemother. Pharmacol.* 69, 253–261

337. Cheon, E. C., Strouch, M. J., Krantz, S. B., et al. (2012) Genetic Deletion of 5-Lipoxygenase Increases Tumor-Infiltrating Macrophages in ApcΔ468 Mice. *J. Gastrointest. Surg.* 16, 389–393

338. Poczobutt, J. M., Nguyen, T. T., Hanson, D., et al. (2016) Deletion of 5-Lipoxygenase in the Tumor Microenvironment Promotes Lung Cancer Progression and Metastasis through Regulating T Cell Recruitment. *J. Immunol.* 196, 891–901

339. Iacona, J. R., Monteleone, N. J., and Lutz, C. S. (2018) miR-146a suppresses 5-lipoxygenase activating protein (FLAP) expression and Leukotriene B4 production in lung cancer cells. *Oncotarget* 9, 26751–26769

340. Ye, X., An, L., Wang, X., et al. (2021) ALOX5AP Predicts Poor Prognosis by Enhancing M2 Macrophages Polarization and Immunosuppression in Serous Ovarian Cancer Microenvironment. *Front. Oncol.* 11

341. Jiang, W. G., Douglas-Jones, A. G., and Mansel, R. E. (2006) Aberrant expression of 5-lipoxygenase-activating protein (5-LOXAP) has prognostic and survival significance in patients with breast cancer. *Prostaglandins, Leukot. Essent. Fat. Acids* 74, 125–134

342. Sveinbjörnsson, B., Rasmuson, A., Baryawno, N., et al. (2008) Expression of enzymes and receptors of the leukotriene pathway in human neuroblastoma promotes tumor survival and provides a target for therapy. *FASEB J.* 22, 3525–3536

343. Park, J., Jang, J.-H., Park, G.-S., et al. (2018) BLT2, a leukotriene B4 receptor 2, as a novel prognostic biomarker of triple-negative breast cancer. *BMB Rep.* 51, 373–377

344. Seo, J.-M., Cho, K.-J., Kim, E.-Y., et al. (2011) Up-regulation of BLT2 is critical for the

survival of bladder cancer cells. *Exp. Mol. Med.* 43, 129

345. Hennig, R., Osman, T., Esposito, I., et al. (2008) BLT2 is expressed in PanINs, IPMNs, pancreatic cancer and stimulates tumour cell proliferation. *Br. J. Cancer* 99, 1064–1073

346. Magnusson, C., Ehrnström, R., Olsen, J., et al. (2007) An Increased Expression of Cysteinyl Leukotriene 2 Receptor in Colorectal Adenocarcinomas Correlates with High Differentiation. *Cancer Res.* 67, 9190–9198

347. Venerito, M., Kuester, D., Harms, C., et al. (2011) Upregulation of Leukotriene Receptors in Gastric Cancer. *Cancers (Basel).* 3, 3156–3168

348. Riedl, A., Schlederer, M., Pudelko, K., et al. (2017) Comparison of cancer cells in 2D vs 3D culture reveals differences in AKT-mTOR-S6K signaling and drug responses. *J. Cell Sci.* 130, 203–218

349. Bunz, F., Dutriaux, A., Lengauer, C., et al. (1998) Requirement for p53 and p21 to Sustain G 2 Arrest After DNA Damage. *Science* 282, 1497–1501

350. Kowarz, E., Löscher, D., and Marschalek, R. (2015) Optimized Sleeping Beauty transposons rapidly generate stable transgenic cell lines. *Biotechnol. J.* 10, 647–653

351. Davis, P. K., Ho, A., and Dowdy, S. F. (2001) Biological methods for cell-cycle synchronization of mammalian cells. *Biotechniques* 30, 1322–1326, 1328, 1330–1331

352. Wan, M.-L., Wang, Y., Zeng, Z., et al. (2020) Colorectal cancer (CRC) as a multifactorial disease and its causal correlations with multiple signaling pathways. *Biosci. Rep.* 40

353. Hastings, J. F., Gonzalez Rajal, A., Latham, S. L., et al. (2020) Analysis of pulsed cisplatin signalling dynamics identifies effectors of resistance in lung adenocarcinoma. *Elife* 9

354. Trousil, S., Chen, S., Mu, C., et al. (2017) Phenformin Enhances the Efficacy of ERK Inhibition in NF1-Mutant Melanoma. *J. Invest. Dermatol.* 137, 1135–1143

355. Ponton, A., Thirion, J. P., and Sirois, P. (1997) Repression of the 5-lipoxygenase gene by c-myb overexpression in differentiated HL-60 cells. *Prostaglandins* 53, 49–58

356. Ringleb, J., Strack, E., Angioni, C., et al. (2018) Apoptotic Cancer Cells Suppress 5-Lipoxygenase in Tumor-Associated Macrophages. *J. Immunol.* 200, 857–868

357. Wächtershäuser, A., Steinhilber, D., Loitsch, S. M., et al. (2000) Expression of 5-Lipoxygenase by Human Colorectal Carcinoma Caco-2 Cells during Butyrate-Induced Cell Differentiation. *Biochem. Biophys. Res. Commun.* 268, 778–783

358. Nielsen, C. K., Ohd, J. F., Wikström, K., et al. (2003) The leukotriene receptor CysLT1 and 5-lipoxygenase are upregulated in colon cancer. *Adv. Exp. Med. Biol.* 525, 201–204

359. Costa, H., Touma, J., Davoudi, B., et al. (2019) Human cytomegalovirus infection is correlated with enhanced cyclooxygenase-2 and 5-lipoxygenase protein expression in breast cancer. *J. Cancer Res. Clin. Oncol.* 145, 2083–2095

360. Kutzner, L., Rund, K. M., Ostermann, A. I., et al. (2019) Development of an Optimized LC-MS Method for the Detection of Specialized Pro-Resolving Mediators in Biological Samples. *Front. Pharmacol.* 10

361. Jeong, C.-H., Bode, A. M., Pugliese, A., et al. (2009) [6]-Gingerol Suppresses Colon Cancer Growth by Targeting Leukotriene A4 Hydrolase. *Cancer Res.* 69, 5584–5591

362. YOSHIMURA, R., MATSUYAMA, M., TSUCHIDA, K., et al. (2003) Expression of Lipoxygenase in Human Bladder Carcinoma and Growth Inhibition by Its Inhibitors. *J. Urol.* 170, 1994–1999

363. Hennig, R., Ding, X.-Z., Tong, W.-G., et al. (2002) 5-Lipoxygenase and leukotriene B(4) receptor are expressed in human pancreatic cancers but not in pancreatic ducts in normal tissue. *Am. J. Pathol.* 161, 421–428

364. Ahmed, D., Eide, P. W., Eilertsen, I. A., et al. (2013) Epigenetic and genetic features of 24 colon cancer cell lines. *Oncogenesis* 2, e71–e71

365. Riffle, S. and Hegde, R. S. (2017) Modeling tumor cell adaptations to hypoxia in multicellular tumor spheroids. *J. Exp. Clin. Cancer Res.* 36, 102

366. Gáti, I., Bergström, M., Muhr, C., et al. Leukotriene and 5-lipoxygenase inhibitor induced variations in thymidine uptake in a human glioma cell line cultured as monolayers or as multicellular spheroids. *Anticancer Res.* 14, 453–459

367. Kerjaschki, D., Bago-Horvath, Z., Rudas, M., et al. (2011) Lipoxygenase mediates invasion of intrametastatic lymphatic vessels and propagates lymph node metastasis of human mammary carcinoma xenografts in mouse. *J. Clin. Invest.* 121, 2000–2012

368. Sha, W., Olesch, C., Hanaka, H., et al. (2013) Necrosis in DU145 prostate cancer spheroids induces COX-2/mPGES-1-derived PGE 2 to promote tumor growth and to inhibit T cell activation. *Int. J. Cancer* 133, 1578–1588

369. Sutoo, S., Maeda, T., Suzuki, A., et al. (2020) Adaptation to chronic acidic extracellular pH elicits a sustained increase in lung cancer cell invasion and metastasis. *Clin. Exp. Metastasis* 37, 133–144

370. Wu, T.-C., Liao, C.-Y., Lu, W.-C., et al. (2022) Identification of distinct slow mode of reversible adaptation of pancreatic ductal adenocarcinoma to the prolonged acidic pH microenvironment. *J. Exp. Clin. Cancer Res.* 41, 137

371. Rauschner, M., Lange, L., Hüsing, T., et al. (2021) Impact of the acidic environment on gene expression and functional parameters of tumors in vitro and in vivo. *J. Exp. Clin. Cancer Res.* 40, 10

372. Lee, S. and Shanti, A. (2021) Effect of Exogenous pH on Cell Growth of Breast Cancer Cells. *Int. J. Mol. Sci.* 22

373. Leontieva, O. V., Demidenko, Z. N., and Blagosklonny, M. V. (2014) Contact inhibition and high cell density deactivate the mammalian target of rapamycin pathway, thus suppressing the senescence program. *Proc. Natl. Acad. Sci.* 111, 8832–8837

374. Saqcena, M., Menon, D., Patel, D., et al. (2013) Amino Acids and mTOR Mediate Distinct Metabolic Checkpoints in Mammalian G1 Cell Cycle. *PLoS One* 8, e74157

375. Fingar, D. C., Richardson, C. J., Tee, A. R., et al. (2004) mTOR Controls Cell Cycle Progression through Its Cell Growth Effectors S6K1 and 4E-BP1/Eukaryotic Translation Initiation Factor 4E. *Mol. Cell. Biol.* 24, 200–216

376. Arodin Selenius, L., Wallenberg Lundgren, M., Jawad, R., et al. (2019) The Cell Culture Medium Affects Growth, Phenotype Expression and the Response to Selenium Cytotoxicity in A549 and HepG2 Cells. *Antioxidants* 8, 130

377. KIM, S. W., KIM, S.-J., LANGLEY, R. R., et al. (2015) Modulation of the cancer cell transcriptome by culture media formulations and cell density. *Int. J. Oncol.* 46, 2067–2075

378. Werz, O., Tretiakova, I., Michel, A., et al. (2005) Caspase-mediated degradation of human 5-lipoxygenase in B lymphocytic cells. *Proc. Natl. Acad. Sci.* 102, 13164–13169

379. Chiang, C.-T., Lau, R., Ghaffarizadeh, A., et al. (2021) High-throughput microscopy reveals the impact of multifactorial environmental perturbations on colorectal cancer cell growth. *Gigascience* 10

380. Medico, E., Russo, M., Picco, G., et al. (2015) The molecular landscape of colorectal cancer cell lines unveils clinically actionable kinase targets. *Nat. Commun.* 6, 7002

381. Sadanandam, A., Lyssiotis, C. A., Homicsko, K., et al. (2013) A colorectal cancer classification system that associates cellular phenotype and responses to therapy. *Nat. Med.* 19, 619–625

382. Hamada, K., Monnai, M., Kawai, K., et al. (2008) Liver metastasis models of colon cancer for evaluation of drug efficacy using NOD/Shi-scid IL2Rγnull (NOG) mice. *Int. J. Oncol.* 32, 153–159

383. Kakiuchi, Y., Yurube, T., Kakutani, K., et al. (2019) Pharmacological inhibition of mTORC1 but not mTORC2 protects against human disc cellular apoptosis, senescence, and extracellular matrix catabolism through Akt and autophagy induction. *Osteoarthr. Cartil.* 27, 965–976

384. Li, Q., Li, Z., Luo, T., et al. (2022) Targeting the PI3K/AKT/mTOR and RAF/MEK/ERK pathways for cancer therapy. *Mol. Biomed.* 3, 47

385. Zhu, G., Pei, L., Xia, H., et al. (2021) Role of oncogenic KRAS in the prognosis, diagnosis and treatment of colorectal cancer. *Mol. Cancer* 20, 143

386. Waters, A. M. and Der, C. J. (2018) KRAS: The Critical Driver and Therapeutic Target for Pancreatic Cancer. *Cold Spring Harb. Perspect. Med.* 8, a031435

387. Xie, M., Xu, X., and Fan, Y. (2021) KRAS-Mutant Non-Small Cell Lung Cancer: An Emerging Promisingly Treatable Subgroup. *Front. Oncol.* 11

388. Dou, R., Zhang, L., Lu, T., et al. (2018) Identification of a novel HRAS variant and its association with papillary thyroid carcinoma. *Oncol. Lett.* 15, 4511–4516

389. Dietrich, P., Gaza, A., Wormser, L., et al. (2019) Neuroblastoma RAS Viral Oncogene Homolog (NRAS) Is a Novel Prognostic Marker and Contributes to Sorafenib Resistance in Hepatocellular Carcinoma. *Neoplasia* 21, 257–268

390. Sepp-Lorenzino, L., Ma, Z., Rands, E., et al. (1995) A peptidomimetic inhibitor of farnesyl:protein transferase blocks the anchorage-dependent and -independent growth of human tumor cell lines. *Cancer Res.* 55, 5302–5309

391. Der, C. J. and Cox, A. D. (1991) Isoprenoid modification and plasma membrane association: critical factors for ras oncogenicity. *Cancer Cells* 3, 331–340

392. Odeniyide, P., Yohe, M. E., Pollard, K., et al. (2022) Targeting farnesylation as a novel therapeutic approach in HRAS-mutant rhabdomyosarcoma. *Oncogene* 41, 2973–2983

393. Gimple, R. C. and Wang, X. (2019) RAS: Striking at the Core of the Oncogenic Circuitry. *Front. Oncol.* 9

394. White, E. Z., Pennant, N. M., Carter, J. R., et al. (2020) Serum deprivation initiates adaptation and survival to oxidative stress in prostate cancer cells. *Sci. Rep.* 10, 12505

395. Alessio, N., Aprile, D., Cappabianca, S., et al. (2021) Different Stages of Quiescence, Senescence, and Cell Stress Identified by Molecular Algorithm Based on the Expression of Ki67, RPS6, and Beta-Galactosidase Activity. *Int. J. Mol. Sci.* 22, 3102

396. YU, Y., YU, X., MA, J., et al. (2016) Effects of NVP-BEZ235 on the proliferation, migration, apoptosis and autophagy in HT-29 human colorectal adenocarcinoma cells. *Int. J. Oncol.* 49, 285–293

397. Gong, S., Xu, D., Zhu, J., et al. (2018) Efficacy of the MEK Inhibitor Cobimetinib and its Potential Application to Colorectal Cancer Cells. *Cell. Physiol. Biochem.* 47, 680–693

398. Pal, R., Wei, N., Song, N., et al. (2018) Molecular subtypes of colorectal cancer in pre-clinical models show differential response to targeted therapies: Treatment implications beyond KRAS mutations. *PLoS One* 13, e0200836

399. Smith, M. P., Ferguson, J., Arozarena, I., et al. (2013) Effect of SMURF2 Targeting on Susceptibility to MEK Inhibitors in Melanoma. *JNCI J. Natl. Cancer Inst.* 105, 33–46

400. Hou, G., Zhao, Q., Zhang, M., et al. (2018) Down-regulation of Rictor enhances cell sensitivity to PI3K inhibitor LY294002 by blocking mTORC2-medicated phosphorylation of Akt/PRAS40 in esophageal squamous cell carcinoma. *Biomed. Pharmacother.* 106, 1348–

1356

401. Breuleux, M., Klopfenstein, M., Stephan, C., et al. (2009) Increased AKT S473 phosphorylation after mTORC1 inhibition is rictor dependent and does not predict tumor cell response to PI3K/mTOR inhibition. *Mol. Cancer Ther.* 8, 742–753

402. Julien, L.-A., Carriere, A., Moreau, J., et al. (2010) mTORC1-Activated S6K1 Phosphorylates Rictor on Threonine 1135 and Regulates mTORC2 Signaling. *Mol. Cell. Biol.* 30, 908–921

403. Chen, B. W., Chen, W., Liang, H., et al. (2015) Inhibition of mTORC2 Induces Cell-Cycle Arrest and Enhances the Cytotoxicity of Doxorubicin by Suppressing MDR1 Expression in HCC Cells. *Mol. Cancer Ther.* 14, 1805–1815

404. Zhou, X., Jiang, Y., Li, Q., et al. (2020) Aberrant ALOX5 Activation Correlates with HER2 Status and Mediates Breast Cancer Biological Activities through Multiple Mechanisms. *Biomed Res. Int.* 2020, 1–8

405. Chang, J., Tang, N., Fang, Q., et al. (2019) Inhibition of COX-2 and 5-LOX regulates the progression of colorectal cancer by promoting PTEN and suppressing PI3K/AKT pathway. *Biochem. Biophys. Res. Commun.* 517, 1–7

406. Wen, Z.-H., Su, Y.-C., Lai, P.-L., et al. (2013) Critical role of arachidonic acid-activated mTOR signaling in breast carcinogenesis and angiogenesis. *Oncogene* 32, 160–170

407. Tang, J., Zhang, C., Lin, J., et al. (2021) ALOX5-5-HETE promotes gastric cancer growth and alleviates chemotherapy toxicity via MEK/ERK activation. *Cancer Med.* 10, 5246–5255

408. You, J., Mi, D., Zhou, X., et al. (2009) A Positive Feedback between Activated Extracellularly Regulated Kinase and Cyclooxygenase/Lipoxygenase Maintains Proliferation and Migration of Breast Cancer Cells. *Endocrinology* 150, 1607–1617

409. Horio, Y., Isegawa, Y., and Shichiri, M. (2023) Daidzein phosphorylates and activates 5-lipoxygenase via the MEK/ERK pathway: a mechanism for inducing the production of 5-lipoxygenase metabolite that inhibit influenza virus intracellular replication. *J. Nutr. Biochem.* 114, 109276

410. Chang, X., Luo, F., Jiang, W., et al. (2015) Protective activity of salidroside against ethanol-induced gastric ulcer via the MAPK/NF-κB pathway in vivo and in vitro. *Int. Immunopharmacol.* 28, 604–615

411. Lee, S. J., Kim, C. E., Seo, K. W., et al. (2010) HNE-induced 5-LO expression is regulated by NF- B/ERK and Sp1/p38 MAPK pathways via EGF receptor in murine macrophages. *Cardiovasc. Res.* 88, 352–359

412. Koundouros, N., Karali, E., Tripp, A., et al. (2020) Metabolic Fingerprinting Links Oncogenic PIK3CA with Enhanced Arachidonic Acid-Derived Eicosanoids. *Cell* 181, 1596-1611.e27

413. Marcel, V., Nguyen Van Long, F., and Diaz, J.-J. (2018) 40 Years of Research Put p53 in Translation. *Cancers (Basel).* 10

414. Catalano, A., Rodilossi, S., Caprari, P., et al. (2005) 5-Lipoxygenase regulates senescence-like growth arrest by promoting ROS-dependent p53 activation. *EMBO J.* 24, 170–179

415. Tate, J. G., Bamford, S., Jubb, H. C., et al. (2019) COSMIC: the Catalogue Of Somatic Mutations In Cancer. *Nucleic Acids Res.* 47, D941–D947

416. Lu, Y., Soong, T. D., and Elemento, O. (2013) A Novel Approach for Characterizing Microsatellite Instability in Cancer Cells. *PLoS One* 8, e63056

417. Gu, M., Nishihara, R., Chen, Y., et al. (2017) Aspirin exerts high anti-cancer activity in PIK3CA -mutant colon cancer cells. *Oncotarget* 8, 87379–87389

418. Oda, K., Okada, J., Timmerman, L., et al. (2008) PIK3CA Cooperates with Other

Phosphatidylinositol 3′-Kinase Pathway Mutations to Effect Oncogenic Transformation. *Cancer Res.* 68, 8127–8136

419. Arcaroli, J. J., Quackenbush, K. S., Powell, R. W., et al. (2012) Common PIK3CA Mutants and a Novel 3′ UTR Mutation Are Associated with Increased Sensitivity to Saracatinib. *Clin. Cancer Res.* 18, 2704–2714

420. Beaver, J. A., Gustin, J. P., Yi, K. H., et al. (2013) PIK3CA and AKT1 Mutations Have Distinct Effects on Sensitivity to Targeted Pathway Inhibitors in an Isogenic Luminal Breast Cancer Model System. *Clin. Cancer Res.* 19, 5413–5422

421. Berg, K. C. G., Eide, P. W., Eilertsen, I. A., et al. (2017) Multi-omics of 34 colorectal cancer cell lines - a resource for biomedical studies. *Mol. Cancer* 16, 116

422. Luo, Y., Li, Z., Kong, Y., et al. (2022) KRAS mutant–driven SUMOylation controls extracellular vesicle transmission to trigger lymphangiogenesis in pancreatic cancer. *J. Clin. Invest.* 132

423. Shankar, S., Pitchiaya, S., Malik, R., et al. (2016) KRAS Engages AGO2 to Enhance Cellular Transformation. *Cell Rep.* 14, 1448–1461

424. Swiatnicki, M., Engel, L., Shrestha, R., et al. (2022) Profiling oncogenic KRAS mutant drugs with a cell-based Lumit p-ERK immunoassay. *SLAS Discov.* 27, 249–257

425. Hinoue, T., Weisenberger, D. J., Pan, F., et al. (2009) Analysis of the Association between CIMP and BRAFV600E in Colorectal Cancer by DNA Methylation Profiling. *PLoS One* 4, e8357

426. Cho, E., Lou, H. J., Kuruvilla, L., et al. (2021) PPP6C negatively regulates oncogenic ERK signaling through dephosphorylation of MEK. *Cell Rep.* 34, 108928

427. Patra, S., Young, V., Llewellyn, L., et al. (2017) BRAF, KRAS and PIK3CA Mutation and Sensitivity to Trastuzumab in Breast Cancer Cell Line Model. *Asian Pac. J. Cancer Prev.* 18, 2209–2213

428. Leroy, B., Girard, L., Hollestelle, A., et al. (2014) Analysis of TP53 Mutation Status in Human Cancer Cell Lines: A Reassessment. *Hum. Mutat.* 35, 756–765

429. Allan, L. A. and Fried, M. (1999) p53-dependent apoptosis or growth arrest induced by different forms of radiation in U2OS cells: p21WAF1/CIP1 repression in UV induced apoptosis. *Oncogene* 18, 5403–5412

430. Wu, P.-K. and Park, J.-I. (2015) MEK1/2 Inhibitors: Molecular Activity and Resistance Mechanisms. *Semin. Oncol.* 42, 849–862

431. Wabnitz, P. A., Mitchell, D., and Wabnitz, D. A. M. (2004) In vitro and in vivo metabolism of the anti-cancer agent CI-1040, a MEK inhibitor, in rat, monkey, and human. *Pharm. Res.* 21, 1670–1679

432. Ma, Y., Kurtyka, C. A., Boyapalle, S., et al. (2008) A small-molecule E2F inhibitor blocks growth in a melanoma culture model. *Cancer Res.* 68, 6292–6299

433. Habenicht, A. J., Goerig, M., Rothe, D. E., et al. (1989) Early reversible induction of leukotriene synthesis in chicken myelomonocytic cells transformed by a temperature-sensitive mutant of avian leukemia virus E26. *Proc. Natl. Acad. Sci. U. S. A.* 86, 921–924

434. Tong, W.-G., Ding, X.-Z., Witt, R. C., et al. (2002) Lipoxygenase inhibitors attenuate growth of human pancreatic cancer xenografts and induce apoptosis through the mitochondrial pathway. *Mol. Cancer Ther.* 1, 929–935

435. Ding, X. Z., Iversen, P., Cluck, M. W., et al. (1999) Lipoxygenase inhibitors abolish proliferation of human pancreatic cancer cells. *Biochem. Biophys. Res. Commun.* 261, 218–223

436. Ding, X. Z., Kuszynski, C. A., El-Metwally, T. H., et al. (1999) Lipoxygenase inhibition

induced apoptosis, morphological changes, and carbonic anhydrase expression in human pancreatic cancer cells. *Biochem. Biophys. Res. Commun.* 266, 392–399

437. Ding, X.-Z., Tong, W.-G., and Adrian, T. E. (2003) Multiple signal pathways are involved in the mitogenic effect of 5(S)-HETE in human pancreatic cancer. *Oncology* 65, 285–294

438. Hankin, J. A., Jones, D. N. M., and Murphy, R. C. (2003) Covalent binding of leukotriene A4 to DNA and RNA. *Chem. Res. Toxicol.* 16, 551–561

439. Zhu, P., Lee, S. H., Wehrli, S., et al. (2006) Characterization of a lipid hydroperoxide-derived RNA adduct in rat intestinal epithelial cells. *Chem. Res. Toxicol.* 19, 809–817

440. Liu, Y., Wang, W., Li, Y., et al. (2015) The 5-Lipoxygenase Inhibitor Zileuton Confers Neuroprotection against Glutamate Oxidative Damage by Inhibiting Ferroptosis. *Biol. Pharm. Bull.* 38, 1234–1239

441. Lee, J.-J., Chang-Chien, G.-P., Lin, S., et al. (2022) 5-Lipoxygenase Inhibition Protects Retinal Pigment Epithelium from Sodium Iodate-Induced Ferroptosis and Prevents Retinal Degeneration. *Oxid. Med. Cell. Longev.* 2022, 1792894

442. Wu, C., Du, M., Yu, R., et al. (2022) A novel mechanism linking ferroptosis and endoplasmic reticulum stress via the circPtpn14/miR-351-5p/5-LOX signaling in melatonin-mediated treatment of traumatic brain injury. *Free Radic. Biol. Med.* 178, 271–294

443. Grimminger, F., Mayer, K., Kiss, L., et al. (1997) Synthesis of 4- and 5-series leukotrienes in the lung microvasculature challenged with Escherichia coli hemolysin: critical dependence on exogenous free fatty acid supply. *Am. J. Respir. Cell Mol. Biol.* 16, 317–324

444. Grimminger, F., Mayer, K., Kiss, L., et al. (2000) PAF-induced synthesis of tetraenoic and pentaenoic leukotrienes in the isolated rabbit lung. *Am. J. Physiol. Cell. Mol. Physiol.* 278, L268–L275

445. Wesley Ely, E., Seeds, M. C., Chilton, F. H., et al. (1995) Neutrophil release of arachidonic acid, oxidants, and proteinases: causally related or independent. *Biochim. Biophys. Acta - Lipids Lipid Metab.* 1258, 135–144

446. Walker, C., West, A., Browning, L., et al. (2015) The Pattern of Fatty Acids Displaced by EPA and DHA Following 12 Months Supplementation Varies between Blood Cell and Plasma Fractions. *Nutrients* 7, 6281–6293

447. Saku, N., Kobayashi, J., and Kitamura, S. (1999) Eicosapentaenoic acid modulates arachidonic acid metabolism in rat alveolar macrophages activated by silica. *Prostaglandins, Leukot. Essent. Fat. Acids* 61, 51–54

448. Nathaniel, D. J., Evans, J. F., Leblanc, Y., et al. (1985) Leukotriene A5 is a substrate and an inhibitor of rat and human neutrophil LTA4 hydrolase. *Biochem. Biophys. Res. Commun.* 131, 827–835

449. Archambault, A.-S., Turcotte, C., Martin, C., et al. (2018) Comparison of eight 15-lipoxygenase (LO) inhibitors on the biosynthesis of 15-LO metabolites by human neutrophils and eosinophils. *PLoS One* 13, e0202424

450. Kutzner, L., Goloshchapova, K., Heydeck, D., et al. (2017) Mammalian ALOX15 orthologs exhibit pronounced dual positional specificity with docosahexaenoic acid. *Biochim. Biophys. Acta - Mol. Cell Biol. Lipids* 1862, 666–675

451. Bryant, R. W., Bailey, J. M., Schewe, T., et al. (1982) Positional specificity of a reticulocyte lipoxygenase. Conversion of arachidonic acid to 15-S-hydroperoxy-eicosatetraenoic acid. *J. Biol. Chem.* 257, 6050–6055

452. Kühn, H., Barnett, J., Grunberger, D., et al. (1993) Overexpression, purification and characterization of human recombinant 15-lipoxygenase. *Biochim. Biophys. Acta - Lipids Lipid Metab.* 1169, 80–89

453. Thuresson, E. D., Lakkides, K. M., and Smith, W. L. (2000) Different Catalytically Competent Arrangements of Arachidonic Acid within the Cyclooxygenase Active Site of Prostaglandin Endoperoxide H Synthase-1 Lead to the Formation of Different Oxygenated Products. *J. Biol. Chem.* 275, 8501–8507

454. Hofling, U., Tacconelli, S., Contursi, A., et al. (2022) Characterization of the acetylation of cyclooxygenase-isozymes and targeted lipidomics of eicosanoids in serum and colon cancer cells by the new aspirin formulation IP1867B versus aspirin in vitro. *Front. Pharmacol.* 13

455. Werner, M., Jordan, P. M., Romp, E., et al. (2019) Targeting biosynthetic networks of the proinflammatory and proresolving lipid metabolome. *FASEB J.* 33, 6140–6153

456. Werz, O., Gerstmeier, J., Libreros, S., et al. (2018) Human macrophages differentially produce specific resolvin or leukotriene signals that depend on bacterial pathogenicity. *Nat. Commun.* 9, 59

457. Cortese, J. F., Spannhake, E. W., Eisinger, W., et al. (1995) The 5-lipoxygenase pathway in cultured human intestinal epithelial cells. *Prostaglandins* 49, 155–166

458. Mittal, M., Kumar, R. B., Balagunaseelan, N., et al. (2016) Kinetic investigation of human 5-lipoxygenase with arachidonic acid. *Bioorg. Med. Chem. Lett.* 26, 3547–3551

459. Peters-Golden, M. and Brock, T. G. (2003) 5-Lipoxygenase and FLAP. *Prostaglandins, Leukot. Essent. Fat. Acids* 69, 99–109

460. Rådmark, O., Werz, O., Steinhilber, D., et al. (2015) 5-Lipoxygenase, a key enzyme for leukotriene biosynthesis in health and disease. *Biochim. Biophys. Acta - Mol. Cell Biol. Lipids* 1851, 331–339

461. Amrein, P. and Stossel, T. (1980) Prevention of degradation of human polymorphonuclear leukocyte proteins by diisopropylfluorophosphate. *Blood* 56, 442–447

462. Radmark, O. (2022) Formation of eicosanoids and other oxylipins in human macrophages. *Biochem. Pharmacol.* 204, 115210

463. Hartung, N. M., Mainka, M., Kampschulte, N., et al. (2019) A strategy for validating concentrations of oxylipin standards for external calibration. *Prostaglandins Other Lipid Mediat.* 141, 22–24

464. Göbel, T., Goebel, B., Hyprath, M., et al. (2023) Three-dimensional growth reveals fine-tuning of 5-lipoxygenase by proliferative pathways in cancer. *Life Sci. Alliance* 6, e202201804

9 Danksagung

Declaration of Contribution

The work presented was generated by myself under the supervision of my advisors, Dr. Astrid Kahnt and Prof. Dr. Dieter Steinhilber, during my doctoral studies. All contributions from colleagues are explicitly referenced in the following. The data listed below were obtained in the context of collaborative research:

Figure 4.14: Phosphorylation state of ERK and p70S6K in MCTS. Svenja Simonyi performed the SDS-PAGE separation and Western Blot transfer. Tamara Göbel performed the sample preparation and antibody incubations.

Figure 4.35: Lipid mediator profile in unstimulated and stimulated HT-29 and HCT-116 cells. Carlo Angioni and Sandra Trautmann (Fraunhofer-Institute for Translational Medicine and Pharmacology, Department of Clinical Research (Biomedical Analysis) performed the lipid mediator extraction and analysis via LC-MS/MS. Tamara Göbel performed the sample incubation and preparation.

Figure 4.36: 15-LO expression and chiral 15-LO dependent lipid mediator formation in unstimulated and stimulated HT-29 and HCT-116 cells. Carlo Angioni and Sandra Trautmann (Fraunhofer-Institute for Translational Medicine and Pharmacology, Department of Clinical Research (Biomedical Analysis) performed the lipid mediator extraction and analysis via LC-MS/MS. Tamara Göbel performed the sample incubation and preparation.

Figure 4.37: Substrate-dependent 5-LO activity in HT-29 and HCT-116 cells. Carlo Angioni and Sandra Trautmann (Fraunhofer-Institute for Translational Medicine and Pharmacology, Department of Clinical Research (Biomedical Analysis) performed the lipid mediator extraction and analysis via LC-MS/MS. Tamara Göbel performed the sample incubation and preparation.

Figure 4.38: Comparison of 5-LO activity in tumor cells and leukocytes. Carlo Angioni and Sandra Trautmann (Fraunhofer-Institute for Translational Medicine and Pharmacology, Department of Clinical Research (Biomedical Analysis) performed the lipid mediator extraction and analysis via LC-MS/MS. Tamara Göbel performed the sample incubation, preparation, and Western blot analysis.

Figure 4.39: Comparison of the lipid mediator profile in tumor cells and leukocytes. Carlo Angioni and Sandra Trautmann (Fraunhofer-Institute for Translational Medicine and Pharmacology, Department of Clinical Research (Biomedical Analysis) performed the lipid mediator extraction and analysis via LC-MS/MS. Tamara Göbel performed the sample incubation and preparation.

Figure 4.40: Lipid mediator formation in HT-29 and PMNL co-incubations. Dr. Nadja Kampschulte, under the supervision of Prof. Dr. Nils Helge Schebb (Department of Food Chemistry, Faculty of Mathematics and Natural Sciences, University Wuppertal), performed the lipid mediator extraction and analysis via LC-MS/MS. Tamara Göbel performed the sample incubation and preparation.

App. Figure 7.2: mRNA expression of PTGS1 and PTGS2 in MCTS. qPCR analysis was performed by Marius Mathes. RNA extraction and general sample preparation was performed by Tamara Göbel.

Whenever a figure, table, or text is identical to a previous publication, it is explicitly stated in the figure legend. Copyright permission and/or co-author agreement has been obtained.

Cloning, preparation, and purification of the plasmids listed in Table 40: Summary of plasmid preparations was performed by Bjarne Goebel and Marius Hyprath.

Parts of the following data presented within this thesis have been previously published in a similar form:

Göbel, T., Goebel, B., Hyprath, M., Lamminger, I., Weisser, H., Angioni, C., Mathes, M., Thomas, D., and Kahnt, A. S. (2023) Three-dimensional growth reveals fine-tuning of 5-lipoxygenase by proliferative pathways in cancer. Life Sci. Alliance 6, e202201804 (464)

Figure 4.1, Figure 4.2, Figure 4.3, Figure 4.4, Figure 4.6, Figure 4.10, Figure 4.11, Figure 4.12, Figure 4.13, Figure 4.15, Figure 4.16, Figure 4.17, Figure 4.18, Figure 4.19, Figure 4.20, Figure 4.21, Figure 4.22, Figure 4.23, Figure 4.25, Figure 4.26, Figure 4.27, Figure 4.28, Figure 4.29, Figure 4.31, Figure 4.33, Figure 4.34, App. Figure 7.1, App. Figure 7.4, App. Figure 7.6, App. Figure 7.9, App. Figure 7.11, App. Figure 7.12

Following figures were created using BioRender.com and exported under a paid subscription:

Figure 1.1, Figure 1.3, Figure 1.4, Figure 1.5, Figure 1.6, Figure 1.7, Figure 1.8, Figure 1.9, Figure 1.11, Figure 1.12, Figure 1.14, Figure 3.1, Figure 3.2, Figure 5.1